Role of RAB25 and RAB11 GTPases in bladder tumorigenesis

Thuy Trang To

COMPARTIMENTATION ET DYNAMIQUE CELLULAIRES
INSTITUT CURIE/CNRS UMR144

THÈSE DE DOCTORAT
DE L'UNIVERSITÉ PIERRE ET MARIE CURIE

Spécialité: **BIOLOGIE CELLULAIRE**

Rôle des GTPases RAB25 et RAB11 dans la tumorigénèse des cancers de la vessie

présentée par

Thuy Trang TO

pour obtenir le grade de

DOCTEUR DE L'UNIVERSITÉ PIERRE ET MARIE CURIE

Soutenue le 08/07/2016 devant le jury composé de:

Pr.	Germain TRUGNAN	Président
Dr.	Jacky BONAVENTURE	Rapporteur
Dr.	Christophe LAMAZE	Rapporteur
Dr.	Thierry GALLI	Examinateur
Pr.	Françis VACHEROT	Examinateur
Dr.	Bruno GOUD	Directeur de thèse
Dr.	François RADVANYI	Directeur de thèse

To Long and Nhã Anh

This page intentionally left blank.

Remerciement

Au terme de ce travail, c'est avec émotion que je tiens à remercier tous ceux qui, de près ou de loin, ont contribué à la réalisation de ce projet.

Je tiens à remercier vivement Dr. **Jacky Bonaventure** et Dr. **Christophe Lamaze**, qui ont accepté de consacrer du temps pour évaluer mon travail en qualité de rapporteurs ainsi que Dr. **Thierry Galli**, Pr. **Germain Trugnan** et Pr. **Françis Vacherot**, qui ont également accepté de faire partie du jury de cette thèse.

Merci aux **membres de mon comité de thèse**, qui se sont rendus disponibles chaque année pour évaluer la progression de ma thèse et formuler des conseils avisés.

Un grand merci pour leur œil d'expert à mes **directeurs de thèse, Isabelle, Anh, Minh, Matt et Virginia** et pour le temps consacré à la relecture et à la correction de ce manuscrit.

Mes remerciements vont également à mes deux responsables de thèse, **François et Bruno**, qui pendant quatre ans ont dirigé et encadré mes travaux. Merci de m'avoir offert l'opportunité de réaliser un projet de thèse ambitieux et particulièrement de la liberté d'action que vous m'avez confiée à chaque étape de cette aventure. Aussi, merci **François** pour les nombreux chocolats suisses fourrés de liqueur Williams, sans oublier les oranges, pommes, clémentines, fraises à partager. Merci **Bruno** pour ta disponibilité lorsque je t'ai sollicité même à la dernière minute.

Je tiens également à remercier **Isabelle** pour ta présence lors des réunions d'avancement du projet, pour tes bons conseils afin de planifier les manipulations.

Un grand merci aux filles du laboratoire, **Marion, Vera, Mélanie, Céline, Daniella, Elodie, Jennifer, Alice, Clems, Hélène, Mériem, Virginia, Laure, Narjesse, Aura** et également les gars, **Florent, Mingjun, Damien, Thibault, Rémy**. Je tiens à vous remercier pour m'avoir toujours accueillie très chaleureusement, pour la bonne ambiance de travail que vous avez su créer, pour vos conseils scientifiques pertinents, votre soutien, votre écoute, votre dynamisme, les afterworks avec de la bière et des frites.

Un vif merci à **Sabine** pour ta générosité sans limites, ton soutien pendant mes périodes de doutes et pour tes multiples encouragements répétés. Merci aussi **Jean-Baptiste** pour ton aide pour la génération des constructions, **Stéphanie** pour tes conseils en spectrométrie de masse, à **Kristine, Lena et Carina** pour nos discussions scientifiques. Je remercie **Camilla, Bruno, Amal, Guillaume** pour les bons moments partagés et je vous souhaite à tous bon courage pour vos thèses.

Je remercie à mes deux secrétaires, **Michèle et Aurélie**, pour toute l'aide que vous nous apportez au quotidien. Aussi, merci **Michèle** pour tes cours sur l'Histoire de France et **Aurélie** pour les moments partagés.

Je vous remercie **Fatima, Edwige et Pierre** pour vos sourires et votre bonne humeur quotidienne.

Je remercie naturellement **l'équipe de la plateforme d'imagerie** de l'Institut Curie, particulièrement **Lucie et Vincent**, sans qui mes images seraient toujours inexploitables. Je n'oublie pas **l'équipe de la plateforme protéomique** de l'Institut Jacques Monod.

Merci **les collègues de l'UMR144**, en particulier l**es collègues du premier étage** et de **l'équipe Raposo** pour les discussions, les anticorps, les équipements, les bons moments partagés dans la salle de culture.

Mes remerciements s'adressent aussi à **ma famille** qui m'a toujours soutenue et encouragée, et tout particulièrement à **ma mère** qui a parcouru 10 000 km pour m'apporter son aide au quotidien et sans laquelle je n'aurai pas pu achever cette thèse.

Merci **ma puce**, qui, bien que tu sois toute petite, es et seras toujours ma source d'énergie. Enfin, un merci tout particulier à **Long**, pour ton soutien affectif et pour m'avoir toujours encouragé et épaulé depuis que ce projet de thèse était encore en germe. Merci pour tout, chéri !

Je remercie par avance ceux dont le nom n'apparaît pas dans cette page et qui m'ont aidé d'une manière ou d'une autre. Ils se reconnaîtront.

Summary

Activation of Fibroblast Growth Factor Receptor 3 (FGFR3) by point mutation, translocation is one of the most frequent events in bladder cancer, in particular in non-invasive muscle tumors. Growing evidence shows the dysfunction of RAB25 in many cancers. RAB25, RAB11A and RAB11B belong to the RAB subfamily involved in the endocytic recycling process of many transmembrane receptors. During this thesis, gene expression analysis in bladder cancer indicates that *RAB25* expression is significant higher in tumors carrying altered FGFR3 (translocation and mutation) compared to non-altered tumors. Then the thesis project aimed to unveil the potential role of RAB25, RAB11A and RAB11B and their effectors RAB11FIP2 and MYO5B in 1) the tumorigenesis of tumors carrying altered FGFR3 and 2) the trafficking and the signaling of FGFR3. Our results demonstrate that depletion of RAB25, RAB11, RAB11FIP2 or MYO5B by siRNA significantly reduces cell viability in cells expressing constitutively activated forms of FGFR3. FGFR3 accumulates in TFRC-positive compartments in RAB25 and RAB11-depleted cells, indicating that RAB25 and RAB11 are important for the endocytic recycling of FGFR3. This RAB11- and RAB25-mediated recycling can sustain the signaling by protecting altered FGFR3 from the degradation pathway. The effects of RAB25 and RAB11 silencing on FGFR3 signaling and the expression of FGFR3 target genes suggest that the endocytic recycling compartment can provide a platform for FGFR3 signaling. We also compared the subcellular distribution of wild type and mutant (S249C) forms of FGFR3. These two forms localize to different compartments including early endosomes, late endosomes and recycling compartments. The S249C FGFR3 mutant preferentially localizes to the endocytic recycling compartment. The depletion of RAB11/RAB25 induces an accumulation of the two forms of FGFR3 in the TFRC-positive endocytic recycling compartments. Our findings shed light to the molecular mechanisms underlying the relationships between the trafficking and signaling of FGFR3 in the context of bladder cancer. It could pave the way for the identification of new targets and new therapeutic strategies for tumors associated with an abnormal FGFR3 pathway.

This page intentionally left blank.

Contents

This page intentionally left blank.

List of Figures

This page intentionally left blank.

List of Tables

This page intentionally left blank.

Abbreviations

ACH achondroplasia. 25

CCV Clathrin-coated vesicle. 37
CDE Clathrin-dependent endocytosis. 37
CIE Clathrin-independent endocytosis. 37
CIS Carcinoma *in situ*. 9

EE Early endosomes. 39
EEA1 Early endosome antigen 1. 21
EGFR Epidermal growth factor receptor. 11
ER endoplasmic reticulum. 27
ERC endocytic recycling compartment. 41
ESCRT Endosomal sorting complex required for transport. 40

FGF Fibroblast growth factor. 13
FGFR3 Fibroblast growth factor receptor 3. 9

GAP GTPases activating protein. 51
GDI Guanine exchange dissociation inhibitor. 51
GEF guanine nucleotide exchange factor. 51

HCH hypochondroplasia. 25

LAMP1 Lysosomal-Associated Membrane Protein 1. 21
LE Late endosomes. 40

M6PRs mannose-6-phosphate receptors. 51
MIBC muscle invasive bladder cancer. 8

NMIBC non-muscle invasive bladder cancer. 8

PI3K Phosphatidylinositol 3-kinase. 9
PI3P Phosphatidylinositol-3-phosphate. 39
PIP2 Phosphatidylinositol 4,5-bisphosphate. 19
PLC Phospholipase C. 18

RAS/MAPK Rat Sarcoma/Mitogen-Activated Protein Kinase. 18
REP RAB escort protein. 51
RTK Receptor tyrosine kinase. 13

SADDAN severe ACH with developmental delay and acanthosis nigricans. 25
STAT Signal transducer and activator of transcription. 18

TD thanatophoric dysplasia. 25
TUR Transurethral resection. 7

I.

Introduction

1 Bladder cancer

Bladder cancer is a major health issue worldwide that causes a considerable morbidity, mortality and overall health care costs due to frequent recurrences and ineffective therapeutics. It is, therefore, essential to better understand the molecular mechanisms underlying bladder tumor progression to develop targeted therapies. In this chapter, I first introduce general facts and features about bladder cancer and then report current understanding of genetic alterations in bladder cancer.

1.1 The urinary bladder

First, I will begin by presenting some key features of the normal structure and functions of the normal bladder to more understand bladder cancer. The urinary bladder is a muscular balloon-shaped organ in the pelvic area. Its main function is to store urine from kidneys by stretching itself and to evacuates urine via ureters by contracting.

Though the bladder seems like a simple flexible sack of flesh, its structure is actually complex. The bladder wall consists of several distinct layers: the urothelium, the lamina propria, the muscularis propria and the adventitia layer. The urothelium, so-called transitional epithelium, is composed by 3 different cell types: basal cells, intermediate cells and surface umbrella cells (Figure 1.1). Basal cells are composed of cylindrical cells which are in contact with the basement membrane. Intermediate urothelial cells are cuboidal cells with well-defined borders. Large "umbrella" cells with an asymmetric apical membrane helps bladder relax or contract. The urothelium layer usually contacts toxic substances in urine that may explain why urothelial carcinoma is the most common type of bladder cancer, 90% [49]. Lamina propria is a thin layer of connective tissue, blood vessels and nervous tissue. Muscularis propria, the thickest layer of the bladder wall, consists of spindle-shape muscle cells which provides the bladder's ability to relax and contract. Finally, the adventitia layer containing fatty connective tissue separating the bladder from adjacent organs.

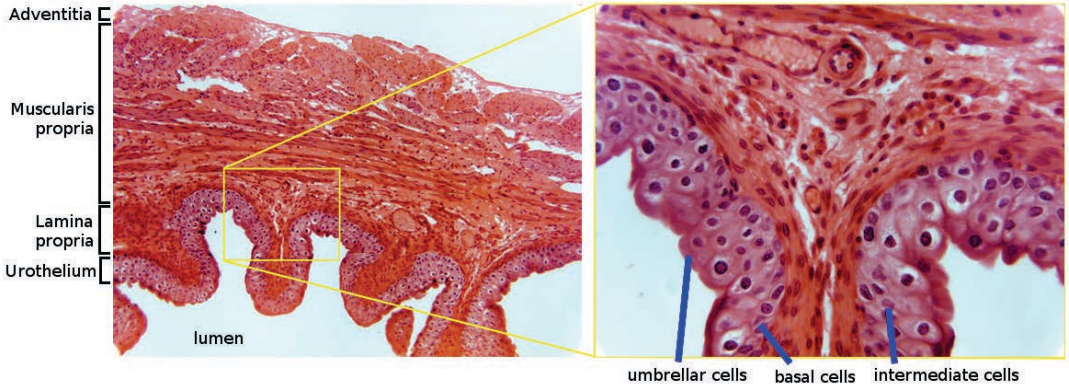

Figure 1.1 Layers of the bladder wall. Left. Cross-section of the bladder wall stained with hematoxylin/eosin (objective of 10X). The bladder wall showing a number of folds is composed of several distinct layers: adventitia, muscularis propria, lamina propria, urothelium (in contact with lumen). Right. Higher magnification (objective of 40X) of yellow frame on the left. Urothelium consist of different cell types, outside to inside: umbrella, intermediate and basal cells [2].

1.2

Key statistics about bladder cancer

Bladder cancer has always been on the top-10 list of cancers in term of morbidity and mortality. A recent study estimated, worldwide, 429 800 new cases of bladder cancer and 165 100 deaths occurring in 2012. Europe, Northern American, Western Asia and Northern Africa have higher incidence rates than other geographic area [209]. In Europe, an estimated 151 200 patient were newly diagnosed and 52 400 patients died from bladder cancer in 2012. In France, an estimated 11 170 new cases diagnosed and 17 150 deaths occurred in 2012 [57]. The American Cancer Society estimated for bladder cancer in the United States in 2015: 74 000 new cases and 16 000 deaths [187]. Compare to other cancers, bladder cancer incidence and mortality rates have been declining or stable in developed countries over the past decades.

Bladder cancer occurs mainly in elderly people. The average age at diagnosis is seventy [209].

The majority of bladder cancer is diagnosed in men with about a 3.8 to 1-fold difference to women in worldwide incidence rates. In men, bladder cancer is the fourth most common cancer in term of incidence and is ranked ninth leading cause of death from cancer [209].

Tobacco smoking is the well-established risk factor of bladder cancer. It is estimated that the risk of bladder cancer in smokers is approximately 2- to 6-fold higher than in non-smokers. Exposure to toxic chemicals such as arsenic, phenols, aromatic amines increases the risk of getting bladder cancer [209]. Growing evidences have indicated that air pollution including occupational and residential exposure to traffic or traffic emissions was associated with an increased risk of unitary bladder cancer [53]. Chronic infections caused by *Schistosoma haematobium* is mostly responsible for bladder cancer in the developing countries, particularly Africa and Western Asia [209, 49].

1.3 Clinical features

Signs and symptoms. Painless gross hematuria is the most common symptom of bladder cancer (in 85% of patients) [94]. Sometimes the bleeding in the urine may be associated with pain due to the blood clotting. Tumors located at the bladder neck or having large size may cause irritative symptoms, i.e. dysuria, urgency and frequency.

Diagnosis. Here, I present some examinations and methods proposed in the guideline for bladder cancer established by "Haute Autorité de Santé" and "Institut National du Cancer" [80].

An ultrasound examination is the first method in case of clinical suspicion. This test allows exploring the bladder and the upper urinary systems to detect bladder cancer. Urine cytology is a systematic test which is to detect presence of abnormal cancerous cells. The test is quite specific for cancer though it has a poor sensitivity for low grade bladder cancers. Therefore, in case of negative result, a cystoscopy will be performed. This method indicates the number of tumors, their size and their topography. The suspected lesion will be prepared for histological sections, which are examined under a microscope by a pathologist to characterize the histopathology of the tumors. When bladder cancer is detected, it is recommended to find the localization of tumor and to evaluate the tumor by different imaging techniques, such as intravenous urography, magnetic resonance imaging, computational tomography.

1.4 Classification of bladder cancer

From the diagnosis tests, the pathologists evaluate the bladder tumors according to the clinical and pathological features of tumors. First, the bladder cancers are staged using the TNM which is based on the invasive characteristic of tumor (Figure 1.2) [213]. Second, the tumors are graded according to their differentiated characteristic by using the WHO 1973 or WHO/ISUP classification 2004 [225, 49]. The figure 1.3 summarizes the key features between these classification systems.

At initial diagnosis, approximately 70-80% of patients with bladder cancer present non-muscle invasive papillary tumors (pTa, pT1) of low grade (G1, G2) [9, 90]. These tumors frequently recur (50-70%) and less frequently progress to muscle-invasive disease (10-30%). 5-year survival is $\sim 80\%$ [187]. On the other hand, at initial diagnostic, 20-30% patients have muscle-invasive bladder cancer which are generally pT≥ 2 and often associated with carcinoma *in situ*. These tumors have poor prognosis with 5-year survival less than 40% and frequent progression to metastasis [187].

1.5 Treatment

The actual therapeutic protocol is mainly established according to the stage and grade of the tumor described in the diagnostic assessment [80, 9, 228]. Other parameters

TNM classification [1,2]

T – Primary tumour

TX	Primary tumour cannot be assessed
T0	No evidence of primary tumour
Ta	Non-invasive papillary carcinoma
Tis	Carcinoma in situ: "flat tumour"
T1	Tumour invades subepithelial connective tissue
T2	Tumour invades muscle
T2a	Tumour invades superficial muscle (inner half)
T2b	Tumour invades deep muscle (outer half)
T3	Tumour invades perivesical tissue:
T3a	Microscopically
T3b	Macroscopically (extravesical mass)
T4	Tumour invades any of the following: prostate, uterus, vagina, pelvic wall, abdominal wall
T4a	Tumour invades prostate, uterus or vagina
T4b	Tumour invades pelvic wall or abdominal wall

N – Regional lymph nodes

NX	Regional lymph nodes cannot be assessed
N0	No regional lymph node metastasis
N1	Metastasis in a single lymph node 2 cm or less in greatest dimension
N2	Metastasis in a single lymph node more than 2 cm but not more than 5 cm in greatest dimension, or multiple lymph nodes, none more than 5 cm in greatest dimension
N3	Metastasis in a lymph node more than 5 cm in greatest dimension

M – Distant metastasis

MX	Distant metastasis cannot be assessed
M0	No distant metastasis
M1	Distant metastasis

Stage Grouping

Stage 0a	Ta	N0	M0
Stage 0is	Tis	N0	M0
Stage I	T1	N0	M0
Stage II	T2a, b	N0	M0
Stage III	T3a, b	N0	M0
	T4a	N0	M0
Stage IV	T4b	N0	M0
	Any T	N1, N2, N3	M0
	Any T	Any N	M1

[1] {944,2662}.
[2] A help desk for specific questions about the TNM classification is available at http://www.uicc.org/tnm/

Figure 1.2 TNM classification of carcinomas of the urinary bladder [49].

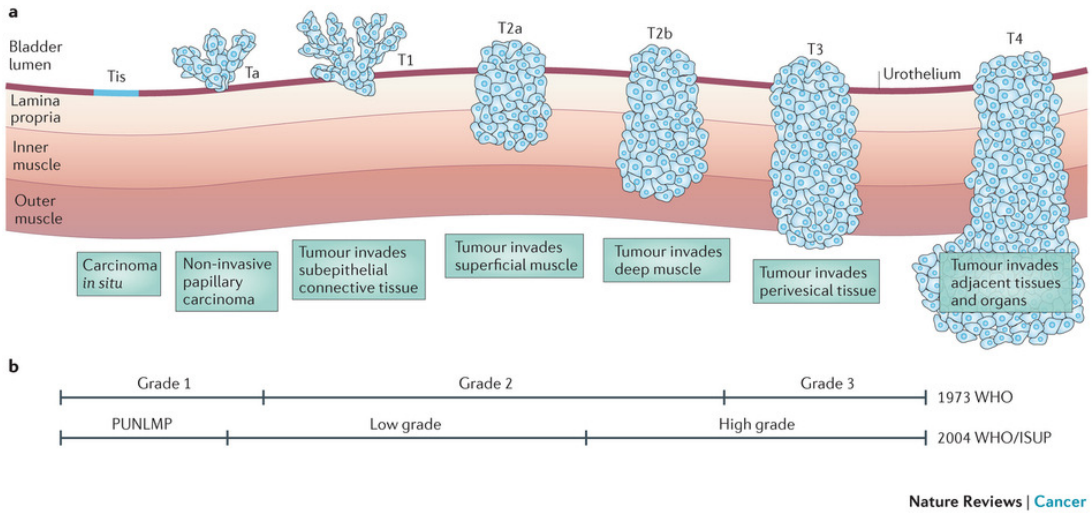

Figure 1.3 Bladder cancer grading and staging. a. Staging of bladder cancer according to TNM system is shown. b. Grading according to 1973 WHO and 2004 WHO/ISUP criteria is shown. The major difference is in the classification of papillary tumors, which are classified as grades 1, 2 and 3 in the older system and as papillary urothelial malignancy of low malignant potential (PUNLMP; equivalent to grade 1), low-grade or high-grade papillary urothelial carcinoma in the WHO/ISUP 2004 classification [104].

such as tumor multiplicity as well as frequence of recurrences are also take into account.

Non-muscle invasive tumor. Transurethral resection (TUR) of the bladder is the first-line treatment for non-muscle invasive tumor. Immediately after TUR, the patient can get one post-operative intravesical instillation of Mytomycin C which is an antineoplastic antibiotic inhibiting DNA synthesis. In a meta-analysis of 1476 patients, one immediate post-operative instillation had significant reduction of recurrence rate by 11.7% compared to TUR alone [201]. Additional intravesical chemotherapy instillation may be necessary depending on the risk of recurrence and of progression. Bacillus Calmette-Guerin (BCG) immunotherapy can be prescribed for the patients in case of tumors with high risk of progression. Non-muscle invasive tumors tend to recur frequently, 50-70%, and also can progress, therefore high surveillance of the urinary tract after treatment is essential.

Muscle-invasive non metastatic tumor. Radical cystectomy is the standard treatment of choice for muscle-invasive non metastatic tumors, pT2-T4a and N0M0. Radical cystectomy should be performed within 3 months after diagnosis, otherwise the risk of progression increases. Neoadjuvant and/or adjuvant chemotherapy can be used to reduce the risk of metastasis. Cisplatin-based chemotherapy will be discussed for localized bladder cancer and response to chemotherapy should be interpreted with caution. In case the patients get radiotherapy, this treatment is frequently associated with chemotherapy. It is indicated that a 10-year disease-specific survival by 35% was better after radiotherapy and concurrent chemotherapy than after radiotherapy alone [228].

Metastatic disease. Cisplatin-containing combination chemotherapy has been the standard first-line systematic chemotherapy for eligible patients. Cisplatin, Methotrexate, Vinblastin, Doxorubicin regimen or Gemcitabin, Cisplatin regimen are generally used. For Cisplatin-ineligible patients, treatment with Carboplatin-containing combination chemotherapy, i.e. Gemcitabin/Carboplatin is indicated. In case tumors progress $\geq$6-12 months after first-line treatment, a challenge with regimen with molecules having different mode of action is recommended. Bone metastases occur in 30-40% of patients with muscle-invasive and metastatic bladder cancer. Thus, Denosumad and Zoledronic acid are recommended to use [228].

Over the two past decades, treatment has remained unchanged and the survival of bladder cancer has not been significantly improved with 5-year relative survival rates for regionally advanced and metastatic disease of 34% and 5%, respectively [187]. Recently, a promising direction in bladder cancer treatment is targeted therapy by using immune checkpoint inhibitors, such as a PD-L1 antibody (in phase III trial for patients with high-risk muscle invasive bladder cancer) or PD-1 antibody (in phase II trial for patients with high-risk non-muscle invasive bladder) [163, 6]. Using monoclonal antibodies against FGFR3 is another promising avenue (in phase II trial for patients with locally advanced or metastatic bladder cancer, NCT02401542). A better understanding the molecular mechanisms underlying bladder tumorigenesis to help develop treatment strategies and new therapeutic targets for systematic therapy is essential.

1.6
Genetics behind bladder cancer

According to clinico-pathological features, there are two distinct groups of lesions, non-muscle invasive bladder cancer (NMIBC) and muscle invasive bladder cancer (MIBC). Along with molecular profiles observed in bladder cancer, several models of two-pathway progression in bladder cancer have been proposed, Figure 1.4 represents one of them. Here, I review several alterations which are frequent events in bladder cancer.

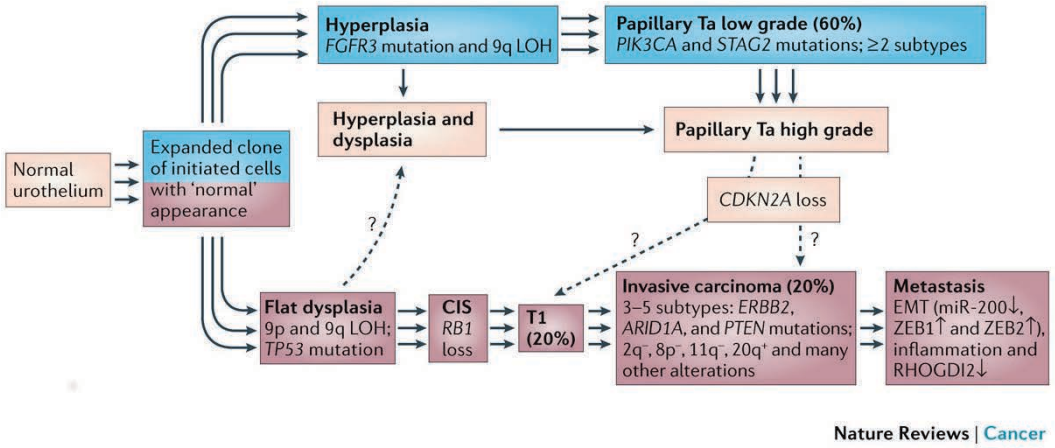

Figure 1.4 Potential pathogenesis pathways are shown based on histopathological and molecular observations. The blue and purple pathways indicate the two major pathways with distinct histopathological and molecular features that have been recognized for the past two decades. Percentages at diagnosis and key molecular features are indicated. The recent identification of multiple distinct molecular subtypes of NMIBC and MIBC suggests multiple subpathways within each of the major pathways. It should be noted that the existence of multiple subtypes within all of the histologically recognizable intermediates remains hypothetical. Development of histopathologically recognizable urothelial alterations is preceded by clonal expansion of altered cells within the urothelium. Low-grade papillary tumours may arise via simple hyperplasia and minimal dysplasia, and these are characterized at the molecular level by loss of heterozygosity (LOH) of chromosome 9 and activating mutations of fibroblast growth factor receptor 3 (*FGFR3*), *PIK3CA* (which encodes p110α of PI3K) and stromal antigen 2 (*STAG2*). These non-invasive tumours recur frequently but are genetically relatively stable. Muscle -invasive carcinoma is thought to arise mainly via flat dysplasia and carcinoma in situ (CIS), which commonly show TP53 mutation in addition to chromosome 9 deletions but no FGFR3 mutations. Muscle-invasive tumours are genetically unstable and accumulate many genomic alterations. Uncertainty about the possible development of high-grade non-invasive papillary tumours from flat dysplasia is indicated by a dashed arrow. The finding of a subtype of invasive carcinomas with FGFR3 mutation and loss of cyclin-dependent kinase inhibitor 2A (*CDKN2A*) may suggest a route by which low-grade non-invasive papillary tumours can progress to muscle invasion (dashed arrow). ARID1A, AT-rich interactive domain 1A; EMT, epithelial–mesenchymal transition; RHOGDI1, RHO-GDP dissociation inhibitor 2; ZEB1, zinc-finger E-box binding homeobox 1 [104].

Deletion of chromosome 9 or parts of chromosome 9 is the most frequently observed alteration in bladder cancer, in 50% of all stages and grades [140]. It is likely that deletions of chromosome 9 are present during the early stage of tumor progression [216]. Several works reported that there is no difference in prevalence of chromosome 9 deletions between the 2 tumorigenesis pathways [79, 161]. One of critical regions of deletion is 9p21 containing *CDKN2A* and *CDKN2B*, which encode for

the p16/p14 and p15, respectively. These genes are well known as tumor suppressor genes. Our group demonstrated that *CDKN2A* homozygous deletion was associated with high risk progression in non muscle-invasive tumors presenting *Fibroblast growth factor receptor 3 (FGFR3)* mutations [170].

Ta pathway. Tumors of the Ta pathway are non-invasive muscle tumors (stage pTa) which are thought to be developed via flat urothelial hyperplasia. These tumors recur frequently (50-70%) but rarely progress to stage ≥pT2 [90]. Several well-established genetic alterations in this pathway contain *FGFR3* alterations, activating alterations in Phosphatidylinositol 3-kinase (PI3K) pathway.

FGFR3 alteration is the most common event in the Ta pathway, >60%. These alterations will be discussed in more detail in section 2.5.

PI3K/AKT/mTOR pathway plays an important role in cancer cell survival, proliferation [113, 84]. Figure 1.5 summarizes major actors and functions of this pathway. In tumors of the Ta pathway, PI3K pathway is frequently activated by activating mutation of the p110-α-catalytic subunit of PI3K (encoded by *PIK3CA* gene). In a recent study, 17% patients presented mutated *PIK3CA* in a set of 218 patients [191]. A significant association between *FGFR3* and *PIK3CA* mutations was also reported. Another component of this pathway, *TSC1*, presents loss of functions due to mutations in 17% in bladder cancer [191]. These mutations were found to be associated with the deletion of the region 9q34 [104].

Carcinoma *in situ* (CIS) pathway. Tumors of the CIS pathway are muscle-invasive high grade tumors which are thought to arise from flat urothelial dysplasia and CIS lesions. These tumors recur frequently but also progress with high probability to stage pT≥2 or metastasis. Although carcinma *in situ* is rare, most of the muscle-invasive tumors are thought to arise from these lesions. The major characteristic in this progression pathway is alterations in *TP53*, *RB1* genes.

TP53 encodes for a tumor suppressor protein which is implicated in cell-cycle arrest and apoptosis. Somatic *TP53* gene mutations occurring in many codons in bladder cancers have been reported in many studies [65]. A recent meta-analysis of 827 tumors indicated that *TP53* mutations are more frequent in high stage: pT1 (40.6%) and pT2-4 (50.7%) and also in high grade G3 (46.3%) [147]. In low grade, low stage tumors, *FGFR3* mutations but not *TP53* mutations are observed but mutations of both genes can occur in high stage- and grade-tumors of Ta pathway. Thus the authors proposed that *TP53* mutations occur in the earliest stage of the CIS pathway , whereas they would occur much later in the Ta pathway, at the T1G3 or muscle-invasive stage.

RB1 encodes for a tumor suppressor protein which was identified in retinoblastoma for the first time. RB1 is a negative regulator of the cell cycle. Loss of heterozygosity of the *RB1* locus was found in more than 50% of muscle invasive tumors at cystectomy.

The 2-pathway progression model gathered the molecular and clinicopathological features of bladder cancers that could help pathological evaluation, nonetheless, this model still does not represent the ful heterogeneity of bladder cancers. In recent years, many studies have made effort to better characterize the sub-groups of bladder cancers, especially in muscle-invasive tumors [192, 35, 41, 205, 13].

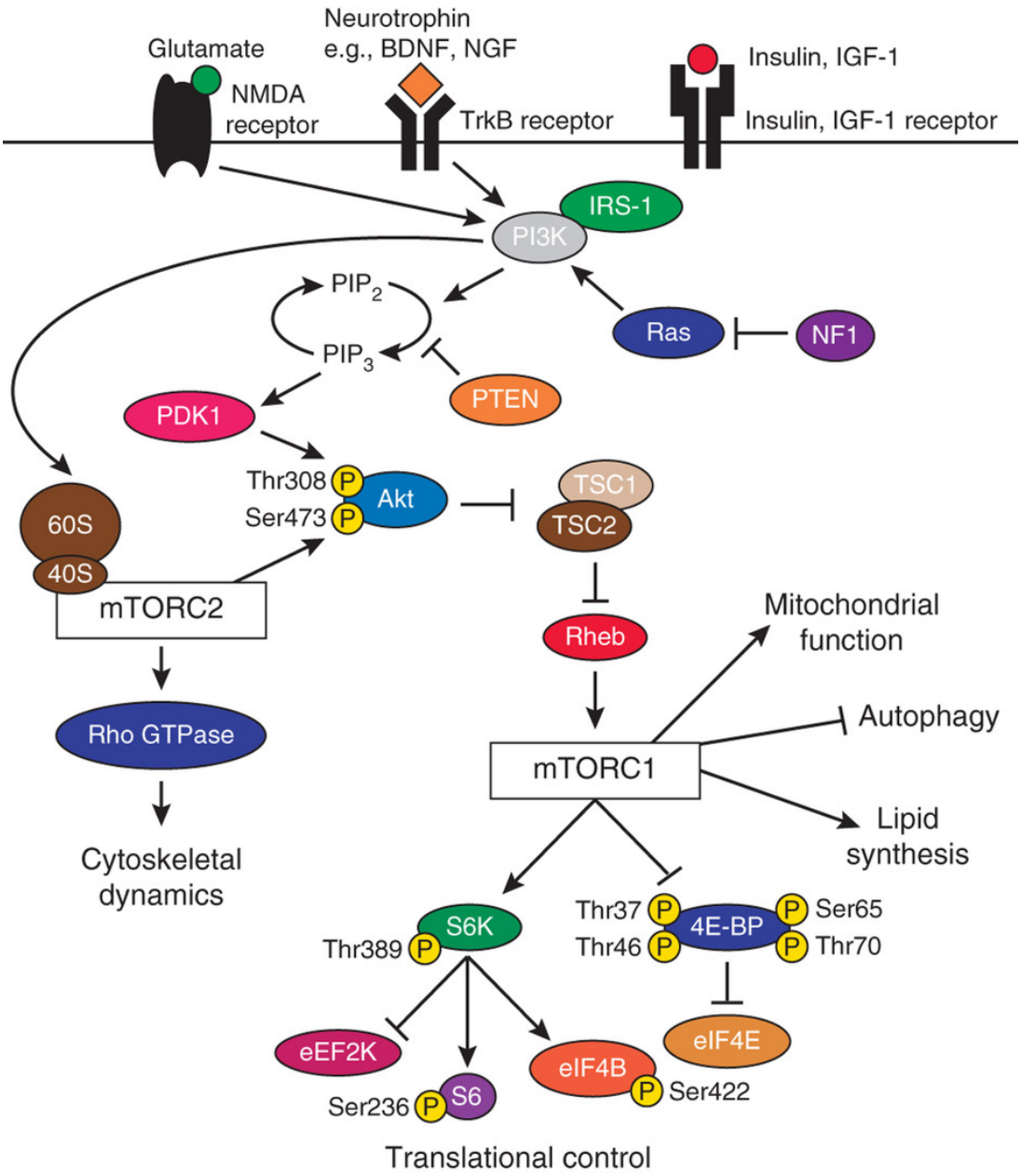

Figure 1.5 PI3K/AKT/mTOR pathway. mTORC1 is activated by growth factors through the PI3K/AKT signaling pathway which phosphorylates and inhibits TSC1/TSC2 complex. This complex is an upstream negative regulator and acts as a GTPase-activating protein for Rheb GTPase. The activation of Rheb consequently promotes the mTOR activity which targets several downstream proteins such as 4E-BP and S6K. 4E-BP is a family of translational repressor proteins which interacts with eukaryotic translation initiation factor (eIF4E) depending their phosphorylation level. When hyperphosphorylated, 4e-BP can not bind to eIF4E which results in the recruitment of the translation initiation factor. S6K, for Ribosomal Protein S6 Kinase, regulates mRNA translation by activating or inhibiting some substrates, e.g. Ribosomal protein S6, eIF4B, eEF2K. These activities of mTOR on translational control result in the positive regulate cell growth and proliferation [39].

A recent study from our group has allowed to define a sub-group, named ”basal-like”, which is characterized by an upregulation of epithelial basal cell markers including *keratins (KRT5, KRT6A, KRT14)* and *Epidermal growth factor receptor (EGFR)* and which shared a gene signature with the well-known basal subgroup in breast cancer [169]. Tumors of this sub-group are muscle-invasive and are associated with a short overall survival. EGFR pathway is activated in these tumors. Additionally, EGFR inhibitors reduce the cell proliferation and tumor appearance of cancer cells of this subgroup *in vitro* and *in vivo*. These results support therefore the advantage of classification of sub-groups of bladder cancer according to gene expression profile for diagnostic tools and anti-cancer therapy [169].

This page intentionally left blank.

Fibroblast growth factor receptor signaling

2

In the previous chapter, I mentioned that genetic alteration in *Fibroblast Growth Factor Receptor 3 (FGFR3)* is one of the most frequent events in non-muscle invasive bladder cancer. The aim of this chapter is to introduce several aspects of the Fibroblast Growth Factor receptor (FGFR) pathway, including the components, intracellular signaling cascades, physiological and pathological functions in bone development. Finally, I will discuss about *FGFR3* alterations in bladder cancer.

2.1 Pathway components

2.1.1 Fibroblast Growth Factors

Fibroblast growth factor (FGF) was first found in an extract from bovine pituitary and brain [72]. FGF purified from these extracts had a mitogenic activity which stimulated the DNA synthesis of NIH-3T3 mouse embryo fibroblasts. Since this discovery, 22 members of the FGF family have been identified and can be grouped into 7 subfamilies (Figure 2.1). 5 subfamilies of paracrine FGFs and one subfamily of endocrine FGFs mediate their cellular responses through interaction with FGF receptors. The last subfamily encodes intracellular FGFs which are not secreted and have no interaction with FGF receptors.

2.1.2 Fibroblast Growth Factor Receptors

18 secreted FGF ligands trigger their signaling by binding to different cell surface FGF receptors (FGFR), which are encoded by four distinct genes in mammals, *FGFR1, FGFR2, FGFR3,* and *FGFR4* [151]. FGFRs constitute a subfamily of Receptor tyrosine kinase (RTK) family. They share a common core with other RTKs with ligand-binding domains in the extracellular region, a single transmembrane helix and in a cytoplasmic region containing the protein tyrosine kinase domain and juxtamembrane regulatory region (Figure 2.2) [117]. This receptor is composed of $\sim$ 800 amino acids

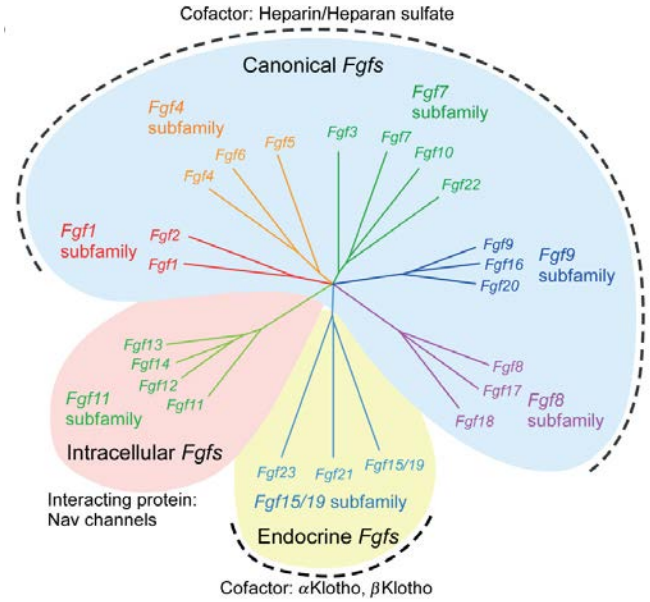

Figure 2.1 Fibroblast Growth Factor families. Phylogenetic analysis suggests that 22 *FGF* genes can be classed into seven subfamilies. Branch lengths are proportional to the evolutionary distance between each gene. The *FGF1*, *FGF4*, *FGF7*, *FGF8*, and *FGF9* subfamily genes encode secreted canonical FGFs, which bind to and activate FGFRs with Heparin/Heparin sulfate as a cofactor. The *FGF15/19* subfamily members encode endocrine FGFs, which bind to and activate FGFRs with the Klotho family proteins (α and β Klotho) as a cofactor. The *FGF11* subfamily genes encode intracellular FGFs, which are non-signaling proteins serving as cofactors for voltage gated sodium channels (Nav channels) and other molecules [151].

with a conserved structure comprising three extracellular Immunoglobulin (Ig)-like domains, an acidic box, a single transmembrane (TM) domain and a cytoplasmic domain containing the catalytic tyrosine kinase (TK) core (Figure 2.3.a) [151]. The acidic box appears to play an important role in glycosaminoglycan modification, and is required for modification by heparan sulfate glycosaminoglycan. Of note, in *FGFR1, 2* and *3* but not in *FGFR4*, *FGFR* isoforms are generated by alternative splicing of exons encoding their third Ig-like domain. Ig III domain is generated by splicing an invariant exon (IIIa) to either exon IIIb or IIIc, both of which splice to the exon that encodes the transmembrane region (Figure 2.3.b). In general, the IIIb of FGFR receptors are found in epithelial cells while the IIIc variants are preferentially expressed in mesenchymal cells [151].

The affinity of ligand binding to the four distinct receptors is generally determined by the Ig-like domain II and III and the linker region between these 2 domains. Furthermore, in FGFR1, FGFR2 and FGFR3, the specificity of ligand interaction is profoundly determined by alternative splicing of the FGFRb and FGFRc isoforms. The specificity of the interaction of the 18 secreted FGFs to the different isoforms of FGFR has been studied by various mitogenic assay and/or by directly measuring affinity for FGFRs in BaF3 cells or L6 myoblasts that have no or little endogenous FGFR [153, 235]. Results from these studies are summarized in Figure 2.3.c. Of note, there is no ligand with high specificity for FGFR3b apart from FGF1.

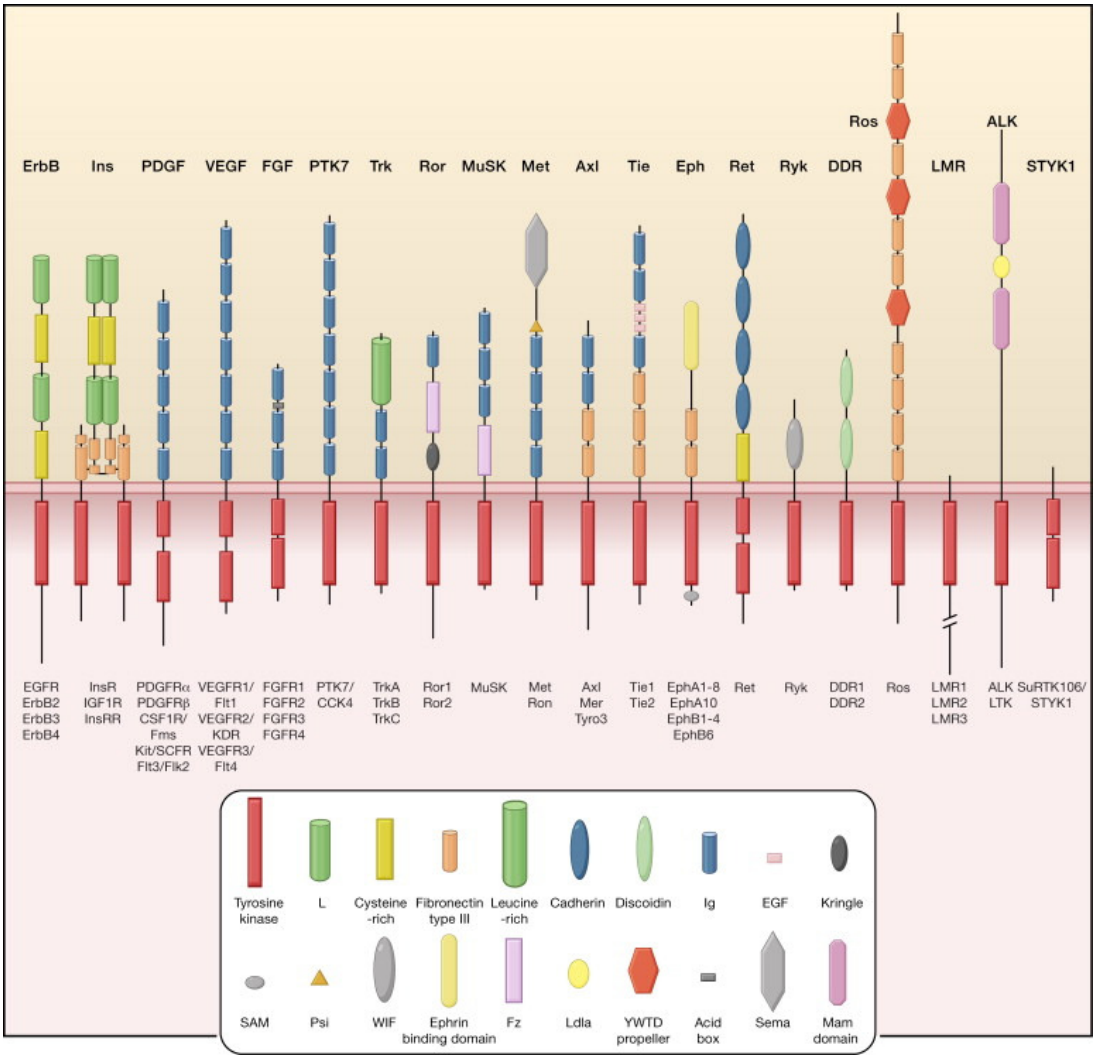

Figure 2.2 Receptor Tyrosine Kinase families. Human RTKs contain 20 subfamilies, shown here schematically with the family members listed beneath each receptor. Structural domains in the extracellular regions, identified by structure determination or sequence analysis, are marked according to the key. The intracellular domains are shown as red rectangles [117].

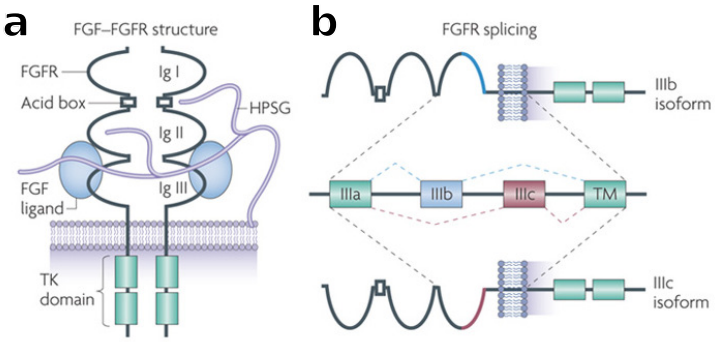

c

FGF subfamily	FGF	Cofactor	Receptor specificity
FGF1 subfamily	FGF1 FGF2		All FGFRs FGFR 1c, 3c > 2c, 1b, 4Δ
FGF4 subfamily	FGF4 FGF5 FGF6		FGFR 1c, 2c > 3c, 4Δ
FGF7 subfamily	FGF3 FGF7 FGF10 FGF22	+ Heparin or Heparan sulfate	FGFR 2b > 1b
FGF8 subfamily	FGF8 FGF17 FGF18		FGFR 3c > 4Δ > 2c > 1c >> 3b
FGF9 subfamily	FGF9 FGF16 FGF20		FGFR 3c > 2c > 1c, 3b >> 4Δ
FGF15/19 subfamily	FGF15/19	+βKlotho	FGFR 1c, 2c, 3c, 4Δ
	FGF21		FGFR 1c, 3c
	FGF23	+αKlotho	FGFR 1c, 3c, 4

Figure 2.3 FGFR structure and control of ligand specificity. a. The basic structure of the FGFR consists of three extracellular immunoglobulin (Ig)-like domains, an acid box, a single transmembrane helix and an intracellular split tyrosine kinase (TK) domain. HSPG: Heparan Sulfate proteoglycans. **b.** The alternative splicing of the Ig III domain. The first half of Ig III is encoded by an invariant exon (IIIa), which is spliced to either exon IIIb or IIIc, both of which splice to the exon that encodes the transmembrane (TM) region [212]. **c.** Receptor specificity of paracrine and endocrine FGFs. FGFR4Δ is a two Ig-like domain form of FGFR4 [151].

2.2

Mode of activation

A reservoir of paracrine FGF ligands near the site of action is maintained by the interaction between FGF ligands and heparan sulfate and a specific core proteins heparan sulfate proteoglycans which are components of extracellular matrix. To trigger the signaling, FGF is released from the extracellular matrix by heparinases, proteases or specific FGF-binding protein. Liberated FGF subsequently binds to FGFR that leads to conformational changes and a symmetric FGF-FGFR dimer. Paracrine FGFs require heparan sulfate as co-factor to establish a stable ternary FGF-heparin-FGFR complex at a ratio 2:2:2 (Figure 2.4). In contrast, endocrine FGFs (FGF15/19 subfamily) depend on the Klotho family proteins for signaling [66]. Finally, FGFR dimerization leads to transphosphorylation of the intracellular TK domain and intracellular tail that results in the activation of intracellular signaling pathways.

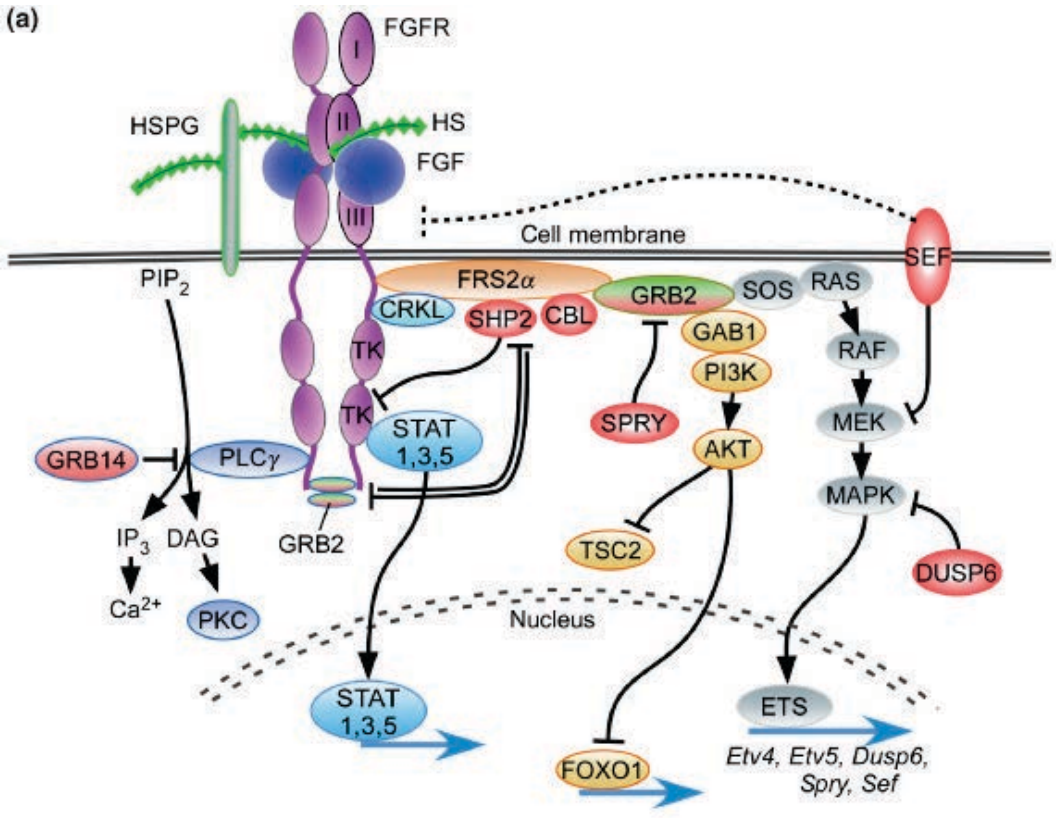

Figure 2.4 FGF signaling pathways. Binding of paracrine FGFs to FGFR with heparan sulfate (HS) and/or Heparan Sulfate proteoglycans (HSPG) as cofactor induces the formation of ternary FGF-heparin-FGFR complex, which activated the FGFR intracellular TK domain by phosphorylation of specific tyrosine residues. The activated receptor is coupled to intracellular signaling pathways including the RAS-MAPK, PI3K-AKT, PLCγ, and STAT pathways [151].

2.3
Intracellular signaling pathways

Following ligand activation, FGFRs recruit different substrates to trigger signal transduction cascades or inhibitory regulators. Also, activated receptors undergo endocytosis into the cytoplasm to continue signaling or to be degraded. In this section, I will discuss about these different fates of activated FGFR.

2.3.1
Downstream signaling

In response to FGF-stimulation, the protein tyrosine kinase core of FGF receptors is autophosphorylated and serves as a docking site for adaptor proteins. These adaptors may be phosphorylated and then recruit other proteins to activate four major signal transductions pathways including Rat Sarcoma/Mitogen-Activated Protein Kinase (RAS/MAPK), PI3K/AKT, Phospholipase C (PLC)γ and Signal transducer and activator of transcription (STAT) [54, 212, 151]. Figure 2.4 illustrates these four cascades of phosphorylation events.

RAS/MAPK pathway. The activation of RAS-MAPK pathway by FGF stimulation is via the recruitment of Fibroblast growth factor receptor substrate (FRS2), which specifically binds to FGFRs. The activated FGFR phosphorylates FRS2 that recruits the complex Growth Factor Receptor-Bound Protein 2 (GRB2) and son of sevenless (SOS) [105]. This complex then recruits to the membrane the inactive RAS leading to its conformational change to become active. The GTP bound active RAS subsequently recruits RAF to the plasma membrane. RAF is in turn activated and activates MEK which then phosphorylates MAPKs such as ERK1/2. Finally, the downstream targets of ERK1/2 are transcription factors including ETS, c-JUN and c-MYC [133]. Thus, FGFRs use the RAS/RAF/MEK/MAPK cascade to transduce signals from the cell surface to transcription factors which regulate the expression of many genes involved in proliferation, anti-apoptosis, differentiation and cell migration.

PI3K/AKT pathway. PI3K-AKT pathway links to FGFR via the docking site FRS2-GRB2. Unlike in RAS-MAPK pathway, GRB2-associated binding protein 1 (GAB1) is the upstream activator of PI3K-AKT pathway [110]. GAB1 activates the enzyme PI3K leading to the phosphorylation of AKT. Activated AKT then phosphorylates Forhead box O 1 (FOXO1) which consequently results in the nuclear exclusion of FOXO1. FOXO1 is a transcription factor which has a pro-apoptotic property [236].

On the other hand, phosphorylated AKT inhibits the TSC1/TSC2 complex, a modulator of mTOR pathway (Figure 1.5). In fact this complex acts as a negative regulator for Rheb GTPase. The activation of Rheb consequently promotes the mTOR activity which targets several downstream proteins such as 4E-BP and S6K. 4E-BP is a family of translational repressor proteins which interacts with eukaryotic translation initiation factor (eIF4E) depending on their phosphorylation level. When hyperphosphorylated, 4e-BP cannot bind to eIF4E, that results in the recruitment of the translation initiation factor. S6K, for Ribosomal Protein S6 Kinase, regulates mRNA translation

by activating or inhibiting some substrates, e.g. Ribosomal protein S6, eIF4B, eEF2K. These activities of mTOR on translational control result in the positive regulation of cell growth and proliferation [84].

PLCγ pathway. In addition to the FRS2 binding site, on the intracellular part of the activated FGFRs, another specific phosphotyrosine at residue 766 next to the carboxy terminal can bind to PLCγ via the Src homology 2 domain of this protein [158]. Phosphorylation of PLCγ catalyzes Phosphatidylinositol 4,5-bisphosphate (PIP2) to produce inositol 1,4,5-triphosphate (IP3) and diacylglycerol (DAG). IP3 serves as a second messenger that diffuses in cytosol and binds to IP3 receptor on the membrane of the endoplasmic reticulum. This receptor is composed of a calcium channel at the C-terminus which helps to release calcium from the endoplasmic reticulum [137]. DAG is another lipid second messenger, but unlike IP3, DAG remains in the plasma membrane thanks to its hydrophobic properties. DAG activates protein kinase C (PKC) family which then phosphorylates other intracellular targets such as MAPK pathway promoting the growth of tumors [63]. Figure 2.5 illustrates the different components of this pathway.

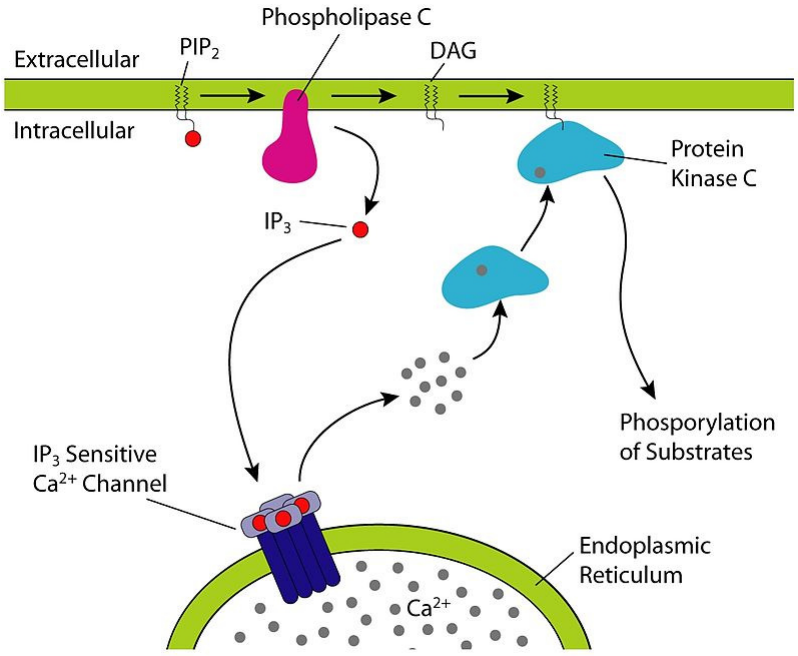

Figure 2.5 Phospholipase C γ pathway. Activated PLCγ cleaves PIP2 to produce IP3 and DAG [1].

STAT pathway. STAT pathway is another signal transduction cascade to translate an extracellular signal into a transcriptional response.

In mammals, the STAT family consists of seven closely related proteins, including STAT1, STAT2, STAT3, STAT4, STAT5A, STAT5B, and STAT6. STATs are phosphorylated by activated cytokine receptors or tyrosine kinase receptors. STAT can directly bind to TK receptor but interacts to cytokine receptor via JAK. Phosphorylation of STAT at tyrosine residue results in homo- or hetero-dimeric STATs which are rapidly translocated into the nucleus. STAT dimers bind specifically to an 8– to

10–base pair inverted repeat DNA element with a consensus sequence of 5′-TT(N4-6)AA-3′ within the gene promoter. Some target genes can be cited including cell-cycle inhibitor p21/WAF1, suppressors of cytokine signaling (SOCS) [168].

Phosphorylated FGFR3 by ligand stimulation or mutation had been shown to activated STAT1 for the first time in the work of Xin-Yuan Fu's group [200]. They showed that the overexpression of mutant K644E FGFR3 induced activation of STAT, leading to the nuclear translocation of the protein. Consequently, a high level of mRNA and protein of p21WAF1, a cell-cycle inhibitor was observed compared to control cells. This explains the growth arrest of 293T cells transiently expressing mutant FGFR3. STAT3 or STAT5 have been also reported to be activated by other FGFRs [151].

2.3.2 Negative regulators of signaling

Following ligand stimulation, inhibition activity of receptor tyrosine kinase signaling in general and FGFR signaling in particular is essential for the precise control of cellular functions. Although the mechanism is not fully understood, several mechanisms have been proposed including degradation of the receptor, regulation of receptor kinase activity, inhibitory molecules. Some of them are represented in Figure 2.4.

Following FGF fixation on the receptor, phosphorylated FRS2 can form a ternary complex with GRB2-CBL resulting in the ubiquitination and degradation of FRS2 and FGFR. In fact, SOS and CBL compete for the same binding site (Src homology 3 domain) of GRB2 to come together with FRS2 that allows a balanced FGF signal transduction [229].

After being activated by FRS2, ERK1/2 can subsequently phosphorylate FRS2 at several threonine residues which prevents the recruitment of GRB2. This ERK-mediated negative feedback mechanism is important for the control of signaling pathways via FRS2 [73].

Many inhibitory regulators (molecules shaded red in figure 2.4) of receptor kinase activity have been characterized [151, 212]. First, the Sprouty (SPRY) and Sprouty-related (SPRED) proteins were identified as an intracellular negative regulator of receptor tyrosine kinase signaling such as FGFR, EGFR, platelet-derived growth factor receptor, and nerve growth factor receptor. In FGF signaling, binding of SPRY on GRB2 prevents the recruitment of GRB2 to phosphorylated FRS2 which results in the attenuation of RAS-MAPK pathway. Of note, SPREDs are likely more potent inhibitors of MAPK activity than Sprouty [190]. Second, Similar Expression of FGF (SEF) is another antagonist of RAS-MAPK pathway which interacts with activated MEK then inhibits the dissociation of MEK-MAPK complex. The inhibition of SEF thus interrupts nuclear translocation of activated MAPK. SEF may act as a transmembrane protein to interact with FGFR for inhibiting receptor phosphorylation. Third, Mitogen-Activated Protein Kinase Phosphatase 3 (MKP3 or known as DUSP6) dephosphorylates ERK1/2 on phosphotyrosine and phosphothreonine residues to attenuate MAPK signaling [51].

2.3.3 Intracellular trafficking of receptor

There is now clear evidence that endocytic membrane trafficking promotes receptor-mediated signaling and vice versa (reviewed in [196, 135]). I first introduce the trafficking of the four FGFRs and then cite two studies investigating the link between endocytic membrane trafficking and signaling.

FGFR trafficking. The intracellular trafficking of four FGFRs was systematically studied in the work of Haugsten in 2005 for the first time [82]. The different constructions of FGFRs were introduced in HeLa cells which do not express detectable amount of any FGFR. Labeled FGF1, a ligand having a strong affinity to the four receptors, was chosen as a marker to follow the intracellular trafficking of the FGFRs. After 15 minutes incubation of labeled FGF1 at 37°C, the complexes of FGF1 and different FGFRs were localized in Early endosome antigen 1 (EEA1)-positive early/sorting endosomes. After a 2-hour chase in the presence of leuceptin, a protease inhibitor to inhibit degradation into the lysosomes, the distribution of the four FGFRs was sorted in different compartments. FGFR1-3 were mainly sorted to lysosomes where it was colocalized with Lysosomal-Associated Membrane Protein 1 (LAMP1), a marker of late endosomes/lysosomes while FGFR4 showed a remarkable overlap with transferrin, a marker of recycling compartment. The biotinylation assay and radiolabelled FGF1 allowed investigating the degradation of internalized receptors and FGF1 ligand in HeLa cells expressing transiently different FGFRs. The results indicated that endocytosed FGFR4 was degraded more slowly than the other receptors. Additionally, internalized FGF1 was degraded more slowly in cells expressing FGFR4 than in cells expressing other FGFRs. Moreover the rate of recycling for FGF1 internalized by FGFR4 was higher than those internalized by FGFR1. FGFR4 was also shown less ubiquitinated than FGFR1 which was probably the molecular mechanism for determining the different sorting of the receptors after internalization [82].

FGFR3 endocytosis. The endocytic trafficking and sorting of FGFR3 has been characterized in a few studies. The study of Haugsten and colleagues in 2011 was the first report about the molecular mechanism involved in endocytosis of wild type FGFR3 and the role of internalization in FGFR3 signaling [83]. In UO2S cells expressing FGFR1 following by depletion of clathrin, the rate of labeled FGF1 internalization was significantly reduced compared to control cells. In contrast, in cells expressing FGFR3 knockdown for clathrin, the rate of FGF1 endocytosed was only partly reduced compared to control cells. In cells expressing FGFR3 and either wild-type dynamin or dominant negative mutant of dynamin K44A, FGF1 internalized was mostly found in EEA1 positive early endosomes. However FGF1 was excluded in EEA1 positive endosomes in FGFR1 and dynamin K44A expressing cells. Together these results showed that internalization of FGF1 via FGFR3 was partly via clathrin- and dynamin-dependent endocytosis while ligand-bound FGFR1 was internalized by clathrin- and dynamin-dependent manner.

To study the latter pathway of endocytosis, the authors utilized cells stably expressing FGFR3 with siRNA or dominant negative mutant of Arf6, Cdc42, Flotillin 1

and 2 which are the proteins involved in the clathrin-dependent endocytosis. The rate of internalization of labeled FGF1 via FGFR3 was then measured. The results however indicated that none of these proteins were implicated in the clathrin- and dynamin-independent endocytic pathways of FGFR3. To further investigate the impact of the internalization of FGFR3 in its signaling, the authors studied FGFR3's protein level and signaling in FGFR3-stably expressing cells that were depleted of clathrin. FGFR3 was degraded more slowly in cells depleted of clathrin but there were no remarkable changes in different downstream signaling pathways of FGFR3 over time. Altogether, the data from this study showed that FGFR3 used both clathrin-dependent and -independent endocytic pathways for efficient signaling [83].

FGFR4 intracellular trafficking. The molecular mechanism underlying the recycling of FGFR4 has been recently revealed by the same authors [81]. By using biochemical assays including recycling of radiolabelled FGF1 (^{125}I-FGF1) assay and cell surface biotinylation recycling assay for FGFR4 recycling, the authors indicated that recycling of both ligand and receptor was reduced when RAB11A and RAB11B were depleted. They performed another approach providing more visualized quantitative data in which FGFR4 was fused with a photoactivatable green fluorescent (PA-GFP) protein. Indeed, the trafficking of photoactivated FGFR4-PA-GFP was followed at any time point of interest, for example, from endocytic recycling compartments to the plasma membrane. The results showed that this membrane transport was dependent on RAB11. To investigate more about the FGFR4-positive structure after RAB11 depletion, correlative light and electron microscopy analysis were performed. The data revealed that beyond being accumulated in tubular network, FGFR4 was localized in small vesicles budding or separating of 30-40 nm diameter. Interestingly, in RAB11-depleted cells, phosphorylated FGFR4 as well as PLCγ was maintained for a longer period than in control cells. In contrast, the phosphorylation of AKT and ERK was found to be rapidly decreased following RAB11 knockdown [81].

2.4 Context-dependent signaling

FGF-FGFR signaling plays a fundamental role in embryogenesis, tissue homeostasis, wound healing and inflammation. At the cellular level, FGFR pathways promote different processes including proliferation, differentiation, survival and migration. An important remark is that the functional outcome of FGF signaling depends on cellular context. In this section, I will first introduce the physiological role of FGFR signaling in bone development. I will then report about aberrant FGF-FGFR signaling in heritable skeletal disease mutations in FGFRs focusing on FGFR3-related skeletal dysplasias.

2.4.1 FGF signaling in endochondral and intramembranous bone development

Endochondral and intramembranous bone development are two main processes contributing to form skeletal elements that occur during fetal development until late puberty. Endochondral ossification allows the development of the skeleton, facial bones,

vertebrae and the lateral medial clavicles where cartilage is replaced by bone. Intramembranous ossification, where bone develops within sheets of connective tissue, gives rise to flat bones (e.g. the cranium and medial clavicles). Both types of ossification need an initial condensation of mesenchyme followed by formation of calcified bone [152].

FGF signaling in the developing endochondral bone

The mesenchymal condensation is the first event in the developing endochondral bone (reviewed in [150]). Figure 2.6 illustrates *FGFR* and *FGF* gene expression during endochondral and intramembranous bone development. FGF2, FGF9 are expressed in the developing condensation. FGFR1 is expressed in the surrounding loose mesenchyme and also in the periphery of the mesenchymal condensation. FGFR2 is however upregulated in condensing mesenchyme. How FGF signaling functions in condensing mesenchyme is however poorly understood. It is suggested that FGF signaling may regulate the expression of SOX9, an essential transcription factor for chondrocyte differentiation [144]. FGF2 and FGF9 can stimulate proliferation of chondrocytes.

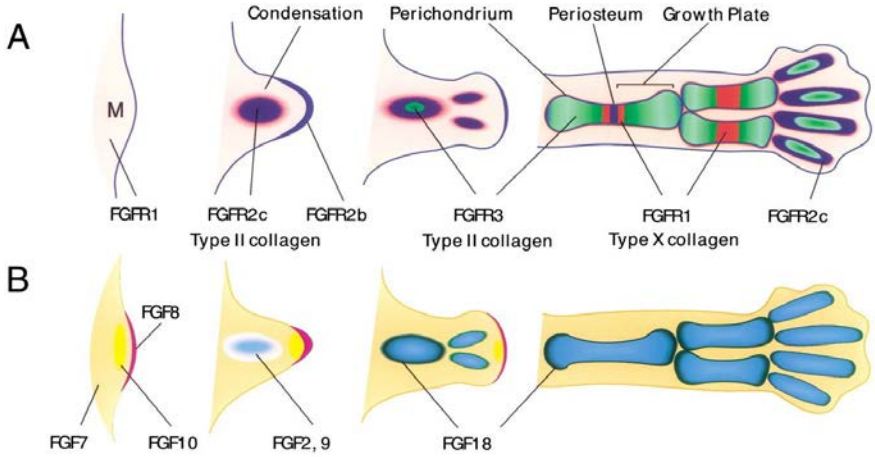

Figure 2.6 *FGF* and *FGFR* gene expression in developing endochondral bone. (A) *FGFR* gene expression. FGFR1 is expressed in limb mesenchyme (M) and in the periphery of the mesenchymal condensation (pink). *FGFR2* is first expressed in condensing mesenchyme (purple). *FGFR3* expression is initiated as chondrocytes differentiate and proliferate (green). *FGFR1* expression is present as chondrocytes hypertrophy (red), and *FGFR2* expression is prominent in osteoblasts in the ossification center (purple). Both FGFR1 and FGFR2 appear to be coexpressed in the perichondrium (pink). (B) FGF gene expression. At the limb bud stage, FGF10 is expressed in distal mesenchyme (M) (yellow) and FGF8 is expressed in the overlying apical ectodermal ridge (AER) (pink). FGF2 and FGF9 expression is observed in the developing condensation (blue), and FGF18 expression is observed in the perichondrium and presumptive joint positions (green). FGF7 is expressed in loose mesenchyme and perichondrium surrounding the mesenchymal condensation (tan) [150].

Shortly after formation of the condensing mesenchyme, FGFR3 is expressed in proliferating chondrocytes in the central core of the mesenchymal condensation that suggests a direct role of FGFR3 in proliferation of chondrocytes. FGFR1 is however expressed in prehypertrophic and hypertrophic chondrocytes which suggests a role for FGFR1 in controlling cell survival, cell differentiation and cell death. FGFR2 continues to be expressed in osteoblasts in the ossificated region of mature bone.

Endochondral bone development requires an orchestrated regulation between chondrocyte proliferation, differentiation to hypertrophic chondrocyte and ossification. These signaling pathways will be more discussed in the section 2.4.2.2.

FGF signaling in the developing intramembranous bone

Intramembranous ossification is responsible for the formation of the cranium and medial clavicles. Intramembranous ossification begins with the mesenchymal condensation. Undifferentiated mesenchymal cells then differentiate into osteoprogenitor cells which become bone matrix-forming mature osteoblasts. Osteoblasts either die by apoptosis or are embedded in the matrix, becoming osteocytes [152].

During this progressive process, the expression of FGFs and FGFRs is temporally and spatially controlled to assure the balance between proliferation, apoptosis and differentiation of osteogenic cells. FGF2, FGF18, FGFR1 and FGFR2 are the key regulators in intramembranous bone formation [152]. In recent years, essential molecular mecha-

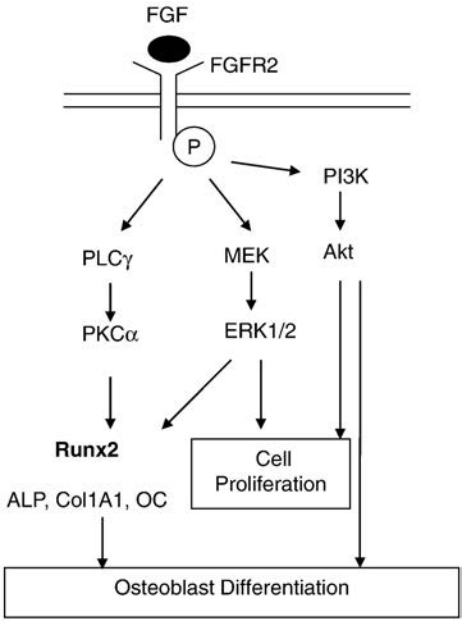

Figure 2.7 Signaling pathways activated by FGF/FGFR2 control osteoblast proliferation and differentiation [129].

nisms by which FGF/FGFR signaling promotes intramembranous bone development has been revealed by analyzing FGFR mutations involved in human skeletal disorders and using genetically altered mouse models. Three downstream pathways in response to FGF-stimulation are well characterized during osteoblastogenesis. There are ERKs, AKT and PKC pathways which are coordinated to promote cell proliferation and differentiation (Figure 2.7). First, activation of ERK1/2 signaling is partly involved in cell proliferation of osteoprogenitors [34]. Osteoblast differentiation promoted by FGFR2 is thought via ERK-induced expression of RUNX2, an essential transcription factor involved in osteoblastogenesis. The activation of ERK-MAP kinase also induces expression of osteogenic marker genes [155]. Second, PKC activation by FGFR2 also results in RUNX2 activity in mesenchymal cells and osteoblasts [138]. Third, PI3K-AKT pathway is activated by FGF2 or FGF4 that promotes the proliferation and differentiation

of osteoblast precursor cells [34].

Many studies also demonstrated that there are crosstalks between FGF/FGFR signaling, Wnt signaling and other receptor tyrosine kinase signaling which control osteoblast functions (further detail in [129]).

2.4.2 Heritable skeletal disease mutations in FGFRs

Due to the essential role of FGFR1, 2 and 3 in skeletal development, alterations in particular the mutations of these receptors, are the etiology in many heritable skeletal diseases.

2.4.2.1 Craniosynostosis

Craniosynostosis consists of premature fusion of one or more cranial sutures, occuring in ∼1 in 2500 newborns [94]. Syndromic craniosynostosis is usually associated with many complications affecting sensory, respiratory and neurological function. The majority of craniosynostosis syndromes are associated with mutations in FGFR2. Autosomal dominant gain-of-function missense mutations, deletions, and insertions in FGFR2 result in Apert syndrome, Crouzon syndrome, non syndromic craniosynostosis syndrome, Saethe-Chotzen syndrome, Pfeiffer syndrome, and Jackson-Weiss syndrome [94, 151]. The consequence of the classic Apert syndrome mutations (S252W and P253R FGFR2) is modification of ligand binding affinity. Gain-of-function missense mutations in FGFR1 are found in several craniosynostosis syndromes including Pfeiffer syndrome, Jackson-Weiss syndrome, Muenke syndrome, and osteoglophonic dysplasia. Several mutations of FGFR3 can cause specific craniosynostosis syndromes but at low prevalence (about 5-10%) [94].

2.4.2.2 Chondrodysplasia syndromes

Chondrodysplasia syndromes are characterized by reduced growth of long bones with proximal elements more severely affected than distal elements. Since the point mutation in FGFR3 in achondroplasia was first reported in 1994 [184, 173], many studies have contributed to identify different mutations in FGFR3 in the dwarfism chondrodysplasia syndromes, which include hypochondroplasia (HCH), achondroplasia (ACH), severe ACH with developmental delay and acanthosis nigricans (SADDAN), thanatophoric dysplasia (TD) (TDI and II). ACH is the most common form of short-limb dwarfisms, and its birth incidence is estimated to occur in 1 in 10000 to 1 in 30000 newborns [87]. The consequences of FGFR3 mutations in these syndromes will be discussed further below.

Mutations of FGFR3 in different forms of chondrodysplasia syndromes

Like others FGF receptors, FGFR3 has three extracellular Ig-like domains (I, II, III), a single transmembrane domain and an intracellular domain that contains a split tyrosine kinase subdomain. The alternative splicing of the third Ig-like domain produces 2 isoforms of FGFR3 (FGFR3b and FGFR3c). FGFR3b is mainly expressed in epithelial cell populations while the form FGFR3c is present in non-epithelial cells. Among

22 known FGFs, the specific physiological ligand(s) for FGFR3 is still not identified, although FGFs 1, 2, 4, 9, and 18 are probably the best candidates based on the distribution of expression, the capacity of binding and activating FGFR3, and the phenotype of mice lacking these particular ligands [150, 235, 123].

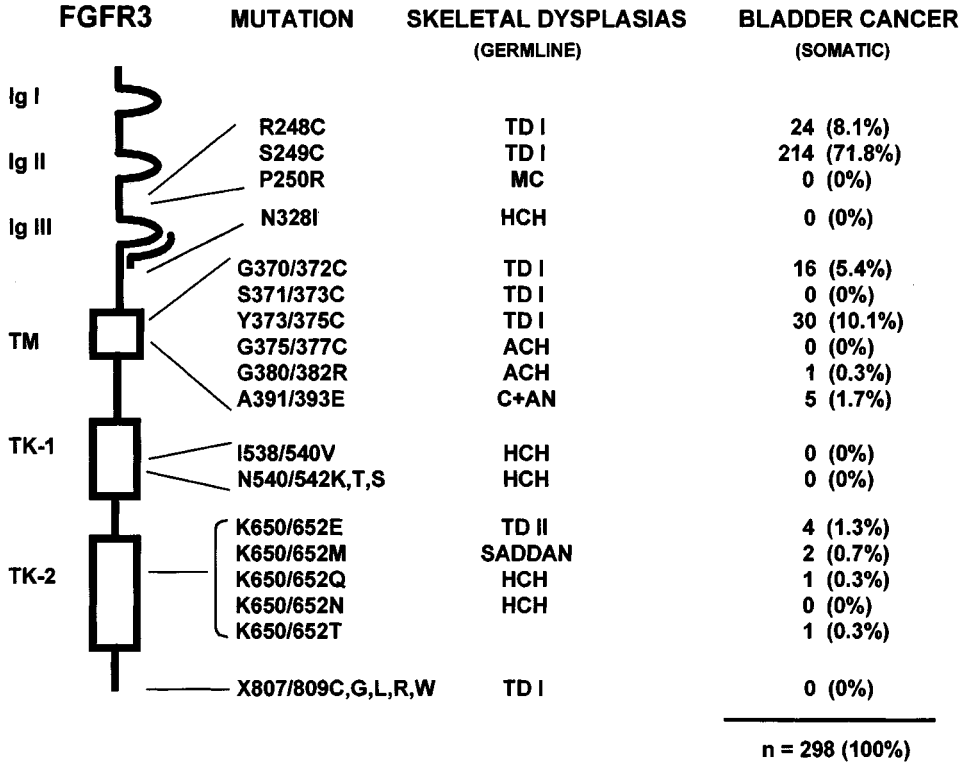

Figure 2.8 *FGFR3* mutations associated with skeletal disorders. The locations of the missense mutations associated with skeletal dysplasias: Hypochondroplasia (HCH), achondroplasia (ACH), severe ACH with developmental delay and acanthosis nigricans (SADDAN), thanatophoric dysplasia (TDI and TDII), Crouzono syndrome zith acanthosis nigricans (C+AN), Muenke craniosynostosis (MC) [217].

From the first discovery of FGFR3 mutation in skeletal dysplasias, 18 mutations have been identified. FGFR3 mutations in skeletal dysplasias are summarized in figure 2.8.

The common consequence of these mutations is constitutive FGFR3 activation. The transmembrane mutation (G380R in ACH) is thought to ligand-independent stabilization of FGFR3 dimers via hydrogen bonds formed between the side-chains of the two arginine residues [223]. TDI-associated Y373C and R248C substitutions activate FGFR3 via forming covalently bound dimers by a disulfide bond between the free cysteine residues which are introduced into the juxtamembrane domain (Y373C) or to the region linking two Ig domains in the extracellular part of FGFR3 (R248C) [42, 146]. Finally, mutations in the activation loop kinase domain, such as K650M (TDI) or K650E (TDII), result in constitutive FGFR3 activation by mimicking the conformational shifts in this domain that are normally induced by ligand-stimulation followed by autophosphorylation [223].

Lievens and colleagues proposed that different types of amino acid substitution at the Lysine 650 of FGFR3 interferes with its biosynthesis and its intracellular transport.

Two highly phosphorylated FGFR3 (K650M and K650E), which are associated with severe pathologies, were located as immature glycosylated proteins in the endoplasmic reticulum (ER), and failed to be degraded. They could even activate JAK/STAT signaling pathway from ER [119, 120]. The ER localization of murine K644E FGFR3 corresponding to the human K650E substitution in ER is still controversial, because these results in HEK293 cells were different compared to the same construction in COS7 cells where mutant FGFR3 was located in vesicular structures [33].

Another consequence of mutant FGFR3 is the increased stability of the receptor. The work of Cho and colleagues suggested that ACH-G380R and TDII-K650E disrupted c-Cbl-mediated ubiquitination that resulted in the escape of mutant receptor from lysosomal targeting into recycling pathway to increase the signaling capacity [33].

Although all FGFR3-related skeletal dysplasias are characterized by shortening of the long bones, they display a graded spectrum of phenotypic severity, ranging from relatively mild HCH to the neonatal lethal TD. Some studies have suggested that the phenotypic severity depends on the phosphorylated states, the intracellular localization of the mutated FGFR3 and the duration of FGFR3 phosphorylation [146, 78]. Figure 2.9 shows the factors which potentially decide the severity of different FGFR3-related chondrodysplasia syndromes.

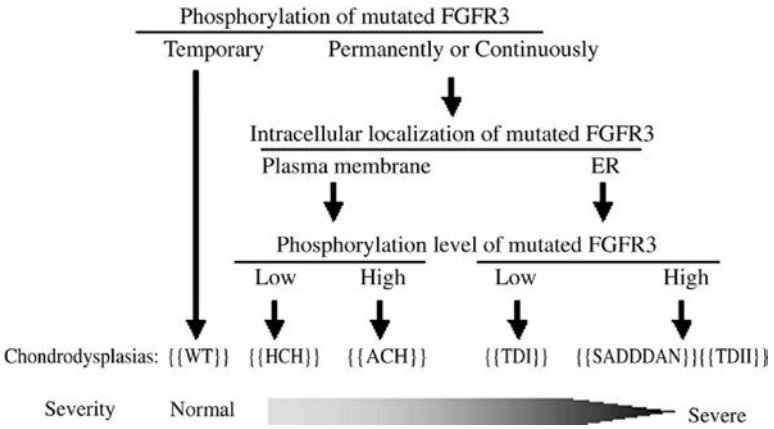

Figure 2.9 Flow chart for the classification of the suggested crucial factors concerning the pathogenesis or severity of the FGFR3-related skeletal dysplasias. Continuous phosphorylation either dependent or independent on ligand stimulation is the crucial factor to distinct mutated FGFR3s from WT-FGFR3. Among mutants, ER localization of the receptor and phosphorylation level of mutated FGFR3 are the factors which determine the severity of the skeletal dysplasias [78].

FGFR3 signaling in chondrodysplasia syndromes

FGFR3 functions as a physiological negative regulator of growth of long bones. FGFR3 signaling plays different roles in chondrocyte including inhibiting the proliferation, promoting the differentiation, regulating the synthesis of chondrocyte extracellular matrix and cellular shape. The dwarfism phenotypes in patients carrying gain-of-mutations in *FGFR3* are thought to exaggerate the physiological function [58].

Three main signaling pathways of FGFR3 implicating chondrodysplasia syndromes are: STAT, ERK-MAPK, stabilization of FGFR3. Figure 2.10 illustrates these pathways.

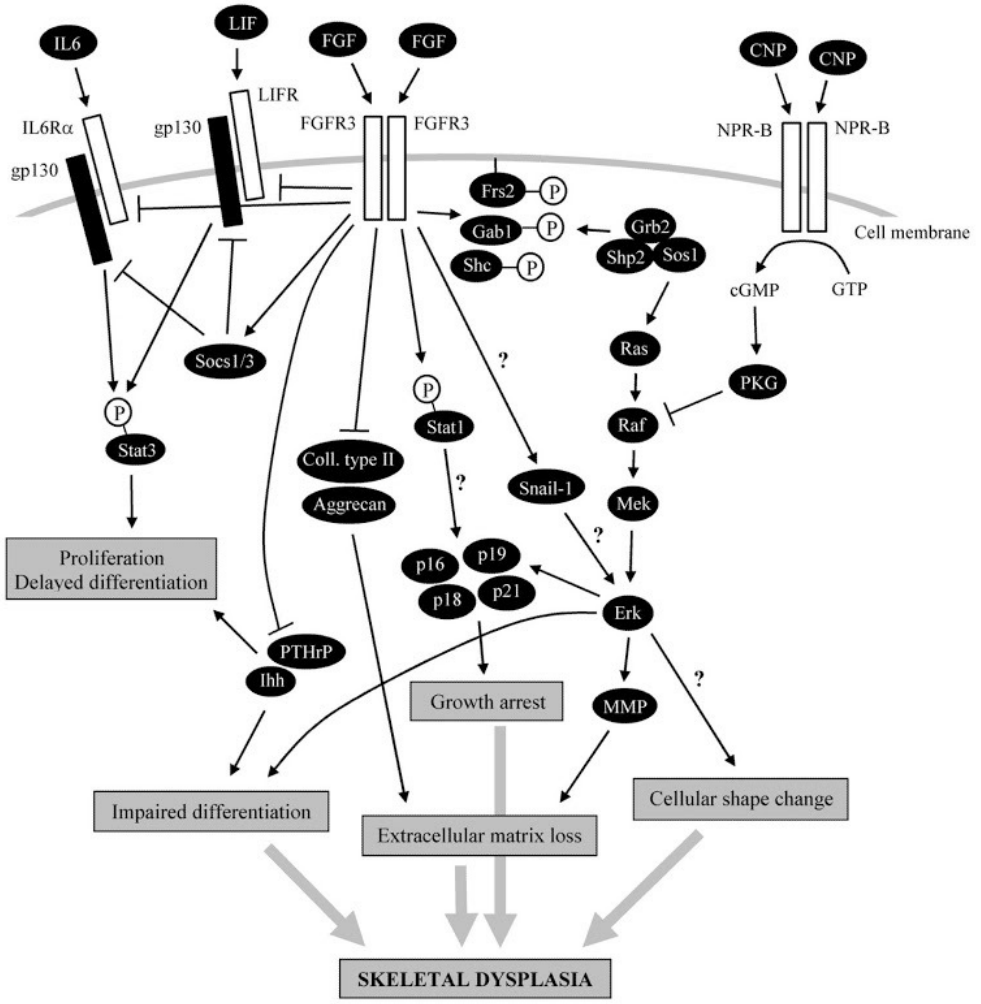

Figure 2.10 Molecular mechanisms of FGFR3 signaling in cartilage. Aberrant activation of FGFR3 alters chondrocyte behavior by inducing premature growth arrest, loss of extracellular matrix, altered differentiation, and changes in cell shape. Together, these cellular phenotypes (gray arrows) contribute to profound disruption of the growth plate cartilage resulting in skeletal dysplasia. At the molecular level, the growth arrest phenotype is mediated by induction of several inhibitors of the cell cycle, belonging to cip/kip family (p21) or INK4 family (p16, p18, p19), whereas the loss of the extracellular matrix originates from both inhibition of production of major matrix components (collagen type II and aggrecan), and active matrix degradation, mediated by several members of MMP family. Expression of two important physiological regulators of chondrocyte differentiation, Indian hedgehog (Ihh) and parathyroid hormone-related protein (PTHrP), is inhibited by FGFR3 in cartilage, likely contributing to impaired chondrocyte hypertrophic differentiation. ERK MAP kinase is a major pathway for growth arrest, extracellular matrix loss, and impaired chondrocyte differentiation. FGFR3 causes prolonged activation of the ERK signaling module (RAS-RAF-MEK-ERK), mediated by adapter (GAB1, FRS2, and SHC) driven recruitment of SHP2-GRB2-SOS1 complexes to the cell membrane, where they activate RAS. In addition, SNAIL1 transcription factor is involved in regulation of FGFR3-mediated ERK activity, although the exact nature of this regulation is not presently clear (question marks). The FGFR3-mediated activation of the ERK pathway is antagonized by CNP signaling, which inhibits ERK pathway by inactivation of RAF kinase, via inhibitory phosphorylation mediated by cGMP-activated protein kinase (PKG). Some FGFR3 mutants also activate STAT1, possibly via direct phosphorylation at Y701. It is, however, currently unclear whether activated STAT1 or other STATs induce cell cycle inhibitor expression in cartilage, thereby contributing to the FGFR3-mediated growth arrest (question mark). Finally, chronic activation of FGFR3 leads to inhibition of canonical cytokine–STAT signaling in chondrocytes, via both induction of SOCS inhibitors of cytokine signaling and inhibition of expression of receptors for IL6 (IL6Rα) or LIF (LIFR). As the latter cytokines represent positive regulators of chondrocyte proliferation, their inhibition might contribute to the pathological effects of FGFR3. NPR-B, natriuretic peptide receptor B/guanylyl cyclase B; GTP, guanosine-5'-triphosphate; cGMP, cyclic guanosine monophosphate; gp130, glycoprotein 130 [58].

Signal Transducer and Activator of Transcription (STAT) is characterized as a mediator in mutated FGFR3 signaling in many studies. STAT signal was first reported in Su's work [200]. They showed that mutant TDII FGFR3 (K650E) can specifically induce activation and nuclear translocation of the transcription factor STAT1. This correlates with the accumulation in the nuclei of p21(WAF/CIF), a cell-cycle inhibitor, and growth arrest of the 293T cells expressing K650E FGFR3. It was suggested that STAT1 activation and P21 induction might be responsible for delayed growth in bone development. Many studies have then given evidences to support this model in which lethal FGFR3 mutants (K650M or K650E) use STAT1 as a mediator to regulate chondrocyte proliferation and differentiation [175, 143, 120, 116, 78]. Strikingly, Krejci and his colleagues systematically compared the capacity of phosphorylation by STATs of wild type FGFR3 and different mutants which are associated with chondrodysplasia syndromes. Only K650M and K650E FGFR3 mutants of tyrosine kinase domain, significantly activated STAT1 or STAT5 [106]. These results were similar to data from other studies in which K650 mutants were used as models to identify the pathways implicated in bone growth in FGFR3-related skeletal dysplasia. Krejci and his colleagues suggested that STAT pathway is just an unusual signaling restricted to K650 Mutants (reviewed in [58]). They proposed an alternative model for the implication of STATs in FGFR3 downstream signaling pathways that FGFR3 may inhibit directly canonical cytokine-STAT signaling activated by interferon γ, Interleukin 6, Interleukin 11, and leukemia inhibitory factor (LIF); or indirectly via induction of Suppressor Of Cytokine Signaling 1 and 3 (SOCS1 and SOCS3), inhibitors of cytokine signaling. Thus, constitutively activated FGFR3 in FGFR3-related skeletal dysplasia might inhibit cytokine-STAT signaling leading to altered chondrocyte proliferation and differentiation (Figure 2.10).

Many studies have revealed that the RAS–RAF–MEK–ERK pathway is activated by mutated FGFR3 in ACH and TD. In Murakami's work, mice expressing the achondroplasia mutant of FGFR3 displayed uncompleted hypertrophic chondrocytes and a high phosphorylation of MEK1 in the growth plate. In addition, expression of a constitutively active mutant of MEK1 in chondrocytes of *fgfr3-/-* mice delayed hypertrophic chondrocyte differentiation. These results suggested a model in which FGFR3 signaling uses the MAPK pathway to inhibit chondrocyte differentiation [143]. Lievens and colleagues demonstrated that mice K644E/M mutants, corresponding to K650E/M in human, which causes the severe skeletal dysplasia SADDAN and TDII, may activate ERK1/2 from the endoplasmic reticulum [121]. Moreover, constitutive activation of FGFR3 inhibited longitudinal bone growth by decreasing the extracellular matrix synthesis through the MAPK pathway [232].

In ACH or TD growth plates, FGFR3 mutation has a tendency to be upregulated in comparison to wild type FGFR3. It may be due to the fact that mutated FGFR3 escapes from lysosomal degradation by c-CBL-dependent ubiquitination, that results in recycling of activated receptors and amplification of FGFR3 signals [33]. Results from the same group [76] further proposed a precise mechanism of this model: constitutively active FGFR3 induces phosphorylation of SPRY2 leading to increased c-CBL sequestration by SPRY2. These results are consistent with previous observations that c-CBL is unable to interact with mutant FGFR3 for ubiquitination and degradation. However, the implication of c-CBL in degradation of mutated FGFR3 by ubiquitination is

still controversial, as those of data mentioned above are different from other studies reporting strong ubiquitination of other FGFR3 mutants having no effect on FGFR3 stability [142, 16].

2.4.3 Deregulation of FGFR signaling in cancer

Deregulation of FGFR signaling pathways can be originated from aberrant expression, mutation in FGF ligands and receptors, or from alterations in downstream signaling pathways. This deregulation has been found in many types of cancers (extensively reviewed in [212]). Figure 2.11 summarizes the contribution of FGF ligands and FGF receptors in cancer. Particularly, in bladder cancer, FGFR3 alteration is one of the most frequent events. Thus, I dedicate the next section 2.5 to introduce the alterations of FGFR3 in bladder cancer.

2.5 Alterations of FGFR3 in bladder cancer

As mentioned above, the functions of FGFR signaling in general and FGFR3 signaling in particular depend on the cellular context. FGFR3 acts as a physiological negative regulator of skeletal growth via inhibition of chondrocyte proliferation and the gain-of-function mutations of FGFR3 cause the enhanced inhibition in this cell type. However, the gain-of-function mutations of FGFR3, even the same point mutations, cause excessive cell proliferation in epithelial cells [124, 12]. In this section, I will report the current understanding of the alterations of FGFR3 and their consequences in tumorigenesis and signaling in bladder cancer.

2.5.1 Activating mutations

FGFR3 mutations in bladder cancer were first reported by Radvanyi's group over fifteen years ago [22]. They found single nucleotide substitutions of *FGFR3* in 9 of 26 bladder carcinomas (35%). Since then, 11 different mutations have been identified in urothelial tumors. All FGFR3 mutations described to date are shown in Figure 2.12. The most frequent mutations are S249C (66.6%), Y375C (15.1%), R248C (9.7%) and G372C (4.3%). They are identical to the mutations causing lethal TDI (Figure 2.8). Data from our group and cBioPortal indicate that FGFR3 mutations seem to be restricted to a few tumor types including bladder cancer (50-60% in non-invasive muscle tumors, 12-20% in muscle-invasive tumors), lung cancer (around 6%), melanoma (around 3%). Other types of cancers have low frequency of FGFR3 mutations [98, 61, 28].

Many studies established that *FGFR3* mutations is strongly associated with low tumor grade and stage [102, 122, 208, 147]. The recent meta-analysis of 916 tumors about the distribution of *FGFR3* mutations by stage and grade indicated that the frequency of *FGFR3* mutations significantly decreased while gravity of stage and grade increased. In term of stage, 65% pTa tumor samples, 30% of pT1 tumor samples, 11.5% in pT2-4 tumors samples present mutant FGFR3. Also, by grade, 69.8% G1 tumors,

Gene Name	Mutation	Type of Cancer
(a) Contributions of FGFs to malignancy (*in vivo*)		
FGF1	Amplification	Ovarian cancer
FGF2	Over expression	Bladder cancer, Prostate cancer, Small cell lung carcinoma, Melanoma, Hepatocellular carcinoma
FGF3	Amplification	Breast cancer
FGF4	Amplification	Breast cancer
FGF5	Over expression	Glioblastoma
FGF6	Over expression	Prostate cancer
FGF7	Over expression	Lung adenocarcinoma
FGF8	Over expression	Breast cancer, Prostate cancer, Hepatocellular carcinoma, Colorectal cancer
Fgf9	Frameshift/missense/ nonsense mutation	Colorectral and endometrial carcinomas
	Over expression	Non small cell lung cancer
FGF10	Over expression	Breast carcinomas, Prostate cancer
FGF15/19	Over expression	Prostate cancer, Hepatocellular carcinoma
FGF16	Over expression	Ovarian cancer
FGF17	Over expression	Prostate cancer, Hepatocellular carcinoma
FGF18	Over expression	Hepatocellular carcinoma
FGF22	Knockout	Suppresses skin papilloma (in mice)
FGF23	Polymorphism	Increased risk of prostate cancer
(b) Contributions of FGFRs to malignancy (*in vivo*)		
FGFR1	Amplification	Small cell lung cancer, Squamous cell lung cancer, Breast cancer, Ovarian cancer, Pancreatic ductal adenocarcinoma, Tongue squamous cell carcinoma
	Missense mutation	Melanoma, Pilocytic astrocytoma
	Translocation	Leukemia, Lymphoma, Alveolar rhabdomyosarcoma, Glioblastoma, Myeloproliferative syndrome (fusion with CUX1, FGFROP2, FIM, RANBP2/NUP358, SQSTM1, TRP, ZNF198)
	Over expression	Glioblastoma
FGFR2	Amplification	Gastric cancer, Breast cancer
	Missense mutation	Endometrial carcinoma, Gastric cancer
	Translocation	Cholangiocarcinoma
FGFR3	Missense mutation	Gastric cancer, Colorectal cancer, Breast cancer, Endometrial carcinoma, Urothelial carcinoma, Bladder tumor, Skin tumor, Myeloma
	Mis-localization	Brest cancer
	Translocation	Myeloma, Squamous cell lung cancer, Bladder cancer, Glioblastoma, Lymphoma
	Over expression	Breast cancer, Colon cancer (FGFR3c)
FGFR4	Missense mutation	Rhabdomyosarcoma, Adenoid cystic carcinoma, Breast Cancer (resistance to adjuvant therapy)
	Over expression	Ovarian cancer, hepatocellular carcinoma

Figure 2.11 Acquired and heritable mutations in FGFs and FGFRs in malignancy [151].

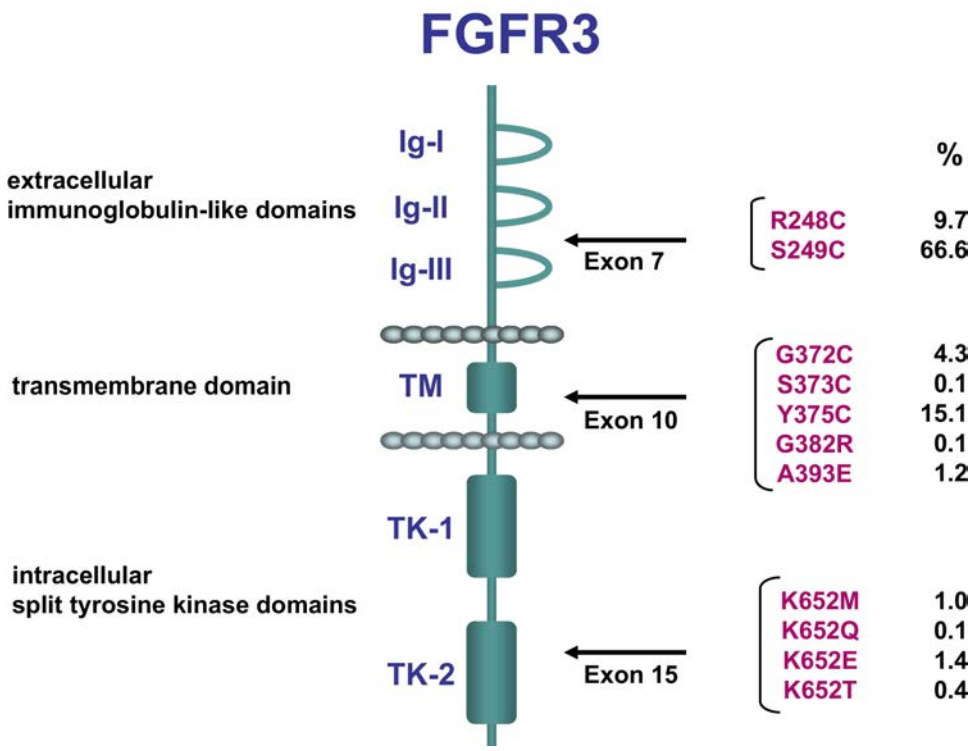

Figure 2.12 Relative frequencies and positions of FGFR3 mutations in bladder cancers [65].

68% G2 tumors and only 18.6% of total G3 tumor sample present mutant FGFR3 [148].

The S249C or Y375C mutations create a cysteine residue in the extracellular domain or the transmembrane region of the receptor, respectively that results in the formation of disulfide bonds between adjacent monomer receptors [42]. This ligand-independent dimerization leads to the constitutive activation of mutant receptors [12]. Mutations in kinase domain (lysine residue at position 652, K650E, identical to the TDII mutation) which are more frequent in non-lethal dysplasias, are rare in urothelial cancer with frequency of around 2%. In skeletal dysplasia, these mutations are thought to mimic the conformational changes leading to ligand-independent receptor activation and signaling [223].

2.5.2 Overexpression

The levels of FGFR3 transcripts and protein examined by RT-qPCR or immunohistochemistry, respectively have been reported in several studies [70, 12, 208, 14]. There was an association of FGFR3 expression levels with tumor stage and grade. Overexpression of FGFR3 was more prevalent in low-stage and low-grade tumors. The expression of FGFR3 in pTa and pT1 tumors was increased compared to normal human urothelial cells. Moreover, superficial bladder tumors expressed significantly higher FGFR3 than muscle-invasive tumors [12, 208]. Interestingly, there was a correlation between mutation status and expression level of FGFR3. Mutant tumors had increased *FGFR3* mRNA levels by 2.2- and 3.1-fold compared to normal human urothelial cells and non-mutated tumors, respectively [12]. A recent study by analyzing tissue mi-

croarrays has been in accordance with this observation [164]. They have shown that FGFR3 was identified in 113/207 tumor samples (54.6%) and was significantly associated with FGFR3 mutation, low tumor stage, low histological grade and a papillary growth pattern. 74% of tumors with positive FGFR3 expression presented an FGFR3 mutation.

The molecular mechanisms driving the overexpression of FGFR3 in bladder cancer however are partly understood. One study of microRNA (miR) alterations in 78 normal and malignant urothelial samples indicated that loss of miR-99a and miR-100 leads to overexpression of FGFR3 in tumors [27]. Normally, these microRNAs bind directly to the 3'UTR region of the *FGFR3* mRNA leading to the degradation of the mRNA.

One group found overexpression of FGFR3 in 50% of muscle-invasive tumors in which wild type FGFR3 was expressed more commonly [70]. Thus, it is suggested that FGFR3 is necessary for bladder tumor progression in both superficial and muscle-invasive tumors.

2.5.3 Translocations

Chromosomal translocation is another mechanism of abnormal FGFR3 activation in bladder cancer. Figure 2.13 shows two types of FGFR3 fusion identified in bladder cancer, FGFR3-TACC3 and FGFR3-BAIAP2L1.

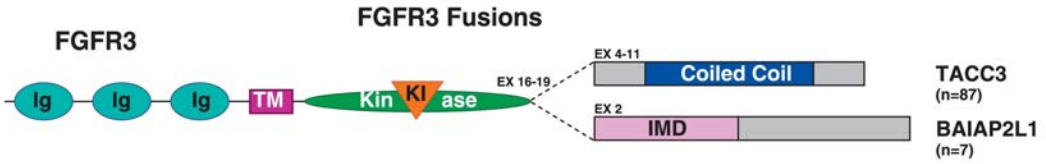

Figure 2.13 Schematic representation of two FGFR3 fusions identified in bladder cancers. The most common breakpoint of each fusion is shown. Occurence numbers (n) indicate the total number of times the fusion has been identified, including breakpoints not shown in the figure [60].

The fusion gene which occurs between FGFR3 and the transforming acidic coiled-coil containing protein 3 (TACC3) gene has been reported in glioblastoma in 2012 for the first time [188]. They found that the fusion gene has oncogenic properties. Indeed, cells expressing FGFR3-TACC3 was able to grow in anchorage-independent conditions and the mice transduced with FGFR3-TACC3 developed malignant brain tumors. FGFR3-TACC3 displayed constitutive phosphorylation and inhibition of FGFR kinase rescued the aneuploidy defect and oral administration of an FGFR inhibitor prolongs survival of mice bearing intracranial FGFR3-TACC3-initiated glioma. FGFR3-TACC3 has been subsequently identified in other cancers including lung cancer, head and neck cancer, oral cancer, cervical cancer and also bladder cancer [21, 234, 23, 227].

In bladder cancer, to date, several isoforms of FGFR3-TACC3 have been identified. The group of Knowles found 3 isoforms which contain commonly exon 1-18 FGFR3 fused with different lengths of TACC3: from exon 11 in RT112 or LUCC2 cell lines, from exon 4 in RT4 cell line, and from exon 8 in one tumor sample [227]. TCGA study identified 2 isoforms of FGFR3-TACC3 of which the breakpoint was in intro 16 or exon

17 of FGFR3 and intro 10 of TACC3 [205]. Results from our laboratory by Western Blot and PCR indicated that FGFR3-TACC3 were detected in 4 of 200 tumor samples examined. Chromosomal rearrangement results in the loss of the 3'-UTR of FGFR, a region that contains various microRNA regulation sites. In glioblastoma, it was shown that the formation of FGFR3-TACC3 fusion resulted in a loss of microRNA-99a site leading to the overexpression of FGFR3-TACC3 [156]. This could also explain why FGFR3-TACC3 is generally overexpressed in bladder cancer cell lines or tumor samples.

FGFR3-BAI1-associated protein 2-like 1 (BAIAP2L1) is another gene fusion identified in bladder cancer. FGFR3-BAIAP2L1 has been detected in 4 of 46 patients with bladder cancer [145] and in one bladder cancer cell line, SW780 [227].

2.5.4 Consequences in the downstream signaling of FGFR3 alterations

It has been shown that FGFR3 mutants display oncogenic properties in bladder cancers. Indeed, they have transforming capacity *in vitro* and induce the tumorigenicity *in vivo* mouse models. NIH-3T3 cells expressing S249C FGFR3 increases cell proliferation and presents anchorage-independent cell growth. In addition, in nude mice xenografted with cells expressing S249C FGFR3, tumors develops after 10 days [12]. In the same study, the authors indicated that Y375C mutation is required for the transforming properties of MGH-U3 cell line. Another study confirms these observations in NIH-3T3 cells, however, in immortalized normal human urothelial TERT-NHU cells, S249C and Y375C mutants promotes cell proliferation and viability [46]. Also, the knockdown of S249C FGFR3 in the urothelial cell line 97-7 reduces the proliferation and anchorage independent growth [208]. However, the introduction of only K652E FGFR3 is not sufficient to induce urothelial tumor in mice or to transform TERT-NHU cells [4]. Only when this mutation iss combined with the deletion of PTEN, a negative regulator of PI3K-AKT, cell proliferation is increased [59].

Although the oncogenic property of mutated FGFR3 is well established, consequences of FGFR3 mutations in FGFR3 signaling in bladder cancer is partly understood. A recent work of our laboratory has revealed new elements in the signaling pathway activated by altered FGFR3 in bladder cancer [125]. Constitutively activated FGFR3 phosphorylates P38 that results in stabilization of MYC mRNA by translocating Human antigen R protein into the nucleus. On the other hand, the FGFR3-induced AKT phosphorylation inhibits Glycogen synthase kinase 3 (GSK3β) which prevents proteasome-mediated degradation of MYC protein (Figure 2.14). Together, it showed that constitutive FGFR3 activation results in the activation of a MYC transcription program. The study was performed on two bladder cancer cell lines presenting constitutively activated FGFR3: MGH-U3 cells express a mutated activated FGFR3 (Y375C) and RT112 cells show a high amplification and upregulation of both wild-type FGFR3 and a fusion form of FGFR3, FGFR3-TACC3. The signaling pathway described above is identical in the two cell lines suggesting that different activated forms of FGFR3 have the same effects on P38 and AKT pathway [125].

Recently, TGFβ-activated kinase 1 (TAK1) has been identified as a novel partner protein of FGFR3 [176] and was phosphorylated by FGFR3 *in vitro*. In MGH-U3, activated FGFR3 modulated NFκB transcriptional activity in a TAK1-dependent manner.

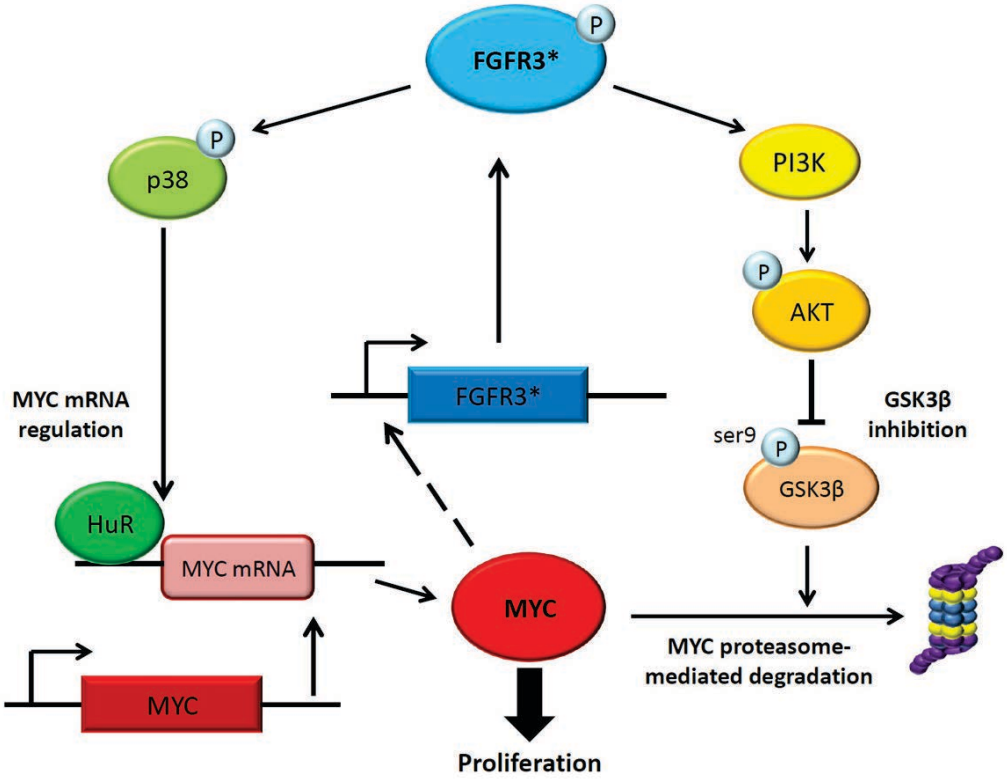

Figure 2.14 Signaling pathways activated by altered FGFR3 in bladder cancer [125].

FGFR3-TACC3 was generally upregulated in bladder cancer cell lines or tumor samples. These cell lines were more sensitive to FGFR inhibition than cell lines with point mutations. All FGFR3-TACC3 fusion proteins are constitutively phosphorylated probably due to the auto-dimerization via the coiled-coil domain of TACC3 [231]. In immortalized normal human urothelial cells TERT-NHU expressing FGFR3-TACC3, ERK1/2 were phosphorylated, but not PLCγ due to a deletion of the last exon of FGFR3 which is the binding site of PLCγ [227, 188].

Rat-2 fibroblast cells stably expressing FGFR3-BAIAP2L1 had an anchorage independent growth in a soft agar assay and in a spheroid formation assay transforming activity, and had a high tumorigenic potential in mice. These cells were sensitive to the selective FGFR kinase activity inhibitor CH5183284/Debio 1347, indicating that FGFR3 kinase activity is crucial for tumorigenesis. The ligand-independent dimerization of fusion protein was created through the BAR domain of BAIAP2L1. The gene signature analysis revealed that this constitutively activated FGFR3 kinase domain led to the activation of MAPK pathway and the inhibition of tumor-suppressive pathways involving RB, p53 and CDKN2A [145]. Also, the study of Wu and colleagues [231] suggested that FGFR3-BAIAP2L1 fusion protein induced ERK1/2 and STAT1 activation.

2.6 FGF- and FGFR-targeted therapy

On the basis of the evidence for the role of FGF signaling in tumorigenesis, so far three approaches of FGF- or FGFR-targeting anticancer agents have been generated, including small-molecule tyrosine kinase inhibitors, monoclonal antibodies and FGF-ligand traps.

Small-molecule kinase inhibitors. Kinase inhibitors are the agents targeting the ATP-binding site of the tyrosine kinase domain of FGFRs [18, 45]. The first-generation of kinase inhibitors which has a weak FGFR inhibitory activity is brivanib, lenvatibib, ponatinib and nintedanib. They have instead dominant anti-vascular endothelial factor receptor (VEGFR) and anti-platelet derived growth factor receptor (PDGFR) activity. In the past few years, the second-generation compounds have been developed which are potent kinase inhibitors and selective to FGFRs versus others tyrosine kinase receptors. *In vitro* studies indicated that AZD4547 (AstraZeneca) and BGJ398 (Novartis) are more potent inhibitors of FGFR1-3 whereas LY2874455 (Eli Lilly) and JNJ-4275649 (Johnson and Johnson) are pan-FGFR inhibitors. Currently, AZD4547 is being introduced in phase II and III in non-small cell lung cancer; BGJ398 is being tested in phase II trials in patients having different tumor types and presenting FGFR genetic alterations; whereas, LY2874455 and JNJ42756493 are being tested in phase I trials in advanced solid tumors. Due to the physiological role of FGFR signaling pathway in normal phosphate and vitamin D homeostasis, hyperphosphatemia has been a big problem as a mechanism-based toxicity of potent FGFR inhibitors. Thus, the challenge for specific FGFR inhibitors in the clinic is to determine a therapeutic dose that will balance anti-tumor efficacy with side effects [18].

Monoclonal antibodies and FGF-ligand traps. Monoclonal antibodies and FGF-ligand traps are being developed with the hope to have a higher selectivity to a particular FGF ligand or FGF receptor. Thus, these approaches may potentially reduce the side effects of FGFR kinase inhibitors. The first FGFR antibody to be tested in clinical phase I trial is the anti-FGFR3 antibody MFGR1877S (Roche) in t(4;14) translocated multiple myeloma patients. Recently, anti-FGFR3 monoclonal antibody B-701 has been evaluated in a phase II trial study for patients with locally advanced or metastatic urothelial cell Carcinoma (NCT02402542). The FGF-trap, FP-1039 (GlaxoSmithKline), is a soluble fusion protein which consists of the extracellular FGFR1-IIIc domain fused to the Fc portion of IgG1. This FGF-trap prevents the binding of FGF1, FGF2, and FGF4 to their corresponding receptors. FP-1039 is currently being introduced in a phase II in patients with endometrial cancer carrying FGFR2 mutations [18].

Lessons from others growth-factor-targeting anticancer agents indicated that cancer cells frequently develop drug resistances to targeted monotherapy. Using a drug cocktail which targets different altered genes in cancer cells should be a good approach to reduce these resistances.

Endocytosis and signaling

3

In the previous chapter, I mentioned that FGFRs as well as other RTKs transfer the extracellular stimuli to the cellular interior through activating several signaling cascades that finally result in physiological responses. In the classical model of signal transduction, transmembrane receptors can recruit many downstream substrates to the plasma membrane to activate signaling pathways and endocytosis serves as receptor clearance pathway to attenuate receptor signaling. However, growing evidence supports the idea that endocytosis has many effects on signal transduction and conversely, the receptor signaling can regulate the endocytic trafficking. In this chapter, I first report general features of endocytosis at different steps during membrane trafficking. Then, I summarize the current understanding of the mechanistic and functional principles underlying this bidirectional relationship, with focus on those of RTKs.

3.1
Intracellular trafficking of transmembrane receptors

3.1.1
Endocytic uptake pathways

There are many distinct mechanisms for endocytosis and generally, one molecule can be internalized through several endocytic routes [47, 103, 93]. Figure 3.1 summarizes the ten endocytic pathways identified to date. They can be divided into 2 groups: Clathrin-dependent endocytosis (CDE) and Clathrin-independent endocytosis (CIE). Here, I only focus on the CDE and the caveolae-/caveolin 1-dependent pathway, which represents a well-documented CIE.

Clathrin-dependent pathway. CDE is well-established in terms of morphology, structure and participating molecules. Five steps have been identified during the Clathrin-coated vesicle (CCV) cycle, illustrated in Figure 3.2 (reviewed in [134, 103]). This cycle initiates with the nucleation step where a low curvature membrane invagination, so-called a pit, is formed. This formation requires membrane-bending activity and some molecules such as FCH domain only (FCHO) proteins and EGFR pathway substrate 15 (EPS15). During the second step, AP2 and other cargo-specific adaptor proteins are recruited to the pit to specifically promote cargo selection. AP2 can bind to PIP2

Endocytic mechanisms	Morphology	Implicated cargoes[a]	Small G-protein dependence	Dynamin implicated?	Other proteins implicated
Clathrin mediated	Vesicular	RTKs, GPCRs, transferrin receptor, anthrax toxin	Rab5, Arf6 implicated	Well established	Clathrin, AP2, epsin, SNX9, synaptojanin, actin amphiphysin, plus many others
Caveolae-/ caveolin1-dependent	Vesicular/ tubulovesicular	CTxB, SV40, GPI-linked proteins	Unclear (caveolins may regulate cdc42 activity)	Some evidence	Caveolins, PTRF, src, PKC, actin (many signaling proteins localize to these sites)
CLIC/GEEC	Tubular/ring like	Fluid phase markers, CTxB, GPI-linked proteins	Cdc42, Arf1	Not as yet	ARHGAP10, actin, GRAF1, other GRAFs
IL2Rβ pathway	Vesicular?	IL2Rβ, FCεRI, Kir3.4, γc-cytokine receptor	RhoA, Rac1	Implicated	PAK1, PAK2
Arf6 dependent	Vesicular/tubular	MHC class I proteins, CD59, carboxypeptidase E	Arf6	Not as yet	Unclear as yet
Flotillin dependent	Vesicular	CTxB, CD59, proteoglycans	Unclear	Implicated but unclear	Flotillin 1 and 2
Phagocytosis	Cargo shaped	Pathogens, apoptotic remnants	Arf6/cdc42/rac1/rhoA (depending on type)	Implicated	Actin, IQGAP1, amphiphysin1, Rho kinase, adhesion proteins
Macropinocytosis	Highly ruffled	Fluid phase markers, RTKs	Rac1	Not as yet (CtBP1/BARS implicated in scission)	Actin, PAK1, PI3K, Ras, Src, HDAC6
Circular dorsal ruffles	Highly ruffled	Fluid phase markers, RTKs	Unclear	Implicated	Cortactin, actin
Entosis	Cell shaped	Matrix-deligated cells	RhoA	Not as yet	Adherens junctions

[a]Abbreviations: CLIC, clathrin-independent carrier; GEEC, GPI-AP enriched early endosomal compartment; GPCRs, G protein–coupled receptors; GPI, glycosylphosphatidylinositol; MHC, major histocompatibility complex; RTK, receptor tyrosine kinase.

Figure 3.1 Morphological and molecular summary of the endocytic pathways [47].

and specific motifs of transmembrane receptors through its μ- and α-subunits; also, it interacts with the cargo via adaptor proteins. Some examples of cargo-specific adaptor proteins can be cited, β-arrestin recruits GPCRs to AP2 or ARH links LDLR to AP2. The next step is the clathrin coat assembly around the defined pit by AP2 and cargo-specific adaptor proteins. A clathrin unit, the triskelion formed by three heavy chains associated with three light chains, is recruited from the cytosol to the defined pit at the plasma membrane. Clathrin units then assemble to form a curved lattice, which consequently stabilizes the curvature. Dynamin (DNM) is then recruited to the neck of the pit for CCV budding step. The polymerization of dynamin facilitates GTP hydrolysis and results in membrane fission. Following the detachment from the plasma membrane, the vesicle uncoats the clathrin lattice by the activity of ATPase heat shock cognate 70 (HSC70) and its cofactors (auxilin and GAK). The clathrin machinery, therefore, comes back to the cytosol for another CCV cycle [134]. CDE has been virtually identified as the major route of internalization for every family of signaling receptors and this hypothesis has been mostly proven under physiological conditions (for example, RTKs, Notch receptors, integrins or G protein-coupled receptors (GPCRs) [196].

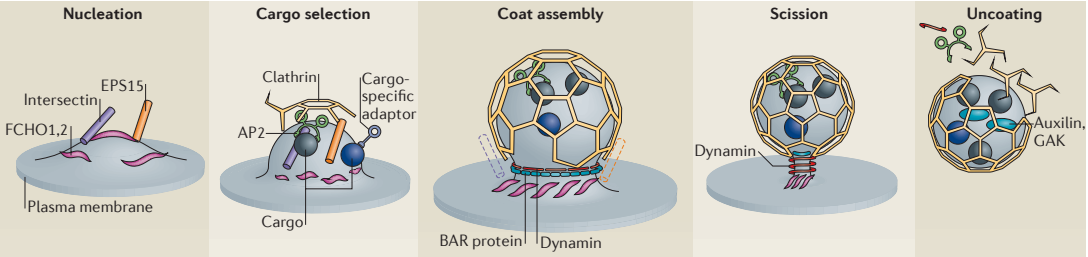

Figure 3.2 The proposed five steps of clathrin-coated vesicle formation. Nucleation: FCHO proteins bind phosphatidylinositol-4,5-bisphosphate (PtdIns(4,5)P2)-rich zones of the plasma membrane and recruit EPS15–EPS15R and Intersectins to initiate clathrin-coated pit formation by recruiting AP2. **Cargo selection**: AP2 recruits several classes of receptors directly through its μ-subunit and σ-subunit. Cargo-specific adaptors (for example, stonin, HRB and Numb) bind to AP2 appendage domains and recruit specific receptors to the AP2 hub. **Coat assembly**: clathrin triskelia are recruited by the AP2 hub and polymerize in hexagons and pentagons to form the clathrin coat around the nascent pit. **Scission**: the GTPase dynamin is recruited at the neck of the forming vesicle by BAR domain-containing proteins, where it self-polymerizes and, upon GTP hydrolysis, induces membrane scission. The actin machinery module can be added at this stage for actin polymerization at the neck of the pit, which can aid in vesicle production (not shown). **Uncoating**: auxilin or cyclin G-associated kinase (GAK) recruit HSC70 to disassemble the clathrin coat and produce an endocytic vesicle containing the cargo molecules. Synaptojanin probably facilitates this by releasing adaptor proteins from the vesicle membrane through its PtdIns lipid phosphatase activity. The components of the clathrin machinery are then freed and become available for another round of CCV formation [134].

Caveolae-/caveolin 1-dependent pathway. Caveolae are small invaginations, which have a morphology close to clathrin-coat pits and are enriched in cholesterol and sphingolipids (reviewed in [109, 131]). This endocytic pathway has been initially described to function in membrane trafficking, cell signaling and recently, to serve as plasma membrane sensors to mechanical stimuli [189]. Caveolin (CAV1, 2, 3) and cavins (Cavin 1, 2, 3, 4) are major players for the generation of caveolae structure. This pathway is dependent on dynamin which is localized to the neck of the caveolae and functions as budding actor. In contrast, EHD2, an ATPase, is required to stabilize the caveolae at the plasma membrane. In addition, EHD2 interacts with Pacsin2 which is able to sense and modulate membrane curvature. To date, it is known that albumin, SV40, cholera toxin B subunit, β1-integrin and glycosylphosphatidylinositol (GPI)-linked proteins use the caveolae-dependent endocytosis to enter the cell [47].

3.1.2 Post-endocytic trafficking

Early endosome as a cargo-sorting station

Following internalization through either CDE or CIE, receptors reach the Early endosomes (EE) as the first sorting station. RAB5, EEA1, PI3K and its product Phosphatidylinositol-3-phosphate (PI3P) are markers of EE. EE are large vesicles (~400 nm) containing regions of thin tubular extensions (~60 nm diameter). They are highly dynamic and able to fuse each other. The unique morphology of EE is thought to be important for the subsequent cargo sorting [96]. From EE, receptors can be delivered to three destinations, illustrated in Figure 3.4 [181]. The first destination is the fast recycling route back to the plasma membrane in which RAB4 and RAB35 have been identified as being im-

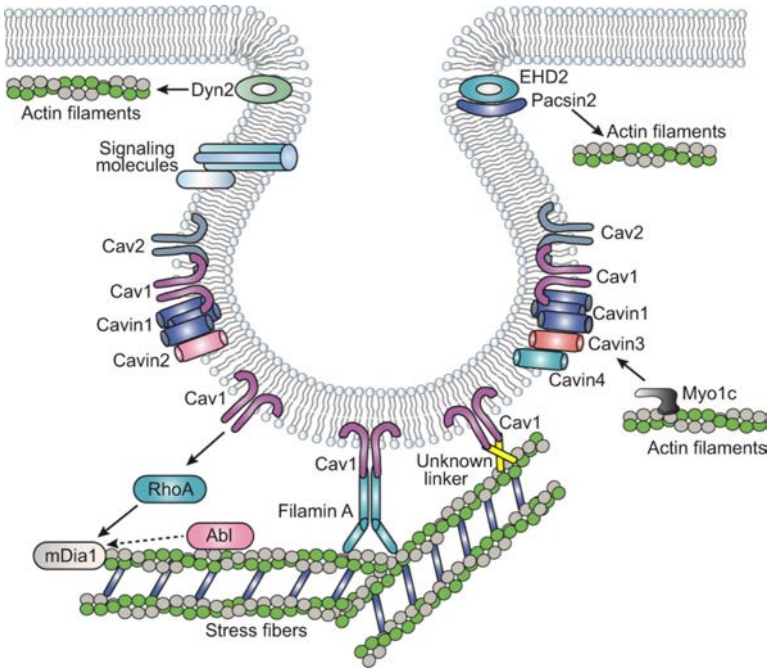

Figure 3.3 Caveolae composition and their links to stress fibers and the actin cytoskeleton. The main molecules that shape caveolae (caveolins, cavins and pacsin2) and the proteins that regulate their dynamics (Dyn2, EHD2 and filamin A) are depicted. The caveolar molecules that have functional or physical association with the actin cytoskeleton, and therefore potentially mediate the physical and functional interaction between caveolae and actin fibers, are also indicated. Filamin A is depicted here as the main protein mediating a linkage with stress fibers, but other yet unidentified linkers might exist (indicated as unknown linker). Regulators of stress fibers (Abl kinases and mDia1) that impinge on caveolae organization and trafficking are shown next to RhoA, the main regulator of stress fibers, which is regulated by Cav1 [50].

portant for recycling of Transferrin receptor (TFRC) (t1/2 = 2 min). Second, transmembrane receptors are sorted to a later, mainly juxtanuclear compartment, well-known as endocytic recycling compartment, from which recycling endosomes are generated and come back to the plasma membrane. Third, ubiquitylated receptors can be transfered to multivesicular bodies before being delivered to late endosomes and lysosomes for degradation. Indeed, ubiquitylated receptors are recognized by multiprotein complexes, known as Endosomal sorting complex required for transport (ESCRT) (0, I, II and III), which facilitates the entry of receptors to multivesicular bodies [167]. Trafficking between the endosomal compartments is spatiotemporally controlled by small RAB GTPases (further described in Chapter 4). An important feature of the endosomal sorting is the specific targeting to each destination. The mechanism specifying the intracellular trafficking of RTKs can be dependent on the ligand for a given receptor, RTK type for a given ligand, co-receptor for ligand-RTK complexes and specific sequences on RTK [135].

Late endosomes and lysosomes

Late endosomes (LE) are composed of round or oval vesicles having a diameter of 250-1000 nm. LE are characterized by the presence of LAMP1 at its membrane and a component of acid hydrolases in the lumen (Figure 3.5). The lumen contains numer-

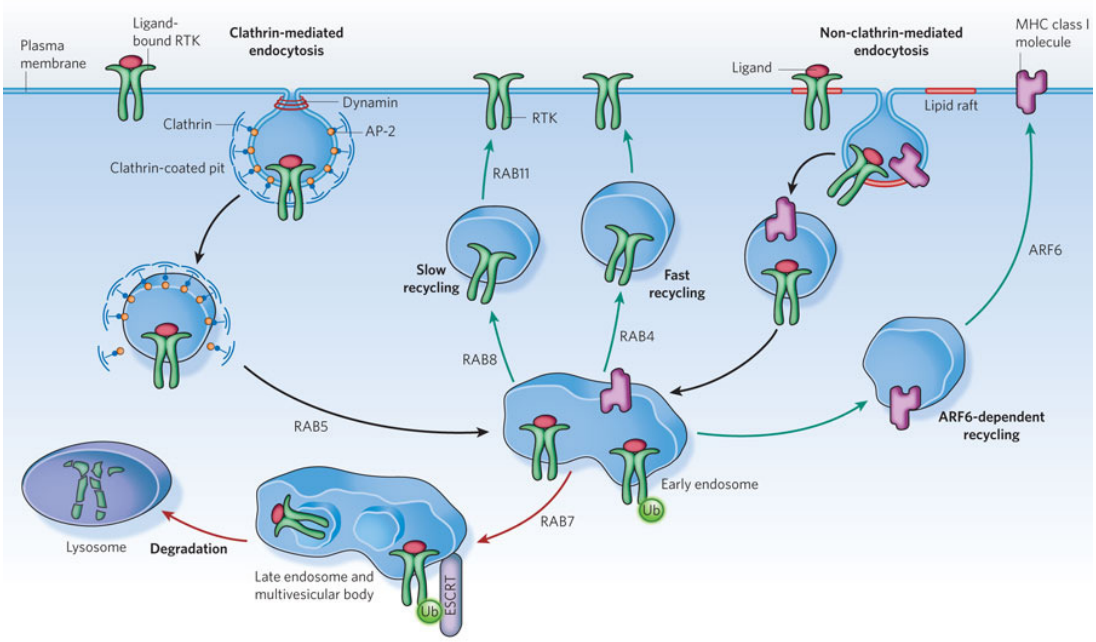

Figure 3.4 Post-endocytic trafficking of signaling receptors. See further detail in the text [181].

ous intralumenal vesicles with a diameter of $\sim$ 50-100 nm and has a pH in the 6.0-4.8 range [88]. The transition from early to LE is regulated by the crosstalk between RAB5, key player of EE and RAB7, key player of LE. It was shown that RAB7 recruits HOPS complex in which VPS39 subunit is a RAB7 GEF in a RAB5-dependent manner. Mathematical prediction suggests that RAB5 activates RAB7 until the latter reaches a threshold upon which it inactivates RAB5 via a negative-feedback loop. This loop recruits a RAB5 GAP in a RAB7-dependent manner [197]. Late endocytic compartments were initially considered as platforms for degradation, resulting in attenuate receptor signaling. However, MAPK scaffold complex is detected at LE, suggesting that signaling continues even receptors are sorted to a degradation pathway [198].

Endocytic recycling pathways

Due to technical challenges, the fast recycling route is still poorly understood. Here, I only discuss about the slow recycling routes that require the full function and positioning of the endocytic recycling compartment (ERC).

The ERC is composed of a tubular network with a diameter of about 60 nm where recycling endosomes are generated. The ERC network is closely associated with microtubule and actin cytoskeleton. In some cell types, the ERC is mainly condensed at the perinuclear region around the centrosome, but in other cells, this network is distributed more widely throughout the cytoplasm [130]. Figure 3.6 illustrates the role of RAB11 and other proteins in the control of endocytic recycling. The RAB11 GTPase subfamily and their effectors play a crucial role in the traffic to and from the ERC (further detail in the section 4.2). Along with these proteins, ARF6 and their effectors are thought to be important actors of recycling pathway of CIE cargoes through their

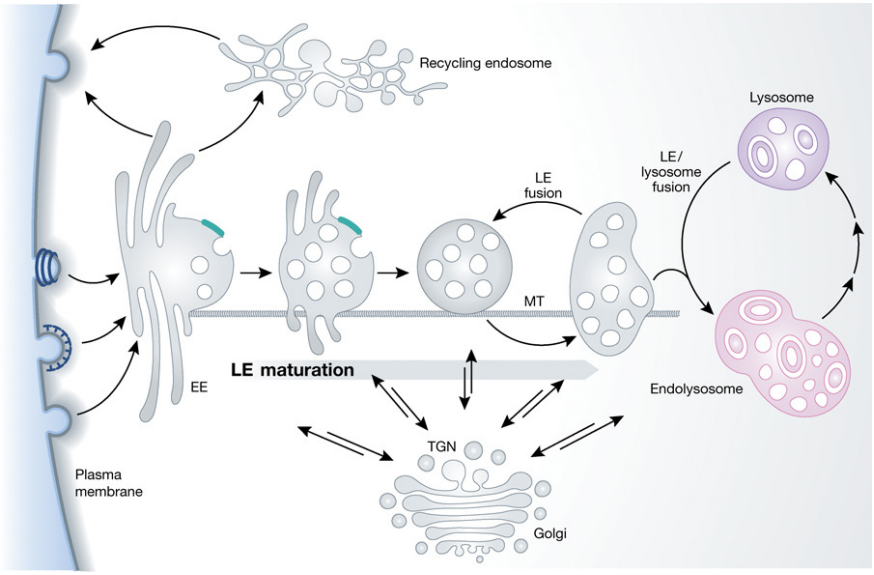

Figure 3.5 The endosome/lysosome system. The primary endocytic vesicles deliver their contents and their membrane to EE in the peripheral cytoplasm. After a period of about 8–15 min during which the EE accumulate cargo and support recycling to the plasma membrane (directly or via recycling endosomes in the perinuclear region), conversion of the EE to LE takes place. Thus, as the endosomes are moving towards the perinuclear space along microtubules (MT), the nascent LE are formed inheriting the vacuolar domains of the EE network. They carry a selected subset of endocytosed cargo from the EE, which they combine en route with newly synthesized lysosomal hydrolases and membrane components from the secretory pathway. They undergo homotypic fusion reactions, grow in size, and acquire more intralumenal vesicles. Their role as feeder system is to deliver this mixture of endocytic and secretory components to lysosomes. To be able to do it, they continue to undergo a maturation process that prepares them for the encounter with lysosomes. The fusion of an endosome with a lysosome generates a transient hybrid organelle, the endolysosome, in which active degradation takes place. What follows is another maturation process; the endolysosome is converted to a classical dense lysosome, which constitutes a storage organelle for lysosomal hydrolases and membrane components [88].

implication in membrane fusion with the plasma membrane or interactions with the actin cytoskeleton, which reflects the role of ARF6 in cell spreading, cell migration and metastasis. For example, the recycling of the syndecan 1 and FGFR complex required ARF6, PIP2 and syntenin which can bind to the C-terminus of syndecan. Introduction of different syntenin mutants, that can not bind to PIP2, in MCF-7 cells leads to the accumulation of syndecan and FGFR in the cells. Inhibiting syndecan recycling back to the plasma membrane results in impaired cell spreading [237]. This is one of the examples showing that the trafficking of internalized receptor back to the plasma membrane can influence its signaling.

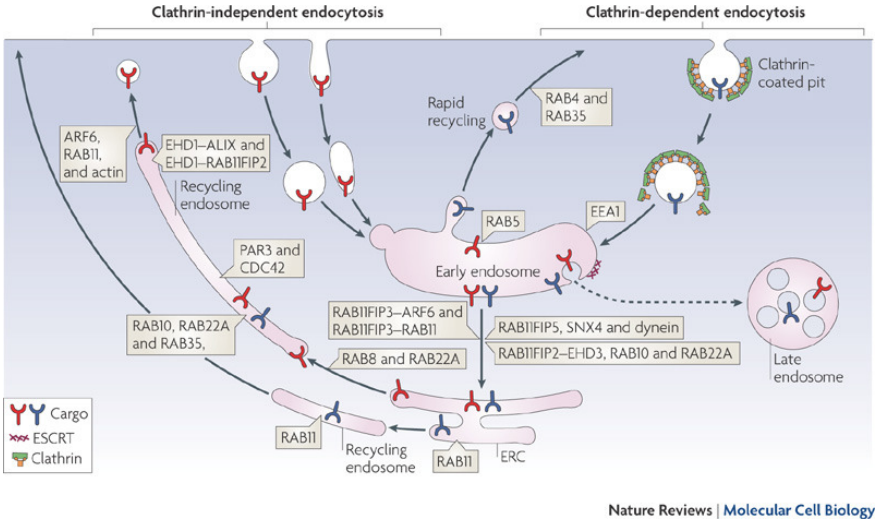

Figure 3.6 Pathways of endocytosis and endocytic recycling. Itinerary of cargo proteins entering cells by clathrin-dependent (blue cargo) and clathrin-independent (red cargo) endocytosis. Clathrin-dependent cargoes can recycle back to the cell surface through a rapid recycling pathway that requires RAB4 and RAB35. Both types of cargo can move from the early endosome to the ERC by a process that requires sorting nexin 4 (SNX4), dynein, RAB10, RAB22A, RAB11FIP2 (in complex with carboxy-terminal epidermal growth factor receptor substrate 15 homology domain-containing protein 3 (EHD3)), RAB11FIP3 (in complex with ARF6 or RAB11) and RAB11FIP5. From the ERC, recycling of both types of cargo requires RAB11, and recycling of clathrin-independent cargoes involves the generation of distinctive RAB8- and RAB22A-dependent tubules, in addition to many other factors. Some clathrin-dependent cargoes might also recycle through these different pathways. RAB10, RAB11, RAB22A and RAB35 are associated with the tubular recycling endosome and, along with EHD1 (homologous to receptor mediated endocytosis protein 1 (RME-1) in C. elegans) in complex with the mammalian apoptosis-linked gene 2-interacting protein X1 homologue ALIX (also known as PDCD6IP) and RAB11FIP2, are required for recycling. In the periphery, the tubules seem to break up into vesicles prior to fusing with the cell surface, a process that initially requires partitioning defective protein 3 (PAR3) and CDC42 and subsequently ADP-ribosylation factor 6 (ARF6), RAB11 and cortical actin. This is a composite description of endocytic recycling and all of the components shown here may not be evident in a given cell type. Adapted from [74].

3.2
Bidirectional link between membrane trafficking and signaling

Numerous findings with different types of receptors support the concept of a bidirectional link between membrane trafficking and signaling. Here, I focus on those described for RTKs.

3.2.1

Receptor trafficking regulates RTK signaling

In the classical model, following ligand stimulation, activated RTKs generate multiple docking sites for adaptor and effector proteins, thus enabling the activation of various signaling pathways, for example, the MAPK cascades or PI3K-AKT pathway. It has long been considered that ligand-bound endocytosis is one of the main ways for negatively regulating signaling from the cell surface. This negative regulation is executed by physically reducing the concentration of transmembrane receptor accessible to the ligand, and by separating the receptors from substrates and adaptors exclusively localized at or near the plasma membrane. However, it is now clear that signal transduction of various receptors can occur from different endosomal compartments (extensively reviewed in [196, 160, 135]). Indeed, endosomes provide an excellent platform for signal transduction because of their unique features including: a small volume facilitating ligand-receptor association; a residence of active receptors for a long duration; a fast capacity of motility over long distance by using microtubules; the presence of specific resident proteins. Two types of signaling at endosomes, hereafter called endosomal signaling, have been identified: first, signaling initiates at the plasma membrane and continues in endosomes; second, signaling occurs only in endosomal compartments.

Continuous RTK signaling in endosomes

In systems in which active receptors are rapidly internalized into endosomes, endosomal signaling is important to ensure the duration of signaling. The first evidence was reported in the work of Vieira and colleagues in which ERK1/2 activation requires the internalization of EGFR for full activation [218]. Recent evidence also supports this concept [160], such as the fact that several RTKs remain bound to their ligand, phosphorylated and active in endosomes until late stages. In addition, a wide range of components of MAPK cascades including GRB2, SHC, SOS, Ras proteins, RAF, MEK1 and MEK2, are detected in different endosomes. This collection of adaptor and effector proteins in endosomes ensures the activation of different cascades. The existence of a MAPK scaffold complex in late endosomes is in favor of the requirement of endocytosis for the full activation of ERK1/2. For example, the phosphorylated p14 and MP1 recruit MEK1 to late endosomes to continue EGFR-initiated signaling for early embryogenesis and tissue homeostasis (Figure 3.7.a) [206].

Endosomes with their capacity to move over a long distance are ideal for a precise, directional delivery of signaling into their site of action. For example, neuron Trk receptors (NTRK) are activated by NGF ligand which requires endocytosis and retrograde transport for the full activation of ERK5 and phosphorylation of the cAMP responsive element-binding protein (CREB) in the neuron soma[222]. To ensure an efficient signaling, endosomes containing NGF-bound Trk are delivered from distal axonal termini to the cell body in a microtubule-mediated manner [230]. In addition, these endosomes contain PLCγ, PI3K, MEK1, p38, B-Raf, Gab2 and Rap1 which are involved in the activation of ERK signaling (Figure 3.7.b) [135].

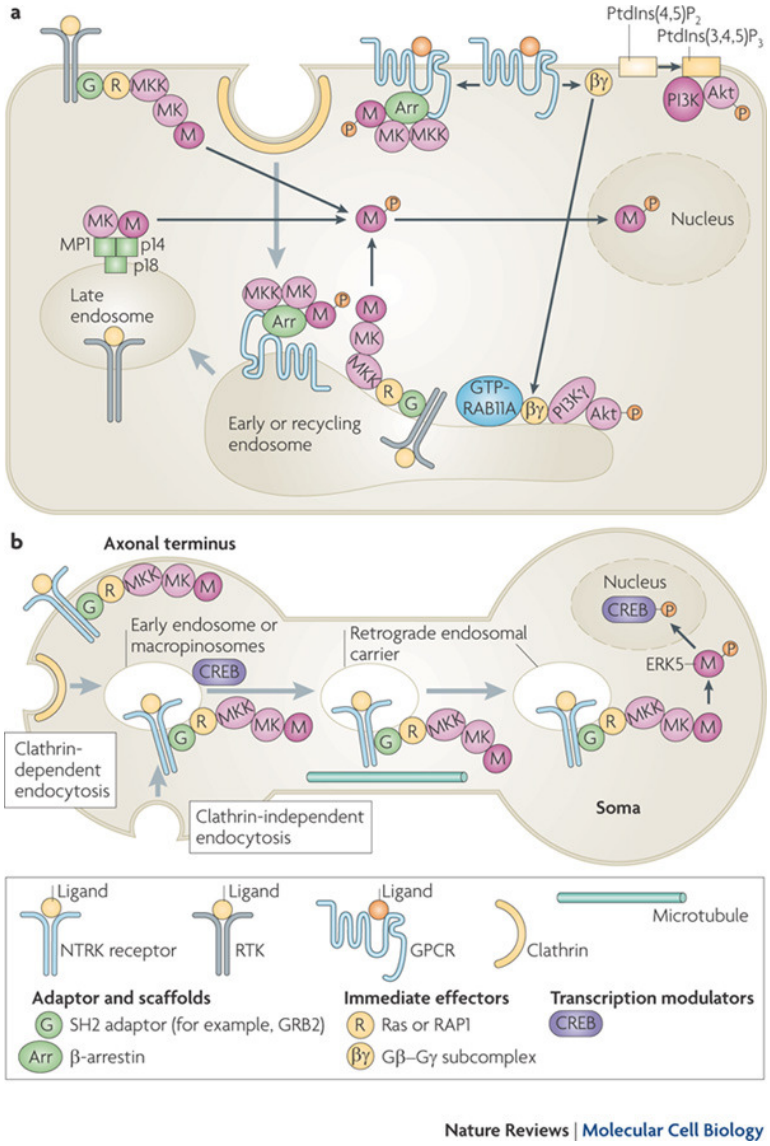

Figure 3.7 Signaling processes begin at the cell surface and continue in endosomes. **a** Activation of mitogen-activated protein kinase (MAPK) and phosphoinositide 3-kinase (PI3K)–Akt signaling cascades by receptor tyrosine kinases (RTKs) and G protein-coupled receptors (GPCRs) occurs at the plasma membrane and in early, recycling and late endosomes. In all of these locations activated, phosphorylated MAPK dissociates from the MAPK kinase (MK), unless stably associated with a scaffold protein such as beta-arrestin, and phosphorylates substrates in the cytoplasm and nucleus. When GPCRs are stimulated by lysophosphatidic acid, the activated G protein subcomplex Gbeta–Ggamma can activate PI3K and Akt at the plasma membrane and also translocate to the early and recycling endosomes to activate endosomal PI3K gamma-isoform, which leads to the phosphorylation and activation of Akt in endosomes. **b** Model of retrograde endosome signaling in neurons. Ligand-bound nerve growth factor receptors (NTRKs) are internalized by clathrin-dependent and clathrin-independent endocytosis, with associated components of the MAPK signaling cascade, into early endosomes or macropinosomes that have a multivesicular body-like morphology. NTRK signaling complexes are delivered to the soma in retrograde endosomal carriers, which are a population of early or late endosomes and macropinosomes, by dynein motor-mediated microtubular transport. The MAPK extracellular signal-regulated kinase 5 (ERK5) is then phosphorylated and activated in the soma. It phosphorylates the cAMP responsive element-binding protein (CREB), which regulates the transcription of anti-apoptotic genes. Grey arrows show trafficking pathways. Black arrows show protein translocations or complex assembly. GRB2, growth factor receptor-bound protein 2; MP1, MEK1 partner 1; PtdIns(3,4,5)P3, phosphatidylinositol-3,4,5-trisphosphate; PtdIns(4,5)P2, phosphatidylinositol-4,5-bisphosphate; SH2, Src homology 2. [196].

Specific signaling in endosomes

In some cases, endosomes serve as a unique platform for the recruitment of specific signaling substrates to amplify signals of activated RTK. An example is the activation mechanism of STAT3 by HGF [101]. STAT3 is weakly activated by HGF stimulation on c-Met receptor; however, increased phosphorylation and subsequent nuclear translocation of STAT3 was observed when activated Met was delivered to the perinuclear endosomes.

Another example is the case of APPLs-mediated AKT recruitment on EE. APPLs (APPL1, APPL2) are RAB5 effectors, and can interact with EGFR or other RTKs on EE [136]. APPLs can recruit AKT which is mostly localized to the plasma membrane. This results in the activation of GSK3β but not TSC2 for prosurvival response. Indeed, a small pool AKT and GSK3β is found to be transiently associated with RAB5 and APPL-positive endosomes [177]. Together, APPLs-positive endosomes provide a platform for selective recruitment and activation of signaling components.

Balance between degradation and recycling of RTKs influences their signaling

The balance between degradation and recycling of a given RTK has an important impact on the signal quality, duration, and magnitude [117]. Generally, ubiquitinylated EGFR is delivered to late endosomes then to lysosomes. Inhibiting EGFR ubiquitinylation by mutating ubiquitin sites on the receptor induces EGFR signaling, and conversely increasing ubiquitinylation downregulates signaling [196]. Moreover, ESCRT complexes are essential for the maturation of late endosomes to lysosomes. It was shown that the depletion of one of these complexes is enough to impair EGFR degradation, leading to enhancing EGFR-induced ERK signaling [160]. Another example is FGF signaling negatively controlled by SRED2. SPRED2 was shown to interact and colocalize with NBR1, a late endosome resident protein. This association leads to diverting FGFR into the lysosomal degradation pathway. Also, the inhibition of ERK1/2 signaling by SPRED2 is dependent on its interaction with NBR1 [128]. The endocytic recycling plays an important role in sustaining receptor signaling. For example, in cells expressing FGFR4, blocking the recycling pathway by depletion of RAB11 induces the prolongation of phosphorylation of PLCγ but reduced the phosphorylation of AKT and ERK [81]. The molecular mechanism however remains unknown. Also, it was shown that Met receptor can sustain ERK1/2 activation from endosomes and the receptor recycling plays a major role in the full activation of ERK1/2 [92].

3.2.2

RTK signaling regulates endocytosis

Although this regulation remains poorly understood, several recent evidence supports this idea. Early evidence came from the fact that ligand-induced activation of EGFR increases the total number and surface density of clathrin-coated pits. This event was then shown to be dependent on the Src kinase activity [196]. Similarly, Src plays a role in clathrin-mediated FGFR2 internalization. In addition, Eps8, phosphorylated by Src, is required for FGFR internalization and intracellular trafficking. Inhibiting Src activity by Src kinase inhibitor or depletion of Eps8 reduces clathrin-mediated FGFR2

internalization. Eps8 is important for the trafficking of FGFR into early endosome and out of this compartment [8].

This page intentionally left blank.

4 RAB GTPase family

RAB proteins constitute the largest family of small GTPases with 11 Rab identified in yeast (also called Ypt) and 70 members in human. RAB GTPases virtually regulate all transport steps between cell compartment. Therefore, alterations in RAB functions are directly or indirectly responsible for a wide range of diseases. In particular, growing evidence points out their roles in cancer development and progression [197, 100].

4.1 Role of RAB in intracellular transport

4.1.1 Structural characteristics

RAB proteins are typically 20-25 kDa monomers and share a common core fold with other small GTPases of the Ras superfamily (Figure 4.1). The fold contains a six-stranded β-sheet flanked by five α-helices. RABs distinguish however from other members of the Ras superfamily through five conserved RAB specific sequences, RABF1-F5 and four conserved sub-family motifs, RABSF1-4 [159].

In terms of functional features, RAB contains two "switch regions" called Switch I and Switch II that are responsible for guanine nucleotide and Mg2+ binding, as well as GTP hydrolysis. Following GTP binding, the switch regions undergo conformational changes that allow binding of RAB effectors. The hypervariable region at the C-terminus of RAB was originally proposed to be involved in targeting RABs to specific membranes. However, growing evidence indicates that RAB targeting relies on other mechanisms, in particular on interactions with Guanine nucleotide Exchange Factor (GEF) proteins [100]. The extreme C-termini contain a cysteine-motif box that can exist as several forms (CXXX, CXC, CCXX or CCXXX; where X is any other amino acid). One or two cysteine residues are geranylgeranylated, which allows RABs to stably insert in the outer leaflet of intracellular membranes [89].

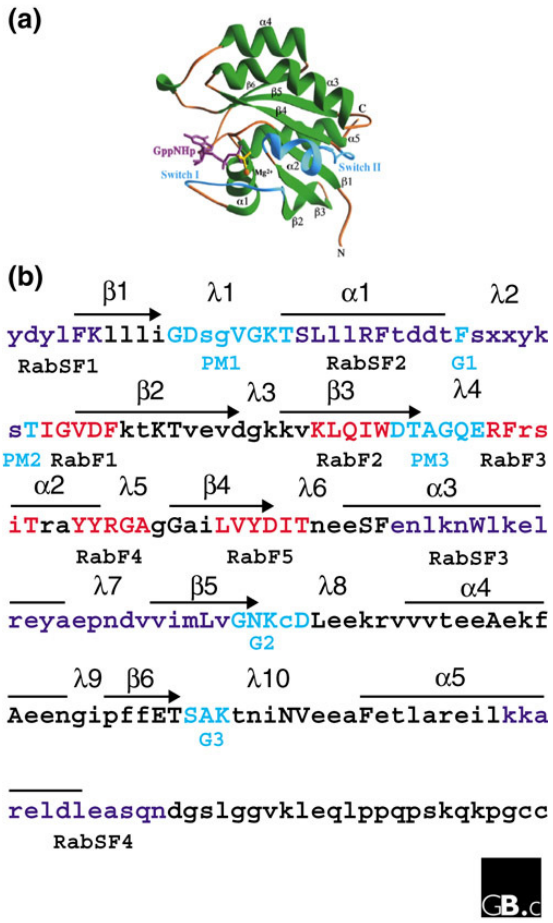

Figure 4.1 Structural features of RAB GTPases. (a) Ribbon drawing of RAB3A complexed with the GTP analog GppNHp. Purple, bound nucleotide; orange sphere, Mg2+ ion; blue, switch I and II regions; green, α helices and β sheets; yellow, loops. **(b)** A profile amino-acid sequence of the RAB GTPase subfamily generated using the hidden Markov model (HMM) method. The uppercase/lowercase coding represents outcome of the profile HMM method. Upper-case characters, residues found in the profile with a probability of p<0.5; red, RAB-specific residues (RABF1-5); dark blue, subfamily-specific motifs (RABSF1-4); cyan, highly conserved nucleotide-binding motifs; G, guanine-base-binding motif; PM, phosphate/magnesium-binding motif. The secondary structure units (α helices, β strands, and loops, λ) are indicated above the sequence [199].

4.1.2 The RAB cycle

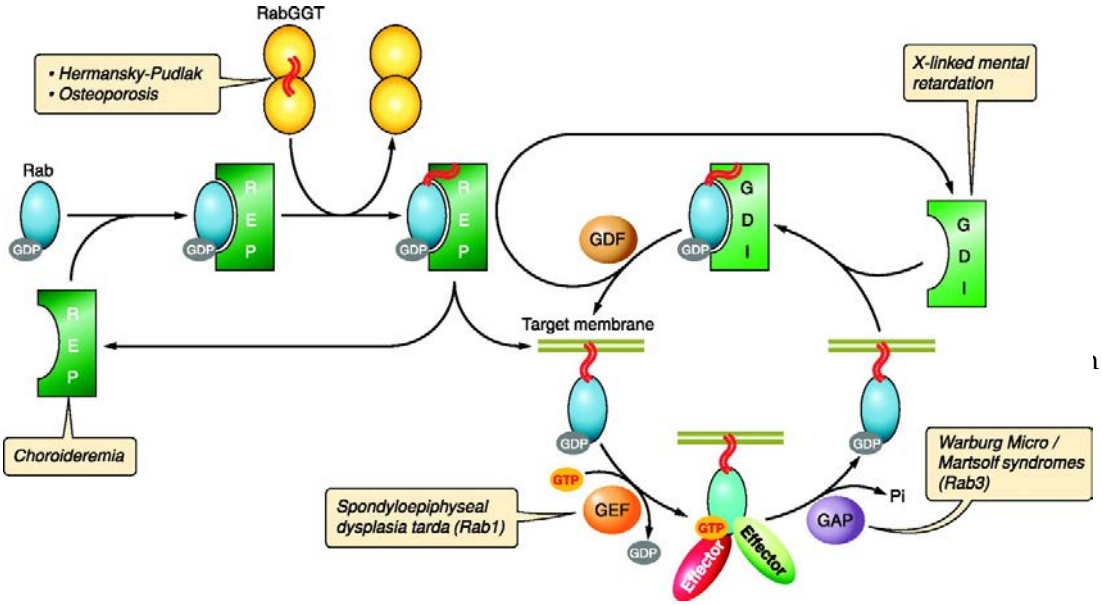

Figure 4.2 The RAB cycle. The newly synthesized RAB protein associates with RAB escort protein (REP) that then directs it to RAB geranylgeranyl transferase (RabGGT) to receive its prenyl tails (red wavy lines). REP delivers the RAB to its target membrane. Throughout this process, the RAB is GDP-bound. A guanine nucleotide exchange factor (GEF) catalyzes exchange of GDP for GTP to activate the RAB. The GTP-bound RAB interacts with effector proteins that mediate membrane traffic in the pathway regulated by its associated RAB. The RAB then interacts with its associated GTPase activating protein (GAP) that catalyzes hydrolysis of GTP to GDP by the RAB. The RAB is then removed from the membrane by guanine nucleotide dissociation inhibitor (GDI) in preparation for the next cycle. Loss-of-function mutations at each of the above steps produce disease phenotypes as indicated by the yellow text boxes [89].

4.1.3 Downstream effectors and related functions

RAB GTPases are key determinants in all steps of membrane transport because of their capacity in recruiting a wide range of diverse effectors. Figure 4.3 illustrates the main classes of RAB effectors and their role in RAB-mediated processes. To date, more than 300 RAB effectors have been identified and the list still keeps getting longer [89]. Below, I provide some examples of several well-studied RAB:RAB effector couples in regulating cargo selection, uncoating, motility, tethering and fusion.

Cargo selection. Transport from one compartment to the other is thought to be regulated by vesicular cargoes which are selectively formed by the assembly of coat protein complexes at donor membrane. For example, clathrin, AP2 and dynamin are involved in clathrin-dependent endocytosis; coatomer protein type I (COPI) is involved in membrane trafficking between ER and the Golgi apparatus. Along with coat proteins in cargo selection, RAB proteins also contribute to ensuring the recruitment of specific coat machinery to distinct membrane. The role of RAB9 in the transport of mannose-6-phosphate receptors (M6PRs) is a good example [118]. M6PRs function as

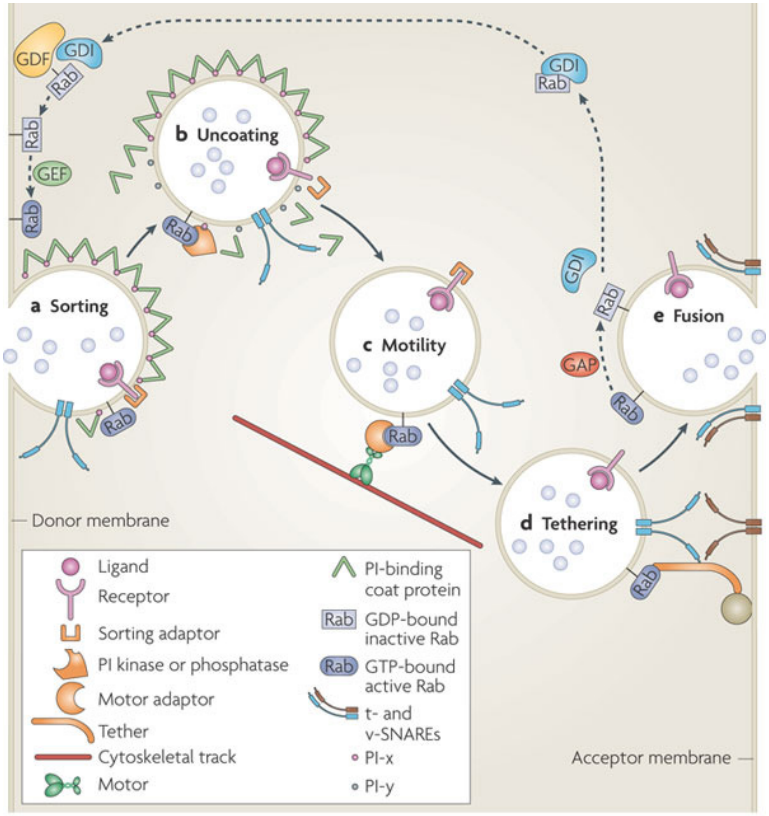

Figure 4.3 RAB GTPases functions in vesicle trafficking. Distinct membrane trafficking steps that can be controlled by a RAB GTPase and its effectors (indicated in orange). **a.** An active GTP-bound RAB can activate a sorting adaptor to sort a receptor into a budding vesicle. **b.** Through recruitment of phosphoinositide (PI) kinases or phosphatases, the PI composition of a transport vesicle might be altered (the conversion of PI-x into PI-y) and thereby cause uncoating through the dissociation of PI-binding coat proteins. **c.** RAB GTPases can mediate vesicle transport along actin filaments or microtubules (collectively referred to as cytoskeletal tracts) by recruiting motor adaptors or by binding directly to motors (not shown). **d.** RAB GTPases can mediate vesicle tethering by recruiting rod-shaped tethering factors that interact with molecules in the acceptor membrane. Such factors might interact with SNAREs and their regulators to activate SNARE complex formation, which results in membrane fusion. **e.** Following membrane fusion and exocytosis, the RAB GTPase is converted to its inactive GDP-bound form and comes back to the donor membrane [197].

carriers to deliver newly synthesized lysosomal enzymes from TGN to the lysosome. Thus, M6PRs are mainly transported from Golgi to early endosomes then to either the cell surface or late endosomes, then it is required to be recycled back to TGN for a new cycle. RAB9 which generally resides on late endosomes, functions in this retrograde transport of M6PRs. RAB9:GDI is first recruited from the cytosol onto late endosome membranes where it is activated by a GEF. RAB9 effector, Tail interacting protein of 47kDa (TIF47), is then recruited onto the membrane by activated RAB9. RAB9:TIP47 complexes then bind to the C-terminal of M6PRs that creates a specific and stable microdomain. Therefore, RAB9 enables the formation of nascent M6PR vesicles ready to bud from late endosome [118].

Vesicle uncoating. Intracellular trafficking mainly relies on the formation of coated vesicle from donor membranes. These coats must be shed before the vesicles reach their target membranes. RAB5 has been shown not only to be necessary for the formation of clathrin-coated vesicles but also for the subsequent uncoating process. Once the clathrin-coated vesicles are formed from donor membrane, RAB5 is activated by hRME-6 and binds to AP2. This association of RAB5 and AP2 displaces μ2 kinase from AP2. The μ2 subunit of AP2 complex is consequently dephosphorylated and the level of PIP2 on the vesicles decreases. In addition, RAB5 can also recruit phosphoinositide 3 kinases or phosphoinositol phosphatases for the turnover of PIP2 [185].

Vesicle motility. Actin cytoskeleton and microtubules are essential actors in intracellular vesicle motility. Actin cytoskeleton serves as tracks for vesicle motility via molecular motors of the myosin family. The transport vesicles can also move along microtubules toward the cell interior or the cell periphery via the interaction with the dynein-dynactin complex or kinesins, respectively. Many studies have revealed the capacity of RAB proteins to recruit molecular motors on transport vesicles. Of note, a given RAB can interact with several motors, as exemplified in the case of RAB11A.

RAB11A is a member of the RAB11 family that includes three proteins (RAB11A, RAB11B, RAB25) encoded by three distinct genes. These proteins are implicated in the recycling process of many cell surface receptors and in cytokinesis [100]. RAB11A recruits RAB11 family-interacting protein 2 (RAB11FIP2) which serves as an adaptor for Myosin Vb (MYO5B) [112]. Another studies indicates that MYO5B can directly bind to RAB11A in the endocytic recycling pathway [172]. Recently, Delavoye et al [44] reported that active GTP-bound form of RAB11A binds to microtubule motor KIF13A to regulate peripheral transport of recycling endosome tubules. I come back to this family in further detail in the section 4.2.

Vesicle tethering and fusion. To ensure the fidelity of membrane transport, the recruitment of tethering and fusion factors is essential. Fusion is mediated by the proteins of the SNARE family and RABs are involved in the recruitment of many tethering complexes that dock transport vesicles to their target membranes. For example, the RAB5 machinery has been shown to function in efficient fusion from endocytic vesicles to early endosomes as well as in clustering early endosomes together [37, 174, 149]. Rabaptin-5-Rabex-5, Early endosome antigen 1 (EEA1), Rabenosyn-5 and hVPS34-PI3KR4 are essential effectors for the functional RAB5 machinery. Rabex-5, a RAB5

GEF, forms a tight physical complex with Rabaptin-5, a RAB5 effector to activate and stabilize the active state of RAB5. Active RAB5 (GTP-bound) in turn recruits Early endosome antigen 1 (EEA1) and Rabenosyn-5. These RAB5 effectors contain at the C-terminus a RAB 5 binding domain (R5BD); and a FYVE domain, a conserved phosphotidylinositol 3-phosphate (PI3P) binding motif. Interestingly, EEA1 plays a role in membrane docking thanks to another R5BD at its N-terminus that allows its interaction with another RAB5-GTP on fusion membranes. EEA1 and Rabenosyn-5 are important for the coordination of tethering and fusion. On one hand, Rabenosyn-5 directly interacts with vacuolar protein sorting-associated protein 45 (VPS45), a SNARE regulator. On the other hand, EEA1 and Rabenosyn-5 directly interact with early endosomal SNAREs including Syntaxin 13 and Syntaxin 6. Moreover, RAB5 recruits a PI-3-OH kinase VPS34 and PI(4)- and (5)-phosphatases to ensure the production of PI(3)P [37].

4.1.4
RAB GTPases and diseases

Since RAB GTPases play an important role in membrane trafficking, these proteins and effectors have been reported to be associated with many diseases including infectious diseases, inherited disorders and cancers. For example, *Helicobacter pylori* secretes a toxin that sequesters RAB7 and creates a protective niche for intracellular survival of the bacterium. Mutations in RAB7 are associated with neuropathies such as Charcot-Marie-Tooth disease type 2B. RAB25 is found dysregulated in many cancers such as breast cancer and ovarian cancer. An extensive review about the roles of GTPases in diseases can be found in [197] and particularly those in cancer [38]. A systematic analysis in bladder cancer was performed in our laboratories to investigate the deregulation of expression of 61 *RAB* genes and 223 genes encoding RAB-interacting proteins [86].

4.2
The RAB11 subfamily

Below, I review our current understanding of the RAB11 family, which is involved in membrane trafficking of a wide range of receptors and identified as a key player in many human disorders.

The three members of the RAB11 (RAB11A, RAB11B and RAB25) share a high sequence homology (RAB11A:RAB11B, 91% identity; RAB11A:RAB25, 62% identity; RAB11B:RAB25, 61% identity). Of note, RAB25 contains WDTAGLE motif, instead of WDTAGQE, which results in a dominant active phenotype [69]. RAB11 proteins serve as regulators in recycling trafficking of many cell surface receptors and for endosomal membrane transport during cytokinesis [100, 178].

4.2.1
Localization and functions

RAB11A is ubiquitously expressed and predominantly localized to the pericentriolar ERC. RAB11A was identified as the first small GTPase implicated in slow endo-

cytic recycling pathway of transferrin through ERC [214]. From this discovery, many studies have revealed the role of RAB11A in the recycling pathway of a wide range of receptors, for example, $\alpha 5\beta 1$ integrin, Langerin and FGFR4 [221]. Depletion of RAB11A results in the accumulation of receptors in pericentriolar transferrin-positive ERC [162, 64, 81]. RAB11A also colocalizes with TGN38, a *trans*-Golgi network (TGN) resident protein, and regulates transport from endosomes back to the TGN [226]. RAB11A is also involved in other physiological process such as cytokinesis [166] and long-term potentiation [221].

RAB11B was subsequently identified [108] and was also shown to localize to the ERC and essential for the efficient recycling of transferrin [179]. However, a number of reports have indicated that RAB11B plays a distinct role compared to RAB11A in the endocytic recycling pathway. In rabbit gastric parietal cells or MDCK cells, RAB11B localizes to cellular compartments distinct from RAB11A [111]. RAB11A and RAB11B were suggested to function at overlapping but also in different steps of the recycling pathway of FGFR4 [81]. Recently, RAB11B but not RAB11A has been shown to be a key regulator of recycling of protease-activated receptor-1 (PAR1) [75]. The authors proposed a model for the differential regulation of PAR constitutive recycling and basal degradation by RAB11B and RAB11A (Figure 4.4).

RAB25 was initially found to be expressed in epithelial tissue [24] and to colocalize with RAB11A in an apical pericentriolar endosomal compartment. The association of RAB25 and RAB11A with the apical recycling system is required to regulate transcytotic pathways in polarized epithelial MDCK cells [24]. Interestingly, in cultured A2780 cells highly expressing CLIC3, a late endosomal/lysosomal protein, RAB25 was found to localize not only to recycling endosomes but also to a CLIC3-positive late endosomal population [48]. The localization of RAB25 in these cells is distinct from RAB11/transferrin endosomes. Indeed, RAB25 helps active integrins to escape the degradation pathway and transport back to the plasma membrane. This process is shown to be required for effective cell invasion. Accordingly, RAB25 and CLIC3 were both shown to be associated with aggressive cancers.

4.2.2 RAB11 motor protein complexes

To execute its functions in recycling trafficking or cytokinesis, RAB11 recruits distinct motor adaptors. RAB11 forms complexes with myosin for actin-filament-dependent transport or kinesins and dynein for bidirectional movement along microtubule tracks. Here, I introduce some studies investigating the role of RAB11 complexes in endosomal recycling of receptors. The role of RAB11 in cytokinesis can be found elsewhere [178, 165].

To unravel the molecular mechanisms underlying RAB11-dependent membrane transport, many approaches have been developed. By yeast two-hybrid screening, three members of the RAB11 subfamily were identified to interact with the C-terminus of myosin Vb (MYO5B) tail [112]. Proteomic screenings then allowed identifying an evolutionarily conserved family of RAB11-effectors which have been termed the RAB11 family-interacting protein (RAB11FIP) [100]. The RAB11FIPs (or FIPs) share a common C-terminal domain that interacts with RAB11, the so-called the RAB11-binding

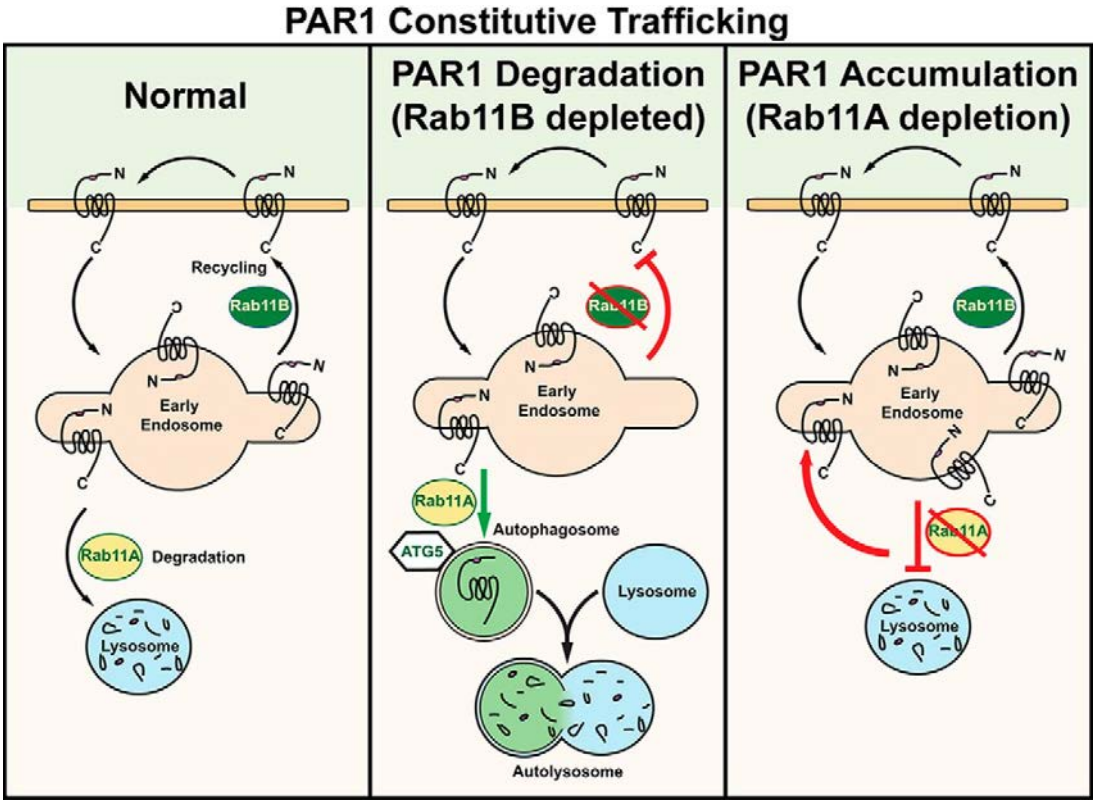

Figure 4.4 Differential regulation of PAR1 constitutive recycling and basal degradation by RAB11A and RAB11B. Unactivated PAR1 is constitutively internalized and recycled back to the cell surface through a RAB11B-dependent pathway, whereas RAB11A regulates basal lysosomal degradation of PAR1 (left panel). In the absence of RAB11A expression (right panel), PAR1 constitutively internalizes, and a marked increase in receptor accumulation in early endosomes is observed, as basal degradation of PAR1 is inhibited. Interestingly, in the absence of RAB11B expression (middle panel), PAR1 exhibits enhanced basal degradation that is blocked by RAB11A and ATG5 depletion, suggesting that the receptor traffics through an autophagic pathway before degradation in the autolysosome. These findings suggest that RAB11B and RAB11A serve distinct functions and regulate PAR1 recycling or basal degradation, respectively [75].

domain.

The best-studied RAB11-FIPs-motor protein complex is the RAB11-FIP2-MYO5B which has been implicated in a wide range of endosomal recycling processes. RAB11 interacts directly with the MYO5B globular tail domain, while the C-terminal MYO5B sequences interact with FIP2. MYO5B and FIP2 recognize the same binding area of GTP-bound RAB11A [224]. An interaction model has been proposed in which FIP2 dimerization and MYO5B dimerization require four available RAB11-GTP to form the tripartite RAB11-FIP2-MYO5B complex (Figure 4.5). Temporal and spatial characterization of the dynamic processes of the recycling pathway mediated by the RAB11-FIP2-MYO5B complex has been addressed in the work of Gidon and colleagues [64]. The authors performed a combination of high resolution imaging techniques to investigate the recycling pathways of langerin, a C-type lectin receptor which is constitutively endocytosed and recycled. A working model has been proposed in which the formation of RAB11A and FIP2 is required to sort langerin toward the late steps of the recycling pathway. MYO5B then interacts with RAB11A which provides part of the force required to generate transport recycling vesicles (Figure 4.6).

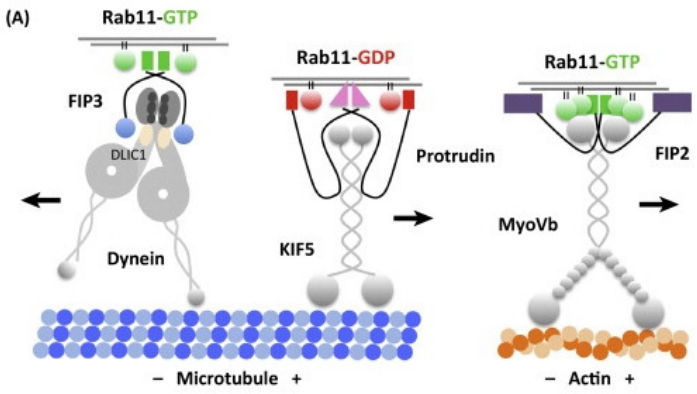

Figure 4.5 Diversity of RAB11 motor protein complexes. RAB11–GTP (green sphere) forms a complex with the microtubule minus-end directed dynein motor protein complex. The interaction is mediated by the interaction of the FIP3 adaptor protein with the DLIC1. The RAB11/protrudin/KIF5 complex represents a RAB11 microtubule plus-end directed motor protein complex. Of note is the adaptor protein protrudin, which belongs to the FYVE zinc finger family of membrane binding proteins; it interacts with RAB11 in its GDP bound form (RAB11–GDP, red sphere). The RAB11-GTP/FIP2/MyoVb complex allows RAB11 vesicles to slide along actin filaments. The unconventional MyoVb actin motor protein interacts directly with both the FIP2 adaptor and the RAB11 protein [224].

In addition to MYO5B, the microtubule-based motor kinesin KIF13A has been recently shown to interact with active GTP-bound forms of RAB11 proteins [44] in yeast two-hybrid and Förster resonance energy transfer (FRET) and fluorescence lifetime imaging microscopy (FLIM) experiments. The overexpression of KIF13A induced a dramatic tubulation of RAB11A- and FIP1-positive compartments. Conversely, depletion of KIF13A leads to the accumulation of large transferrin-positive structures and reduces the number of transferrin containing tubules, that results in the decrease of recycled transferrin. Altogether, these results indicate that KIF13A is required to generate recycling endosomal tubules along microtubule tracks from the vacuolar sorting endosomes. This process is also dependent on RAB11 since in RAB11-depleted cells, KIF13A-positive recycling compartment tubules were significantly decreased compared to control [44].

4.2.3 RAB11 subfamily in cancer

Given the physiological importance of RAB11 proteins and their effectors in membrane trafficking of many receptors, it is found that this subfamily is associated with many cancers. For example, RAB11FIP1 acts as a negative regulator in ErbB2-mediated mammary tumor progression [17]. RAB11FIP3 regulates breast cancer cell motility by modulating the actin cytoskeleton [91]. In particular, there is growing attention toward RAB25 owing to its appearance in a number of cancer screens in different studies (Table 4.1). Here, I outline the current knowledge regarding to the implication of RAB25 in several hallmarks of cancer and its mechanism of action underlying this relationship.

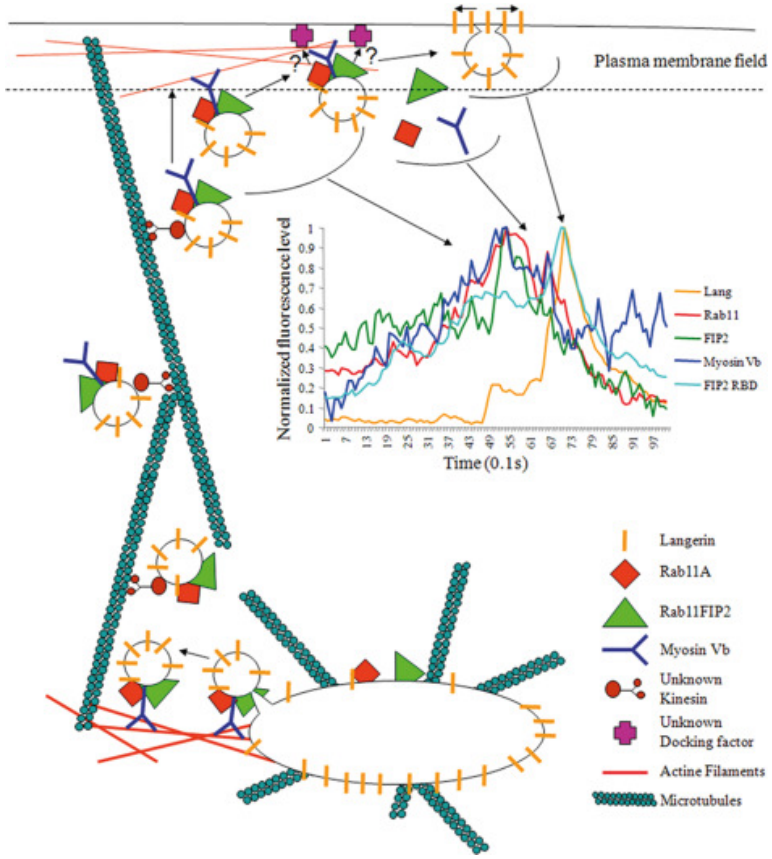

Figure 4.6 RAB11A/RAB11-FIP2/MYO5B at the level of the recycling endosomes of langerin. Working model for chronological events implicated in the recycling of langerin, from recycling endosomes to the plasma membrane. TIRF temporal characterizations of molecular events that lead to the docking/fusion at the plasma membrane of the recycling vesicles bearing langerin, are summarized in the graphs. Curves represent the average of normalized fluorescence levels in a specific region of the plasma membrane where a double fluorescent vesicle is detected, for each time point after temporal registration based on the langerin maximum fluorescence level for normalization (Lang-RAB11A n = 15, Lang-RAB11-FIP2 n = 12 and Lang-RAB11-FIP2RBD n = 13) or on RAB11A maximum fluorescence level for RAB11A-Myosin Vb and RAB11A-RAB11-FIP2 conditions (n = 10 and 12, respectively). Around 40 frames before and 40 frames after the temporal occurrence of these maximums, are then considered for both fluorescence channels in order to obtain values close to baseline of fluorescence intensities and are plotted here [64].

Expression of RAB25 in human cancers. RAB25 was shown for the first time to be upregulated in breast and ovarian cancers in the work of Mills and colleagues [31]. Since then, dysregulated expression of RAB25 has been reported in a range of human cancers, summarized in the Table 4.1. Strikingly, elevated expression of this GTPase was reported in estrogen receptor- and HE2-positive breast cancers but an apparent loss of expression was observed in ER-negative and progesterone receptor-negative tumors [31, 29, 3]. This suggests that RAB25 may play different roles in cancers, depending on the subtype.

Table 4.1 A summary of RAB25 with dysregulated expression level in human cancers

Cancer	Expression level	References
Ovarian cancer	Upregulated	[31, 56, 26, 183]
ER-positive breast cancer	Upregulated	[31, 48]
Triple-negative breast cancer	Downregulated	[29, 30]
Head and neck cancer squamous cell carcinoma	Downregulated	[207, 5]
Prostate cancer	Upregulated	[20]
Mullerian serous carcinoma	Upregulated	[19]
Colorectal cancer	Downregulated	[68]
Hepatocellular carcinoma	Upregulated	[62]

RAB25 in cell proliferation and apoptosis. The overexpression of RAB25 in ovarian cancer cells results in cell transformation *in vitro* and increases aggressiveness of cancer cells *in vivo* [31]. Conversely, downregulation of RAB25 by siRNA or short hairpin RNA (shRNA) inhibits cell proliferation, increases apoptosis *in vitro* and decreases tumor growth *in vivo* xenograft models [31, 56]. In contrast, in basal- and triple-negative breast tumor representing cells, expression of RAB25 decreased cell transformation properties including proliferation and anchorage-independent growth, and reduces tumor growth of xenografted breast carcinoma cells in nude mice [29, 30]. The mechanism of action of RAB25 in cell proliferation and apoptosis remains however poorly understood.

RAB25 in cell migration and invasion. RAB25 was identified as a component of the invasive and metastatic signature of breast cancer cells *in vivo* and *in vitro* [220]. The mechanisms by which RAB25 promotes invasive migration and tumor aggressiveness were extensively reported in the studies of the Norman group [26, 25, 48]. RAB25 stably expressing cells display a significant increase in $\alpha5\beta1$ integrin-dependent migration in 3D matrices containing fibronectin. An association between RAB25 and $\beta1$ integrin can be detected within invading pseudopodia. In addition, using cells expressing photoactivable paGFP-$\alpha5$ integrin and Cherry-RAB25 in combination with time-lapse microscopy, Norman and colleagues have demonstrated that the pool of $\alpha5\beta1$ integrin at RAB25 vesicles is highly dynamic, and continuously delivered to the plasma membrane at pseudopodial tips. Interestingly, elevated expression of RAB25 leads to the retention of a pool of integrin at the pseudopodial tips [26]. Subsequent study has revealed that increased recycling of $\alpha5\beta1$ integrin also requires the presence of RAB11FIP1 at the tips of invading pseudopods [25]. In a recent work of the same

group, RAB25 was shown, in coordination with CLIC3, to promote the recycling of integrins from late endosomes/lysosomes to the plasma membrane. They proposed that in tumors lacking CLIC3, RAB25 will sort active integrins to lysosomes, thus attenuating integrin signaling. Conversely, in tumors with upregulated RAB25 and CLIC3, active integrins escape the degradation pathway and recycle back to the plasma membrane, thus enabling their signaling to drive tumor progression [48]. Taken together, these results revealed that RAB25 contributes to the tumorigenesis by promoting the trafficking of integrins, key players in tumor invasion and metastasis.

When cancer cells invade in hypoxic 3D environments, they adapt to generate energy in oxygen independent ways and they express a range of genes involved in angiogenesis, cell survival, invasion and tumor progression, genes that are mostly regulated by the hypoxia inducible factors (HIF-1α and 1β). In hypoxic conditions, HIF-1α enters the nucleus, binds to HIF-1β and triggers the expression of HIF1 target genes [71]. Ovarian cancer cell lines stably expressing RAB25 induce, in an oxygen-independent way, the expresion of HIF-1α which is found located in the nucleus. This HIF-1α induction by RAB25 was proposed to occur via ErbB2 regulation as well as ERK1/2 and mTOR signaling pathways.

RAB25 and chemotherapy-resistance. RAB25 was identified in an ovarian cancer subgroup resistant to chemotherapy [31, 71]. In addition, it is suggested that chemoresistance induced by RAB25 is through HIF-1-dependent activation [71].

II.

Objectives

5 Objectives

Bladder cancer is a major health issue worldwide that causes a considerable morbidity, mortality and overall health care costs due to frequent recurrences and ineffective therapeutics. It is, therefore, essential to better understand the molecular mechanisms underlying bladder tumorigenesis to develop targeted therapies. FGFR3 is a promising candidate owing to the fact that FGFR3 alteration has been identified as one of the most frequent events in bladder cancer, in particular in non-invasive tumors. FGFR3 is frequently activated by point mutation, translocation and overexpression. Although aberrant FGFR3s display oncogenic properties in bladder cancer, it remains partly characterized how FGFR3 activates the downstream signaling pathways, and whether there is a difference in the downstream signaling induced by the different aberrant forms of FGFR3.

As shown in Chapter 3, numerous evidence supports the view that trafficking of a receptor tyrosine kinase may affect its signaling. To our knowledge, no study has addressed the relationship between FGFR3 trafficking and signaling in the context of cancer, and in particular of bladder cancer. RAB25, along with closely related RAB11A and RAB11B known as key players of endocytic recycling process, is found to be upregulated or downregulated in a number of cancer screens in different studies. In addition, depending on the context, RAB25 has been found to display either protumorigenic or tumor suppressor properties. Gene expression data obtained in our laboratory or from a publicly available source indicate that *RAB25* expression is significant higher in bladder tumors associated with altered FGFR3 compared to tumors without FGFR3 alterations. This suggests that RAB25 can play a protumorigenic role in tumors carrying altered FGFR3, potentially through an effect on the trafficking of the receptor.

The Thesis project aims to investigate the role of endocytosis/endocytic recycling of FGFR3 in its signaling during bladder tumorigenesis.

Specific objectives were designed:

1. Elucidate the role of RAB25, RAB11A, RAB11B and two of their effectors, RAB11FIP2 and MYO5B, in bladder cancer cells presenting FGFR3 alterations.

2. Compare the trafficking and signaling of wild type and mutant S249C forms of FGFR3, and study the role of RAB11 and RAB25 in these processes.

3. Identify interaction partners of FGFR3 by mass spectrometry.

This page intentionally left blank.

III.

Results

Roles of RAB25/RAB11, RAB11FIP2, MYO5B in bladder cancer

6

6.1 Introduction

FGFR3 along with closely related FGFR1, FGFR2 and FGFR4 constitute a subfamily of the receptor tyrosine kinase (RTK) family [117]. FGFR3 has three extracellular Immunoglobulin-like domains (I, II, III), a single transmembrane domain and an intracellular domain that contains a split tyrosine kinase domain. The alternative splicing of the third Immunoglobulin-like domain produces 2 isoforms of FGFR3 (FGFR3b and FGFR3c). FGFR3b is mainly expressed in epithelial cell populations while the FGFR3c isoform is present in non-epithelial cells [150]. FGFR3 activities promote different processes including proliferation, differentiation, survival and migration. An important remark is that the functional outcome of FGFR3 signaling depends on the cellular context. FGFR3 acts as a physiological negative regulator of skeletal growth via inhibition of chondrocyte proliferation and the activating mutations of FGFR3 enhances the inhibition of cell growth in this cell type [150]. However, the activating mutations of FGFR3, even the same point mutation, cause excessive cell proliferation in epithelial cells [124, 12].

From the first discovery of four FGFR3 mutations in bladder and cervix cancers [22], other FGFR3 mutations have been identified and these mutations were found in various types of cancer such as multiple myeloma, lung cancer, prostate cancer and melanoma [212, 28]. However, high frequency of FGFR3 mutations seem to be restricted to bladder carcinomas, 50% in non-invasive muscle tumors and 10-15% in muscle-invasive tumors [147]; and to benign epidermal tumors, such as seborrheic keratosis (40-80% of samples tested) [124, 77] as well as to epidermal nevi [77, 85]. Recently, FGFR3 translocations leading to FGFR3-gene fusions, including FGFR3-TACC3 and FGFR3-BAIAP2L1 have been identified in bladder carcinoma but also in glioblastoma and lung cancer [188, 231]. Both mutations and translocations result in constitutively activated FGFR3 that displays oncogenic properties in bladder cancer [12, 46, 227]. However, how FGFR3 activates the downstream signaling pathways remains

poorly understood. Thus, it is necessary to better understand the molecular mechanisms underlying FGFR3 signaling to develop a FGFR3-targeted therapy and treatment strategies for bladder cancer. This cancer is a major health issue worldwide that causes a considerable morbidity, mortality and overall health care costs due to frequent recurrences and ineffective therapeutics [209].

FGFRs as well as other RTKs transfer the extracellular stimuli to the cellular interior through activating several signaling cascades that finally results in physiological responses. In the classical model of signal transduction, transmembrane receptors can recruit many downstream substrates to the plasma membrane to activate signaling pathways, and endocytosis serves as receptor clearance pathway to attenuate receptor signaling. However, growing evidence supports the view that trafficking of a RTK may affect its signaling [196, 135]. To date, no study has addressed the relationship between FGFR3 trafficking and signaling in the context of cancer, and in particular of bladder cancer.

Endosomal trafficking is spatiotemporally controlled by small RAB GTPases, which constitute the largest family of small GTPases with 70 members in human [99]. The traffic of cargoes to the endocytic recycling compartment and from there to the plasma membrane is regulated by the RAB11 GTPase subfamily. This subfamily is composed of three proteins (RAB11A, RAB11B, RAB25) encoded by three distinct genes which share a high sequence homology [100]. RAB11 proteins serve as regulators of endocytic recycling of many cell surface receptors and of endosomal membrane transport during cytokinesis [100, 178]. To execute these functions, RAB11 proteins recruit motor adaptors directly or indirectly via RAB11 family-interacting proteins (RAB11FIPs). The best studied RAB11-RABFIPs-motor protein complex is the complex made by RAB11 with RAB11FIP2 and myosin Vb (MYO5B). This complex has been implicated in a wide range of endosomal recycling processes, for example recycling of transferrin receptor and integrins [224].

Alterations in RAB functions have been reported to be directly or indirectly responsible for many diseases, in particular, for cancers [197, 32]. Among RAB GTPases involved in cancers, RAB25 is the protein whose association with tumor progression is the best known [139, 3]. Depending on the cellular context, RAB25 has been found to have either protumorigenic or tumor suppressor properties. The overexpression of RAB25 in ovarian cancer cells results in cell transformation *in vitro* and increases aggressiveness of cancer cells *in vivo* [31, 56]. In contrast, in basal- and triple-negative breast tumor cells, overexpression of RAB25 decreases cell transformation properties such as, cell proliferation and anchorage-independent growth, and reduces tumor growth of xenografted breast carcinoma cells in nude mice [29, 30]. The mechanisms underlying the role of RAB25 in cell proliferation and apoptosis remain however poorly understood. On the other hand, several works have reported that RAB25 promotes tumor invasion and metastasis by regulating the endocytic recycling of integrins [26, 48, 211].

In this study, we first determined the status of genes coding for RAB and RAB-interacting proteins in two groups of bladder cancers: tumors carrying mutated or translocated FGFR3, hereafter called altered FGFR3 tumors and tumors without these alterations, called non-altered FGFR3 tumors. Next, we investigated the role RAB25, RAB11A, RAB11B and two of their effectors, RAB11FIP2 and MYO5B, in bladder can-

cer cells carrying FGFR3 alterations by using siRNA depletion. We analyzed the effects of these depletions on cell viability, endocytic recycling, FGFR3 downstream signaling pathways and expression of FGFR3 target genes.

6.2 Results

6.2.1 RAB25 is upregulated in bladder tumos carrying altered FGFR3

In order to identify genes coding for RAB and RAB-interacting proteins associated with bladder cancer presenting alterations of FGFR3 (mutation and translocation genes), we performed a differential expression analysis by using the LIMMA method between two groups: altered FGFR3 tumors and non-altered FGFR3 tumors. The list of 270 genes coding for RAB proteins and RAB-interacting proteins was established in a previous study [86]. Two data sets were collected, one from our laboratory (HuExon dataset), constituting of 98 superficial tumors and 106 muscle invasive tumors (63 and 15 tumors carrying FGFR3 alteration, respectively), and the other from a publicly available source The Cancer Genome Atlas (TCGA dataset), consisting of 371 muscle-invasive tumors among which 50 tumors carry FGFR3 alteration. 42 genes out of 270 genes tested are differentially expressed between the two groups of altered and non-altered superficial tumors (Figure 6.1). For muscle-invasive tumors in the HuExon dataset and the TCGA dataset, we obtained 15 genes and 122 genes, respectively, differentially expressed (Figures 6.2, 6.3). The results indicated that *RAB25* expression was significantly higher in altered FGFR3 tumors compared to non-altered FGFR3 tumors (Figure 6.4.A). In superficial tumors and muscle-invasive tumors of the HuExon dataset, the fold change (FC) was 1.2 and 1.7, respectively; in invasive tumors of the TCGA dataset, the FC was 2.3. *RAB25* appeared twice as the *RAB* having the most upregulated expression in tumors presenting alterations of FGFR3 (Figures 6.1, 6.2, 6.3). Moreover, *RAB11A* and *RAB11B* are also significantly upregulated in the 50 altered-FGFR3 tumors of 371 muscle-invasive tumors of TCGA with FC of 1.5 and 1.2, respectively (Figure 6.4.B,C). On the other hand, there was no difference in the expression levels of RAB11 effectors including *RAB11FIP2* and *MYO5B* in tumors presenting or not alterations of FGFR3 (Figure 6.4.D,E). Our findings suggest that in tumors carrying altered FGFR3, the altered endocytic recycling due to the upregulation of RAB25 and RAB11 can promote bladder progression.

6.2.2 Depletion of RAB25/RAB11 proteins and their effectors inhibits cell viability of altered FGFR3 expressing cells

In order to investigate the role of *RAB25, RAB11A, RAB11B, RAB11FIP2* and *MYO5B* in bladder cancer, we examined the mRNA expression of these genes in normal human urothelium cells (NHU cells) and 6 human bladder cancer cell lines (Figure 6.5.A-E). The characteristics of these cancer cell lines is summarized in Figure 6.6. *RAB11A, RAB11B* and *RAB11FIP2* were expressed at about the same levels in the NHU cells and

superficial HuExon data set			
rank	**symbol**	**adjusted P-Value**	**Foldchange**
1	PIK3R1	0,000188947	1,539968736
2	RIMS2	0,026997051	1,474632875
3	RAB38	0,027841026	1,405831019
4	TBC1D4	0,001983594	1,401916598
5	TRAPPC1	3,13E-06	1,379190849
6	CASP1	0,000134854	1,371910077
7	SDC1	8,58E-05	1,370668009
8	SYTL1	6,28E-06	1,351344304
9	ARL6IP5	0,0041291	1,31544224
10	MADD	0,001546274	1,259644611
11	RAB13	2,50E-05	1,241570712
12	ANKFY1	0,001058843	1,234284217
13	ARHGAP1	0,012123341	1,222363577
14	RAB25	0,005958683	1,212426267
15	ATG5	0,002837457	1,202575817
16	RAB40A	0,000820313	1,196018227
17	MICAL1	0,015962224	1,195739034
18	VPS52	0,003679771	1,183041163
19	RAB3GAP1	0,0041291	1,178574247
20	RAB19	0,039223502	1,168075099
21	GCC2	0,035364187	1,164983868
22	GOPC	0,003016732	1,164557379
23	RAB4A	0,0406342	1,152543272
24	VPS11	0,028589834	1,14471658
25	VPS39	0,012902615	1,143180691
26	CEP290	0,03785452	1,127132044
27	TSC2	0,035364187	1,118595899
28	RPH3AL	0,012902615	1,116185441
29	ATG16L1	0,042029964	1,114190956
30	STX4	0,042458806	1,097606414
31	TBC1D17	0,039223502	1,092332195
32	CTBP1	0,037665171	1,091766709
33	TBC1D3B	0,0041291	1,070800851
34	GNB1	0,026313005	0,914986003
35	RAB8A	0,035364187	0,893828255
36	ITGB1	0,004543994	0,888062689
37	RAB5A	0,018640413	0,886781259
38	RAB1A	0,012329798	0,884933748
39	GNG2	0,014161156	0,879689273
40	ODF2	0,037535659	0,874997826
41	YWHAQ	0,003236383	0,869812089
42	GOLGA2	0,026869759	0,86060278

Figure 6.1 Differentially expressed genes in superficial bladder tumors from the HuExon data set. This table provides results of the differential expression analysis, performed with the LIMMA method, between superficial tumors associated with altered FGFR3 and without FGFR3 alterations from the HuExon data set. symbol, Gene symbols; adjusted P-value, adjusted p-value using Benjamini et Hochberg procedure; Foldchange, estimate the fold change tumors associated with altered FGFR3 versus without FGFR3 alterations.

invasive HuExon data set			
rank	**symbol**	**adjusted P-Value**	**Foldchange**
1	SDC1	0,000675877	2,407568583
2	PIK3R1	0,000369297	1,858906697
3	RAB25	0,036350205	1,726434901
4	RAB19	0,000968118	1,670995335
5	SYTL1	4,18372E-06	1,587077481
6	ALS2CL	0,047203843	1,578594711
7	RAB11A	0,019349988	1,338720002
8	VPS35	0,027367285	1,283480731
9	DENND1A	0,019349988	0,759125844
10	ERC1	0,019349988	0,757020264
11	LEPRE1	0,042189453	0,713209774
12	GNG2	0,008947891	0,678566508
13	MYO5A	0,024060497	0,633283592
14	MICAL2	0,032321388	0,631038863
15	STXBP1	0,006117843	0,503061626

Figure 6.2 Differentially expressed genes in invasive bladder tumors from the HuExon data set. This table provides the results of the differential expression analysis, performed with the LIMMA method, between invasive tumors associated with altered FGFR3 and without FGFR3 alterations from the HuExon data set. symbol, Gene symbols; adjusted P-value, adjusted p-value using Benjamini et Hochberg procedure; Foldchange, estimate the fold change tumors associated with altered FGFR3 versus without FGFR3 alterations.

invasive TCGA data set (1)			
rank	symbol	adjusted P-Value	Foldchange
1	SYTL1	6,03E-09	3,055054651
2	MLPH	1,26E-05	2,553810413
3	OTOF	0,001232766	2,347246647
4	RAB25	0,001714843	2,26741529
5	SDC1	0,000148969	2,250560098
6	RAB26	0,000553367	2,17754529
7	RAB15	4,75E-05	2,12548073
8	RPH3AL	6,10E-08	2,091117987
9	RAB17	0,000449901	1,930939288
10	ALS2CL	0,000128078	1,898650103
11	ICA1	0,000695707	1,754847848
12	TBC1D3B	0,000148969	1,717469353
13	RAB19	0,018729337	1,606288906
14	SYTL4	0,00019751	1,569350604
15	GAPDH	4,04E-06	1,528420871
16	RAB11A	4,75E-08	1,501377038
17	NDRG1	0,018729337	1,487005447
18	RABEP2	5,11E-05	1,455065593
19	RILP	0,000780461	1,446714548
20	CEP290	8,16E-05	1,43464028
21	RAB11FIP3	0,023901495	1,415157718
22	TRAPPC1	4,04E-06	1,410081118
23	CD2AP	0,000251303	1,405731433
24	TRAPPC5	0,000489903	1,389143502
25	MICALL2	0,001861668	1,369498084
26	RAB40C	0,000553367	1,354286464
27	RIN1	0,043337692	1,353507076
28	RAB3A	0,00986944	1,334234891
29	CTBP1	6,13E-06	1,309043196
30	TBC1D4	0,02146894	1,298624327
31	MADD	0,000106257	1,289220111

invasive TCGA data set (2)			
rank	symbol	adjusted P-Value	Foldchange
32	VPS52	4,04E-06	1,26625043
33	RAB24	0,001304836	1,261929313
34	MICALL1	0,02308131	1,245596636
35	RAB4A	0,000148969	1,240887255
36	RAB13	0,003296464	1,240673331
37	RAB4B	0,008717868	1,237667375
38	VPS33B	1,76E-05	1,234418843
39	NSF	0,003913507	1,225143933
40	TSC2	0,000148969	1,215465793
41	EVI5L	0,009116263	1,21533956
42	HPS4	0,008233756	1,211192444
43	TBC1D2B	0,007378603	1,210380785
44	RAC1	0,001113514	1,207925213
45	VPS35	0,002250204	1,207450326
46	VPS39	0,000148969	1,206983803
47	HPS1	0,004307102	1,206976517
48	TBC1D17	0,004602969	1,20274616
49	ZFYVE27	0,002873326	1,20117308
50	RAB11B	0,003513539	1,199246129
51	GAS8	0,018986795	1,188221194
52	CTNNA1	0,001364181	1,184801045
53	TRAPPC2	0,018729337	1,180216892
54	TRAPPC9	0,016600318	1,180206579
55	ARL6IP5	0,035469788	1,179433135
56	RAB5B	0,007296844	1,175571257
57	RAB10	0,018287843	1,170261497
58	VPS29	0,013538382	1,150845307
59	RUFY1	0,014504887	1,149297274
60	GRIPAP1	0,010626637	1,140050803
61	RAB1B	0,017681472	1,136838567
62	RAB21	0,044042883	1,136280054

invasive TCGA data set (3)			
rank	symbol	adjusted P-Value	Foldchange
63	GOLGA1	0,001701333	0,853984014
64	RAB33B	0,045542105	0,853249545
65	DCTN1	0,001693511	0,849958215
66	INPP5E	0,035569027	0,841118357
67	RAB14	0,001232766	0,84014812
68	ACAP2	0,007378603	0,832116946
69	MICAL3	0,031332417	0,830854052
70	ITGB1	0,015449217	0,828671019
71	WDR44	0,032857762	0,812213112
72	RABEPK	0,004532116	0,811139799
73	SMCHD1	0,016977318	0,811077214
74	RAB9A	0,008233756	0,81045821
75	DYNC1LI1	0,000239554	0,807240949
76	ZFYVE20	0,002728235	0,804838714
77	RABGAP1	0,00047591	0,798958174
78	GOLGA2	0,000148969	0,796544211
79	INPP5B	0,000539707	0,795782582
80	YWHAQ	0,001701333	0,793547178
81	RIN2	0,035547259	0,788442109
82	LEPRE1	0,023589339	0,778233245
83	PIK3CB	0,000591303	0,775232188
84	ANKRD27	0,000110252	0,743358893
85	TBXA2R	0,049139422	0,740118653
86	RNF115	7,50E-05	0,738441745
87	ODF2	1,15E-06	0,731192327
88	OSGIN2	0,000116822	0,728566905
89	BICD2	0,000541115	0,718060226
90	RAB6B	0,033459137	0,699671227
91	PRKAR2A	0,021892483	0,691717917
92	VCL	0,000211701	0,68984344
93	GAPVD1	4,83E-11	0,687028861

invasive TCGA data set (4)			
rank	symbol	adjusted P-Value	Foldchange
94	DENND1A	2,37E-07	0,659950834
95	RABGAP1L	4,75E-05	0,628380452
96	ERC1	2,08E-06	0,62087021
97	DENND5A	1,15E-06	0,613256471
98	SYTL3	0,001364181	0,603257573
99	MYO5A	0,000656026	0,594465713
100	RUSC2	0,000469632	0,593093048
101	PTGIR	0,001671952	0,576585626
102	PEX5L	0,009116263	0,574726444
103	WDR38	0,009116263	0,565596042
104	MICAL2	4,88E-05	0,561912578
105	RIMS1	0,026595181	0,551561059
106	RAB23	0,000109006	0,543862586
107	RAB3C	0,012479574	0,533856896
108	TBC1D10C	0,010903306	0,532239316
109	ITGA5	0,000576308	0,52533673
110	RAB31	0,000109006	0,517107345
111	RAB33A	8,02E-05	0,512864267
112	RAB30	1,21E-06	0,48581967
113	RAB39B	0,000823133	0,464478202
114	GNG2	3,11E-05	0,460572151
115	GNAL	0,003008379	0,459418955
116	LRRK2	0,000325562	0,415287428
117	STXBP1	2,10E-05	0,413921253
118	RAB39	0,000110276	0,408795722
119	RAB42	3,18E-07	0,404269661
120	RAB3IL1	2,38E-06	0,352730821
121	CAV1	4,04E-06	0,328798108
122	SNAP25	6,95E-07	0,23055123

Figure 6.3 Differentially expressed genes in muscle-invasive bladder tumors from the TCGA data set. This table provides the results of the differential expression analysis, performed with the LIMMA method, between superficial tumors associated with altered FGFR3 and without FGFR3 alterations from the TCGA data set. symbol, Gene symbol; adjusted P-value, adjusted p-value using Benjamini et Hochberg procedure; Foldchange, estimate the fold change tumors associated with altered FGFR3 versus without FGFR3 alterations.

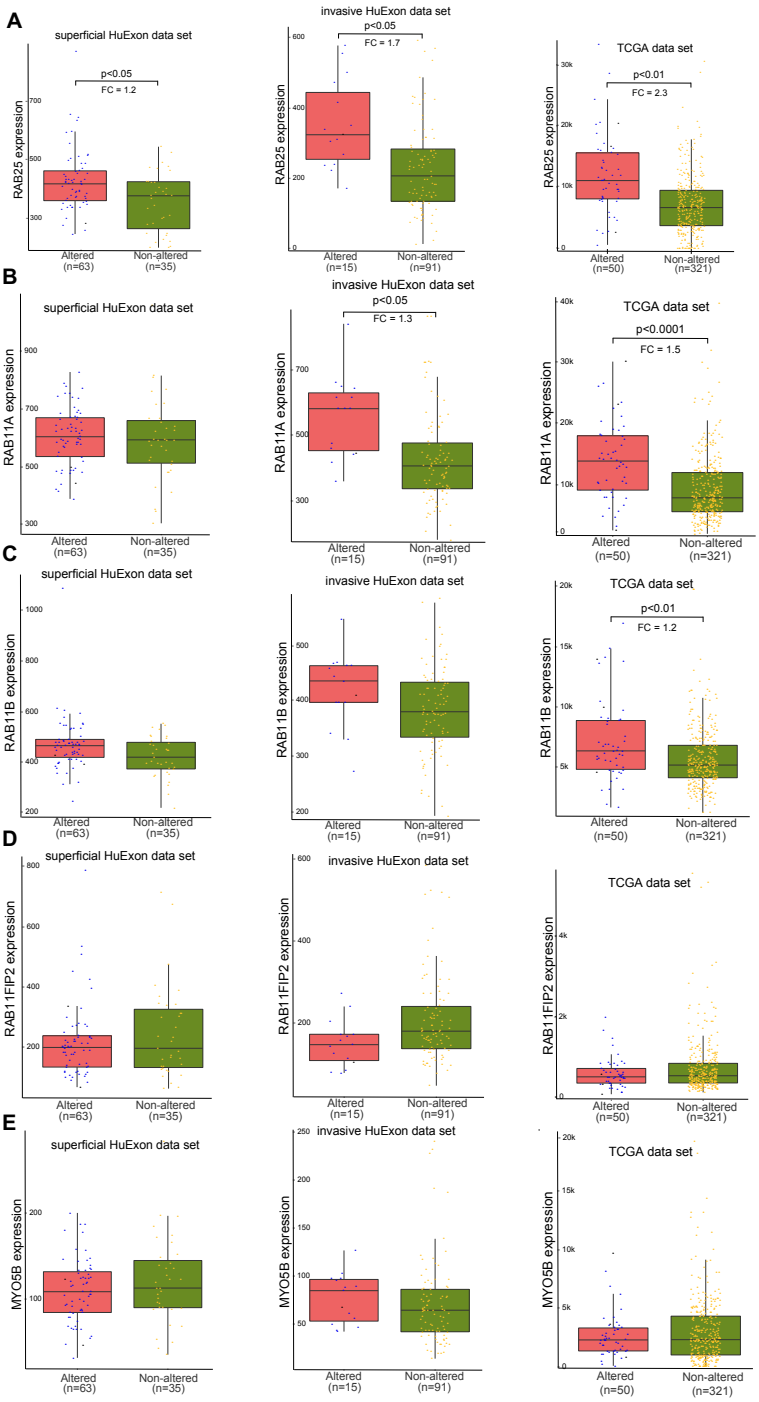

Figure 6.4 *RAB25, RAB11A, RAB11B, RAB11FIP2, MYO5B* expressions in bladder cancer. Box plots showing gene expression values of *RAB25* (A), *RAB11A* (B), *RAB11B* (C), *RAB11FIP2* (D) and *MYO5B* (E) in bladder cancer samples from microarray data set (HuExon data set) and from RNA-seq (TCGA data set) comparing tumors carrying mutated and translocated FGFR3 (Altered) and tumors with non-mutated and non-translocated of FGFR3 (Non-altered). Box plots represent the first and third quartiles and median values; whiskers represent all values from the smallest value up to the largest value. The number of samples for each group was indicated under box plots. Differential expression analysis was performed by using the LIMMA method. Left: superficial tumors from HuExon data set. Center: muscle-invasive tumors from HuExon data set. Right: muscle-invasive tumors from TCGA dataset. TCGA: The Cancer Genome Atlas; FC: fold change in gene expression of indicated gene between group of altered tumors versus group of non-altered tumors.

the cancer cell lines (Figure 6.5.B-D). Interestingly, *RAB25* and *MYO5B* mRNA levels displayed higher variability among the cell lines (Figure 6.5.A and E). Confirmed by Western blotting, the RAB25 protein level displayed variability among the cell lines tested (Figure 6.5.G). Therefore, to examine the role of these proteins in cell viability of bladder cancer cells carrying altered FGFR3, we selected two cell lines, MGHU3 and RT112 cells. Indeed, MGHU3 cells endogenously express FGFR3 with a point mutation (Y375C). RT112 cells show a high level of *FGFR3* amplification and upregulation of both wild type FGFR3 and the FGFR3-TACC3 fusion protein (Figure 6.5.F). Moreover, cell proliferation and transforming properties of these cell lines are dependent on constitutively activated FGFR3 [12, 227].

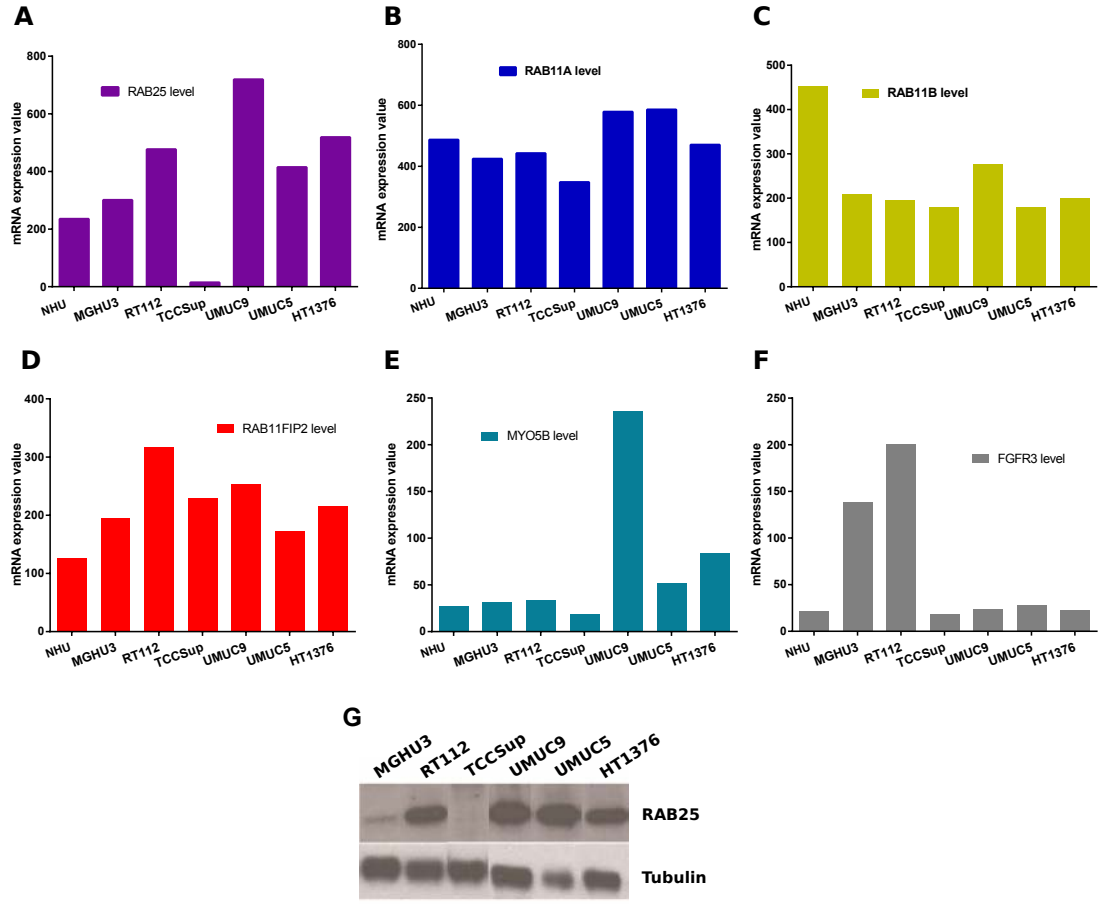

Figure 6.5 *RAB25, RAB11A, RAB11B, RAB11FIP2 and MYO5B* expressions in normal human urothelial cells and bladder cancer cell lines. Expression values from microarray data set (Affymetrix Human Exon 1.0 ST Array, RMA normalization) of *RAB25* (A), *RAB11A* (B), *RAB11B* (C), *RAB11FIP2* (D), *MYO5B* (E) and *FGFR3* (F) in normal human urothelial cells (NHU) and six bladder cancer cell lines (MGHU3, RT112, TCCSup, UMUC9, UMUC5, HT1376). (G) Protein level of RAB25 was measured by Western Blot in bladder cancer cell lines. Tubulin was used as loading control.

We first investigated the effects of RAB11A, RAB11B, RAB25, RAB11FIP2 and MYO5B depletion by siRNA on cell viability. For a given gene, we tested knockdown efficiency by RT-qPCR of three individual siRNAs targeting different sites of this gene. Then, one siRNA for each gene was selected for following experiments if the expression of target gene is reduced over 80% (data not shown). After 72h siRNA transfection, the viability

Cell lines	Classification (gene expression data)	FGFR3 alteration	FGFR3 expression	*PIK3CA*	*RAS*	Grade
HT1376	basal-like	WT	no	WT	WT	III
MGHU3	basal-like	Y375C	upregulated (low)	WT	WT	I
RT112	luminal	WT/FGFR3-TACC3	upregulated (high)	WT	WT	II
TCCSup	luminal	WT	no	E545K	WT	IV
UMUC5	basal-like	WT	no	E545K	WT	no information
UMUC9	luminal	WT	no	WT	WT	no information

Figure 6.6 Characteristics of bladder cancer cell lines used in the study.

of RT112 and MGHU3 cells was measured by MTT assays (Figure 6.7). This assay allows indirect measurement of cell viability after siRNA silencing or a drug treatment. In parallel, the efficacy of siRNAs was evaluated by RT-qPCR or Western blot depending on the availability of antibodies (Figure 6.8). Compared to cells transfected with control siRNA, in MGHU3 cells, the inhibitory effect on cell viability ranged from 50% to 70% (Figure 6.7.A). Also, the viability was reduced to ∼50% in RT112 cells with all siRNAs (Figure 6.7.B). Because RAB25, RAB11A and RAB11B share a high sequence identity [100], these proteins were simultaneously depleted by using a combination of siRNAs to test their functional redundancy (Figure 6.7.A,B). In both cell lines, the cell viability was decreased to the same level by either one or two or three siRNA against the RAB11 subfamily genes, indicating that RAB11A, RAB11B, RAB25 are necessary for the viability of RT112 and MGHU3 cells. In other words, the three members of the RAB11 subfamily have a distinct role in the cell viability.

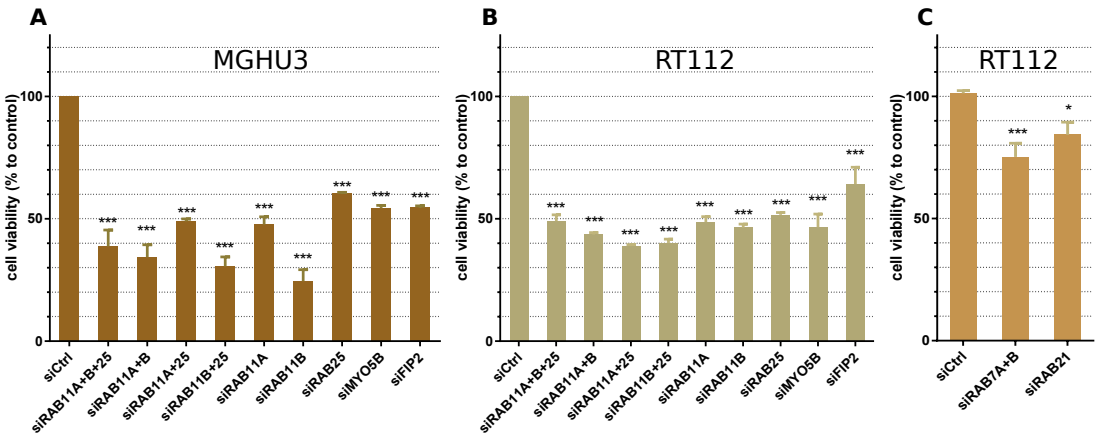

Figure 6.7 Depletion of RAB25/RAB11 and their effectors inhibits cell viability. MGHU3 cells (A) and RT112 cells (B) were transfected with different siRNA targeting *RAB11A*, *RAB11B*, *RAB25*, *RAB11FIP2* and *MYO5B*. (C) RT112 cells were transfected with different siRNA targeting *RAB7A/B* and *RAB21*. After 72h transfection, cell viability was determined by the MTT assay. Error bars, SEM from three independent experiments each performed in triplicate. t-test was performed between siRNA targeting indicated genes with control siRNA; *, $p<0.05$; **, $p<0.01$; ***, $p<0.001$.

To verify whether this effect on cell viability is specific for RAB25, RAB11A, RAB11B and their effectors RAB11FIP2 and MYO5B, we transfected RT112 cells with siRNA targeting other RAB GTPases, including RAB7A, RAB7B and RAB21. RAB7A and RAB7B localize to late endosomes and are involved in the degradation pathway [95]. RAB21 is implicated in transport events at the level of early endosomes [157]. The effects on cell viability induced by depletion of RAB7 or RAB21 was ∼20%, lower than that

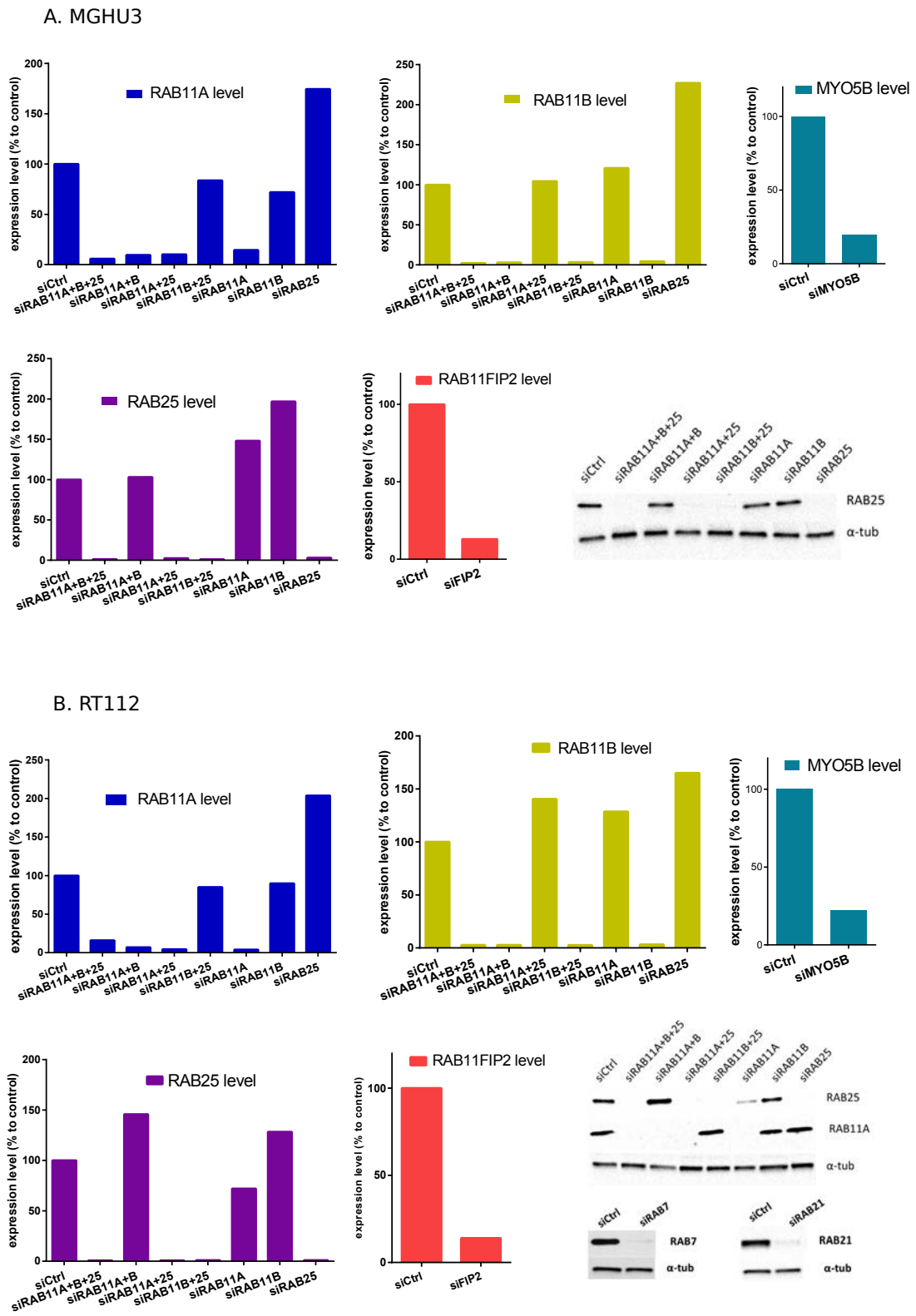

Figure 6.8 Efficiency of siRNA silencing in MGHU3 and RT112 cells. (A) In MGHU3 cells, the expression levels of *RAB11A*, *RAB11B*, *RAB25*, *RAB11FIP2* and *MYO5B* after 72h siRNA transfection were verified by RT-qPCR. Western Blot analysis confirmed the efficiency of siRNA targeting *RAB25*. (B) In RT112 cells, the expression levels of *RAB11A*, *RAB11B*, *RAB25*, *RAB11FIP2 and MYO5B* after 72h siRNA transfection were verified by RT-qPCR; and Western blotting confirmed the efficiency of siRNA targeting *RAB25*, *RAB11A*, *RAB21 and RAB7A/B*. In RT-qPCR, target gene expressions were normalized to *TBP* level. Tubulin (α-tub) was used as loading control in Western Blot analysis. The figure is representative data from one of three independent experiments.

observed after depletion of members of the RAB11 subfamily (Figure 6.7.C). Taken together, these results suggest that altering the endocytic recycling results in the inhibition of cell viability of cells displaying alterations of FGFR3.

To determine whether this effect is specific to bladder cancer cells expressing FGFR3 or more general in different subgroups of bladder cancers, we next repeated the depletion experiments in several bladder cancer cell lines, including TCCSup, UMUC9, UMUC5 and HT1376 cell lines (Figure 6.9). These cell lines do not express FGFR3 (Figure 6.5.F). Knockdown efficiency was confirmed by RT-qPCR or Western blot (Figure 6.10). In these cell lines, the RAB11/RAB25 or MYO5B depletion had no effect or induced a lower inhibition in cell viability than in RT112 and MGHU3 cells (Figure 6.9). Of note, the siRNA targeting RAB11B had an important effect on HT1376 (~80%), therefore, we examined this effect with another siRNA targeting *RAB11B*. The inhibition of cell viability was less important (20%) (data not shown), suggesting that the first siRNA targeting *RAB11B* had an off-target in HT1376 cells. Taken together, these findings suggest that the inhibition of cell viability induced by the depletion of RAB11/RAB25 and their effectors is specific in bladder cancer cells presenting alterations of FGFR3.

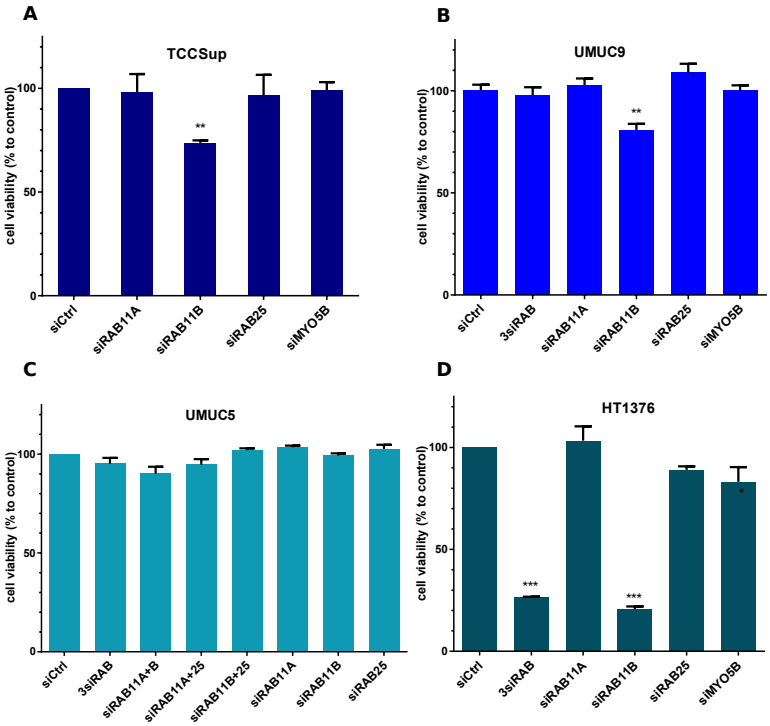

Figure 6.9 Cell viability after depletion of RAB25/RAB11 and their effectors in other bladder cancer cell lines. TCCSup (A), UMUC9 (B), UMUC5 (C), HT1376 (D) cells were transfected with control siRNA or other indicated siRNAs. After 72h transfection, cell viability was determined by the MTT assay. Error bars, SEM from 2-3 independent experiments each performed in triplicate. t-test was performed between siRNA targeting indicated genes with control siRNA; *, $p<0.05$; **, $p<0.01$, ***, $p<0.001$.

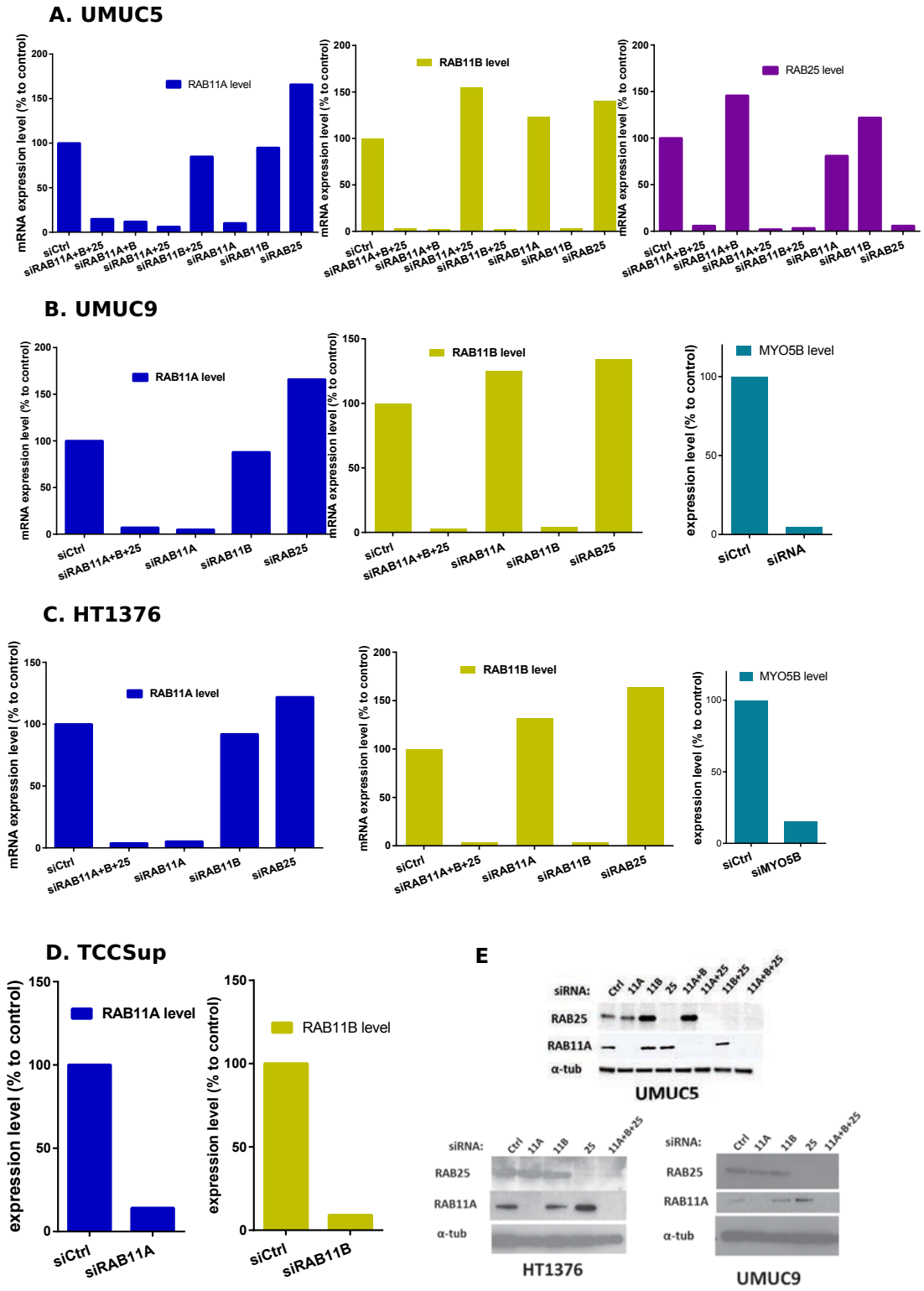

Figure 6.10 Efficiency of siRNA silencing in bladder cancer cell lines. Expression levels of target genes after 72h transfection with indicated siRNA were verified by RT-qPCR in UMUC5 cells (A), UMUC9 (B), HT1376 (C) and TCCSup(D). (E) Western Blot analysis using anti-RAB25 and anti-RAB11A confirms the efficiency of knockdown in UMUC5 (top), HT1376 (bottom left) and UMUC9 (bottom right). In RT-qPCR, target gene expressions were normalized to *TBP* levels. Tubulin (α-tub) was used as loading control in Western Blot analysis. The figure is representative data from one experiment.

6.2.3

Effects on cell viability of a combination of RAB11/RAB25 depletion with FGFR3 depletion or treatment with a FGFR inhibitor

Altered FGFR3 has been shown to display oncogenic properties in bladder cancer cells *in vitro* and *in vivo* [12, 46, 227]. Indeed, previous studies from our laboratory revealed that knockdown of FGFR3 in RT112 and MGHU3 cells inhibited cell viability. We therefore wanted to determine whether the impact on cell viability of RAB25/RAB11 silencing reflects the role of FGFR3 in these cell lines. We transfected RT112 cells with a cocktail of siRNAs targeting FGFR3 and RAB25/RAB11. In cells transfected with only siRNA against FGFR3, the effect on cell viability was ~80%, a value higher than that obtained following RAB25/RAB11 or MYO5B depletion (50% or 40%, respectively) (Figure 6.11.A). Of note, the simultaneous depletion of FGFR3 with either RAB25/RAB11 or MYO5B has the same effect (80% inhibition) compared to the depletion of FGFR3 alone. In parallel, we treated RT112 cells depleted for RAB25/RAB11 with either a FGFR inhibitor PD173074 (0.5 μM) or DMSO (0.1%) as control for 24h. The treatment with the FGFR inhibitor induced a dramatic reduction in cell viability and the number of surviving cells were about the same in RAB11/RAB25-depleted cells treated with the FGFR inhibitor (Figure 6.11.B). These results indicate that the depletion of RAB11/RAB25 is not sufficient to induce an effect on cell viability as important as FGFR3 depletion does. The inhibition of RAB25/RAB11 or MYO5B however does not have an additive effect on the inhibition of cell viability by either a siRNA targeting *FGFR3* or a tyrosine kinase inhibitor, suggesting that RAB25/RAB11 proteins could be involved in FGFR3 signaling. On the other hand, it is possible that the complex of endocytic recycling and FGFR3 signaling represent two separate pathways that are both required for cell viability.

6.2.4

FGFR3 localizes to TFRC-, RAB25- and RAB11A-positive vesicles

To date, the cellular localization of FGFR3 has not been characterized in the context of bladder cancer. We therefore addressed this question by using RT112 cells transiently expressing FGFR3-GFP due to the lack of antibodies specifically recognizing endogenous FGFR3 by immunofluorescence staining. We generated the C-terminal GFP tagged FGFR3 for the wild type form (FGFR3-GFP). FGFR3-GFP was shown by co-immunoprecipitation to interact with HSP90, a well-known partner of FGFR3 [107], suggesting that FGFR3-GFP is fully functional in RT112 cells (data not shown). 24h after transfection, RT112 cells were fixed and the subcellular distribution of FGFR3 was analyzed using 3D deconvolution microscopy. FGFR3 displayed a characteristic punctuate, vesicular pattern throughout the cytoplasm (Figure 6.12.B). Fluorescent signal was weakly detected on the plasma membrane probably due to limitations of widefield light microscopy.

We then used various antibodies against marker proteins of endosomal compartments, including anti-TFRC (transferrin receptor), anti-EEA1, anti-LAMP1, anti-CD63 and anti-RAB25 to further identify the nature of FGFR3 punctuate structures (Figure 6.12.A). No difference in the subcellular localization of these markers was observed between non-transfected RT112 cells and cells transfected with FGFR3-GFP (data not

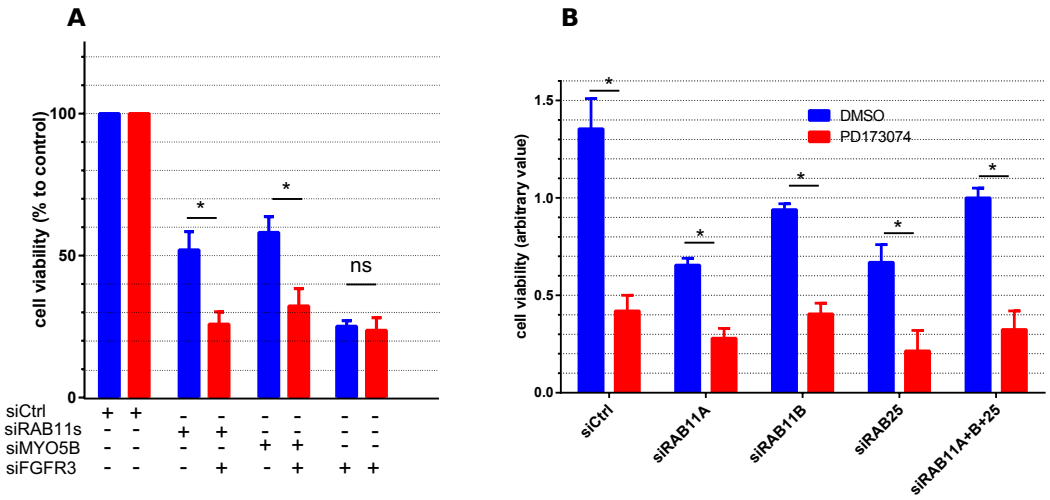

Figure 6.11 Effects on cell viability of a combination of RAB11/RAB25 depletion with FGFR3 depletion or treatment of FGFR inhibitor. (A) RT112 cells were transfected with different siRNA targeting indicated genes or in combination with siRNA targeting *FGFR3*. (B) RT112 cells were first transfected with siRNA targeting RAB25/RAB11 then treated with dimethyl sulfoxide (DMSO) as control or 0.5 μM FGFR inhibitor PD173074 for 24h. Cell viability was determined by the MTT assay. In (A) the graph represents the cell viability relative to control siRNA. In (B) the bar plots represent the raw value in MTT assays. t-test was performed, *, p-value$<$0.05 Error bars, SEM from three independent experiments each performed in triplicate.

shown). We quantified the colocalization between two structures containing FGFR3 and these markers by using the plugin JACOP in ImageJ software to calculate Manders' overlap coefficients [126, 15] (Figure 6.12.C). TFRC localizes mainly to recycling endosomes at steady state. A significant degree of colocalization of TFRC with FGFR3 (Manders' coefficient=0.18) was observed in punctuate structures throughout the cytoplasm. A similar degree of colocalization was observed with RAB25 (Manders' coefficient=0.2). Immunolabelling of the early endosomes with EEA1 indicated that FGFR3 was found in the early endosomal compartment (Manders' coefficient=0.15). There was a small fraction of FGFR3 structures which colocalized with LAMP1 or CD63, markers of late endosomes and lysosomes (Manders' coefficient =0.1). Of note, the degree of colocalization between FGFR3 and RAB25 or TFRC was significant higher than that of LAMP1 or CD63. In addition, we co-transfected RT112 cells with FGFR3-GFP and RAB11A-mcherry, and quantified the colocalization between FGFR3 and RAB11A. As for RAB25, 25% of FGFR3-positive structures colocalized with RAB11A (Figure 6.12.A,C). Thus, these results indicate that FGFR3 resides in different intracellular compartments but preferentially localizes to TFRC-, RAB25-, RAB11A- positive recycling compartments.

6.2.5

RAB25 and RAB11 depletion alters the subcellular distribution of FGFR3

To investigate the role of RAB25/RAB11 on the subcellular localization of FGFR3, RT112 cells were transfected with control or a cocktail of RAB11A, RAB11B and RAB25-targeting siRNAs for 48h, followed by FGFR3-GFP transfection for 24h. Knockdown efficiency was confirmed by RT-qPCR and Western Blot. In control RT112 cells, TFRC-

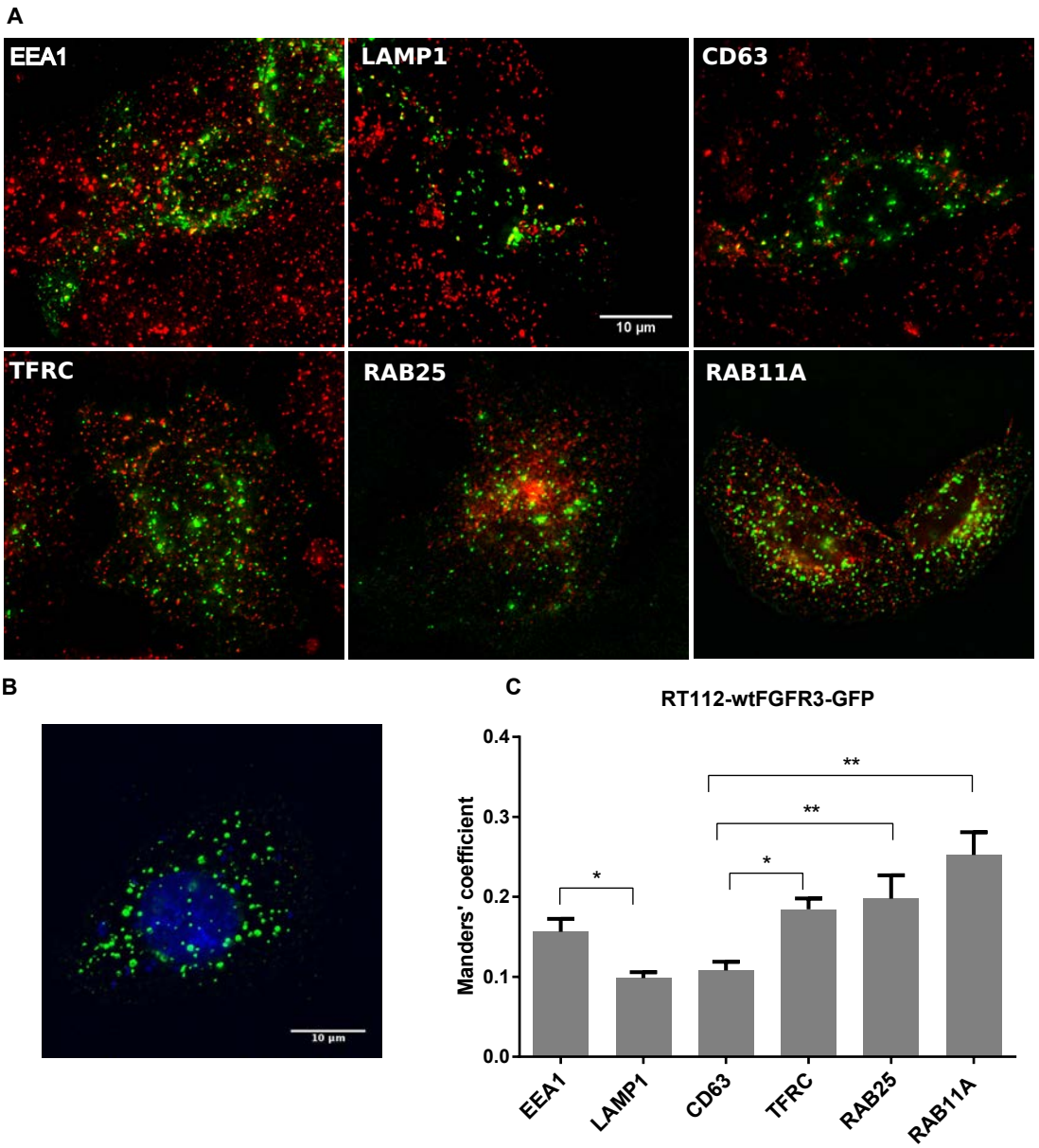

Figure 6.12 FGFR3 localizes to RAB25- and RAB11-positive vesicles. (A) RT112 cells transiently expressing wild type FGFR3-GFP were fixed and stained with anti-EEA1, anti-LAMP1, anti-CD63, anti-TFRC and anti-RAB25. Also, RT112 cells were cotransfected with RAB11A-mcherry. The cells were then fixed and analyzed by 3D deconvolution microscopy. Red signal: EEA1, LAMP1, CD63, TFRC, RAB25 and RAB11A. Green signal: FGFR3. Scale bar, 10 μm. (B) RT112 cells transiently expressing WT FGFR3-GFP were fixed and analyzed by 3D deconvolution microscopy. Blue signal: DAPI, green signal: FGFR3. Scale bar, 10 μm.(C) Colocalization between FGFR3 and different markers was quantified and Manders' overlap coefficients were calculated using Jacop plugin in ImageJ. The histogram represents the mean $\pm$SEM of two independent experiments. A total of 35-45 cells were analyzed for each condition. t-test was performed. *, $p \leq 0.05$; **, $p \leq 0.01$.

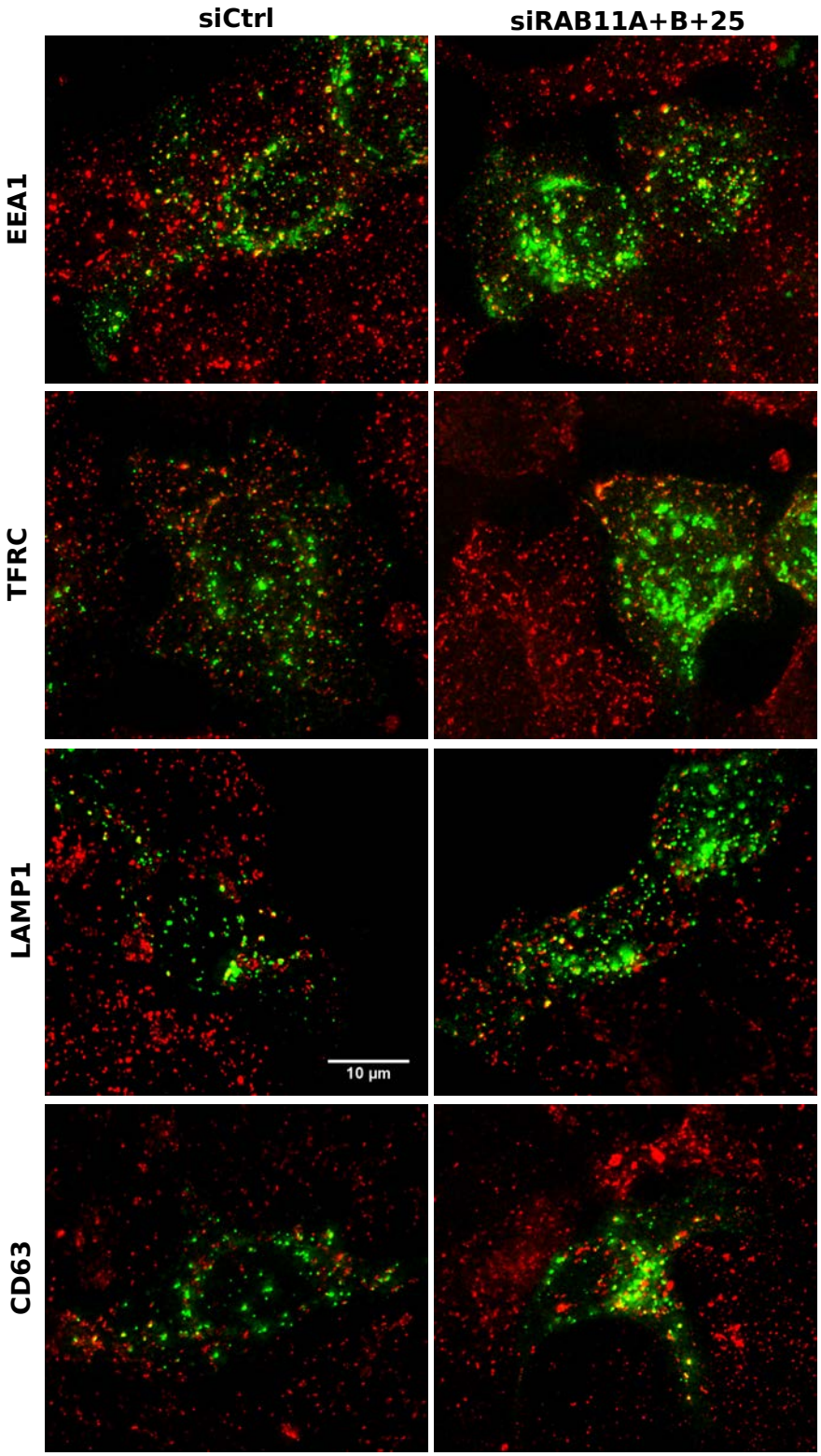

Figure 6.13 FGFR3 accumulated in different compartments in cells depleted for RAB11. RT112 cells were transfected with control siRNA (siCtrl) or siRNA targeting *RAB11A, RAB11B* and *RAB25* (siRAB11A+B+25) for 48 h, followed by FGFR3-GFP transfection for 24h. The cells were then fixed and stained with anti-EEA1, anti-TFRC, anti-LAMP1 and anti-CD63, followed with analysis by 3D deconvolution microscopy. Red signal: EEA1, LAMP1, CD63 and TFRC. Green signal: FGFR3. Scale bar, 10 μm.

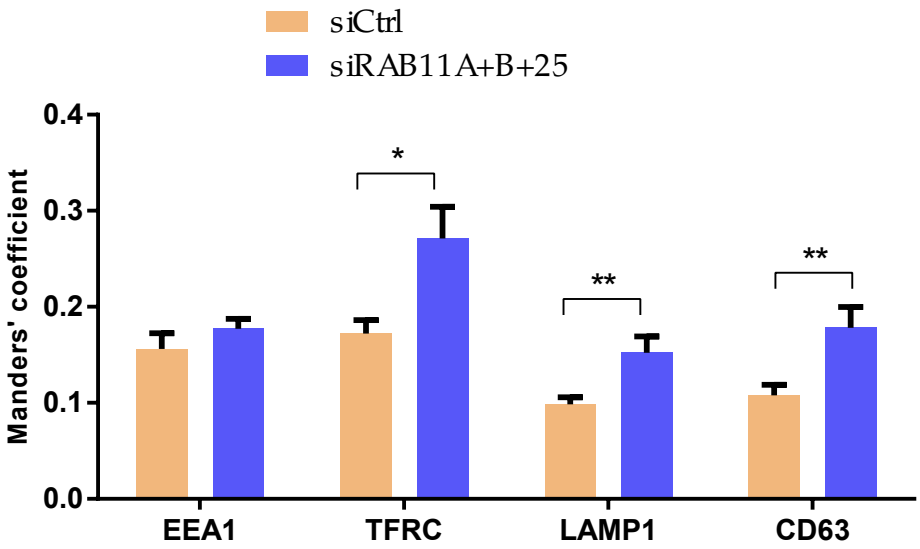

Figure 6.14 FGFR3 accumulates in different compartment in cells depleted for RAB11. Colocalization between FGFR3 and different markers shown in 6.13 was quantified and Manders' overlap coefficients were calculated. The histogram represents the mean ±SEM of two independent experiments. A total of 35-40 cells were analyzed for each condition. t-test was performed. *, $p<0.05$; **, $p<0.01$.

and FGFR3-positive vesicles were both distributed throughout the cytoplasm. In RAB25- and RAB11-depleted cells, we observed tubular TFRC-positive structures (Figures 6.13), as previously reported in other cell lines [214, 81]. In these cells, FGFR3-positive structures appeared larger and more concentrated in the perinuclear region than in controls. In addition, the extent of colocalization with TFRC was significantly increased (28% versus 18% in controls) (Figure 6.14). Of note, colocalization of FGFR3 with CD63 or LAMP1 was also significantly increased (Figures 6.13 and 6.14) but not that with EEA1. These data suggest that RAB11/RAB25 proteins play a role in the recycling of FGFR3 and that the inhibition of recycling favors its degradation.

6.2.6 Depletion of RAB25/RAB11 has differential effects on the known signaling pathways of FGFR3

RAB25/RAB11 depletion leading to altered recycling of FGFR3, we tested whether this can potentially affect its signaling. We analyzed activation of downstream substrates of FGFR3 in RAB25/RAB11-depleted RT112 cells. Previous studies in our laboratory demonstrated that PI3K-AKT, P38 and ERK1/2 are three main signaling pathways activated by altered FGFR3 in bladder cancer [12, 125]. Interestingly, elevated level of phosphorylated P38 was observed following RAB25 depletion. P-AKT was increased only when cells were depleted for RAB11A or RAB11B or RAB25. RAB11B depletion induced an increase in phosphorylation of ERK1/2 (Figure 6.15.A). We then investigated whether the differential effects on downstream signaling substrates reflect the altered activity of FGFR3 in these pathways. The P38 as well as the AKT pathway were shown to play a more important role than the ERK1/2 pathway in the proliferation of RT112 cells. We determined the phosphorylation of P38 after simultaneously depleting RAB25 and FGFR3 or after FGFR inhibitor PD173074 treatment

in RAB25-depleted cells (as described in the experiments on cell viability). The results indicate that the depletion of FGFR3 alone reduced the phosphorylation levels of P38, in contrast to the depletion of RAB25 alone (Figure 6.15.B). The level of P-P38 after simultaneous depletion for FGFR3 and RAB25 was slightly reduced compared to control. In cells depleted for RAB25 and treated with PD173074, P-P38 was higher than in control cells, maybe due to the fact that PD173074 did not completely inhibit P-P38.

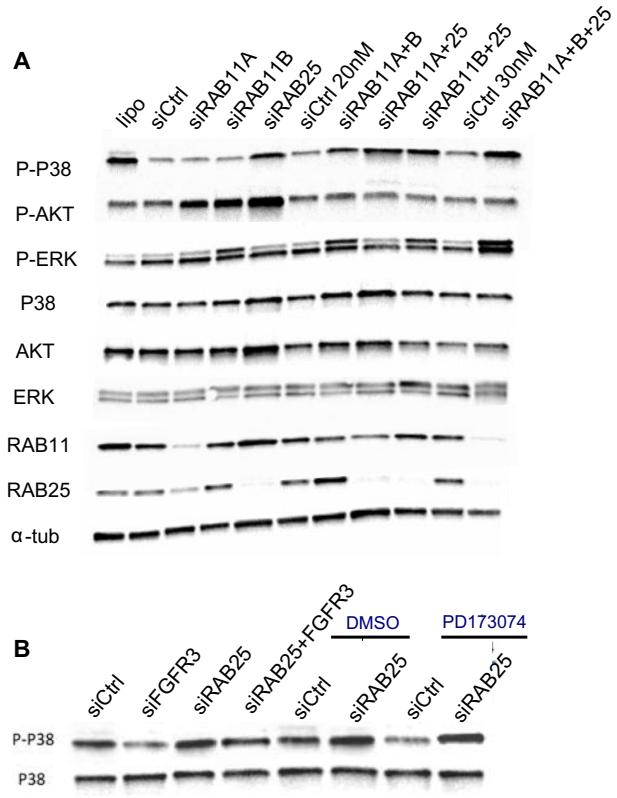

Figure 6.15 Differential effects of RAB25/RAB11 depletion on FGFR3 downstream signaling pathways. (A) After 72h transfection with indicated siRNAs, RT112 cells were lysed, and proteins were analyzed by Western blotting using antibodies against indicated proteins or phospho-proteins. (B) Phosphorylation of P38 levels was determined after depletion of FGFR3 or RAB11 alone, and after combination of siRNA against *RAB25* with either siRNA against *FGFR3* or FGFR inhibitor treatment. Tubulin (α-tub) was used as loading control in Western Blot analysis. The blot is a representative data of three independent experiments.

6.2.7

RAB25/RAB11 depletion has not the same effect compared to FGFR3 depletion on the expression of FGFR3 target genes

To further unravel the origin of the inhibitory effects on cell viability observed after knockdown of RAB11 and their effectors in cells carrying altered FGFR3, we tested whether the expression of FGFR3 target genes was affected. FGFR3 target genes were identified in a separate study performed in our laboratory. Briefly, we compared the transcriptome of the RT112 and MGHU3 cell lines treated with two or three siRNAs targeting FGFR3 or with the transfection reagent (Lipofectamine) as control. We

found that 414 genes were significantly deregulated by siRNA treatment (283 genes downregulated and 131 genes upregulated compared to control). Among deregulated genes, we selected three genes which have a potential function in FGFR3 activity including *DUSP6, TIMP2* and *GATA3*. DUSP6 is a well-known negative regulator of FGFR signaling via the inhibition of the ERK1/2 pathway [51]; TIMP2 is an inhibitor of metalloproteinases [182]; GATA3 serves as a transcription factor for differentiation [36]. We also selected *MYC* since this gene was previously shown in our laboratory to be inhibited following FGFR3 depletion in RT112 and MGHU3 cells.

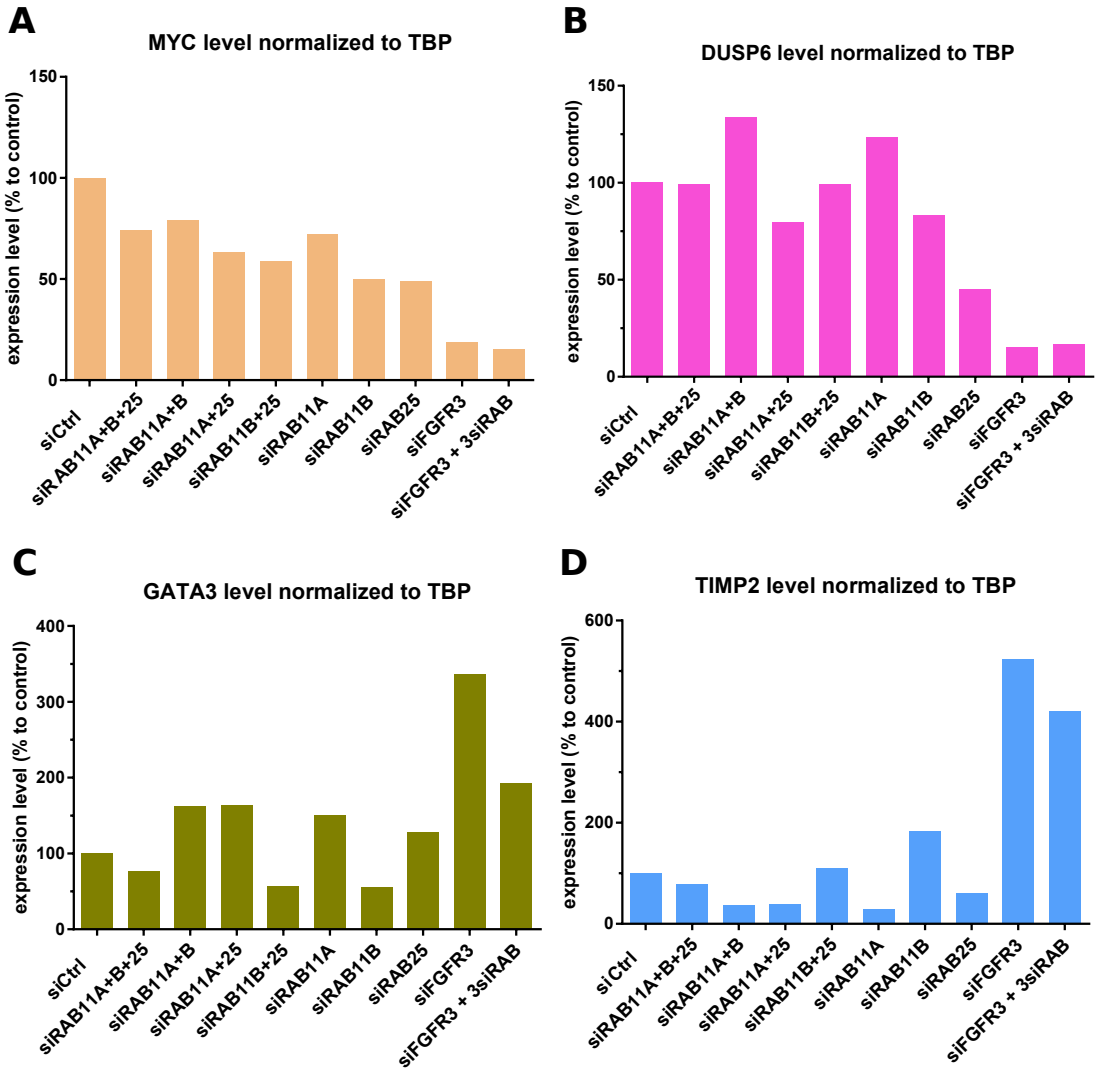

Figure 6.16 Expression of FGFR3 target genes after RAB25/RAB11 and/or FGFR3 depletion in RT112 cells. RT112 cells were transfected with control siRNA (siCtrl) or indicated siRNAs and cultured for 72h. mRNA extraction and cDNA synthesis by reverse transcription-PCR were performed. The expressions of *MYC* (A), *DUSP6* (B), *GATA3* (C) and *TIMP2* (D) were determined by RT-qPCR with normalization to *TBP* gene expression. The graph is data from one experiment.

After 72h transfection with siRNA targeting *RA25B/RAB11* or a cocktail of siRNA targeting these RABs and *FGFR3* in RT112 cells, we performed mRNA extractions and reverse transcription-PCR. Then, the expression of the four genes described above was determined by RT-qPCR, normalized to *TBP* gene expression. The results indicated

that the single, double or triple depletion of RAB11A/RAB11B/RAB25 induced a ∼40-50% inhibition of *MYC* expression compared to control siRNA. However, in FGFR3-depleted cells or in cells depleted for both FGFR3 and RAB11/RAB25, *MYC* expression was inhibited up to 80% (Figure 6.16.A). This effect of FGFR3 on *MYC* expression is consistent with other studies in our laboratory. In the case of *DUSP6*, its expression was also reduced up to ∼80% when cells were knockdown for FGFR3 alone or for FGFR3 and RAB11/RAB25 (Figure 6.16.B). RAB11/RAB25 depletion only moderately affected *DUSP6* expression. We next examined the expression of *GATA3* and *TIMP2* that are upregulated following FGFR3 depletion in microarray data (Foldchange = 1.7 and 2.6, respectively). By RT-qPCR, we obtained the same result, FGFR3 silencing increasing three times the expression of *GATA3* (Figure 6.16.C). *GATA3* was upregulated by 150% compared to control siRNA when RAB11A was depleted but reduced by 50% in RAB11/RAB25-knockdown cells. The upregulation of *GATA3* after simultaneous depletion of RAB11 and RAB25 and FGFR3 was less pronounced than in the case of FGFR3 depletion alone but still two times compared to control siRNA. FGFR3 but not RAB11 depletion induced a massive upregulation of *TIMP2* (Figure 6.16.D). Taken together, these results indicated that RAB11 depletion has less effect than FGFR3 depletion does on the expression of several FGFR3 target genes.

6.2.8

Dyngo4a treatment increases the phosphorylation of AKT and ERK1/2 but not that of P38

In order to investigate the potential role of endocytosis in FGFR3 signaling, we treated RT112 cells with Dyngo4a. Dyngo4a is a potent dynamin inhibitor which acts at an allosteric site in the G domain of dynamin, resulting in blocking dynamin-dependent endocytosis [132]. We first determined the minimum concentration of Dyngo4a required to block endocytosis by testing a range of Dyngo4a concentrations. The impact on transferrin internalization and cell morphology were taken into account. 60 μM appeared as a good concentration because it did not affect the cell morphology and transferrin internalization was blocked at this concentration (Figure 6.17.A). In RT112 cells, although we could not verify whether FGFR3 internalization was effectively blocked due to the lack of FGFR3 antibodies working suitable for immunofluorescence staining. The fact that transferrin was accumulated at the plasma membrane after 30 min treatment with Dyngo4a suggests other receptors including FGFR3 were likely blocked at the plasma membrane.

Following treatment with 60 μM Dyngo4a or DMSO 0.1% for 15 min, 30 min, 1h or 2h, RT112 cells were lysed and protein levels were determined by Western blotting. The results indicate an increased phosphorylation of AKT and ERK1/2 but not that of P38 (Figure 6.17.B-D). In RT112 cells, AKT, ERK and P38 pathways are mainly activated by FGFR3 activity independently of ligand stimulation [12, 125]. These findings suggest that P-38 can be activated by FGFR3 at either the plasma membrane or intracellular compartments. In contrast, the increased phosphorylation of AKT and ERK1/2 observed following Dyngo4a treatment is probably due to the accumulation of FGFR3 at the plasma membrane, suggesting that FGFR3 phosphorylates AKT and ERK1/2 at the plasma membrane.

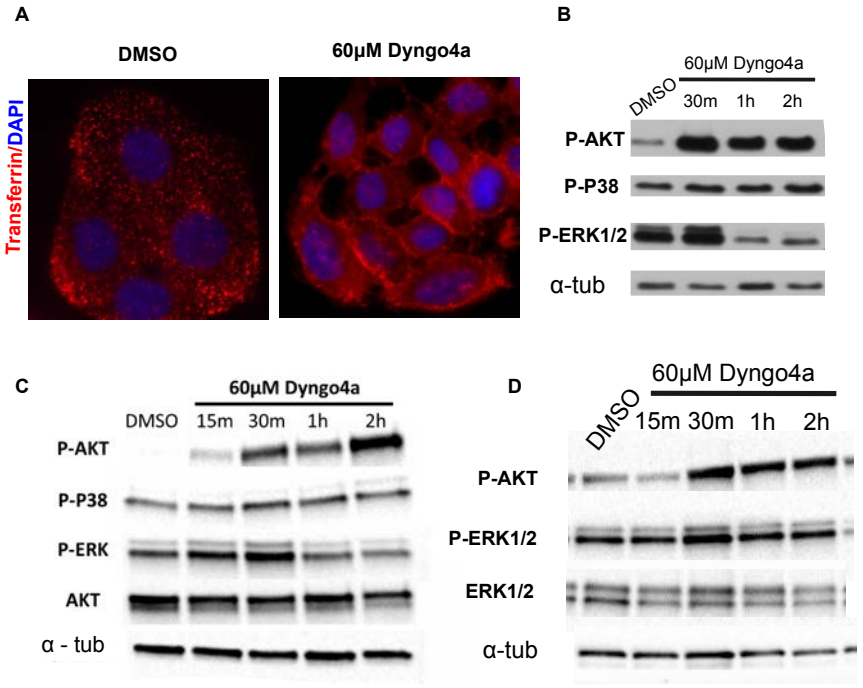

Figure 6.17 Dyngo4a treatment increases the phosphorylation of AKT and ERK1/2 but not P38. (A) RT112 cells were incubated for 30 min at 37°C with 60 μM Dynamin inhibitor Dyngo4a or 0.1% DMSO only in serum-free medium. The cells were then incubated with the same media containing fluorescently labeled Alexa-555 transferrin (red) for 45 min at 4°C. Following two washes, the cells were transferred back to 37°C for 15 min. The cells were fixed with 4% PFA and stained with DAPI as counterstained, images were taken with fluorescence microscopy (objective of 60X). (B)-(D) RT112 cells were treated with 60 μM Dyngo4a or 0.1% DMSO for the indicated times. The cells were then lysed and proteins were separated using SDS-PAGE and analyzed by Western blotting with the indicated antibodies. Three blots from three independent experiments were shown. Tubulin (α-tub) was used as loading control.

6.3 Materials and methods

Microarray data

Transcriptomic data from 204 human bladder samples and seven cell lines were obtained using Affymetrix Human Exon 1.0 ST DNA Array. RNA amplification, cDNA probe labeling and hybridization were performed as described on the Affymetrix website. Raw data were normalized by the robust multiarray average (RMA) method available in the R package *affy*. The annotation used is based on the custom CDF files from BrainArray [40], Ensembl Gene version 17. The Limma of R package from Bioconductor [194] was used to identify genes differentially expressed in FGFR3 altered tumors compared to non-altered tumors. Clinical and RNA-seq data related to 371 muscle-invasive bladder tumor samples were collected from The Cancer Genome Atlas (Provisional data 2015) [205]. Raw data was normalized by the trimmed mean of M values (TMM) method with the R package [171]. Differential expression was analyzed with the *voom* Limma in the R package from Bioconductor [114, 194]. For each differential expression analysis, the p-values were adjusted for multiple testing by Benjamini et Hochber FDR methods. Genes with an adjusted p-value below 0.05 were considered to be differentially expressed.

Cell culture and reagents

Bladder cancer cell lines used in this study (UMUC5, UMUC9, HT1376) were purchased from ECACC and TCCSup cells from ATCC. The MGHU3 cell line was a gift from Yves Fradet (CRC, Quebec). All cell lines were maintained under 5% CO2 at 37°C in Dulbecco's modified Eagle's medium (DMEM) (Gibco, Life Technologies) supplemented with 10% fetal bovine serum (FBS) (Lonza), except for the RT112 cells cultured in RPMI (Gibco, Life Technologies) with 10% FBS.

DMSO, Tyrosine kinase FGFR inhibitor PD173074 (P2499) was purchased from Sigma. Dyngo4a (ab120689) was purchase from Abcam. DAPI (D1306) was purchase from Molecular Probes.

Antibodies

Antibodies were purchased from Sigma Aldrich: anti-FGFR3 (F0425), anti-alpha-tubulin (T6199); from Abcam: anti-FGFR3 (ab133644), anti-CD63 (ab23792); from Cell Signaling Technology: anti-RAB25 (4314); anti-RAB11A (2413); anti-RAB7A/B (9367); anti-p44/42 MAPK (9102); anti-phospho-p44/42 MAPK (Thr202/Tyr204) (9101); anti-AKT (9272); anti-phospho-AKT Ser473 (4060); anti-P38 MAPK (9212); anti-phospho-P38 MAPK (Thr180/Tyr182) (4511); anti-mouse HRP-linked (7076); anti-rabbit HRP-linked (7074); from Santa Cruz Biotechnology: EEA1 antibodies (sc-6414); from BD Pharmingen: anti-LAMP1 CD107a (553792); from Invitrogen: Goat anti-mouse IgG Alexa Fluor 594 (a11032), Goat anti-rabbit IgG Alexa Fluor 594 (a11037), anti-Transferrin (136800); from Jackson ImmunoResearch: Donkey anti-goat IgG Cy3. Anti-RAB21 was a kind gift from Johanna Ivaska's laboratory.

Plasmid constructs and transfection

The FGFR3-GFP construct was generated by subcloning the *Hind*III-*Bam*HI fragment from pcDNA3.1 containing wild type FGFR3 into pEGFP-N3 (Clontech). Full length human wt RAB11A flanked with attB1.1 and attB2.1 were synthesized and inserted into pDONR207 (BP cloning reaction, Invitrogen), then transfered into Gateway compatible versions of pmCherry-C1 (Clontech) (LR cloning reaction, Invitrogen). All constructs were sequence-verified by Sanger sequencing. RT112 cells were transfected with this construct using Fugene HD Transfection Reagent (Promega) according to the manufacturer's instructions.

RNA interference

siRNAs were transfected with Lipofectamine RNAiMAX reagent (Invitrogen) according to the manufacturer's instructions, and cultured for 72h for further manipulations. Depletion efficiency was estimated by RT-qPCR and/or Western blotting ($\geq$80% inhibition). All siRNAs were purchased from Qiagen, except for *FGFR3* (Ambion) and *RAB21* (L-009450-00, Dharmacon). The target sequences of siRNA against RAB7A no5: CACGTAGGCCTTCAACACAAT and siRNA against RAB7B no5: AAGGTGGACCTGAAACTCATT. List of siRNA sequences and concentration used:

Table 6.1 List of siRNA used in the study.

siRNA	Sequence	Concentration
Control siRNA	CGUACGCGGAAUACUUCGATT (sens)	as indicated in figures
	UCGAAGUAUUCCGCGUACGTT (anstisens)	
RAB11A no6	AAAUGAGUUUAAUCUGGAATT (sens)	10nM
	UUCCAGAUUAAACUCAUUUCG (anstisens)	
RAB11B no4	AGUUCAACCUGGAGAGCAATT (sens)	10nM
	UUGCUCUCCAGGUUGAACUCG (antisens)	
RAB25 no3	GGAACUGAGGAAGAUUAUATT (sens)	10nM
	UAUAAUCUUCCUCAGUUCCAT (antisens)	
RAB11FIP2 no6	CCUGGUGGGUCUGGAUAAATT (sens)	20nM
	UUUAUCCAGACCCACCAGGGA (antisens)	
MYO5B no7	GCAUUAGUUUGAUUCCCAATT (sens)	20nM
	UUGGGAAUCAAACUAAUGCTG (antisens)	
FGFR3	CCUGCGUCGUGGAGAACAATT (sens)	4nM
	UUGUUCUCCACGACGCAGGTG (antisens)	

MTT assay

After siRNA transfection or treatment with inhibitor (time as indicated in figures), medium was changed, MTT (3-(4, 5-dimethylthiazolyl-2)-2,5-diphenyltetrazolium bromide) (Sigma) was added to the cells to a final concentration of 1 mg/mL. After 30 min incubation at 37°C in a 5% CO2, the purple formazan was solubilized in DMSO and quantified. Absorbance was measured at 550 nm using a microplate reader. For MTT assay, each condition was performed in triplicate wells.

Real-time quantitative PCR

RNA was extracted from cells with RNAeasy kits (Quiagen). One microgram of total RNA was reverse-transcribed with the High-Capacity cDNA Reverse Transcription kit (Applied Biosystems). Predesigned assay was used to quantify human *TBP* gene expression (Applied Biosystems) and custom assays were used for the other genes (see table). For custom assays, primers and probes were designed with Probe Finder software via the Universal Probe Library Assay Design Center (Roche). RT-qPCR was carried out with the LightCycler 480 Instrument (Roche) in a 20 μl reaction mixture containing 10-20 ng of reverse-transcribed RNA, 1x LightCycler 480 Probe Master, 25 μM each of the forward and reverse primers and 10 μM of the UPL probe (or 1x the predesigned assay probe). All expression assays were run in the same thermal cycling conditions, including an initial step at 95°C (10 min), followed by 40 cycles at 95°C (10 s), 60°C (30 s) and 72°C (10 s). For each gene, the amount of mRNA was normalized to that of the *TBP* gene by the $2^{-\Delta\Delta Ct}$ method.

Table 6.2 List of primers and probes used for RT-qPCR.

Gene (Probe)	Forward primer	Reverse primer
RAB11A (31)	CTGCACCTTTGGCTTGTTTT	CAGGGCAGTTCCTACAGATGA
RAB11B (62)	CGACGAGTACGACTACCTATTCAA	AACTCGTTGCGGGTGAAG
RAB25 (1)	GCTGCTGTCAAGGCTCAGAT	CCCACTGCACCACGATAGTA
RAB11FIP2 (59)	GCAATGAAGACCTCAGGAAAA	CTTCATAGGTCAGACTACGATACCC
MYO5B (49)	CTCCAACAAGGAGCACAAGA	CAGGGTCTCCATGAGCAGAT
MYC (34)	CACCAGCAGCGACTCTGA	GATCCAGACTCTGACCTTTTGC
DUSP6 (66)	CGACTGGAACGAGAATACGG	AATGTACCAAGACACCACAGTTCT
TIMP2 (43)	GAAGAGCCTGAACCACAGGT	CGGGGAGGAGATGTAGCAC
GATA3 (71)	CTCATTAAGCCCAAGCGAAG	TCTGACAGTTCGCACAGGAC

Western blotting

Protein extracts were obtained using lysis buffer (50mM Tris-HCl (pH 6.8), 2% SDS, 5% glycerol, DTT 2mM, 2.5 mM EDTA, 2.5 mM EGTA) freshly supplemented with Protease and phosphatase inhibitor (Roche)). Cell lysates were clarified by centrifugation. Protein concentration was determined with a BCA Protein Assay-Reducing Agent Compatible kit (ThermoFischer). Proteins (8 μg to 20 μg) were separated by SDS-PAGE using 4-15% precast Tris-glycine gel (Biorad) and transferred to nitrocellulose membranes using Trans-Blot Turbo transfer system (Biorad). Membranes were then blocked with 5% non-fat milk or 5% BSA at room temperature. Membranes were then incubated with the primary antibody overnight at 4°C and the secondary antibody for 45 min at room temperature. Signals were detected with the Clarity Western ECL (BioRad), Western blots were analyzed with a Fujifilm LAS-3000 imager or with ChemiDoc MP imaging systems using Imagelab software (Biorad).

Immunofluorescence staining

Cells were fixed for 15 min with 4% PFA in PBS at room temperature. After permeabilization with 0.5% saponin (Sigma-Aldrich) and 2% BSA (Sigma-Aldrich), cells were incubated with primary and secondary antibodies before being mounted with

Mowiol (Biovalley). Fixed samples were imaged with an upright widefield microscope from Leica equipped with 100X CFIPlanAPo VC oil immersion objective (Na 1.4 CFI), a piezoelectric motor (Physik Instrumente) and highly sensitive cooled interlined charge-coupled device (CCD) camera (CoolSNAP HQ2, Photometrics). Z-dimension series of images were taken every 0.2 μm by Metamorph software (Molecular Devices). After deconvolution (Meinel algorithm, [186]), colocalization between structure was analyzed with ImageJ 1.50 software [180]. Manders' overlap coefficients were calculated using the JACOP plugin for ImageJ [15].

Transferrin internalization

For transferrin internalization experiment, RT112 cells were starved for 4h in serum free medium and incubate with transferrin-A555 (10μg/ml) (Invitrogen) for 45 min at 4°C. Cells were then washed with cold PBS and chased at 37°C with serum free medium for 15 min. Cells were fixed with 4% PFA in PBS and mounted with Mowiol.

Statistical analysis

All functional experiments were carried out twice or three times, in triplicate. Data are expressed as means ± SEM. Student's t-tests were used for the statistical analysis. The control siRNA group or the DMSO group was used as the reference group.

This page intentionally left blank.

Trafficking of wild type and mutated S249C FGFR3

7

7.1 Introduction

FGFR3 mutations in bladder cancer were first reported by Radvanyi's group over fifteen years ago [22]. They found single nucleotide substitutions of FGFR3 in 9 of 26 bladder carcinomas (35%). Since then, 11 different mutations have been identified in urothelial tumors. The most frequent mutations are S249C (66.6%), Y375C (15.1%), R248C (9.7%) and G372C (4.3%) [65].

In this study, we first generated plasmid encoding the wild type (WT) and S249C FGFR3 tagged with GFP at the C-terminus. Next, we compared the subcellular distribution of these two forms in HeLa cells transiently expressing WT or S249C FGFR3-GFP. Finally, we evaluated the effects of RAB11A/B depletion by siRNA on the subcellular localization and signaling of the two forms of FGFR3.

7.2 Results

7.2.1 Generation of WT and mutant S249C FGFR3-GFP expressing cells

The cellular distribution of wild type (WT) and mutant S249C forms of FGFR3 was studied in HeLa cells transiently transfected with different FGFR3 constructs. HeLa cells do not express detectable levels of endogenous FGFR3 [82]. This was also confirmed by Western blotting (Figure 7.1.A). We generated the plasmids encoding FGFR3 tagged with GFP at the C-terminus or N-terminus for each form. 24h after transfection with these constructs, HeLa cells were fixed and analyzed by fluorescence microscopy. The N-terminal GFP-tagged constructs of the two forms of FGFR3 localized to the endoplasmic reticulum, suggesting that GFP-FGFR3s may not be correctly folded to exit the endoplasmic reticulum (data not shown). In contrast, the C-terminal GFP-tagged constructs were detected in punctuate and vesicular structures distributed throughout the cytoplasm (Figure 7.1.B). A fluorescence signal was only weakly detected at

the plasma membrane, probably due to the limitations of wide field microscopy. The punctuate structures of the C-terminal fusion FGFR3-GFP were also observed in bladder cancer cell lines transfected with C-terminal GFP-tagged FGFR3 such as RT112 cells, MGHU3 cells and T24 cells. Furthermore, C-terminal tagged GFP-FGFR3 were able to interact, as non-tagged FGFR3, with HSP90 [107], suggesting that the GFP tag did not alter the functionality of FGFR3 (data not shown). We therefore used these C-terminal tagged GFP-FGFR3 constructs for following experiments, hereafter called FGFR3-GFP.

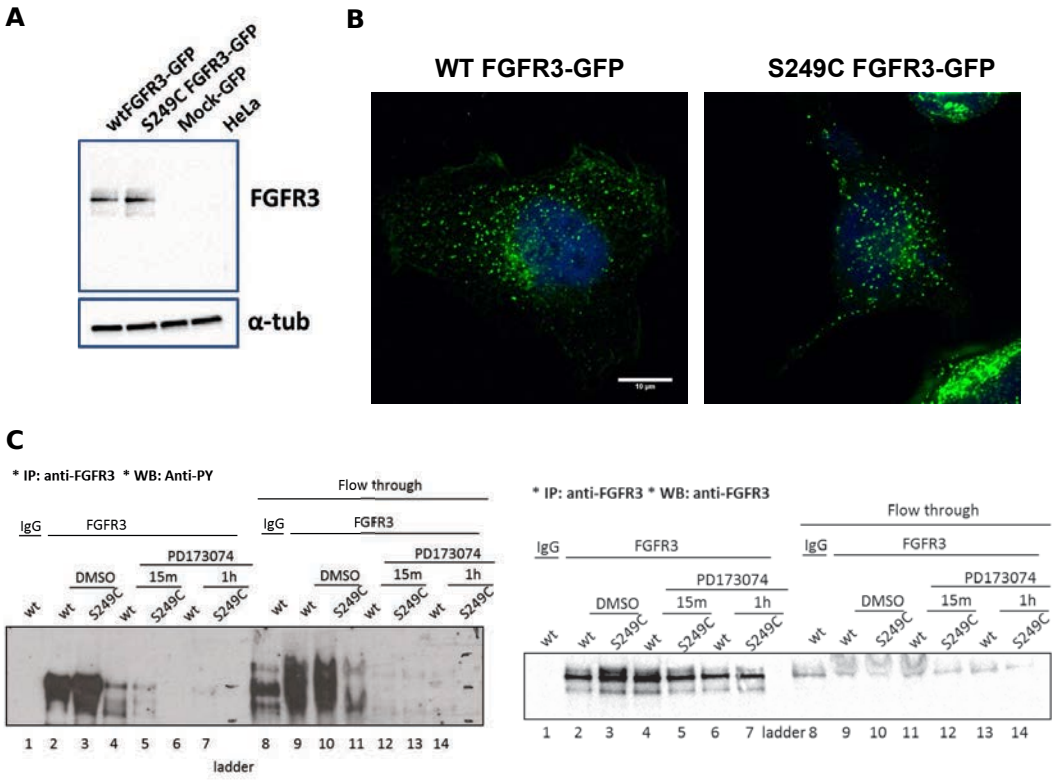

Figure 7.1 Generation of wild type and S249C FGFR3-GFP expressing HeLa cells. (A) HeLa cells were transfected with WT or S249C FGFR3 tagged with GFP at C-terminal (WT FGFR3-GFP, S249C FGFR3-GFP) or with mock GFP plasmid (Mock-GFP). 24h after transfection, the cells were lysed and analyzed by Western blotting with anti-FGFR3. Tubulin was used as loading control. (B) Hela cells transiently expressing WT FGFR3-GFP or S249C FGFR3-GFP were fixed and analyzed by 3D deconvolution microscopy. Scale bar, 10 μm. (C) HeLa cells were transfected with WT FGFR3-GFP (wt) or S249C FGFR3-GFP (S249C) for 24h, then treated with DMSO alone (0.1%) as control or FGFR inhibitor PD173074 (1 μM) for 15 minutes (15m) and 1 hour (1h). The cells were then lysed and immunoprecipated with anti-FGFR3. In addition, the cell lysate from HeLa expressing WT FGFR3-GFP was incubated with IgG control (IgG). The protein complex was then eluted and analyzed by Western blotting using anti-phosphotyrosine (anti-PY) or anti-FGFR3. Flow through of immunoprecipitation was also loaded to verify the binding efficiency of antibody to antigen.

We first verified that HeLa cells expressed WT and mutant FGFR3-GFP at comparable levels (Figure 7.1.A). The functionality of the two GFP fusion proteins was confirmed by evaluating their phosphorylation levels. After 24h transfection with WT or S249C FGFR3-GFP, HeLa cells were treated with DMSO alone (0.1%) or 1 μM FGFR in-

hibitor PD173074 for 15 min or 1h in medium with 10% serum. Cell lysates were then immunoprecipitated with anti-FGFR3 antibody or control IgG antibodies followed by immunoblotting with anti-FGFR3 antibody to validate the efficiency of immunoprecipitation, and with anti-phosphotyrosine to examine the phosphorylation level of the receptors. The results indicated that both WT and S249C FGFR3 were phosphorylated in medium with 10% serum (Figure 7.1.C). The phosphorylation of FGFR3-GFP was strongly reduced with the treatment of 1 μM PD173074 for 15 min and completely inhibited after 1h of treatment. Thus, in HeLa cells transiently expressing FGFR3-GFP, both WT and mutant FGFR3 were activated.

7.2.2

Characterization of the trafficking of WT and mutant forms

The possible difference in the cellular distribution of WT and mutant S249C FGFR3 remains poorly explored in the context of cancer. We addressed this question by comparing the localization of these forms in HeLa cells transfected with the FGFR3-GFP constructs described above. We used various antibodies against marker proteins of endosomal compartments, as described in section 6.2.4 (Figure 7.2). In parallel, we co-transfected RAB11A-mcherry with either WT FGFR3-GFP or S249C FGFR3-GFP. The degree of colocalization between FGFR3 and the different markers was quantified by Manders' overlap coefficient (Figure 7.3). The results showed that WT FGFR3-GFP partly colocalized with TFRC, LAMP1 or CD63 (Manders' coefficient= 0.28, 0.30 and 0.6, respectively). There was no significant difference between these extent of colocalization (Figures 7.2 and 7.3.A). A small fraction of WT FGFR3-GFP was found in EEA1-positive compartment (Manders' coefficient=0.17). Compared to WT FGFR3-GFP, mutant S249C FGFR3-GFP preferentially resided in TFRC-positive compartments (Manders coefficient=0.40) and was less colocalized with LAMP1 or CD63 (Manders' coefficient=0.2, 0.19 respectively) (Figures 7.2 and 7.3.B). Interestingly, the high colocalization of S249C FGFR3 with TFRC was consistent with the overlap between S249C FGFR3-GFP and RAB11A (Manders' coefficient=0.41) (Figures 7.2 and 7.3.B). Figure 7.3.C shows significant differences in the localization of the two forms of FGFR3 in different compartments. S249C FGFR3 is significantly more present in TFRC- or RAB11A-positive compartments than WT FGFR3. Thus, S249C FGFR3 mainly localizes in the endocytic recycling compartment. In contrast, WT FGFR3 can be delivered to the recycling compartment but also to late endosomes and lysosomes.

7.2.3

FGFR3 accumulates in TFRC-positive structures in RAB11-depleted HeLa cells

HeLa cells do not express endogenous RAB25. Thus we examined the role of the RAB11 subfamily in FGFR3 trafficking by depleting RAB11A and RAB11B with siRNA. HeLa cells were transfected with control siRNA or a cocktail of RAB11-targeting siRNAs for 48h, followed with FGFR3-GFP transfection for 24h. Knockdown efficiency was confirmed by RT-qPCR and Western Blot (Figures 7.4.B, 7.5.B, 7.7). In control HeLa cells, TFRC- and FGFR3- positive structures were both distributed throughout the cytoplasm. Moreover, WT FGFR3 was less colocalized with TFRC than S249C

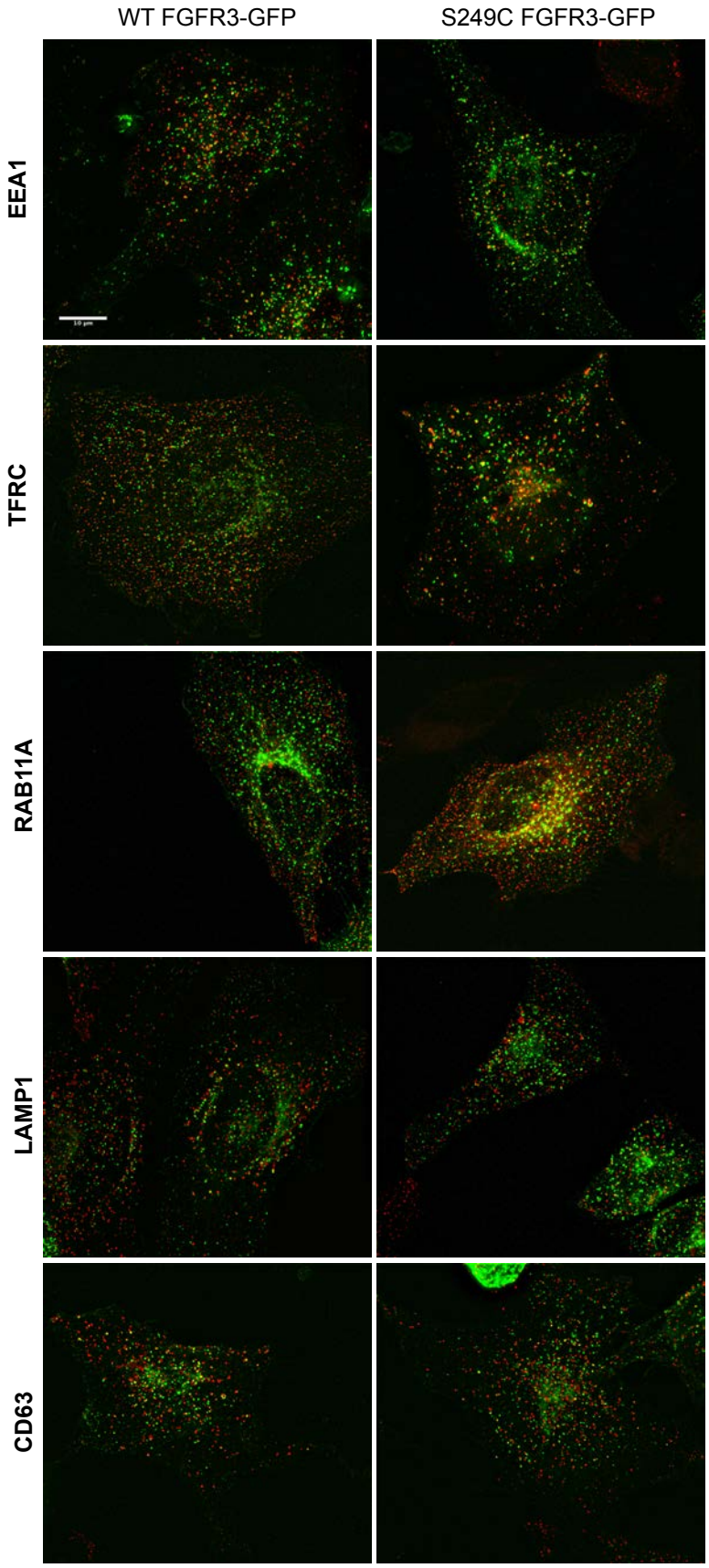

Figure 7.2 Subcellular localization of WT and S249C FGFR3. HeLa cells transiently expressing WT or S249C FGFR3-GFP were fixed and stained with anti-EEA1, anti-TFRC, anti-LAMP1 and anti-CD63. HeLa cells were also co-transfected with a RAB11A-mcherry with either WT FGFR3-GFP or S249C FGFR3-GFP. The cells were then analyzed by 3D deconvolution microscopy. Red signal: EEA1, LAMP1, CD63, TFRC and RAB11A. Green signal: FGFR3. Scale bar, 10μm.

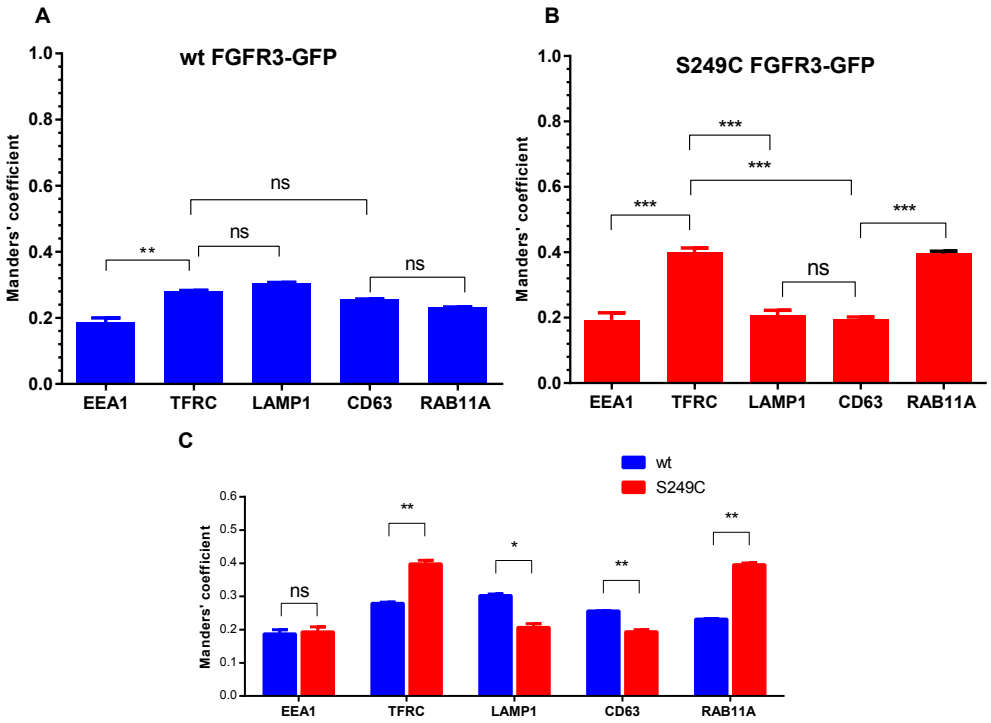

Figure 7.3 Subcellular localization of WT and S249C FGFR3. Colocalization between WT FGFR3 (A) or S249C FGFR3 (B) with different markers shown in Figure 7.2 was quantified and Manders' overlap coefficients were calculated, t-test was performed. The histogram represents the mean ± SEM of three independent experiments. A total of 55-65 cells were analyzed for each condition. (C) Manders' coefficients were compared between two WT and S249C forms of FGFR3, t-test was performed. *, $p<0.05$; **, $p<0.01$; ***, $p<0.001$; ns, non-significant.

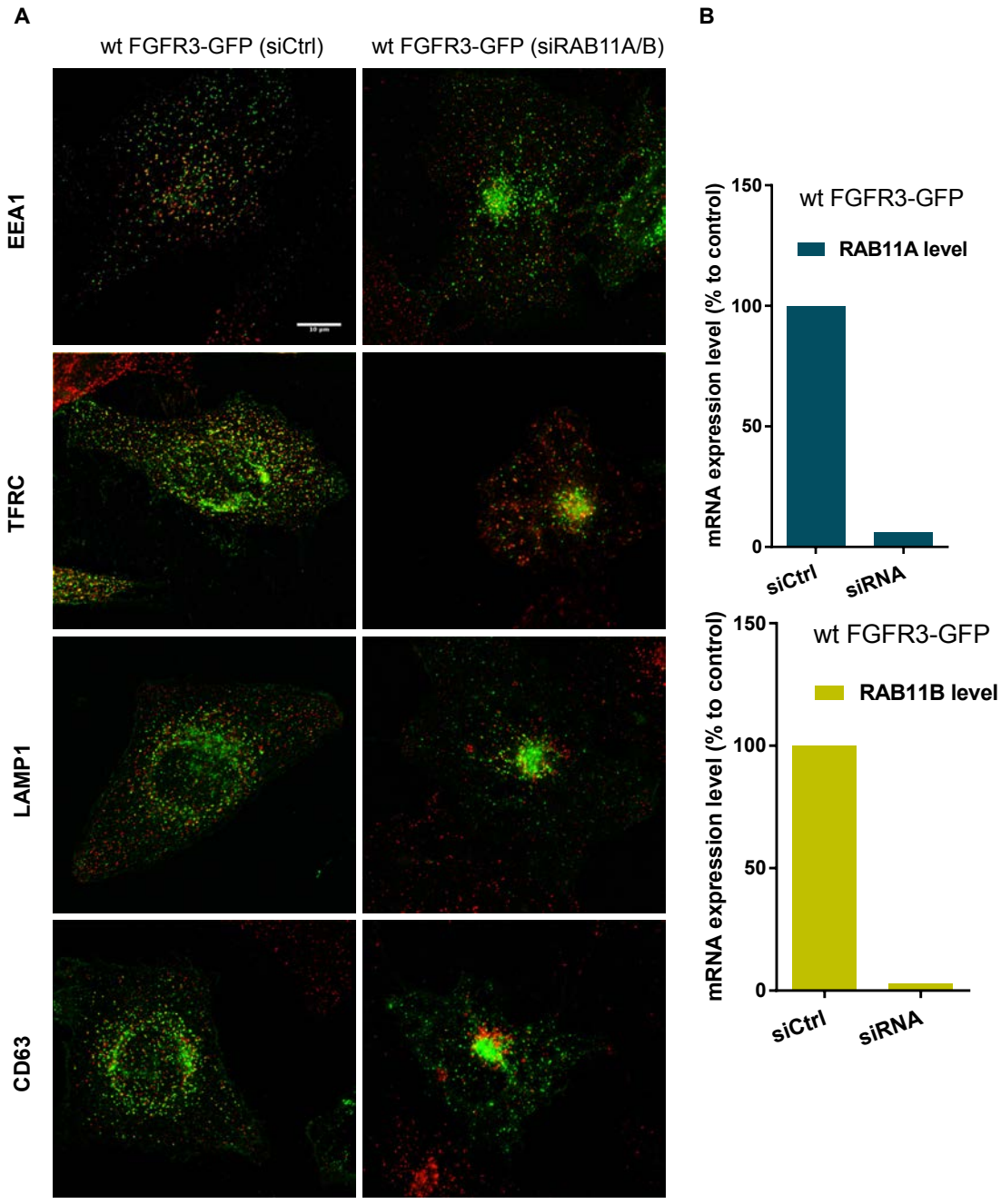

Figure 7.4 WT FGFR3 accumulates in TFRC-positive structures in RAB11-depleted cells. (A) HeLa cells were transfected with control siRNA (siCtrl) or siRNA targeting *RAB11A/B* followed by transfection with WT FGFR3-GFP. The cells were then fixed and stained with anti-EEA1, anti-TFRC, anti-LAMP1 and anti-CD63. Red signal: EEA1, LAMP1, CD63 and TFRC. Green signal: FGFR3. Scale bar, 10μm. (B) Knockdown efficiency was verified by RT-qPCR, normalized to *TBP* expression.

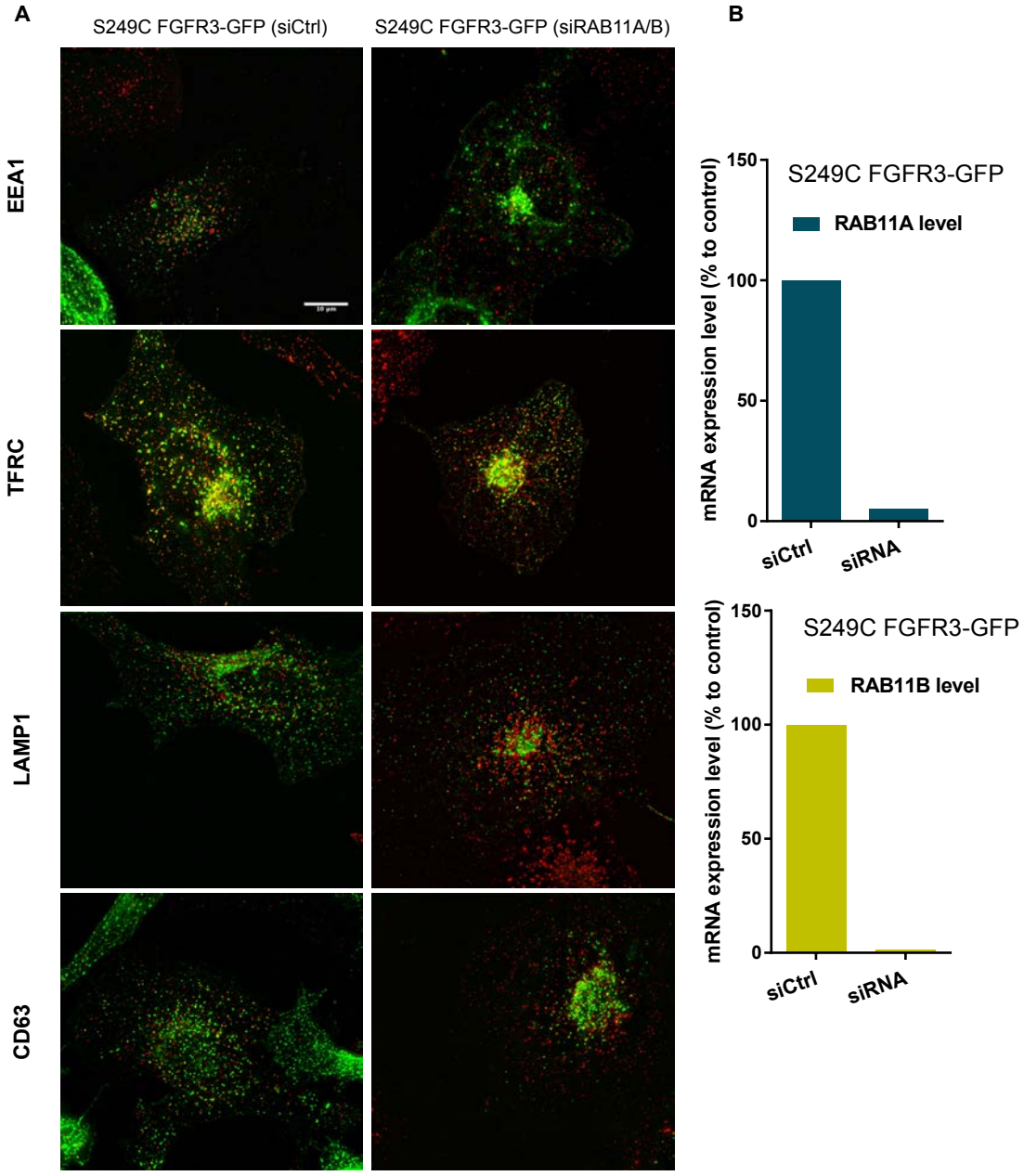

Figure 7.5 S249C FGFR3 accumulates in TFRC-positive structures in RAB11-depleted cells. (A) HeLa cells were transfected with control siRNA (siCtrl) or siRNA targeting *RAB11A/B* followed by transfection with S249C FGFR3-GFP. The cells were then fixed and stained with anti-EEA1, anti-TFRC, anti-LAMP1 and anti-CD63. Red signal: EEA1, LAMP1, CD63 and TFRC. Green signal: FGFR3. Scale bar, 10μm. (B) Knockdown efficiency was verified by RT-qPCR, normalized to *TBP* expression.

FGFR3 as shown previously. In contrast, in RAB11-depleted cells, we observed a tubulation of TFRC-positive structures (Figure 7.4.A and 7.5.A), as previously reported in other cell lines [214, 81]. In these cells, FGFR3-positive structures appeared larger and mostly concentrated in the perinuclear region than in control cells. In addition, the colocalization with TFRC of the two forms of FGFR3 was significantly increased (WT: 66% versus 28% in controls; S249C: 65% versus 39% in controls, Figure 7.6). Of note, the extent of overlap between TFRC with either WT FGFR3 or S249C FGFR3 in RAB11-depleted cells was similar. On the other hand, both forms of FGFR3 were less colocalized with EEA1-positive structures in RAB11-knockdown cells (WT: 9%; S249C: 10%) compared to control cells (WT: 18%; S249C: 18%). Strikingly, the RAB11 depletion induced the accumulation of LAMP1- or CD63-positive structures in the perinuclear region (Figure 7.4.A, Figure 7.5.A). However, the extent of colocalization between these structures with WT or S249C was not affected (Figure 7.6). These data suggest that RAB11A and RAB11B play a role in the recycling of both WT and mutant S249C FGFR3.

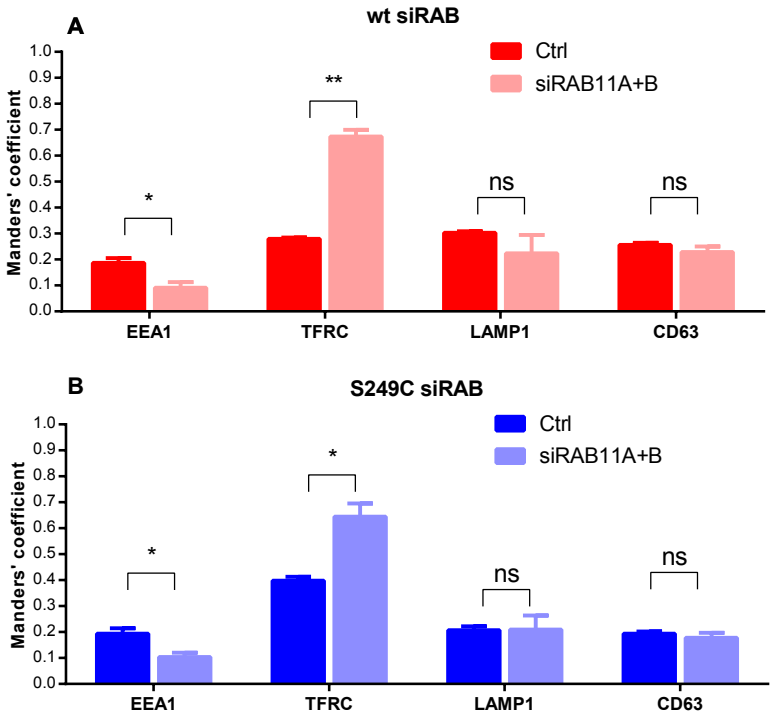

Figure 7.6 FGFR3 accumulated in TFRC-positive structures in RAB11-depleted cells. Colocalization between WT FGFR3 (A) or S249C FGFR3-GFP (B) with different markers shown in Figure 7.4 and Figure 7.5 was quantified and Manders' overlap coefficients were calculated. The histogram represents the mean ± SEM of two independent experiments. A total of 35-45 cells were analyzed for each condition. t-test was performed, *, $p<0.05$; **, $p<0.01$, ns, non-significant.

7.2.4 Signaling of WT and S249C FGFR3

We further examined whether the difference in the trafficking of WT and mutated S249C FGFR3 can have an impact on FGFR3 signaling by using HeLa cells and RAB11-depleted HeLa cells expressing these two forms of FGFR3. We thus analyzed the ac-

tivation of these downstream substrates of FGFR3. Unexpectedly, no difference in phosphorylation levels of AKT, P38 and ERK1/2 between HeLa cells expressing WT and S249C was observed. A similar result was obtained in RAB11-knockdown HeLa cells expressing these two forms (Figure 7.7.B). Of note, the overexpression of FGFR3 in HeLa cells did not induce any accumulation of phosphorylation of P38, PAKT and ERK1/2 (Figure 7.7.A). Thus, HeLa cells may be not an adequate model to investigate the signaling of FGFR3.

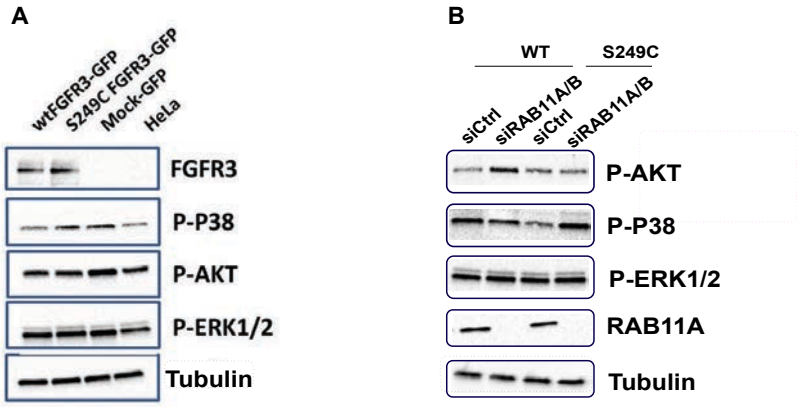

Figure 7.7 Signaling of WT and S249C FGFR in HeLa expressing FGFR3-GFP. (A) Cell lysates from HeLa cells transiently expressing WT or S249C FGFR3-GFP or mock-GFP plasmid and HeLa cells non-transfected were analyzed by Western blotting with anti-FGFR3, anti-phospho-P38, anti-phospho-AKT and anti-phospho-ERK1/2. (B) Cell lysates from RAB11-depleted HeLa cells transfected with WT or S249C FGFR3-GFP were analyzed by Western blotting using anti-phospho-AKT, anti-phospho-P38, anti-phospho-ERK1/2, anti-RAB11A. Tubulin was used as loading control.

7.3 Materials and methods

Cell culture and RNA interference

HeLa cells were grown at 37°C under 5% CO2 in DMEM high-glucose Glutamax (Gibco, Life Technologies) supplemented with 10% fetal bovine serum (Lonza).

For RNA interference, cells were transfected with either control siRNA or siRNA targeting *RAB11A* or *RAB11B* at 10nM each with Lipofectamine RNAiMAX reagent (Invitrogen) according to the manufacturer's instructions, and cultured for 72h for further manipulations. Depletion efficiency was estimated by RT-qPCR and Western blotting. The siRNAs were purchased from Qiagen: Control siRNA (CGUACGCGGAAUACUUCGATT (sens), UCGAAGUAUUCCGCGUACGTT (antisens)); RAB11A no6 (AAAUGAGUUUAAUCUGGAATT (sens), UUCCAGAUUAAACUCAUUUCG (antisens)); RAB11B no4 (AGUUCAACCUGGAGAGCAATT (sens), UGCUCUCCAGGUUGAACUCG (antisens)).

Plasmid constructs

The FGFR3-GFP constructs were generated by subcloning the *Hind*III-*Bam*HI fragment from pcDNA3.1 containing wild type or mutant (S249C) FGFR3 into pEGFP-N3 (Clon-

tech). Full length human wt RAB11A flanked with attB1.1 and attB2.1 were synthesized and inserted into pDONR207 (BP cloning reaction, Invitrogen), then transfered into Gateway compatible versions of pmCherry-C1 (Clontech) (LR cloning reaction, Invitrogen). All constructs were sequence-verified by Sanger sequencing. HeLa cells were transfected with Fugene HD transfection reagent (Promega) according to the manufacturer's instructions.

Antibodies

Antibodies were purchased from Sigma Aldrich: anti-FGFR3 (F0425), anti-alpha-tubulin (T6199); from Cell Signaling Technology: anti-RAB11A (2413); anti-phospho-p44/42 MAPK (Thr202/Tyr204) (9101); anti-phospho-AKT ser473 (4060); anti-phospho-P38 MAPK (Thr180/Tyr182) (4511); anti-rabbit HRP-linked (7074); anti-mouse HRP-linked (7076) from SantaCruz Biotechnology: EEA1 antibodies (sc-6414); from BD Pharmingen: anti-LAMP1 CD107a (553792); from GeneTex: EasyBlot anti Rabbit IgG HRP-linked (GTX221666-01), EasyBlot anti Mouse IgG HRP-linked (GTX221667-01); from Invitrogen: Goat anti-mouse IgG Alexa Fluor 594 (a11032), anti-Transferrin (136800); from Milipore: anti-phospho-tyrosine (05-321); from Jackson ImmunoResearch: Donkey anti-goat IgG Cy3.

Immunoprecipitation

Cells transfected with FGFR3-GFP for 24h treated with FGFR inhibitor PD173074 (Sigma) or DMSO as indicated in figures. Cells were lysed using lysis buffer (25mM Tris pH 7.5, 50mM NaCl and 1% NP40 and freshly supplemented with Protease and phosphatase inhibitor (Roche)). Cell lysates were clarified by centrifugation and the protein concentration was determined with BCA Protein Assay kit (ThermoFischer). 1 mg protein was precleared with 40 μl of protein G agarose beads (50% bead slurry) (GEHealthcare) and then incubated overnight with 20 μl of protein G agarose beads (50% bead slurry) and either anti-FGFR3 (F4025, Sigma) or normal Rabbit IgG control (A-105-C, R&D systems). Beads were rinsed four times with lysis buffer. The protein complex was eluted from the beads with Laemmli sample buffer (Biorad) and boiled at 95°C. The immunoprecipitated proteins were separated by SDS-PAGE using 4-15% Tris-glycine precast gel (Biorad) and analyzed by Western blotting.

Western blotting

Protein extracts were obtained using lysis buffer (50mM Tris-HCl (pH 6.8), 2% SDS, 5% glycerol, DTT 2mM, 2.5 mM EDTA, 2.5 mM EGTA) supplemented with Protease and phosphatase inhibitor (Roche)). Cell lysates were clarified by centrifugation. Protein concentration was determined with a BCA Protein Assay-Reducing Agent Compatible kit (ThermoFischer). Proteins (10 μg) were separated by SDS-PAGE using 4-15% Tris-glycine precast gels (Biorad) and transferred to nitrocellulose membranes using Trans-Blot Turbo transfer system (Biorad). Membranes were then blocked with 5% non-fat milk or 5% BSA at room temperature. Membranes were then incubated with the primary antibody overnight at 4°C and secondary antibody for 45 min at room temperature. Signal detection was performed using the Clarity Western ECL substrates (BioRad) followed with exposure on X-ray film (Thermofischer) or detection

with ChemiDoc MP imaging systems using Imagelab software (Biorad).

Immunofluorescence staining

Cells were fixed for 15 min with 4% PFA in PBS at room temperature. After permeabilization with 0.5% saponin (Sigma-Aldrich) and 2% BSA (Sigma-Aldrich), cells were incubated with primary and secondary antibodies before being mounted with Mowiol (Biovalley). Fixed samples were imaged with an upright widefield microscope from Leica equipped with 100X CFIPlanAPo VC oil immersion objective (1.4 NA CFI), a piezoelectric motor (Physik Instrumente) and highly sensitive cooled interlined charge-coupled device (CCD) camera (CoolSNAP HQ2, Photometrics). Z-dimension series of images were taken every 0.2 μm by Metamorph software (Molecular Devices). After deconvolution (Meine Algorithm [186]), colocalization between structures was analyzed with ImageJ 1.50 software [180]. Manders' overlap coefficients were calculated using the JACOP plugin for ImageJ [15].

Real-time quantitative PCR

RNA was extracted from cells with RNAeasy kits (Quiagen). One microgram of total RNA was reverse-transcribed with the High-Capacity cDNA Reverse Transcription kit (Applied Biosystems). Predesigned assay was used to quantify human *TBP* gene expression (Applied Biosystems) and custom assays were used for *RAB11A* and *RAB11B*. For custom assays, primers and probes were designed with Probe Finder software via the Universal Probe Library Assay Design Center (Roche). RT-qPCR was carried out with the LightCycler 480 Instrument (Roche) in a 20 μl reaction mixture containing 20 ng of reverse-transcribed RNA, 1x LightCycler 480 Probe Master, 25 uM each of the forward and reverse primers and 10 uM of the UPL probe (or 1x the predesigned assay probe). All expression assays were run in the same thermal cycling conditions, including an initial step at 95°C (10 min), followed by 40 cycles at 95°C (10 s), 60C (30 s) and 72°C (10 s). For each gene, the amount of mRNA was normalized to that of the *TBP* gene by the $2^{-\Delta\Delta Ct}$ method. Primers and probes were used for RAB11A: CTGCACCTTTGGCTTGTTTT (forward), CAGGGCAGTTCCTACAGATGA (reverse), probe 31; for RAB11B: CGACGAGTACGACTACCTATTCAA (foward), AACTCGTTGCGGGTGAAG (reverse), probe 62.

This page intentionally left blank.

Identification of FGFR3-interaction partners in bladder cancer

8

In order to better elucidate the molecular mechanisms underlying FGFR3 signaling in bladder cancer, we aimed to identify interaction partners of FGFR3. We generated human bladder cancer RT112 cells transiently expressing GFP-tagged FGFR3 to achieve this goal. Following immunoprecipitation of the FGFR3 protein complexes, interaction partners were identified using mass spectrometry.

8.1 Experimental workflow

To verify the efficiency of transfection, we first transfected RT112 cells with wild type FGFR3 tagged with GFP at its C-terminus or GFP plasmid (control) by using Fugene HD transfection reagent (Promega). The construct FGFR3-GFP is described in section 6.3. 24h after transfection, the cells were either mounted on coverslips or lysed with lysis buffer (25mM Tris pH 7.5, 50mM NaCl and 0.1% NP40 and freshly supplemented with Protease and phosphatase inhibitor (Roche)). The percentage of RT112 transfected cells was low, $\sim$ 20%. Western blot indicated that the FGFR3-GFP fusion protein was not cleaved (data not shown).

To prepare the cell lysate for immunoprecipitation, a seed culture of RT112 cells (at 70–80% confluence) was split and plated with fresh media the day before transfection and then grown to 50–60% confluency. The RT112 cells were then transfected with wild type FGFR3-GFP or GFP plasmid as control. 24h after transfection, the cells were lysed with lysis buffer. Protein concentration was determined with a BCA Protein Assay kit (ThermoFischer). For immunoprecipitation of the protein complexes, we used GFP-TRAP (gta-20, chromotek) which is a GFP binding protein coupled to a monovalent matrix (agarose beads). This method has many advantages including high binding affinity, no heavy and light chains of antibodies present in Western blots and mass spectrometry analysis. Because the percentage of RT112 transfected cells was low, 4 mg of the lysates were incubated with GFP-TRAP overnight at 4°C to enrich the amount of immunoprecipitated protein complexes. After four washes with

lysis buffer, the beads were incubated in H2O and transferred to be analyzed at the proteomics platform (Institut Jacques Monod). Briefly, the beads were trypsinized to digest the baits and the interacting protein. The unfractionated peptides were desalted prior to their analysis using liquid chromatography online coupled to tandem mass spectrometry (LC-MS/MS) (LTQ-Orbitrap Fusion with nano-LC, from ThermoScientific). Enriched proteins were identified using MASCOT (Matrix Science) software using a probabilistic scoring algorithm.

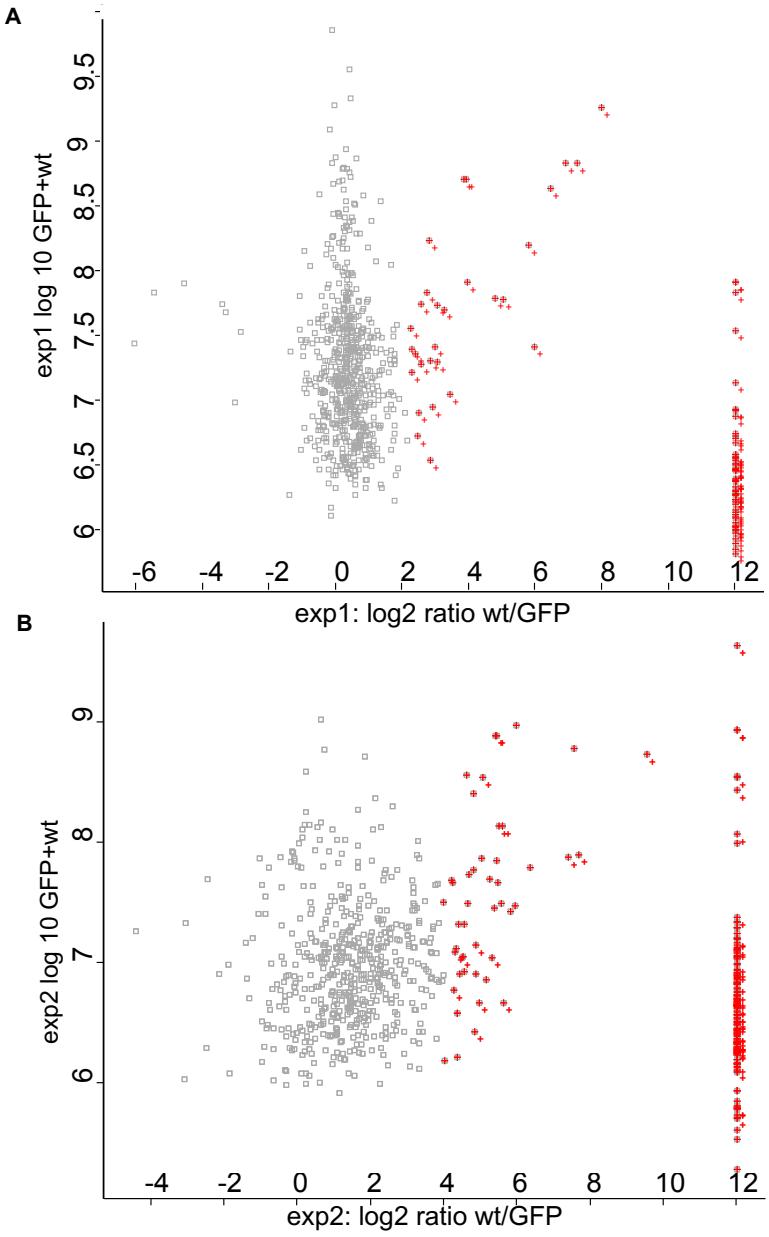

Figure 8.1 Scatter plot of the protein abundance ratios against the intensities of the identified proteins. Scatter plot of the abundance ratios between WT FGFR3-GFP versus GFP control, plotted against the intensities for each protein identified. The square corresponds to proteins that are not significantly enriched. The red cross indicates significant protein abundance differences between WT FGFR3-GFP versus GFP, p-value <0.05 for Experiment 1 (A), and if the abundance ratios between WT FGFR3-GFP versus GFP ≥ 4 for experiment 2 (B).

gene symbol	2	3	4	5	6	7	8
ANXA10	12	6,45	12	6,33	2	2	2,46E-27
AP1S1	12	5,81	12	5,79	2	2	2,46E-27
ATP6V1A	12	6,15	12	6,33	3	5	2,46E-27
ATXN10	12	6,27	12	6,33	3	5	2,46E-27
BAG5	12	6,55	4,29	7,08	3	12	2,46E-27
BAG6	12	6,37	12	6,63	4	9	2,46E-27
BZW1	12	6,87	12	7,12	4	7	2,46E-27
BZW2	5,95	7,41	4,87	7,14	2	11	1,42E-07
CANX	3,04	7,73	5,5	8,13	10	21	0,007663032
CDC37	5,77	8,19	9,55	8,72	19	22	3,41E-07
CDK2	6,91	8,82	12	8,93	4	2	8,30E-10
CDK5	7,26	8,82	12	8,93	5	4	1,05E-10
COG5	12	5,93	12	5,78	2	2	2,46E-27
COPB2	12	6,33	12	6,7	2	11	2,46E-27
COPG1	12	6,05	12	6,47	3	8	2,46E-27
DCAKD	12	6,21	12	6,68	3	8	2,46E-27
DNAJA2	12	6,56	12	7,19	2	6	2,46E-27
DNAJC7	12	6,72	5,32	7,03	5	14	2,46E-27
DNM2	12	6,55	12	6,5	3	11	2,46E-27
ESYT1	2,82	6,53	4,48	7,03	4	26	0,013218235
EZR	5,01	7,77	12	6,32	3	2	1,03E-05
FGFR3	7,97	9,25	12	9,63	31	37	1,15E-12
GBF1	12	5,99	12	8,06	3	8	2,46E-27
GGCX	12	6,47	12	6,52	2	4	2,46E-27
HSP90AA1	3,91	8,7	5,42	8,88	18	27	0,000608987
HSP90AB1	3,84	8,7	5,43	8,88	20	24	0,000763613
HSP90B1	2,73	7,83	5,58	8,13	6	9	0,016342133
HSPG2	12	6,13	12	6,81	3	28	2,46E-27
IPO7	12	6,93	5,61	6,66	3	4	2,46E-27

gene symbol	2	3	4	5	6	7	8
LLGL1	12	6,37	12	5,71	4	2	2,46E-27
LMAN2	12	7,53	12	8,53	7	19	2,46E-27
LMAN2L	12	7,83	12	8,43	11	17	2,46E-27
LRPAP1	12	5,97	12	6,26	2	5	2,46E-27
MFSD10	12	6,09	12	6,36	3	4	2,46E-27
NSF	2,45	6,72	12	6,25	3	7	0,030380
PGK1	12	6,58	12	6,15	3	2	2,46E-27
PIGS	12	6,74	4,27	6,76	2	6	2,46E-27
PLOD1	12	6,92	12	6,1	2	5	2,46E-27
PLXNB2	12	6,51	12	6,31	2	7	2,46E-27
PSMA5	12	6,38	12	6,4	2	3	2,46E-27
PSMC1	12	6,46	12	6,56	2	8	2,46E-27
PSMD12	12	6,23	12	6,28	4	5	2,46E-27
PSMD3	12	6,02	4,85	6,42	3	6	2,46E-27
PTPMT1	12	6,1	4,95	6,66	2	4	2,46E-27
RAB25	2,9	6,94	12	6,97	2	5	0,010888
RPAP3	12	7,13	12	6,62	2	9	2,46E-27
RPS6KA1	12	7,91	7,4	7,87	20	27	2,46E-27
RPS6KA3	12	7,91	7,67	7,89	27	26	2,46E-27
SDC4	12	6,67	12	7,1	4	3	2,46E-27
STAT6	12	6,23	12	6,5	2	6	2,46E-27
STUB1	12	6,29	12	6,74	3	4	2,46E-27
TIMM50	4,79	7,78	12	6,91	5	4	2,52E-05
TM9SF1	12	6,03	12	6,56	2	2	2,46E-27
TOMM70A	12	6,3	12	6,94	2	10	2,46E-27
TRAP1	2,8	8,23	5,05	8,53	15	8	0,013863
UBC	3,05	7,29	12	7,37	3	7	0,007468
UPP1	2,55	7,74	12	6,41	3	5	0,024514
VANGL1	12	6,27	12	7,2	3	11	2,46E-27

Figure 8.2 List of proteins identified in Mass spectrometry. Column 1: Gene symbol; column 2: exp1 wt1 B7:log2 ratio WT1/GFP; column 3: exp1 wt1 B7:log10 GFP+wt; column 4: exp2 wt2 E6 log2 ratio; column 5: exp2 wt2 E6 log10 GFP+wt; column 6: number of unique peptides in experience 1; column 7: number of unique peptides in experience 1; column 8: p-value calculated for experience 1.

To reliably estimate the potential partners of FGFR3, we performed two independent experiments. In order to identify actual interaction partners of FGFR3, we took into account both the abundance ratio between FGFR3-GFP versus GFP and the intensities of the identified proteins. Using a significance B value ($p<0.05$) (Perseus software, Computational systems biochemistry). Our first replica allowed the identification of 88 potential partners for FGFR3 (Figure 8.1.A), while the second replica was not technically successful due to the saturation when the sample were analyzed by mass spectrometry system. Therefore, a manual threshold was set to determine which proteins are probably positive in the list of proteins identified in the second experiment (Figure 8.1.B) (212 proteins). The proteins which were positive in two replicates were uploaded on Ingenuity Pathway Analysis (IPA) developed by Qiagen, then network analysis was performed. The reference set was the IPA knowledge database, all data source in IPA were included for analysis protein-protein interactions. We also searched in the literature for the function of the identified proteins.

8.2 Results

The intersection of 57 proteins identified from the two experiments are presented in Figure 8.2. Analysis by IPA helped us to establish a network of 35 proteins containing proteins identified in the mass spectrometry and additional proteins from the IPA database. The additional proteins have direct or indirect relationship with the proteins identified by mass spectrometry according to the protein-protein interaction algorithm of the IPA knowledge database. Five networks were proposed by IPA.

The first network (Figure 8.3) contained 23 proteins identified in mass spectrometry and 12 additional proteins from IPA database. In this network, we found many well-known partners of FGFR3, such as CDC37 and different isoforms of HSP90 [107], RPS6KA3 (known as RSK2) [97], HSPG2 and SDC4 [7, 52], and STUB1 [107]. Proteins of the HSP90 and HSP70 chaperone complexes were also identified, for instance, TRAP1, DNAJC7, PGK1, LLGL1, TOMM70A, RPAP3, CDK5, BAG6, BAG5 and EZR [202]. Of note, CDK5 has been shown to phosphorylate Dynamin and to be essential for synaptic vesicle endocytosis [204]. In addition, the results indicated an interaction between FGFR3 and a group of proteins involved in proteasome degradation: PSMD12, PSMA3, PSMA5, UBC, STUB1 and PSMC1. ERK1/2 was not detected in the list of proteins identified but we found other substrates of ERK1/2 such as RPS6KA3 and RPS6KA1.

The second network (Figure 8.4) contained less proteins identified in the mass spectrometry experiment (13 proteins) than the first one. The IPA database added the proteins which are substrates of FGFR3 downstream signaling such as PI3K, AKT, P38, RAS. ESYT1 and STAT6 are also of interest because members of the same family have been reported to interact with FGFR [210, 154].

There are 9 proteins identified in our mass spectrometry along with 26 proteins from the IPA constituting the third network (Figure 8.5). This network shows that RAB25 expression is negatively regulated by vimentin [219]. RAB25 has been shown to interact with PKIG by another mass spectrometry analysis [55]. Moreover, AP1S1 is a clathrin adaptor-related protein involving in trafficking [203], but its function remains

poorly explored.

Among the proteins of network 4, there is a group of proteins associated with ubiquitination of receptors such as UBC, ATP6V1A, DCAKD, ATXN10 and TIMM50.

The network 5 points to proteins involved in intracellular transport such as different subunits of COP (Coatomer protein complex), RAB1B, GBF1, ARF, USO1 and LMAN2L. These proteins principally localize to the Golgi complex and the endoplasmic reticulum.

Interestingly, the results showed that there was an interaction between FGFR3 and RAB25 and Dynamin 2 (DNM2). This finding supports our results on the role of RAB25 and DNM2 in the trafficking and signaling of FGFR3, as described in Chapter 6. Of note, STAT6 is upregulated in tumors associated with mutated FGFR3, in contrast to CDK2 that is downregulated in these tumors (transcriptomic data from our laboratory). Also, ANXA10 is negatively associated with the Multiple Regional Epigenetic Silencing (MRES) phenotype of bladder cancer. ANXA10 is expressed in tumors which do not present the MRES phenotype and which comprise most of the FGFR3 mutated tumors [215, 13]. These data suggest that the interaction of FGFR3 with ANXA10, STAT6 and CDK2 should be tested in priority.

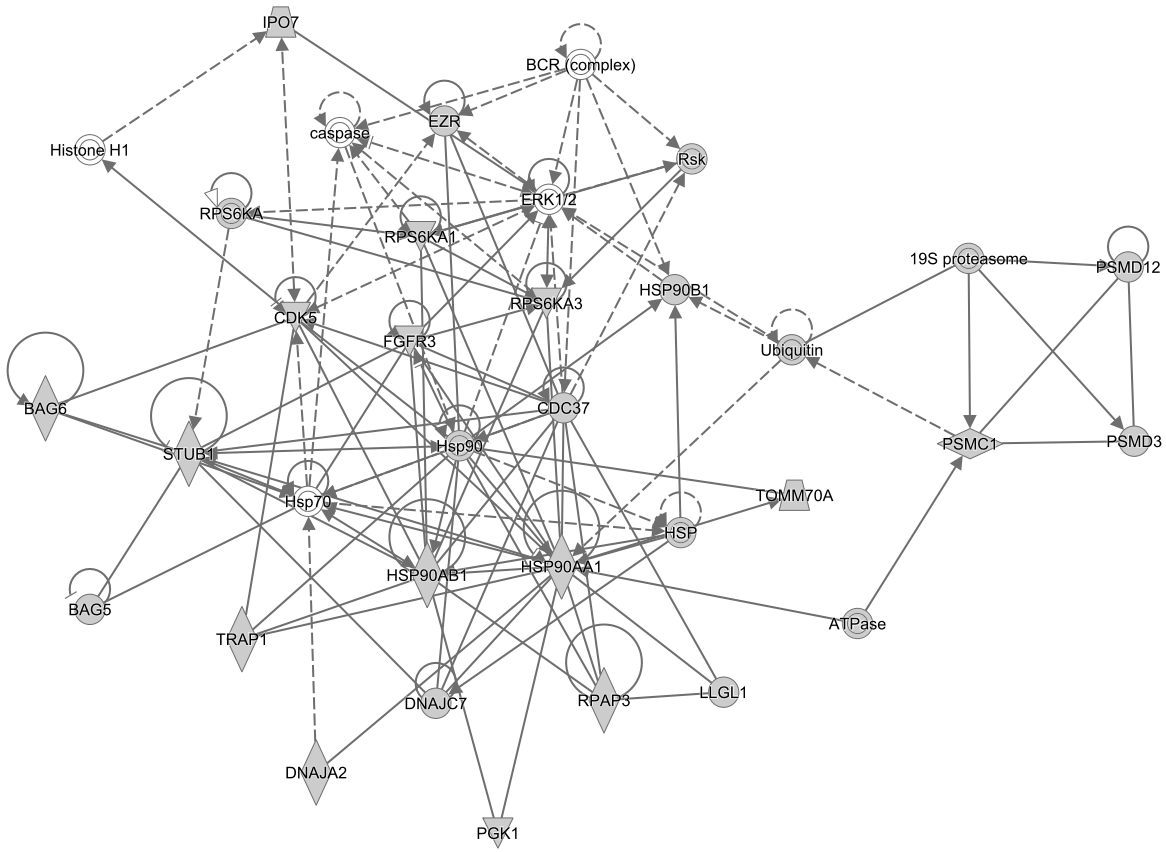

Figure 8.3 Network 1. Continuous line: direct interaction; Dash line: indirect interaction; Line with arrowhead: protein A acts on protein B. Gray node: protein identified in mass spectrometry; white node: protein from IPA database.

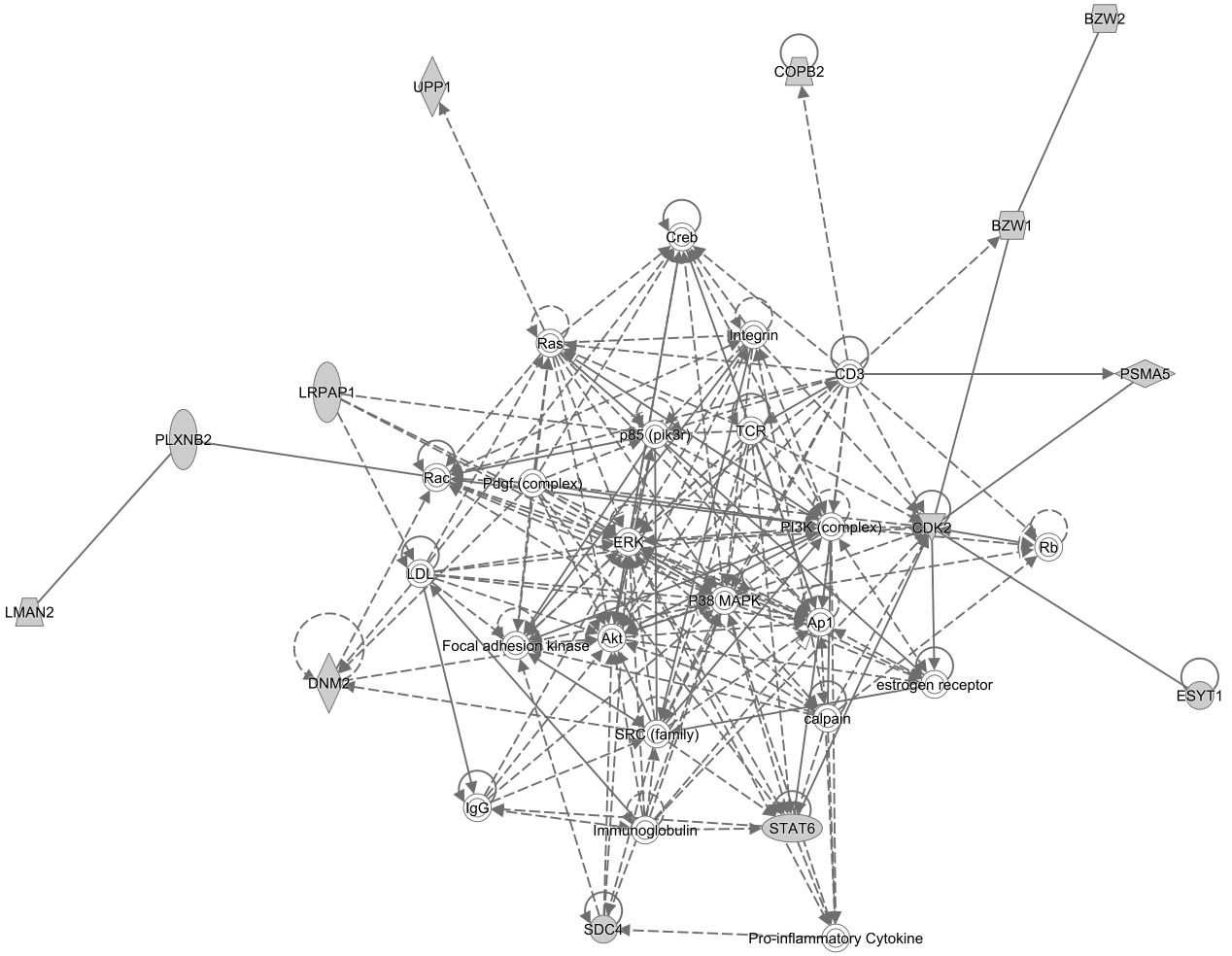

Figure 8.4 Network 2. Continuous line: direct interaction; Dash line: indirect interaction; Line with arrowhead: protein A acts on protein B. Gray node: protein identified in mass spectrometry; white node: protein from IPA database.

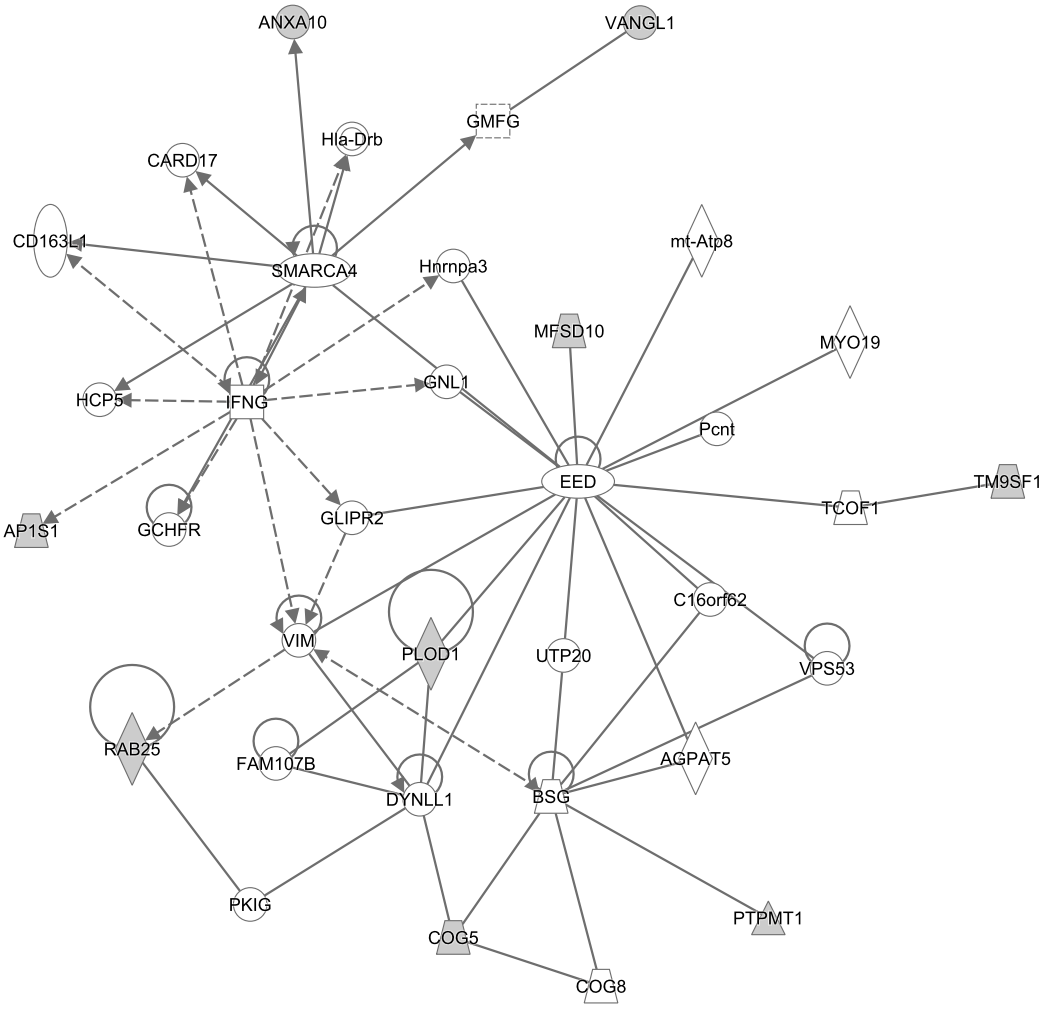

Figure 8.5 Network 3. Continuous line: direct interaction; Dash line: indirect interaction; Line with arrowhead: protein A acts on protein B. Gray node: protein identified in mass spectrometry; white node: protein from IPA database.

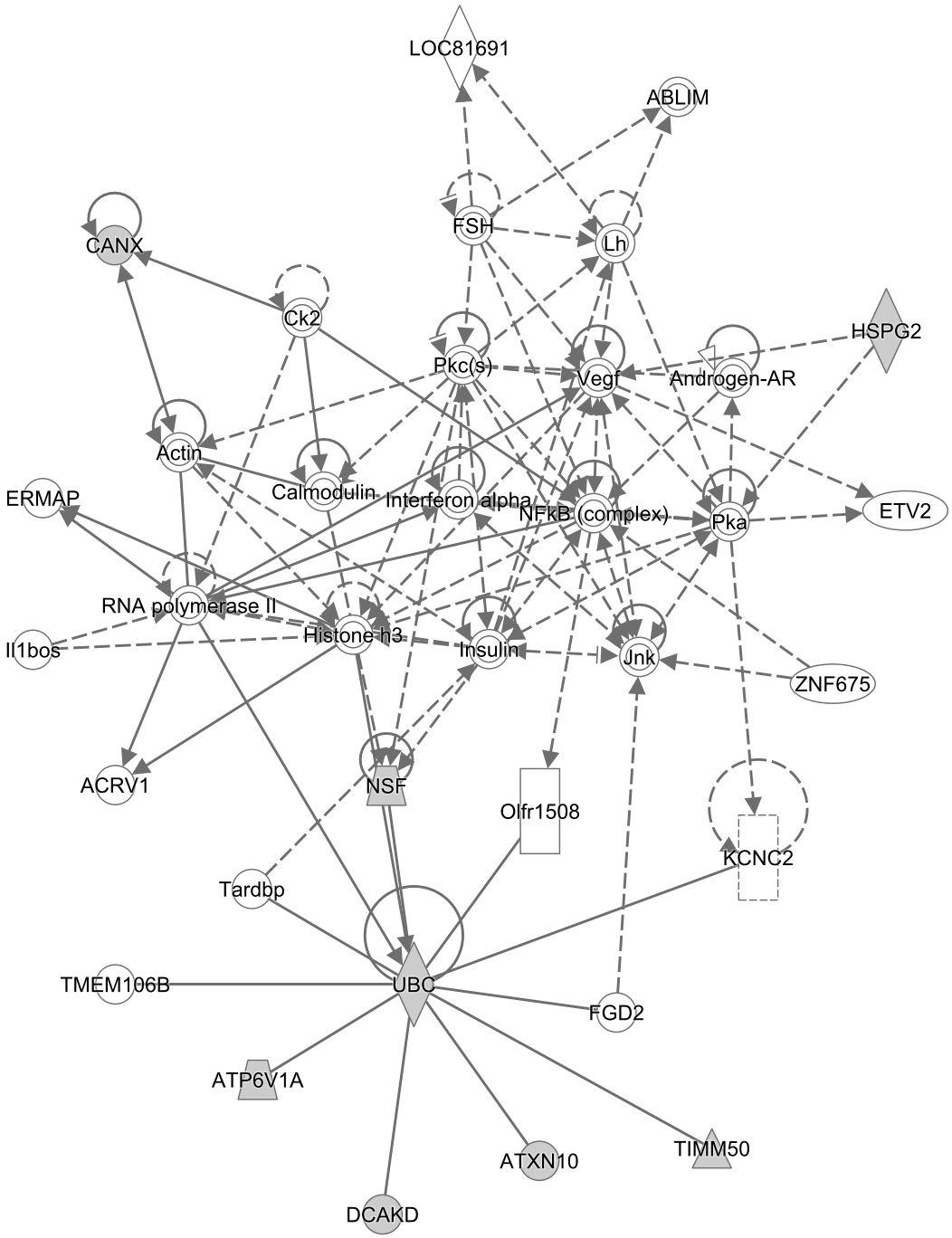

Figure 8.6 Network 4. Continuous line: direct interaction; Dash line: indirect interaction; Line with arrowhead: protein A acts on protein B. Gray node: protein identified in mass spectrometry; white node: protein from IPA database.

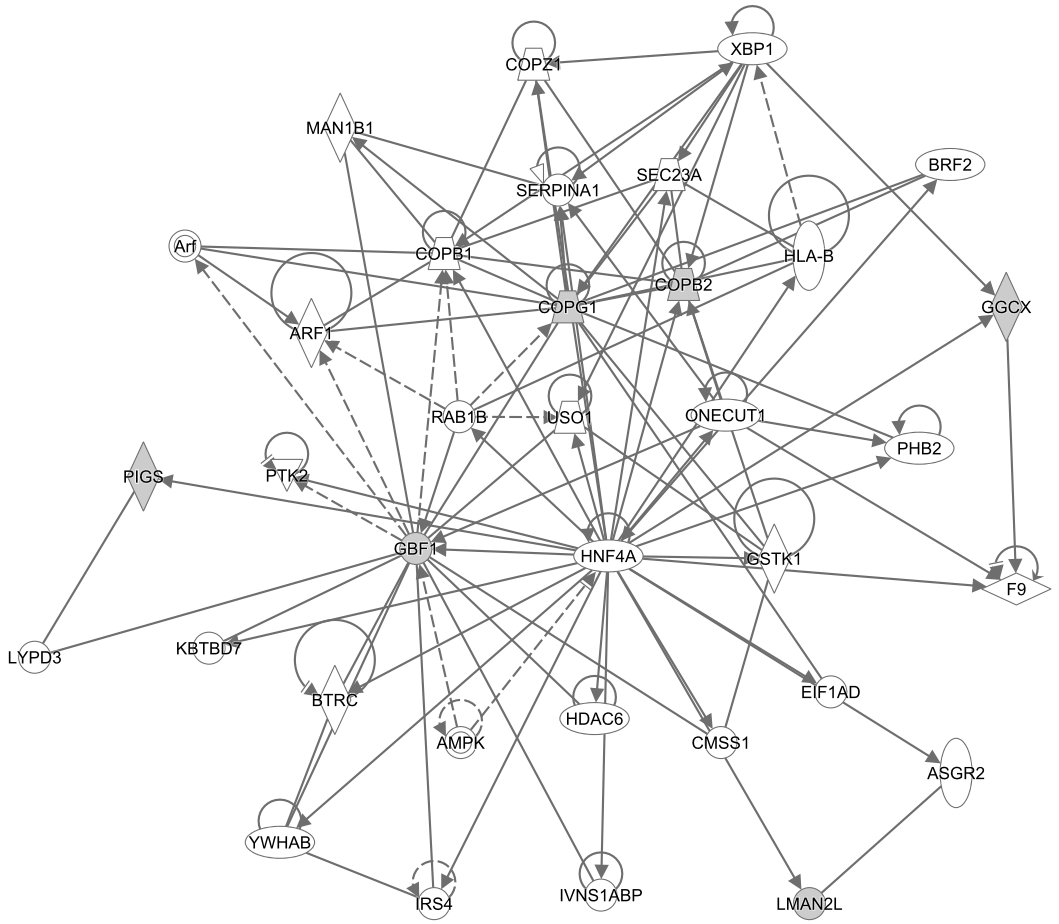

Figure 8.7 Network 5. Continuous line: direct interaction; Dash line: indirect interaction; Line with arrowhead: protein A acts on protein B. Gray node: protein identified in mass spectrometry; white node: protein from IPA database.

8.3 Discussion

The proteins were identified by mass spectrometry from two experiments with different methods setting the threshold due to different efficiency of replicate, therefore another replicate should be performed to validate the results obtained.

Although the results obtained are still preliminary, they suggest new partners of FGFR3 that could help our understanding of its signaling in bladder cancer.

IV.

Discussion

9 Discussion

In the aim to understand the molecular mechanisms underlying FGFR3 signaling in bladder cancer with a particular focus on the importance of FGFR3 trafficking on its signaling, we investigated the potential role of RAB GTPases. We found that proteins of the RAB11 subfamily (RAB11A, RAB11B and RAB25), in particular RAB25, are overexpressed in tumors carrying mutated and translocated FGFR3 compared to tumors without these alterations. Our results indicate that the depletion of RAB11 and RAB25 and two of their effectors, RAB11FIP2 and MYO5B induces an inhibition of cell viability of bladder cancer cell lines expressing activated FGFR3 (mutated or translocated gene) whereas it had little effect on cell viability of other bladder tumor derived cell lines that do not express activated FGFR3. Other RAB such as RAB7 or RAB21, not involved in the recycling process, had no impact on cell viability of cell expressing altered FGFR3. To gain further insight on how RAB11 and RAB25 regulate cell viability in these cells, we first examined whether RAB11 and RAB25 depletion can alter the trafficking of FGFR3. Our results show that RAB11 and RAB25 play an important role in the recycling of FGFR3 and that the inhibition of recycling favors its degradation. We further investigated their role in FGFR3 activity via the activation of downstream signaling pathways (AKT, P38 and ERK1/2) and the expression of FGFR3 target genes (*MYC, DUSP6, TIMP2* and *GATA3*). Our results would favor a model in which the RAB11- and RAB25-mediated recycling of FGFR3 can sustain its signaling by protecting altered FGFR3 from the degradation pathway and providing a unique platform for FGFR3 signaling from the endocytic recycling compartment.

9.1 RAB25 expression

It is thought that RAB25 has an epithelial-restricted expression profile [24, 31, 67, 139]. Gene expression data from our laboratory confirmed this observation in bladder cancer samples. RAB25 as well as MYO5B are highly expressed in normal urothelium and in most low grade and low stage urothelial tumor samples but are weakly expressed in muscle or chorion samples (data not shown). In contrast, RAB11A, RAB11B and RAB11FIP2 are ubiquitously expressed in different cell types (data not shown), which is consistent with findings from other studies [100]. In addition, RAB25 expression is highly correlated to genes associated with differentiated urothelial markers, for ex-

ample, *ELF3, VSIG2, ERBB3, GRHL3, CLDN7, GATA3, UPK2*; and anti-correlated to epithelial-to-mesenchymal transition markers, such as *ZEB1, ZEB2*, and *FYN* (data not shown).

Transcriptome analysis in muscle-invasive bladder tumors has revealed that they are heterogeneous and can be grouped into basal and luminal subtypes like breast cancers [35]. Like in basal breast cancer, basal bladder tumors contain a claudin-low subtype that is enriched with biomarkers characteristic of epithelial-to-mesenchymal transition, for example *ZEB1* and *ZEB2*. Other molecular features characterizing this subgroup are overexpression of *STAT3*, *EGFR*, and *CDH3*. Luminal muscle-invasive bladder cancers are enriched with activating *FGFR3* and *ERBB3* mutations and *ERBB2* amplifications, and their gene expression profiles are controlled by peroxisome proliferator-activated receptor γ (PPARγ). In breast cancers, it was shown that RAB25 is upregulated in luminal ER-positive and PR-positive breast tumors [233, 139]. In contrast, RAB25 is mostly lost in basal-like and triple-negative breast tumors, and displays a tumor suppressor activity in MDA-MB-231, a cell line representative of this group [29]. We expected to obtain the same result in bladder tumors. Following RAB25 depletion, the cell viability of UMUC5 cells, a basal-like bladder cancer cell line, was not inhibited, and unexpectedly the same result was obtained in UMUC9 cells, a luminal bladder cancer cell line that depends on PPARγ for growth. Our results show that RAB25 along with the other members of the RAB11 subfamily play a protumorigenic role specifically in cell lines presenting FGFR3 alterations. Below, I discuss about the putative role of these RAB GTPases in bladder tumorigenesis.

9.2

RAB11/RAB25 GTPases sustain the cell viability via FGFR3 activity

No additive effect on cell viability was observed following simultaneous depletion of RAB11/RAB25 and FGFR3 compared to RAB11/RAB25 or FGFR3 depletion alone, suggesting that RAB11 and RAB25 sustain cell viability via FGFR3 activity. Furthermore, following RAB11/RAB25 knockdown, FGFR3-GFP accumulated in TFRC-positive recycling compartment but the extent of colocalization with LAMP1- or CD63-positive structures was also increased, suggesting that FGFR3 might be degraded. It is possible that the level of total FGFR3 could be partly reduced but not completely depleted in cells knockdown for RAB11/RAB25 compared to control cells. Additionally, compared to control cells, about only 50% of *MYC* expression was inhibited in different conditions of RAB11/RAB25 depletion but about 80% *MYC* expression was reduced following FGFR3 knockdown. It was shown in our laboratory that in RT112 cells, FGFR3 induces MYC upregulation via stabilizing *MYC* mRNA and via protecting MYC protein degradation from proteasome [125]. Taken together, in RAB11/RAB25-depleted cells, the inhibitory effect on cell viability could reflect the effect on *MYC* expression resulting from a decreased FGFR3 activity. It will be important to estimate the amount of FGFR3 present at the plasma membrane following RAB11/RAB25 depletion by using cell surface biotinylation assays. It will be also necessary to examine the MYC protein level after RAB11/RAB25 silencing.

9.3
Proposed working model

From our findings and data from other studies, we propose a model for FGFR3 recycling and signaling in bladder cancer carrying altered FGFR3, illustrated in Figure 9.1.

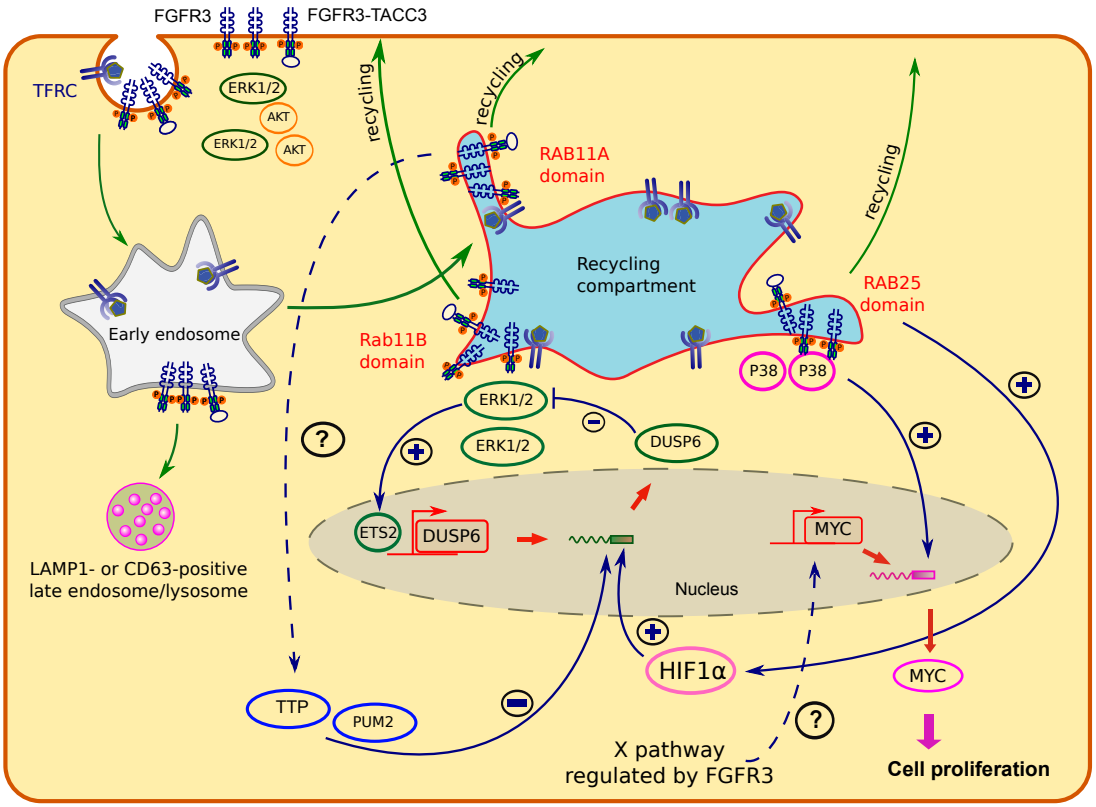

Figure 9.1 FGFR3 trafficking and signaling in bladder cancer carrying altered FGFR3. Green arrow: trafficking pathway, blue arrow: signaling pathway. Continuous line: pathway was proven in our study or other studies. Dash line: proposed pathway. FGFR3: Fibroblast Growth Factor Receptor 3, FGFR3-TACC3: gene fusion between FGFR3 and Transforming Acidic Coiled-Coil containing protein 3, TFRC: Transferrin Receptor, DUSP6: Dual Specificity Phosphatase 6, ETS2: V-Ets Avian Erythroblastosis Virus E26 Oncogene Homolog 2, TTP: Tristetraprolin, PUM2: Pumilio RNA-Binding Family Member 2, HIF1α: Hypoxia Inducible Factor 1 Alpha Subunit.

9.3.1
FGFR3 activates its signaling pathways at the plasma membrane

Our results from the Dyngo4a treatment suggest that AKT and ERK1/2 are activated by FGFR3 from the plasma membrane. This finding is consistent with another study showing that clathrin-dependent endocytosis is not required for efficient activation of FGFR3 on phosphorylation of FRS2, an upstream substrate of AKT in FGFR signaling, and on phosphorylation of ERK1/2 [83]. As in RT112 cells, FGFR3 is constitutively activated in a ligand stimulation-independent manner, we cannot exclude that AKT or ERK1/2 would be still phosphorylated from endosomes after Dyngo4a treatment if FGFR3 was internalized via other pathways. Indeed, the block of a given

endocytic pathway often leads to the activation of others [47]. Moreover, in U2OS cells stably expressing wild type FGFR3, it was shown that FGFR3 is internalized via both clathrin- and dynamin-dependence as well as an unknown clathrin-independent endocytic pathway.

To conclude, we need to verify: i) whether, following Dyngo4a treatment, FGFR3 is completely blocked at the plasma membrane; ii) whether phosphorylation of AKT and ERK1/2 only results from signaling at the plasma membrane; and iii) whether on its way from the endoplasmic reticulum to Golgi and the plasma membrane, FGFR3 can activate its signaling pathways. In addition, to better unravel the role of endocytosis on signaling, several methods to alter receptor internalization should be performed such as depletion of clathrin or AP2.

9.3.2 FGFR3 recycles via distinct domains which are specific for each member of the RAB11 subfamily

This hypothesis comes from the findings that there is no functional redundancy between the RAB11 subfamily proteins in regulating the viability of RT112 and MGHU3 cells. Another line of evidence supporting this hypothesis is that RAB11/RAB25 silencing has differential effects on three FGFR3 downstream signaling pathways: P38, AKT and ERK1/2.

RAB25 domain

Our results show that when RAB25 is depleted (alone or with RAB11), elevated level of P-P38 is detected. This suggests that FGFR3 is trapped into a microdomain of the recycling compartment from which FGFR3 can be recycled in a RAB25-dependent manner. Also, P38 can be specifically recruited to this domain and phosphorylated by FGFR3. In turn, P-P38 will stabilize *MYC* mRNA expression as shown in other studies in our laboratory. In cell simultaneously depleted for RAB11/RAB25 and FGFR3, the P-P38 level was about the same level as control cells, suggesting that P38 was phosphorylated at basal level. This amount of P-P38 may be not enough to stabilize the *MYC* mRNA level because *MYC* expression was dramatically reduced (∼90%) in cells simultaneously depleted for RAB11/RAB25 and FGFR3 compared to control cells. We cannot exclude the possibility that FGFR3 can regulate *MYC* expression via another pathway (termed as X pathway in Figure 9.1). Thus, following RAB25 depletion, the decrease in FGFR3 level can result in a decreased activity of the X pathway, leading to the inhibition of *MYC* expression though an elevated level of P-P38.

Strikingly, *DUSP6* expression was strongly reduced when only RAB25 was depleted (50% compared to control siRNA) or slightly reduced in case of the combination with other siRNAs targeting RAB11A or RAB11B (75% and 90%, respectively). DUSP6 plays a negative role in FGF signaling via a negative feed-back loop at the ERK1/2 level. Indeed, FGF signaling induces phosphorylation of ERK1/2, resulting in binding of Ets2, a transcriptional regulator, to the *DUSP6* promoter [51]. Conversely, when DUSP6 is expressed, this protein in turn inhibits the phosphorylation of ERK1/2 [193]. In our model, after RAB25 silencing, P-ERK1/2 was not altered, suggesting that another mechanism can promote *DUSP6* expression. A recent paper has reported that

overexpression of RAB25 induces Hypoxia-inducible factor 1 alpha (HIF-1α) in an oxygen-independent manner in many cancer cell lines [71]. Furthermore, it was shown that HIF-1α regulates *DUSP6* expression through mRNA stabilization [11]. Therefore, a proposed explanation for our findings is that RAB25 depletion reduces HIF-1α expression, leading to a degradation of *DUSP6* mRNA expression. Thus, it will be important to estimate the level of HIF-1α after RAB25 knockdown.

RAB11B domain

An increased phosphorylation of ERK1/2 was specifically obtained when RAB11B was depleted. In this condition, FGFR3 could be trapped into a microdomain from which FGFR3 can be recycled in a RAB11B-dependent manner. This domain is distinct from the RAB25 domain described above because it specifically recruits and activates ERK1/2. As mentioned above, the ERK pathway appears as a major positive regulator of *DUSP6* mRNA expression in developing embryos and cancer cell lines [193, 51, 11]. The unmodified level of *DUSP6* expression obtained after RAB11B depletion but not after FGFR3 silencing supports the role of RAB11B in FGFR3-induced ERK1/2 activation. Although we cannot clearly explain why *DUSP6* expression remained at the same level compared to control cells, one possibility is that ERK1/2-induced DUSP6 expression has already reached a threshold level. This finding also suggests that ERK1/2 can be activated from the recycling endosomes. Along with the results obtained from the experiment with Dyngo4a treatment, it is possible that following RAB11B depletion, a specific domain for the recruitment of ERK1/2 by FGFR3 is formed on the recycling compartment. To test this hypothesis, a treatment with ERK1/2 inhibitor in cells depleted for RAB11B should be performed. The ERK pathway also regulates DUSP6 expression at the protein level by phosphorylating DUSP6 on Ser159, Ser174 and Ser197 which is followed by the degradation of the phosphatase by the proteasome [127]. We expect that the *DUSP6* mRNA and protein expression will be reduced compared to control cells or cells depleted for RAB11B.

RAB11A domain

This hypothesis comes from the fact that RAB11A depletion alone did not affect the phosphorylation of ERK1/2 or P38. The observation that *MYC* expression in cells knockdown for only RAB11A was 70% compared to control can be explained by the reduction of the activity of the X pathway resulting from a decreased in the total level of FGFR3 protein. Strikingly, an increase of *DUSP6* mRNA level (140% compared to control cells) was obtained after RAB11A silencing. DUSP6 mRNA stability was shown to be positively regulated by HIF-1α as mentioned above, but also to be negatively regulated by Tristetraprolin (TTP) and Pumilio RNA-binding Family Member 2 (PUM2) [11]. Whether RAB11A depletion can alter the function of these proteins should be investigated. In the case of triple-RAB11 depletion, a balance between the inhibitory and activating effects on *DUSP6* expression is possibly established through different pathways.

9.3.3 Evaluation of the proposed model

The fact that RAB proteins localize to distinct endosomal microdomains even on the same compartment has been demonstrated for early and recycling endosomes. These endosomes are formed of multiple RAB4, RAB5 and RAB11 domains that are dynamic but do not significantly intermix overtime [195]. Three main domains have been observed: one that contains only RAB5, a second containing RAB4 and RAB5, and a third containing RAB4 and RAB11. Similarly, late endosomes contain distinct membrane domains that are positive for either RAB7 or RAB9 [10]. Recently, it was proposed that RAB11A and RAB11B play distinct roles in the recycling of FGFR4 or PAR-1 [81, 75]. Our proposed model can be tested by super resolution fluorescence microscopy.

Although we did not directly quantify the protein level of FGFR3 following RAB11 and RAB25 depletion, our results suggest that the FGFR3 level is decreased. However, it is not clear whether RAB11A or RAB11B or RAB25 domains can recruit FGFR3 downstream substrates such as P38 or ERK1/2 under normal condition in RT112 cells or if this recruitment only occurs in cells depleted for RAB11/RAB25. Taken together, our findings clearly indicate that RAB11/RAB25 play an important role in FGFR3 recycling, resulting in sustaining its signaling.

9.3.4 Questions that remain to be elucidated

First, the elevated level of P-AKT was observed in cells depleted for only one of the RAB11 subfamily proteins but not in case of double or triple knockdown. Because the Dyngo4a experiment suggests that AKT is phosphorylated at the plasma membrane, we propose that the endocytic recycling network probably creates a microdomain near the plasma membrane where AKT can be recruited following siRNA targeting only one of the *RAB11* genes.

Two other FGFR3 target genes, GATA3 and TIMP2, displayed a mRNA expression after RAB11/RAB25 silencing different from that obtained after FGFR3 silencing. To our knowledge, the upstream regulation pathway of these genes remains unknown. We thus propose to examine the effects on the expression of *GATA3* and *TIMP2* after RAB11/RAB25 depletion and a treatment with kinase inhibitors of AKT, P38 and ERK1/2.

9.3.5 Limitations of the study

The quantification of the expression of FGFR3 target genes was performed in only one RT-qPCR experiment and needs to be repeated. As reverse-transcribed RNAs are already available after different siRNA transfection, these experiments can be soon performed. We had to investigate the trafficking of FGFR3 in bladder cancer cell lines by using RT112 cells transiently transfected with wild type FGFR3-GFP due to the lack of antibodies specifically recognizing endogenous FGFR3 in immunocytology experiments. Nevertheless, the pattern of subcellular distribution of FGFR3-GFP in RT112

cells is consistent with other studies [82, 43]. The GFP fusion protein seems to be functional in these cells since it interacts with HSP90, a well-known chaperone partner of FGFR3 [107]. Data from our laboratory indicate that in RT112 cells, wild type FGFR3 forms heterodimers with the fusion protein FGFR3-TACC3, suggesting that wild type FGFR-GFP introduced in these cells can interact together with endogenous wild type or translocated FGFR3. We did not choose the labeled ligand stimulation method to follow the trafficking of FGFR3 due to the fact that in RT112 cells displaying altered FGFR3, FGFR3 is constitutively activated and no increase in phosphorylation could be achieved in presence of FGF1 ligand, suggesting that the receptor internalization is independent of ligand stimulation. Also, there is no ligand specific for the FGFR3b isoform which was expressed in bladder cancer cell lines and other FGFRs have the same affinity binding with FGF1. As mentioned before, it will be important to quantify the FGFR3 protein level and the proportion of FGFR3 recycled to confirm the proposed hypothesis.

9.4
Trafficking and signaling of WT and mutated S249C FGFR3

9.4.1
Difference between the subcellular distribution of WT and mutated S249C FGFR3

In an attempt to characterize the potential difference in the trafficking of wild type and mutant FGFR3, we quantified the extent of colocalization between FGFR3 and different markers of intracellular compartments in HeLa cells transiently expressing FGFR3-GFP (WT or S249C forms). As HeLa cells do not express detectable levels of FGFR3, FGFR3-GFP cannot interact with endogenous protein. FGFR3-GFP displayed a vesicular pattern dispersed throughout the cytoplasm. We also observed this vesicular structure in several bladder cancer cell lines (RT112, MGHU3, T24, HT1376). This subcellular distribution is consistent with several studies, for example that of WT and K644E/K650M FGFR3 in Cos-7 stably expressing FGFR3-GFP [33, 43]. Cy3-labeled FGF1 is internalized in vesicular structures in U2OS cells stably expressing FGFR3, suggesting that FGFR3 is found in endosomal compartments [83]. However, in our study, we could not compare the subcellular localization of FGFR3-GFP with that of endogenous FGFR3 in bladder cancer cells due to the lack of anti-FGFR3 antibodies specifically recognizing endogenous FGFR3 by immunofluorescence staining.

Our results indicate that the subcellular distribution of WT FGFR3 differs from that of mutated S249C FGFR3. At steady state, activated WT FGFR3 localizes in several compartments including early endosomes, late endosomes/lysosomes and also the recycling compartment. There was no significant difference between the overlap of FGFR3 with late endosomes and the recycling compartment. In contrast, activated S249C resides preferentially in the recycling compartment, and only a small fraction of mutated FGFR3 was found in late endosomes/lysosomes. This pattern of distribution of WT and mutant FGFR3 was also reported in other studies. Indeed, in Cos-7 stably expressing WT or mutant FGFR3, activated WT FGFR3 is normally targeted for lysosomal degradation through a mechanism involving c-Cbl-mediated ubiquitination [33]; in contrast, mutant forms (K644E, K650M) of FGFR3 escape from lysosomal compart-

ment to enter into a recycling pathway. The consequence of this derailed trafficking is the amplification of the normal inhibitory FGFR3 signals in the skeletal growth plate. The authors suggest that a defect in c-Cbl-mediated ubiquitination of mutant FGFR3 is the cause of this altered trafficking. However, the question of the ubiquitination of mutant FGFR3 is still under debate [33, 16, 141]. Also, the TDI mutant (R248C) localizes in a perinuclear region and colocalizes with nucleoporin; by contrast only a partial or no overlap with late endosomes/lysosomes was observed [115].

However, our findings on the subcellular distribution of FGFR3 differ from those of Bonaventure et al [16]. Wild type FGFR3 was shown to colocalize with GM130, a *cis*-Golgi marker, in 293-VnR cells[16]. Mutated FGFR3 (R248C, Y373C) showed partial colocalization with peptidyl disulfide isomerase (PD1), an endoplasmic reticulum marker. These differences may be due to the two different cell types used (293-VnR cells, a human embryonic kidney cells expressing the vitronectin receptor and HeLa cells, a human cervix carcinoma cell line). Our results also differ from those of Lievens et al [119] that reported that WT FGFR3 localizes mainly at the plasma membrane in HEK293 cells transiently expressing FGFR3-GFP. This difference may be due to the fact that in our model WT FGFR3-GFP is always phosphorylated and activated; in contrast, in their model, WT FGFR3-GFP is not phosphorylated, suggesting that the receptor cannot be internalized.

Aside from S249C FGFR3, we wanted to compare the trafficking of FGFR3-TACC3, a fusion FGFR3 protein recently identified in bladder cancer but also many other cancer type such as glioblastoma and lung cancer [188, 231]. Unfortunately, the PCR amplification of this fusion from RT112 cells failed, maybe due to the length of this gene. Several kits with different types of Taq Polymerase will be tested to obtain this construct.

9.4.2 Signaling of WT and S249C FGFR3

In our studies, we could not conclude whether there was a difference between WT and S249C FGFR3 because the introduction of FGFR3 in HeLa cells did not induce a modification in the AKT, P38 and ERK1/2 downstream signaling pathways of FGFR3. Also, no difference in the phosphorylation of these proteins was observed in cells expressing wild type and S249C FGFR3-GFP. We propose to use human bladder cancer cell lines to directly investigate the impact of the different forms of FGFR3 on trafficking and signaling. These cells will provide the machinery required for FGFR3 transforming activity. For example, MGHU3 cells are dependent on constitutively activated FGFR3 for growth and transformation and expressed weakly mutated FGFR3. However MGHU3 cells are difficult to transfect by using cationic lipid reagents. Thus, electroporation or lentivirus could be better transfection strategy for this cell line.

In conclusion, our results indicate that RAB25 and RAB11 GTPases play an important role in the recycling of FGFR3. They help sustain cell viability by regulating the amplitude of FGFR3 response and probably provide a specific platform for its activity. Our study contributes to understand the molecular mechanisms underlying the relationships between the trafficking and signaling of FGFR3 in the context of bladder cancer. It could pave the way for the identification of new targets and new therapeutic

strategies for tumors associated with an abnormal FGFR3 pathway.

This page intentionally left blank.

Bibliography

[1] *https://en.wikipedia.org/wiki/Diglyceride*.

[2] *http://www.ujaen.es/investiga/atlas/atlas-ingles/vejiga/vejiga10x.htm*.

[3] Agarwal, R., Jurisica, I., Mills, G. B., and Cheng, K. W. The emerging role of the rab25 small gtpase in cancer. *Traffic 10*, 11 (2009), 1561–8.

[4] Ahmad, I., Singh, L. B., Foth, M., Morris, C.-A., Taketo, M. M., Wu, X.-R., Leung, H. Y., Sansom, O. J., and Iwata, T. K-ras and β-catenin mutations cooperate with fgfr3 mutations in mice to promote tumorigenesis in the skin and lung, but not in the bladder. *Dis Model Mech 4*, 4 (Jul 2011), 548–555.

[5] Amornphimoltham, P., Rechache, K., Thompson, J., Masedunskas, A., Leelahavanichkul, K., Patel, V., Molinolo, A., Gutkind, J. S., and Weigert, R. Rab25 regulates invasion and metastasis in head and neck cancer. *Clin Cancer Res 19*, 6 (2013), 1375–88.

[6] Aoun, F., Kourie, H. R., Sideris, S., Roumeguère, T., van Velthoven, R., and Gil, T. Checkpoint inhibitors in bladder and renal cancers: results and perspectives. *Immunotherapy 7*, 12 (Dec 2015), 1259–1271.

[7] Arikawa-Hirasawa, E., Watanabe, H., Takami, H., Hassell, J. R., and Yamada, Y. Perlecan is essential for cartilage and cephalic development. *Nat Genet 23*, 3 (Nov 1999), 354–358.

[8] Auciello, G., Cunningham, D. L., Tatar, T., Heath, J. K., and Rappoport, J. Z. Regulation of fibroblast growth factor receptor signalling and trafficking by src and eps8. *J Cell Sci 126*, Pt 2 (2013), 613–24.

[9] Babjuk, M., Burger, M., Zigeuner, R., Shariat, S. F., van Rhijn, B. W. G., Compérat, E., Sylvester, R. J., Kaasinen, E., Böhle, A., Palou Redorta, J., Rouprêt, M., and , E. A. o. U. Eau guidelines on non-muscle-invasive urothelial carcinoma of the bladder: update 2013. *Eur Urol 64*, 4 (Oct 2013), 639–653.

[10] Barbero, P., Bittova, L., and Pfeffer, S. R. Visualization of rab9-mediated vesicle transport from endosomes to the trans-golgi in living cells. *J Cell Biol 156*, 3 (Feb 2002), 511–518.

[11] Bermudez, O., Pagès, G., and Gimond, C. The dual-specificity map kinase phosphatases: critical roles in development and cancer. *Am J Physiol Cell Physiol 299*, 2 (Aug 2010), C189–C202.

[12] Bernard-Pierrot, I., Brams, A., Dunois-Larde, C., Caillault, A., Diez de Medina, S. G., Cappellen, D., Graff, G., Thiery, J. P., Chopin, D., Ricol, D., and Radvanyi, F. Oncogenic properties of the mutated forms of fibroblast growth factor receptor 3b. *Carcinogenesis 27*, 4 (2006), 740–7.

[13] Biton, A., Bernard-Pierrot, I., Lou, Y., Krucker, C., Chapeaublanc, E., Rubio-Perez, C., Lopez-Bigas, N., Kamoun, A., Neuzillet, Y., Gestraud, P., Grieco, L., Rebouissou, S., de Reynies, A., Benhamou, S., Lebret, T., Southgate, J., Barillot, E., Allory, Y., Zinovyev, A., and Radvanyi, F. Independent component analysis uncovers the landscape of the bladder tumor transcriptome and reveals insights into luminal and basal subtypes. *Cell Rep 9*, 4 (2014), 1235–45.

[14] Bodoor, K., Ghabkari, A., Jaradat, Z., Alkhateeb, A., Jaradat, S., Al-Ghazo, M. A., Matalka, I., Musleh, H., and Haddad, Y. Fgfr3 mutational status and protein expression in patients with bladder cancer in a jordanian population. *Cancer Epidemiol 34*, 6 (Dec 2010), 724–732.

[15] Bolte, S., and Cordelieres, F. P. A guided tour into subcellular colocalization analysis in light microscopy. *J Microsc 224*, Pt 3 (2006), 213–32.

[16] Bonaventure, J., Horne, W. C., and Baron, R. The localization of fgfr3 mutations causing thanatophoric dysplasia type i differentially affects phosphorylation, processing and ubiquitylation of the receptor. *FEBS J 274*, 12 (2007), 3078–93.

[17] Boulay, P.-L., Mitchell, L., Turpin, J., Huot-Marchand, J.-É., Lavoie, C., Sanguin-Gendreau, V., Jones, L., Mitra, S., Livingstone, J. M., Campbell, S., Hallett, M., Mills, G. B., Park, M., Chodosh, L., Strathdee, D., Norman, J. C., and Muller, W. J. Rab11-fip1c is a critical negative regulator in erbb2-mediated mammary tumor progression. *Cancer Res* (Mar 2016).

[18] Brooks, A. N., Kilgour, E., and Smith, P. D. Molecular pathways: fibroblast growth factor signaling: a new therapeutic opportunity in cancer. *Clin Cancer Res 18*, 7 (Apr 2012), 1855–1862.

[19] Brusegard, K., Stavnes, H. T., Nymoen, D. A., Flatmark, K., Trope, C. G., and Davidson, B. Rab25 is overexpressed in müllerian serous carcinoma compared to malignant mesothelioma. *Virchows Arch 460*, 2 (Feb 2012), 193–202.

[20] Calvo, A., Xiao, N., Kang, J., Best, C. J. M., Leiva, I., Emmert-Buck, M. R., Jorcyk, C., and Green, J. E. Alterations in gene expression profiles during prostate cancer progression: functional correlations to tumorigenicity and down-regulation of selenoprotein-p in mouse and human tumors. *Cancer Res 62*, 18 (Sep 2002), 5325–5335.

[21] Capelletti, M., Dodge, M. E., Ercan, D., Hammerman, P. S., Park, S.-I., Kim, J., Sasaki, H., Jablons, D. M., Lipson, D., Young, L., Stephens, P. J., Miller, V. A., Lindeman, N. I., Munir, K. J., Richards, W. G., and Jänne, P. A. Identification of recurrent fgfr3-tacc3 fusion oncogenes from lung adenocarcinoma. *Clin Cancer Res 20*, 24 (Dec 2014), 6551–6558.

[22] Cappellen, D., De Oliveira, C., Ricol, D., de Medina, S., Bourdin, J., Sastre-Garau, X., Chopin, D., Thiery, J. P., and Radvanyi, F. Frequent activating mutations of fgfr3 in human bladder and cervix carcinomas. *Nat Genet 23*, 1 (1999), 18–20.

[23] Carneiro, B. A., Elvin, J. A., Kamath, S. D., Ali, S. M., Paintal, A. S., Restrepo, A., Berry, E., Giles, F. J., and Johnson, M. L. Fgfr3-tacc3: A novel gene fusion in cervical cancer. *Gynecol Oncol Rep 13* (Aug 2015), 53–56.

[24] Casanova, J. E., Wang, X., Kumar, R., Bhartur, S. G., Navarre, J., Woodrum, J. E., Altschuler, Y., Ray, G. S., and Goldenring, J. R. Association of rab25 and rab11a with the apical recycling system of polarized madin-darby canine kidney cells. *Mol Biol Cell 10*, 1 (1999), 47–61.

[25] Caswell, P. T., Chan, M., Lindsay, A. J., McCaffrey, M. W., Boettiger, D., and Norman, J. C. Rab-coupling protein coordinates recycling of alpha5beta1 integrin and egfr1 to promote cell migration in 3d microenvironments. *J Cell Biol 183*, 1 (2008), 143–155.

[26] Caswell, P. T., Spence, H. J., Parsons, M., White, D. P., Clark, K., Cheng, K. W., Mills, G. B., Humphries, M. J., Messent, A. J., Anderson, K. I., McCaffrey, M. W., Ozanne, B. W., and Norman, J. C. Rab25 associates with alpha5beta1 integrin to promote invasive migration in 3d microenvironments. *Dev Cell 13*, 4 (2007), 496–510.

[27] Catto, J. W. F., Miah, S., Owen, H. C., Bryant, H., Myers, K., Dudziec, E., Larré, S., Milo, M., Rehman, I., Rosario, D. J., Di Martino, E., Knowles, M. A., Meuth, M., Harris, A. L., and Hamdy, F. C. Distinct microrna alterations characterize high- and low-grade bladder cancer. *Cancer Res 69*, 21 (Nov 2009), 8472–8481.

[28] Cerami, E., Gao, J., Dogrusoz, U., Gross, B. E., Sumer, S. O., Aksoy, B. A., Jacobsen, A., Byrne, C. J., Heuer, M. L., Larsson, E., Antipin, Y., Reva, B., Goldberg, A. P., Sander, C., and Schultz, N. The cbio cancer genomics portal: an open platform for exploring multidimensional cancer genomics data. *Cancer Discov 2*, 5 (May 2012), 401–404.

[29] Cheng, J.-M., Ding, M., Aribi, A., Shah, P., and Rao, K. Loss of rab25 expression in breast cancer. *Int J Cancer 118*, 12 (Jun 2006), 2957–2964.

[30] Cheng, J. M., Volk, L., Janaki, D. K., Vyakaranam, S., Ran, S., and Rao, K. A. Tumor suppressor function of rab25 in triple-negative breast cancer. *Int J Cancer 126*, 12 (2010), 2799–812.

[31] Cheng, K. W., Lahad, J. P., Kuo, W. L., Lapuk, A., Yamada, K., Auersperg, N., Liu, J., Smith-McCune, K., Lu, K. H., Fishman, D., Gray, J. W., and Mills, G. B. The rab25 small gtpase determines aggressiveness of ovarian and breast cancers. *Nat Med 10*, 11 (2004), 1251–6.

[32] Chia, W. J., and Tang, B. L. Emerging roles for rab family gtpases in human cancer. *Biochim Biophys Acta 1795*, 2 (2009), 110–6.

[33] Cho, J. Y., Guo, C., Torello, M., Lunstrum, G. P., Iwata, T., Deng, C., and Horton, W. A. Defective lysosomal targeting of activated fibroblast growth factor receptor 3 in achondroplasia. *Proc Natl Acad Sci U S A 101*, 2 (Jan 2004), 609–614.

[34] Choi, S.-C., Kim, S.-J., Choi, J.-H., Park, C.-Y., Shim, W.-J., and Lim, D.-S. Fibroblast growth factor-2 and -4 promote the proliferation of bone marrow mesenchymal stem cells by the activation of the pi3k-akt and erk1/2 signaling pathways. *Stem Cells Dev 17*, 4 (Aug 2008), 725–736.

[35] Choi, W., Porten, S., Kim, S., Willis, D., Plimack, E. R., Hoffman-Censits, J., Roth, B., Cheng, T., Tran, M., Lee, I.-L., Melquist, J., Bondaruk, J., Majewski, T., Zhang, S., Pretzsch, S., Baggerly, K., Siefker-Radtke, A., Czerniak, B., Dinney, C. P. N., and McConkey, D. J. Identification of distinct basal and luminal subtypes of muscle-invasive bladder cancer with different sensitivities to frontline chemotherapy. *Cancer Cell 25*, 2 (Feb 2014), 152–165.

[36] Chou, J., Provot, S., and Werb, Z. Gata3 in development and cancer differentiation: cells gata have it! *J Cell Physiol 222*, 1 (Jan 2010), 42–49.

[37] Christoforidis, S., Miaczynska, M., Ashman, K., Wilm, M., Zhao, L., Yip, S. C., Waterfield, M. D., Backer, J. M., and Zerial, M. Phosphatidylinositol-3-oh kinases are rab5 effectors. *Nat Cell Biol 1*, 4 (Aug 1999), 249–252.

[38] Chua, C. E. L., and Tang, B. L. The role of the small gtpase rab31 in cancer. *J Cell Mol Med 19*, 1 (Jan 2015), 1–10.

[39] Costa-Mattioli, M., and Monteggia, L. M. mtor complexes in neurodevelopmental and neuropsychiatric disorders. *Nat Neurosci 16*, 11 (Nov 2013), 1537–1543.

[40] Dai, M., Wang, P., Boyd, A. D., Kostov, G., Athey, B., Jones, E. G., Bunney, W. E., Myers, R. M., Speed, T. P., Akil, H., Watson, S. J., and Meng, F. Evolving gene/transcript definitions significantly alter the interpretation of genechip data. *Nucleic Acids Res 33*, 20 (2005), e175.

[41] Damrauer, J. S., Hoadley, K. A., Chism, D. D., Fan, C., Tiganelli, C. J., Wobker, S. E., Yeh, J. J., Milowsky, M. I., Iyer, G., Parker, J. S., and Kim, W. Y. Intrinsic subtypes of high-grade bladder cancer reflect the hallmarks of breast cancer biology. *Proc Natl Acad Sci U S A 111*, 8 (Feb 2014), 3110–3115.

[42] d'Avis, P. Y., Robertson, S. C., Meyer, A. N., Bardwell, W. M., Webster, M. K., and Donoghue, D. J. Constitutive activation of fibroblast growth factor receptor 3 by mutations responsible for the lethal skeletal dysplasia thanatophoric dysplasia type i. *Cell Growth Differ 9*, 1 (Jan 1998), 71–78.

[43] Degnin, C. R., Laederich, M. B., and Horton, W. A. Ligand activation leads to regulated intramembrane proteolysis of fibroblast growth factor receptor 3. *Mol Biol Cell 22*, 20 (2011), 3861–73.

[44] Delevoye, C., Miserey-Lenkei, S., Montagnac, G., Gilles-Marsens, F., Paul-Gilloteaux, P., Giordano, F., Waharte, F., Marks, M. S., Goud, B., and Raposo,

G. Recycling endosome tubule morphogenesis from sorting endosomes requires the kinesin motor kif13a. *Cell Rep 6*, 3 (Feb 2014), 445–454.

[45] Desai, A., and Adjei, A. A. Fgfr signaling as a target for lung cancer therapy. *Journal of Thoracic Oncology 11*, 1 (2016), 9–20.

[46] di Martino, E., L'Hote, C. G., Kennedy, W., Tomlinson, D. C., and Knowles, M. A. Mutant fibroblast growth factor receptor 3 induces intracellular signaling and cellular transformation in a cell type- and mutation-specific manner. *Oncogene 28*, 48 (2009), 4306–16.

[47] Doherty, G. J., and McMahon, H. T. Mechanisms of endocytosis. *Annu Rev Biochem 78* (2009), 857–902.

[48] Dozynkiewicz, M. A., Jamieson, N. B., Macpherson, I., Grindlay, J., van den Berghe, P. V., von Thun, A., Morton, J. P., Gourley, C., Timpson, P., Nixon, C., McKay, C. J., Carter, R., Strachan, D., Anderson, K., Sansom, O. J., Caswell, P. T., and Norman, J. C. Rab25 and clic3 collaborate to promote integrin recycling from late endosomes/lysosomes and drive cancer progression. *Dev Cell 22*, 1 (2012), 131–45.

[49] Eble, J., Sauter, G., Epstein, J., and Ssterhenn, I. Who classification of ttumour. pathology and genetic of tumour of the urinary system and male genital organs. *IARC Press Lyon* (2004).

[50] Echarri, A., and Del Pozo, M. A. Caveolae - mechanosensitive membrane invaginations linked to actin filaments. *J Cell Sci 128*, 15 (Aug 2015), 2747–2758.

[51] Ekerot, M., Stavridis, M. P., Delavaine, L., Mitchell, M. P., Staples, C., Owens, D. M., Keenan, I. D., Dickinson, R. J., Storey, K. G., and Keyse, S. M. Negative-feedback regulation of fgf signalling by dusp6/mkp-3 is driven by erk1/2 and mediated by ets factor binding to a conserved site within the dusp6/mkp-3 gene promoter. *Biochem J 412*, 2 (Jun 2008), 287–298.

[52] Elfenbein, A., and Simons, M. Syndecan-4 signaling at a glance. *J Cell Sci 126*, Pt 17 (Sep 2013), 3799–3804.

[53] Espina, C., Straif, K., Friis, S., Kogevinas, M., Saracci, R., Vainio, H., and Schüz, J. European code against cancer 4th edition: Environment, occupation and cancer. *Cancer Epidemiol 39 Suppl 1* (Dec 2015), S84–S92.

[54] Eswarakumar, V. P., Lax, I., and Schlessinger, J. Cellular signaling by fibroblast growth factor receptors. *Cytokine Growth Factor Rev 16*, 2 (2005), 139–49.

[55] Ewing, R. M., Chu, P., Elisma, F., Li, H., Taylor, P., Climie, S., McBroom-Cerajewski, L., Robinson, M. D., O'Connor, L., Li, M., Taylor, R., Dharsee, M., Ho, Y., Heilbut, A., Moore, L., Zhang, S., Ornatsky, O., Bukhman, Y. V., Ethier, M., Sheng, Y., Vasilescu, J., Abu-Farha, M., Lambert, J.-P., Duewel, H. S., Stewart, I. I., Kuehl, B., Hogue, K., Colwill, K., Gladwish, K., Muskat, B., Kinach, R., Adams, S.-L., Moran, M. F., Morin, G. B., Topaloglou, T., and Figeys, D.

Large-scale mapping of human protein-protein interactions by mass spectrometry. *Mol Syst Biol 3* (2007), 89.

[56] Fan, Y., Xin, X.-Y., Chen, B.-L., and Ma, X. Knockdown of rab25 expression by rnai inhibits growth of human epithelial ovarian cancer cells in vitro and in vivo. *Pathology 38*, 6 (Dec 2006), 561–567.

[57] Ferlay, J., Steliarova-Foucher, E., Lortet-Tieulent, J., Rosso, S., Coebergh, J. W. W., Comber, H., Forman, D., and Bray, F. Cancer incidence and mortality patterns in europe: estimates for 40 countries in 2012. *Eur J Cancer 49*, 6 (Apr 2013), 1374–1403.

[58] Foldynova-Trantirkova, S., Wilcox, W. R., and Krejci, P. Sixteen years and counting: the current understanding of fibroblast growth factor receptor 3 (fgfr3) signaling in skeletal dysplasias. *Hum Mutat 33*, 1 (Jan 2012), 29–41.

[59] Foth, M., Ahmad, I., van Rhijn, B. W. G., van der Kwast, T., Bergman, A. M., King, L., Ridgway, R., Leung, H. Y., Fraser, S., Sansom, O. J., and Iwata, T. Fibroblast growth factor receptor 3 activation plays a causative role in urothelial cancer pathogenesis in cooperation with pten loss in mice. *J Pathol 233*, 2 (Jun 2014), 148–158.

[60] Gallo, L. H., Nelson, K. N., Meyer, A. N., and Donoghue, D. J. Functions of fibroblast growth factor receptors in cancer defined by novel translocations and mutations. *Cytokine Growth Factor Rev 26*, 4 (Aug 2015), 425–449.

[61] Gao, J., Aksoy, B. A., Dogrusoz, U., Dresdner, G., Gross, B., Sumer, S. O., Sun, Y., Jacobsen, A., Sinha, R., Larsson, E., Cerami, E., Sander, C., and Schultz, N. Integrative analysis of complex cancer genomics and clinical profiles using the cbioportal. *Sci Signal 6*, 269 (Apr 2013), pl1.

[62] Geng, D., Zhao, W., Feng, Y., and Liu, J. Overexpression of rab25 promotes hepatocellular carcinoma cell proliferation and invasion. *Tumour Biol* (Dec 2015).

[63] Geraldes, P., and King, G. L. Activation of protein kinase c isoforms and its impact on diabetic complications. *Circ Res 106*, 8 (Apr 2010), 1319–1331.

[64] Gidon, A., Bardin, S., Cinquin, B., Boulanger, J., Waharte, F., Heliot, L., de la Salle, H., Hanau, D., Kervrann, C., Goud, B., and Salamero, J. A rab11a/myosin vb/rab11-fip2 complex frames two late recycling steps of langerin from the erc to the plasma membrane. *Traffic 13*, 6 (2012), 815–33.

[65] Goebell, P. J., and Knowles, M. A. Bladder cancer or bladder cancers? genetically distinct malignant conditions of the urothelium. *Urol Oncol 28*, 4 (2010), 409–28.

[66] Goetz, R., and Mohammadi, M. Exploring mechanisms of fgf signalling through the lens of structural biology. *Nat Rev Mol Cell Biol* (2013).

[67] Goldenring, J. R., Aron, L. M., Lapierre, L. A., Navarre, J., and Casanova, J. E. Expression and properties of rab25 in polarized madin-darby canine kidney cells. *Methods Enzymol 329* (2001), 225–234.

[68] Goldenring, J. R., and Nam, K. T. Rab25 as a tumour suppressor in colon carcinogenesis. *Br J Cancer 104*, 1 (2011), 33–6.

[69] Goldenring, J. R., Shen, K. R., Vaughan, H. D., and Modlin, I. M. Identification of a small gtp-binding protein, rab25, expressed in the gastrointestinal mucosa, kidney, and lung. *J Biol Chem 268*, 25 (Sep 1993), 18419–18422.

[70] Gómez-Román, J. J., Saenz, P., Molina, M., Cuevas González, J., Escuredo, K., Santa Cruz, S., Junquera, C., Simón, L., Martínez, A., Gutiérrez Baños, J. L., López-Brea, M., Esparza, C., and Val-Bernal, J. F. Fibroblast growth factor receptor 3 is overexpressed in urinary tract carcinomas and modulates the neoplastic cell growth. *Clin Cancer Res 11*, 2 Pt 1 (Jan 2005), 459–465.

[71] Gomez-Roman, N., Sahasrabudhe, N. M., McGregor, F., Chalmers, A. J., Cassidy, J., and Plumb, J. Hypoxia-inducible factor 1 alpha is required for the tumourigenic and aggressive phenotype associated with rab25 expression in ovarian cancer. *Oncotarget* (Mar 2016).

[72] Gospodarowicz, D. Localisation of a fibroblast growth factor and its effect alone and with hydrocortisone on 3t3 cell growth. *Nature 249*, 453 (May 1974), 123–127.

[73] Gotoh, N. Regulation of growth factor signaling by frs2 family docking/scaffold adaptor proteins. *Cancer Sci 99*, 7 (Jul 2008), 1319–1325.

[74] Grant, B. D., and Donaldson, J. G. Pathways and mechanisms of endocytic recycling. *Nat Rev Mol Cell Biol 10*, 9 (Sep 2009), 597–608.

[75] Grimsey, N. J., Coronel, L. J., Cordova, I. C., and Trejo, J. Recycling and endosomal sorting of protease-activated receptor-1 is distinctly regulated by rab11a and rab11b proteins. *J Biol Chem 291*, 5 (Jan 2016), 2223–2236.

[76] Guo, C., Degnin, C. R., Laederich, M. B., Lunstrum, G. P., Holden, P., Bihlmaier, J., Krakow, D., Cho, Y.-J., and Horton, W. A. Sprouty 2 disturbs fgfr3 degradation in thanatophoric dysplasia type ii: a severe form of human achondroplasia. *Cell Signal 20*, 8 (Aug 2008), 1471–1477.

[77] Hafner, C., van Oers, J. M. M., Vogt, T., Landthaler, M., Stoehr, R., Blaszyk, H., Hofstaedter, F., Zwarthoff, E. C., and Hartmann, A. Mosaicism of activating fgfr3 mutations in human skin causes epidermal nevi. *J Clin Invest 116*, 8 (Aug 2006), 2201–2207.

[78] Harada, D., Yamanaka, Y., Ueda, K., Nishimura, R., Morishima, T., Seino, Y., and Tanaka, H. Sustained phosphorylation of mutated fgfr3 is a crucial feature of genetic dwarfism and induces apoptosis in the atdc5 chondrogenic cell line via plcgamma-activated stat1. *Bone 41*, 2 (Aug 2007), 273–281.

[79] Hartmann, A., Schlake, G., Zaak, D., Hungerhuber, E., Hofstetter, A., Hofstaedter, F., and Knuechel, R. Occurrence of chromosome 9 and p53 alterations in multifocal dysplasia and carcinoma in situ of human urinary bladder. *Cancer Res 62*, 3 (Feb 2002), 809–818.

[80] HAS, I. Guide - affection longue durée: Cancer de la vessie, 2010, 2010.

[81] Haugsten, E. M., Brech, A., Liestøl, K., Norman, J. C., and Wesche, J. Photoactivation approaches reveal a role for rab11 in fgfr4 recycling and signalling. *Traffic 15*, 6 (Jun 2014), 665–683.

[82] Haugsten, E. M., Sorensen, V., Brech, A., Olsnes, S., and Wesche, J. Different intracellular trafficking of fgf1 endocytosed by the four homologous fgf receptors. *J Cell Sci 118*, Pt 17 (2005), 3869–81.

[83] Haugsten, E. M., Zakrzewska, M., Brech, A., Pust, S., Olsnes, S., Sandvig, K., and Wesche, J. Clathrin- and dynamin-independent endocytosis of fgfr3–implications for signalling. *PLoS One 6*, 7 (2011), e21708.

[84] Hay, N., and Sonenberg, N. Upstream and downstream of mtor. *Genes Dev 18*, 16 (Aug 2004), 1926–1945.

[85] Hernández, S., Toll, A., Baselga, E., Ribé, A., Azua-Romeo, J., Pujol, R. M., and Real, F. X. Fibroblast growth factor receptor 3 mutations in epidermal nevi and associated low grade bladder tumors. *J Invest Dermatol 127*, 7 (Jul 2007), 1664–1666.

[86] Ho, J. R., Chapeaublanc, E., Kirkwood, L., Nicolle, R., Benhamou, S., Lebret, T., Allory, Y., Southgate, J., Radvanyi, F., and Goud, B. Deregulation of rab and rab effector genes in bladder cancer. *PLoS One 7*, 6 (2012), e39469.

[87] Horton, W. A., Hall, J. G., and Hecht, J. T. Achondroplasia. *Lancet 370*, 9582 (Jul 2007), 162–172.

[88] Huotari, J., and Helenius, A. Endosome maturation. *EMBO J 30*, 17 (Aug 2011), 3481–3500.

[89] Hutagalung, A. H., and Novick, P. J. Role of rab gtpases in membrane traffic and cell physiology. *Physiol Rev 91*, 1 (Jan 2011), 119–149.

[90] Jacobs, B. L., Lee, C. T., and Montie, J. E. Bladder cancer in 2010: how far have we come? *CA Cancer J Clin 60*, 4 (2010), 244–272.

[91] Jing, J., Tarbutton, E., Wilson, G., and Prekeris, R. Rab11-fip3 is a rab11-binding protein that regulates breast cancer cell motility by modulating the actin cytoskeleton. *Eur J Cell Biol 88*, 6 (Jun 2009), 325–341.

[92] Joffre, C., Barrow, R., Menard, L., Calleja, V., Hart, I. R., and Kermorgant, S. A direct role for met endocytosis in tumorigenesis. *Nat Cell Biol 13*, 7 (2011), 827–37.

[93] Johannes, L., Parton, R. G., Bassereau, P., and Mayor, S. Building endocytic pits without clathrin. *Nat Rev Mol Cell Biol 16*, 5 (May 2015), 311–321.

[94] Johnson, D., and Wilkie, A. O. M. Craniosynostosis. *Eur J Hum Genet 19*, 4 (Apr 2011), 369–376.

[95] Jordens, I., Fernandez-Borja, M., Marsman, M., Dusseljee, S., Janssen, L., Calafat, J., Janssen, H., Wubbolts, R., and Neefjes, J. The rab7 effector protein rilp controls lysosomal transport by inducing the recruitment of dynein-dynactin motors. *Curr Biol 11*, 21 (Oct 2001), 1680–1685.

[96] Jovic, M., Sharma, M., Rahajeng, J., and Caplan, S. The early endosome: a busy sorting station for proteins at the crossroads. *Histol Histopathol 25*, 1 (Jan 2010), 99–112.

[97] Kang, S., Dong, S., Gu, T.-L., Guo, A., Cohen, M. S., Lonial, S., Khoury, H. J., Fabbro, D., Gilliland, D. G., Bergsagel, P. L., Taunton, J., Polakiewicz, R. D., and Chen, J. Fgfr3 activates rsk2 to mediate hematopoietic transformation through tyrosine phosphorylation of rsk2 and activation of the mek/erk pathway. *Cancer Cell 12*, 3 (Sep 2007), 201–214.

[98] Karoui, M., Hofmann-Radvanyi, H., Zimmermann, U., Couvelard, A., Degott, C., Faridoni-Laurens, L., Ahomadegbe, J. C., Gazzeri, S., Brambilla, E., Clerici, T., Charbonnier, P., Tresallet, C., Mitry, E., Penna, C., Rougier, P., Boileau, C., Thiery, J. P., Nordlinger, B., Franc, B., and Radvanyi, F. No evidence of somatic fgfr3 mutation in various types of carcinoma. *Oncogene 20*, 36 (Aug 2001), 5059–5061.

[99] Kelly, E. E., Horgan, C. P., Goud, B., and McCaffrey, M. W. The rab family of proteins: 25 years on. *Biochem Soc Trans 40*, 6 (Dec 2012), 1337–1347.

[100] Kelly, E. E., Horgan, C. P., and McCaffrey, M. W. Rab11 proteins in health and disease. *Biochem Soc Trans 40*, 6 (Dec 2012), 1360–1367.

[101] Kermorgant, S., and Parker, P. J. Receptor trafficking controls weak signal delivery: a strategy used by c-met for stat3 nuclear accumulation. *J Cell Biol 182*, 5 (Sep 2008), 855–863.

[102] Kimura, T., Suzuki, H., Ohashi, T., Asano, K., Kiyota, H., and Eto, Y. The incidence of thanatophoric dysplasia mutations in fgfr3 gene is higher in low-grade or superficial bladder carcinomas. *Cancer 92*, 10 (Nov 2001), 2555–2561.

[103] Kirchhausen, T., Owen, D., and Harrison, S. C. Molecular structure, function, and dynamics of clathrin-mediated membrane traffic. *Cold Spring Harb Perspect Biol 6*, 5 (May 2014), a016725.

[104] Knowles, M. A., and Hurst, C. D. Molecular biology of bladder cancer: new insights into pathogenesis and clinical diversity. *Nat Rev Cancer 15*, 1 (Jan 2015), 25–41.

[105] Kouhara, H., Hadari, Y. R., Spivak-Kroizman, T., Schilling, J., Bar-Sagi, D., Lax, I., and Schlessinger, J. A lipid-anchored grb2-binding protein that links fgf-receptor activation to the ras/mapk signaling pathway. *Cell 89*, 5 (May 1997), 693–702.

[106] Krejci, P., Salazar, L., Goodridge, H. S., Kashiwada, T. A., Schibler, M. J., Jelinkova, P., Thompson, L. M., and Wilcox, W. R. Stat1 and stat3 do not participate in fgf-mediated growth arrest in chondrocytes. *J Cell Sci 121*, Pt 3 (Feb 2008), 272–281.

[107] Laederich, M. B., Degnin, C. R., Lunstrum, G. P., Holden, P., and Horton, W. A. Fibroblast growth factor receptor 3 (fgfr3) is a strong heat shock protein 90 (hsp90) client: implications for therapeutic manipulation. *J Biol Chem 286*, 22 (2011), 19597–604.

[108] Lai, F., Stubbs, L., and Artzt, K. Molecular analysis of mouse rab11b: a new type of mammalian ypt/rab protein. *Genomics 22*, 3 (Aug 1994), 610–616.

[109] Lamaze, C., and Torrino, S. Caveolae and cancer: A new mechanical perspective. *Biomed J 38*, 5 (2015), 367–379.

[110] Lamothe, B., Yamada, M., Schaeper, U., Birchmeier, W., Lax, I., and Schlessinger, J. The docking protein gab1 is an essential component of an indirect mechanism for fibroblast growth factor stimulation of the phosphatidylinositol 3-kinase/akt antiapoptotic pathway. *Mol Cell Biol 24*, 13 (Jul 2004), 5657–5666.

[111] Lapierre, L. A., Dorn, M. C., Zimmerman, C. F., Navarre, J., Burnette, J. O., and Goldenring, J. R. Rab11b resides in a vesicular compartment distinct from rab11a in parietal cells and other epithelial cells. *Exp Cell Res 290*, 2 (Nov 2003), 322–331.

[112] Lapierre, L. A., Kumar, R., Hales, C. M., Navarre, J., Bhartur, S. G., Burnette, J. O., Provance, Jr, D., Mercer, J. A., Bähler, M., and Goldenring, J. R. Myosin vb is associated with plasma membrane recycling systems. *Mol Biol Cell 12*, 6 (Jun 2001), 1843–1857.

[113] Laplante, M., and Sabatini, D. M. mtor signaling at a glance. *J Cell Sci 122*, Pt 20 (Oct 2009), 3589–3594.

[114] Law, C. W., Chen, Y., Shi, W., and Smyth, G. K. voom: Precision weights unlock linear model analysis tools for rna-seq read counts. *Genome Biol 15*, 2 (2014), R29.

[115] Legeai-Mallet, L., Benoist-Lasselin, C., Delezoide, A. L., Munnich, A., and Bonaventure, J. Fibroblast growth factor receptor 3 mutations promote apoptosis but do not alter chondrocyte proliferation in thanatophoric dysplasia. *J Biol Chem 273*, 21 (May 1998), 13007–13014.

[116] Legeai-Mallet, L., Benoist-Lasselin, C., Munnich, A., and Bonaventure, J. Overexpression of fgfr3, stat1, stat5 and p21cip1 correlates with phenotypic severity and defective chondrocyte differentiation in fgfr3-related chondrodysplasias. *Bone 34*, 1 (Jan 2004), 26–36.

[117] Lemmon, M. A., and Schlessinger, J. Cell signaling by receptor tyrosine kinases. *Cell 141*, 7 (Jun 2010), 1117–1134.

[118] Li, G., and Segev, N. *Rab GTPases and membrane trafficking*. Bentham Science Publishers, 2012.

[119] Lievens, P. M., and Liboi, E. The thanatophoric dysplasia type ii mutation hampers complete maturation of fibroblast growth factor receptor 3 (fgfr3), which activates signal transducer and activator of transcription 1 (stat1) from the endoplasmic reticulum. *J Biol Chem 278*, 19 (2003), 17344–9.

[120] Lievens, P. M., Mutinelli, C., Baynes, D., and Liboi, E. The kinase activity of fibroblast growth factor receptor 3 with activation loop mutations affects receptor trafficking and signaling. *J Biol Chem 279*, 41 (2004), 43254–60.

[121] Lievens, P. M.-J., Roncador, A., and Liboi, E. K644e/m fgfr3 mutants activate erk1/2 from the endoplasmic reticulum through frs2 alpha and plc gamma-independent pathways. *J Mol Biol 357*, 3 (Mar 2006), 783–792.

[122] Lindgren, D., Liedberg, F., Andersson, A., Chebil, G., Gudjonsson, S., Borg, A., Månsson, W., Fioretos, T., and Höglund, M. Molecular characterization of early-stage bladder carcinomas by expression profiles, fgfr3 mutation status, and loss of 9q. *Oncogene 25*, 18 (Apr 2006), 2685–2696.

[123] Liu, Z., Xu, J., Colvin, J. S., and Ornitz, D. M. Coordination of chondrogenesis and osteogenesis by fibroblast growth factor 18. *Genes Dev 16*, 7 (Apr 2002), 859–869.

[124] Logié, A., Dunois-Lardé, C., Rosty, C., Levrel, O., Blanche, M., Ribeiro, A., Gasc, J.-M., Jorcano, J., Werner, S., Sastre-Garau, X., Thiery, J. P., and Radvanyi, F. Activating mutations of the tyrosine kinase receptor fgfr3 are associated with benign skin tumors in mice and humans. *Hum Mol Genet 14*, 9 (May 2005), 1153–1160.

[125] Mahe, M. *Caractérisation des voies de signalisation des oncogènes FGFR3 muté et FGFR3-TACC3 dans les carcinomes de vessie*. PhD thesis, Université de Paris Sud, 2015.

[126] Manders, E., Verbeek, F., and Aten, J. Measurement of co-localization of objects in dual-colour confocal images. *Journal of microscopy 169*, 3 (1993), 375–382.

[127] Marchetti, S., Gimond, C., Chambard, J.-C., Touboul, T., Roux, D., Pouysségur, J., and Pagès, G. Extracellular signal-regulated kinases phosphorylate mitogen-activated protein kinase phosphatase 3/dusp6 at serines 159 and 197, two sites critical for its proteasomal degradation. *Mol Cell Biol 25*, 2 (Jan 2005), 854–864.

[128] Mardakheh, F. K., Yekezare, M., Machesky, L. M., and Heath, J. K. Spred2 interaction with the late endosomal protein nbr1 down-regulates fibroblast growth factor receptor signaling. *J Cell Biol 187*, 2 (Oct 2009), 265–277.

[129] Marie, P. J. Fibroblast growth factor signaling controlling bone formation: an update. *Gene 498*, 1 (Apr 2012), 1–4.

[130] Maxfield, F. R., and McGraw, T. E. Endocytic recycling. *Nat Rev Mol Cell Biol 5*, 2 (Feb 2004), 121–132.

[131] Mayor, S., Parton, R. G., and Donaldson, J. G. Clathrin-independent pathways of endocytosis. *Cold Spring Harb Perspect Biol 6*, 6 (Jun 2014).

[132] McCluskey, A., Daniel, J. A., Hadzic, G., Chau, N., Clayton, E. L., Mariana, A., Whiting, A., Gorgani, N. N., Lloyd, J., Quan, A., and et al. Building a better dynasore: The dyngo compounds potently inhibit dynamin and endocytosis. *Traffic 14*, 12 (Oct 2013), 1272–1289.

[133] McCubrey, J. A., Steelman, L. S., Chappell, W. H., Abrams, S. L., Wong, E. W. T., Chang, F., Lehmann, B., Terrian, D. M., Milella, M., Tafuri, A., Stivala, F., Libra, M., Basecke, J., Evangelisti, C., Martelli, A. M., and Franklin, R. A. Roles of the raf/mek/erk pathway in cell growth, malignant transformation and drug resistance. *Biochim Biophys Acta 1773*, 8 (Aug 2007), 1263–1284.

[134] McMahon, H. T., and Boucrot, E. Molecular mechanism and physiological functions of clathrin-mediated endocytosis. *Nat Rev Mol Cell Biol 12*, 8 (Aug 2011), 517–533.

[135] Miaczynska, M. Effects of membrane trafficking on signaling by receptor tyrosine kinases. *Cold Spring Harb Perspect Biol 5*, 11 (Nov 2013), a009035.

[136] Miaczynska, M., Christoforidis, S., Giner, A., Shevchenko, A., Uttenweiler-Joseph, S., Habermann, B., Wilm, M., Parton, R. G., and Zerial, M. Appl proteins link rab5 to nuclear signal transduction via an endosomal compartment. *Cell 116*, 3 (Feb 2004), 445–456.

[137] Mikoshiba, K. Ip3 receptor/ca2+ channel: from discovery to new signaling concepts. *J Neurochem 102*, 5 (Sep 2007), 1426–1446.

[138] Miraoui, H., Oudina, K., Petite, H., Tanimoto, Y., Moriyama, K., and Marie, P. J. Fibroblast growth factor receptor 2 promotes osteogenic differentiation in mesenchymal cells via erk1/2 and protein kinase c signaling. *J Biol Chem 284*, 8 (Feb 2009), 4897–4904.

[139] Mitra, S., Cheng, K. W., and Mills, G. B. Rab25 in cancer: a brief update. *Biochem Soc Trans 40*, 6 (Dec 2012), 1404–1408.

[140] Miyao, N., Tsai, Y. C., Lerner, S. P., Olumi, A. F., Spruck, 3rd, C., Gonzalez-Zulueta, M., Nichols, P. W., Skinner, D. G., and Jones, P. A. Role of chromosome 9 in human bladder cancer. *Cancer Res 53*, 17 (Sep 1993), 4066–4070.

[141] Monsonego-Ornan, E., Adar, R., Feferman, T., Segev, O., and Yayon, A. The transmembrane mutation g380r in fibroblast growth factor receptor 3 uncouples ligand-mediated receptor activation from down-regulation. *Mol Cell Biol 20*, 2 (2000), 516–22.

[142] Monsonego-Ornan, E., Adar, R., Rom, E., and Yayon, A. Fgf receptors ubiquitylation: dependence on tyrosine kinase activity and role in downregulation. *FEBS Lett 528*, 1-3 (Sep 2002), 83–89.

[143] Murakami, S., Balmes, G., McKinney, S., Zhang, Z., Givol, D., and de Crombrugghe, B. Constitutive activation of mek1 in chondrocytes causes stat1-independent achondroplasia-like dwarfism and rescues the fgfr3-deficient mouse phenotype. *Genes Dev 18*, 3 (Feb 2004), 290–305.

[144] Murakami, S., Kan, M., McKeehan, W. L., and de Crombrugghe, B. Up-regulation of the chondrogenic sox9 gene by fibroblast growth factors is mediated by the mitogen-activated protein kinase pathway. *Proc Natl Acad Sci U S A 97*, 3 (Feb 2000), 1113–1118.

[145] Nakanishi, Y., Akiyama, N., Tsukaguchi, T., Fujii, T., Satoh, Y., Ishii, N., and Aoki, M. Mechanism of oncogenic signal activation by the novel fusion kinase fgfr3-baiap2l1. *Mol Cancer Ther 14*, 3 (Mar 2015), 704–712.

[146] Naski, M. C., Wang, Q., Xu, J., and Ornitz, D. M. Graded activation of fibroblast growth factor receptor 3 by mutations causing achondroplasia and thanatophoric dysplasia. *Nat Genet 13*, 2 (Jun 1996), 233–237.

[147] Neuzillet, Y., Paoletti, X., Ouerhani, S., Mongiat-Artus, P., Soliman, H., de The, H., Sibony, M., Denoux, Y., Molinie, V., Herault, A., Lepage, M. L., Maille, P., Renou, A., Vordos, D., Abbou, C. C., Bakkar, A., Asselain, B., Kourda, N., El Gaaied, A., Leroy, K., Laplanche, A., Benhamou, S., Lebret, T., Allory, Y., and Radvanyi, F. A meta-analysis of the relationship between fgfr3 and tp53 mutations in bladder cancer. *PLoS One 7*, 12 (2012), e48993.

[148] Neuzillet, Y., van Rhijn, B. W. G., Prigoda, N. L., Bapat, B., Liu, L., Bostrom, P. J., Fleshner, N. E., Gallie, B. L., Zlotta, A. R., Jewett, M. A. S., and van der Kwast, T. H. Fgfr3 mutations, but not fgfr3 expression and fgfr3 copy-number variations, are associated with favourable non-muscle invasive bladder cancer. *Virchows Arch 465*, 2 (Aug 2014), 207–213.

[149] Ohya, T., Miaczynska, M., Coskun, U., Lommer, B., Runge, A., Drechsel, D., Kalaidzidis, Y., and Zerial, M. Reconstitution of rab- and snare-dependent membrane fusion by synthetic endosomes. *Nature 459*, 7250 (Jun 2009), 1091–1097.

[150] Ornitz, D. M. Fgf signaling in the developing endochondral skeleton. *Cytokine Growth Factor Rev 16*, 2 (Apr 2005), 205–213.

[151] Ornitz, D. M., and Itoh, N. The fibroblast growth factor signaling pathway. *Wiley Interdiscip Rev Dev Biol 4*, 3 (2015), 215–266.

[152] Ornitz, D. M., and Marie, P. J. Fgf signaling pathways in endochondral and intramembranous bone development and human genetic disease. *Genes Dev 16*, 12 (Jun 2002), 1446–1465.

[153] Ornitz, D. M., Xu, J., Colvin, J. S., McEwen, D. G., MacArthur, C. A., Coulier, F., Gao, G., and Goldfarb, M. Receptor specificity of the fibroblast growth factor family. *J Biol Chem 271*, 25 (Jun 1996), 15292–15297.

[154] Osorio, E. Y., Travi, B. L., da Cruz, A. M., Saldarriaga, O. A., Medina, A. A., and Melby, P. C. Growth factor and th2 cytokine signaling pathways converge at stat6 to promote arginase expression in progressive experimental visceral leishmaniasis. *PLoS Pathog 10*, 6 (Jun 2014), e1004165.

[155] Park, J., Park, O.-J., Yoon, W.-J., Kim, H.-J., Choi, K.-Y., Cho, T.-J., and Ryoo, H.-M. Functional characterization of a novel fgfr2 mutation, e731k, in craniosynostosis. *J Cell Biochem 113*, 2 (Feb 2012), 457–464.

[156] Parker, B. C., Annala, M. J., Cogdell, D. E., Granberg, K. J., Sun, Y., Ji, P., Li, X., Gumin, J., Zheng, H., Hu, L., Yli-Harja, O., Haapasalo, H., Visakorpi, T., Liu, X., Liu, C. G., Sawaya, R., Fuller, G. N., Chen, K., Lang, F. F., Nykter, M., and Zhang, W. The tumorigenic fgfr3-tacc3 gene fusion escapes mir-99a regulation in glioblastoma. *J Clin Invest 123*, 2 (2013), 855–65.

[157] Pellinen, T., Arjonen, A., Vuoriluoto, K., Kallio, K., Fransen, J. A., and Ivaska, J. Small gtpase rab21 regulates cell adhesion and controls endosomal traffic of beta1-integrins. *J Cell Biol 173*, 5 (2006), 767–80.

[158] Peters, K. G., Marie, J., Wilson, E., Ives, H. E., Escobedo, J., Del Rosario, M., Mirda, D., and Williams, L. T. Point mutation of an fgf receptor abolishes phosphatidylinositol turnover and ca2+ flux but not mitogenesis. *Nature 358*, 6388 (Aug 1992), 678–681.

[159] Pfeffer, S. R. Structural clues to rab gtpase functional diversity. *J Biol Chem 280*, 16 (Apr 2005), 15485–15488.

[160] Platta, H. W., and Stenmark, H. Endocytosis and signaling. *Current Opinion in Cell Biology 23*, 4 (Aug 2011), 393–403.

[161] Pollard, C., Smith, S. C., and Theodorescu, D. Molecular genesis of non-muscle-invasive urothelial carcinoma (nmiuc). *Expert Rev Mol Med 12* (2010), e10.

[162] Powelka, A. M., Sun, J., Li, J., Gao, M., Shaw, L. M., Sonnenberg, A., and Hsu, V. W. Stimulation-dependent recycling of integrin beta1 regulated by arf6 and rab11. *Traffic 5*, 1 (Jan 2004), 20–36.

[163] Powles, T., Eder, J. P., Fine, G. D., Braiteh, F. S., Loriot, Y., Cruz, C., Bellmunt, J., Burris, H. A., Petrylak, D. P., Teng, S.-l., Shen, X., Boyd, Z., Hegde, P. S., Chen, D. S., and Vogelzang, N. J. Mpdl3280a (anti-pd-l1) treatment leads to clinical activity in metastatic bladder cancer. *Nature 515*, 7528 (Nov 2014), 558–562.

[164] Poyet, C., Hermanns, T., Zhong, Q., Drescher, E., Eberli, D., Burger, M., Hofstaedter, F., Hartmann, A., Stöhr, R., Zwarthoff, E. C., Sulser, T., and Wild, P. J. Positive fibroblast growth factor receptor 3 immunoreactivity is associated with low-grade non-invasive urothelial bladder cancer. *Oncol Lett 10*, 5 (Nov 2015), 2753–2760.

[165] Prekeris, R., and Gould, G. W. Breaking up is hard to do - membrane traffic in cytokinesis. *J Cell Sci 121*, Pt 10 (May 2008), 1569–1576.

[166] Prekeris, R., Klumperman, J., and Scheller, R. H. A rab11/rip11 protein complex regulates apical membrane trafficking via recycling endosomes. *Mol Cell 6*, 6 (Dec 2000), 1437–1448.

[167] Raiborg, C., and Stenmark, H. The escrt machinery in endosomal sorting of ubiquitylated membrane proteins. *Nature 458*, 7237 (Mar 2009), 445–452.

[168] Rawlings, J. S., Rosler, K. M., and Harrison, D. A. The jak/stat signaling pathway. *J Cell Sci 117*, Pt 8 (Mar 2004), 1281–1283.

[169] Rebouissou, S., Bernard-Pierrot, I., de Reynies, A., Lepage, M. L., Krucker, C., Chapeaublanc, E., Herault, A., Kamoun, A., Caillault, A., Letouze, E., Elarouci, N., Neuzillet, Y., Denoux, Y., Molinie, V., Vordos, D., Laplanche, A., Maille, P., Soyeux, P., Ofualuka, K., Reyal, F., Biton, A., Sibony, M., Paoletti, X., Southgate, J., Benhamou, S., Lebret, T., Allory, Y., and Radvanyi, F. Egfr as a potential therapeutic target for a subset of muscle-invasive bladder cancers presenting a basal-like phenotype. *Sci Transl Med 6*, 244 (2014), 244ra91.

[170] Rebouissou, S., Hérault, A., Letouzé, E., Neuzillet, Y., Laplanche, A., Ofualuka, K., Maillé, P., Leroy, K., Riou, A., Lepage, M.-L., Vordos, D., de la Taille, A., Denoux, Y., Sibony, M., Guyon, F., Lebret, T., Benhamou, S., Allory, Y., and Radvanyi, F. Cdkn2a homozygous deletion is associated with muscle invasion in fgfr3-mutated urothelial bladder carcinoma. *J Pathol 227*, 3 (Jul 2012), 315–324.

[171] Robinson, M. D., and Oshlack, A. A scaling normalization method for differential expression analysis of rna-seq data. *Genome Biol 11*, 3 (2010), R25.

[172] Roland, J. T., Kenworthy, A. K., Peranen, J., Caplan, S., and Goldenring, J. R. Myosin vb interacts with rab8a on a tubular network containing ehd1 and ehd3. *Mol Biol Cell 18*, 8 (Aug 2007), 2828–2837.

[173] Rousseau, F., Bonaventure, J., Legeai-Mallet, L., Pelet, A., Rozet, J. M., Maroteaux, P., Le Merrer, M., and Munnich, A. Mutations in the gene encoding fibroblast growth factor receptor-3 in achondroplasia. *Nature 371*, 6494 (1994), 252–4.

[174] Rubino, M., Miaczynska, M., Lippé, R., and Zerial, M. Selective membrane recruitment of eea1 suggests a role in directional transport of clathrin-coated vesicles to early endosomes. *J Biol Chem 275*, 6 (Feb 2000), 3745–3748.

[175] Sahni, M., Ambrosetti, D. C., Mansukhani, A., Gertner, R., Levy, D., and Basilico, C. Fgf signaling inhibits chondrocyte proliferation and regulates bone development through the stat-1 pathway. *Genes Dev 13*, 11 (Jun 1999), 1361–1366.

[176] Salazar, L., Kashiwada, T., Krejci, P., Meyer, A. N., Casale, M., Hallowell, M., Wilcox, W. R., Donoghue, D. J., and Thompson, L. M. Fibroblast growth factor receptor 3 interacts with and activates tgfβ-activated kinase 1 tyrosine phosphorylation and nfκb signaling in multiple myeloma and bladder cancer. *PLoS One 9*, 1 (2014), e86470.

[177] Schenck, A., Goto-Silva, L., Collinet, C., Rhinn, M., Giner, A., Habermann, B., Brand, M., and Zerial, M. The endosomal protein appl1 mediates akt substrate specificity and cell survival in vertebrate development. *Cell 133*, 3 (2008), 486–97.

[178] Schiel, J. A., and Prekeris, R. Membrane dynamics during cytokinesis. *Curr Opin Cell Biol 25*, 1 (Feb 2013), 92–98.

[179] Schlierf, B., Fey, G. H., Hauber, J., Hocke, G. M., and Rosorius, O. Rab11b is essential for recycling of transferrin to the plasma membrane. *Exp Cell Res 259*, 1 (Aug 2000), 257–265.

[180] Schneider, C. A., Rasband, W. S., and Eliceiri, K. W. Nih image to imagej: 25 years of image analysis. *Nat Methods 9*, 7 (Jul 2012), 671–675.

[181] Scita, G., and Di Fiore, P. P. The endocytic matrix. *Nature 463*, 7280 (2010), 464–73.

[182] Seo, D.-W., Li, H., Guedez, L., Wingfield, P. T., Diaz, T., Salloum, R., Wei, B.-y., and Stetler-Stevenson, W. G. Timp-2 mediated inhibition of angiogenesis: an mmp-independent mechanism. *Cell 114*, 2 (Jul 2003), 171–180.

[183] Sheach, L. A., Adeney, E. M., Kucukmetin, A., Wilkinson, S. J., Fisher, A. D., Elattar, A., Robson, C. N., and Edmondson, R. J. Androgen-related expression of g-proteins in ovarian cancer. *Br J Cancer 101*, 3 (Aug 2009), 498–503.

[184] Shiang, R., Thompson, L. M., Zhu, Y. Z., Church, D. M., Fielder, T. J., Bocian, M., Winokur, S. T., and Wasmuth, J. J. Mutations in the transmembrane domain of fgfr3 cause the most common genetic form of dwarfism, achondroplasia. *Cell 78*, 2 (Jul 1994), 335–342.

[185] Shin, H.-W., Hayashi, M., Christoforidis, S., Lacas-Gervais, S., Hoepfner, S., Wenk, M. R., Modregger, J., Uttenweiler-Joseph, S., Wilm, M., Nystuen, A., Frankel, W. N., Solimena, M., De Camilli, P., and Zerial, M. An enzymatic cascade of rab5 effectors regulates phosphoinositide turnover in the endocytic pathway. *J Cell Biol 170*, 4 (Aug 2005), 607–618.

[186] Sibarita, J. B. Deconvolution microscopy. *Adv Biochem Eng Biotechnol 95* (2005), 201–43.

[187] Siegel, R. L., Miller, K. D., and Jemal, A. Cancer statistics, 2016. *CA Cancer J Clin* (Jan 2016).

[188] Singh, D., Chan, J. M., Zoppoli, P., Niola, F., Sullivan, R., Castano, A., Liu, E. M., Reichel, J., Porrati, P., Pellegatta, S., Qiu, K., Gao, Z., Ceccarelli, M., Riccardi, R., Brat, D. J., Guha, A., Aldape, K., Golfinos, J. G., Zagzag, D., Mikkelsen, T., Finocchiaro, G., Lasorella, A., Rabadan, R., and Iavarone, A. Transforming fusions of fgfr and tacc genes in human glioblastoma. *Science 337*, 6099 (Sep 2012), 1231–1235.

[189] Sinha, B., Köster, D., Ruez, R., Gonnord, P., Bastiani, M., Abankwa, D., Stan, R. V., Butler-Browne, G., Vedie, B., Johannes, L., Morone, N., Parton, R. G., Raposo, G., Sens, P., Lamaze, C., and Nassoy, P. Cells respond to mechanical stress by rapid disassembly of caveolae. *Cell 144*, 3 (Feb 2011), 402–413.

[190] Sivak, J. M., Petersen, L. F., and Amaya, E. Fgf signal interpretation is directed by sprouty and spred proteins during mesoderm formation. *Dev Cell 8*, 5 (May 2005), 689–701.

[191] Sjödahl, G., Lauss, M., Gudjonsson, S., Liedberg, F., Halldén, C., Chebil, G., Månsson, W., Höglund, M., and Lindgren, D. A systematic study of gene mutations in urothelial carcinoma; inactivating mutations in tsc2 and pik3r1. *PLoS One 6*, 4 (2011), e18583.

[192] Sjödahl, G., Lauss, M., Lövgren, K., Chebil, G., Gudjonsson, S., Veerla, S., Patschan, O., Aine, M., Fernö, M., Ringnér, M., Månsson, W., Liedberg, F., Lindgren, D., and Höglund, M. A molecular taxonomy for urothelial carcinoma. *Clin Cancer Res 18*, 12 (Jun 2012), 3377–3386.

[193] Smith, T. G., Karlsson, M., Lunn, J. S., Eblaghie, M. C., Keenan, I. D., Farrell, E. R., Tickle, C., Storey, K. G., and Keyse, S. M. Negative feedback predominates over cross-regulation to control erk mapk activity in response to fgf signalling in embryos. *FEBS Lett 580*, 17 (Jul 2006), 4242–4245.

[194] Smyth, G. K. Linear models and empirical bayes methods for assessing differential expression in microarray experiments. *Stat Appl Genet Mol Biol 3* (2004), Article3.

[195] Sönnichsen, B., De Renzis, S., Nielsen, E., Rietdorf, J., and Zerial, M. Distinct membrane domains on endosomes in the recycling pathway visualized by multicolor imaging of rab4, rab5, and rab11. *J Cell Biol 149*, 4 (May 2000), 901–914.

[196] Sorkin, A., and von Zastrow, M. Endocytosis and signalling: intertwining molecular networks. *Nat Rev Mol Cell Biol 10*, 9 (2009), 609–22.

[197] Stenmark, H. Rab gtpases as coordinators of vesicle traffic. *Nat Rev Mol Cell Biol 10*, 8 (2009), 513–525.

[198] Stenmark, H. The rabs: a family at the root of metazoan evolution. *BMC Biol 10* (2012), 68–68.

[199] Stenmark, H., and Olkkonen, V. M. The rab gtpase family. *Genome Biol 2*, 5 (2001), REVIEWS3007–REVIEWS3007.

[200] Su, W. C., Kitagawa, M., Xue, N., Xie, B., Garofalo, S., Cho, J., Deng, C., Horton, W. A., and Fu, X. Y. Activation of stat1 by mutant fibroblast growth-factor receptor in thanatophoric dysplasia type ii dwarfism. *Nature 386*, 6622 (Mar 1997), 288–292.

[201] Sylvester, R. J., Oosterlinck, W., and van der Meijden, A. P. M. A single immediate postoperative instillation of chemotherapy decreases the risk of recurrence in patients with stage ta t1 bladder cancer: a meta-analysis of published results of randomized clinical trials. *J Urol 171*, 6 Pt 1 (Jun 2004), 2186–90, quiz 2435.

[202] Taipale, M., Tucker, G., Peng, J., Krykbaeva, I., Lin, Z.-Y., Larsen, B., Choi, H., Berger, B., Gingras, A.-C., and Lindquist, S. A quantitative chaperone interaction network reveals the architecture of cellular protein homeostasis pathways. *Cell 158*, 2 (Jul 2014), 434–448.

[203] Takatsu, H., Sakurai, M., Shin, H. W., Murakami, K., and Nakayama, K. Identification and characterization of novel clathrin adaptor-related proteins. *J Biol Chem 273*, 38 (Sep 1998), 24693–24700.

[204] Tan, T. C., Valova, V. A., Malladi, C. S., Graham, M. E., Berven, L. A., Jupp, O. J., Hansra, G., McClure, S. J., Sarcevic, B., Boadle, R. A., Larsen, M. R., Cousin, M. A., and Robinson, P. J. Cdk5 is essential for synaptic vesicle endocytosis. *Nat Cell Biol 5*, 8 (Aug 2003), 701–710.

[205] TCGA. Comprehensive molecular characterization of urothelial bladder carcinoma. *Nature* (2014).

[206] Teis, D., Taub, N., Kurzbauer, R., Hilber, D., de Araujo, M. E., Erlacher, M., Offterdinger, M., Villunger, A., Geley, S., Bohn, G., Klein, C., Hess, M. W., and Huber, L. A. p14-mp1-mek1 signaling regulates endosomal traffic and cellular proliferation during tissue homeostasis. *J Cell Biol 175*, 6 (Dec 2006), 861–868.

[207] Téllez-Gabriel, M., Arroyo-Solera, I., León, X., Gallardo, A., López, M., Céspedes, M. V., Casanova, I., López-Pousa, A., Quer, M., Mangues, M. A., Barnadas, A., Mangues, R., and Pavón, M. A. High rab25 expression is associated with good clinical outcome in patients with locally advanced head and neck squamous cell carcinoma. *Cancer Med 2*, 6 (Dec 2013), 950–963.

[208] Tomlinson, D. C., Baldo, O., Harnden, P., and Knowles, M. A. Fgfr3 protein expression and its relationship to mutation status and prognostic variables in bladder cancer. *J Pathol 213*, 1 (2007), 91–8.

[209] Torre, L. A., Bray, F., Siegel, R. L., Ferlay, J., Lortet-Tieulent, J., and Jemal, A. Global cancer statistics, 2012. *CA Cancer J Clin 65*, 2 (Mar 2015), 87–108.

[210] Tremblay, M. G., Herdman, C., Guillou, F., Mishra, P. K., Baril, J., Bellenfant, S., and Moss, T. Extended synaptotagmin interaction with the fibroblast growth factor receptor depends on receptor conformation, not catalytic activity. *J Biol Chem 290*, 26 (Jun 2015), 16142–16156.

[211] Tringali, C., Lupo, B., Silvestri, I., Papini, N., Anastasia, L., Tettamanti, G., and Venerando, B. The plasma membrane sialidase neu3 regulates the malignancy of renal carcinoma cells by controlling beta1 integrin internalization and recycling. *J Biol Chem* (2012).

[212] Turner, N., and Grose, R. Fibroblast growth factor signalling: from development to cancer. *Nat Rev Cancer 10*, 2 (2010), 116–29.

[213] UICC, U. I. C. l. C. *TNM classification of Malignant Tumors 7th edition*. UICC, 2009.

[214] Ullrich, O., Reinsch, S., Urbé, S., Zerial, M., and Parton, R. G. Rab11 regulates recycling through the pericentriolar recycling endosome. *J Cell Biol 135*, 4 (Nov 1996), 913–924.

[215] Vallot, C., Stransky, N., Bernard-Pierrot, I., HÃ©rault, A., Zucman-Rossi, J., Chapeaublanc, E., Vordos, D., Laplanche, A., Benhamou, S., Lebret, T., Southgate, J., Allory, Y., and Radvanyi, F. A novel epigenetic phenotype associated with the most aggressive pathway of bladder tumor progression. *J Natl Cancer Inst 103*, 1 (2011), 47–60.

[216] van Oers, J. M. M., Adam, C., Denzinger, S., Stoehr, R., Bertz, S., Zaak, D., Stief, C., Hofstaedter, F., Zwarthoff, E. C., van der Kwast, T. H., Knuechel, R., and Hartmann, A. Chromosome 9 deletions are more frequent than fgfr3 mutations in flat urothelial hyperplasias of the bladder. *Int J Cancer 119*, 5 (Sep 2006), 1212–1215.

[217] van Rhijn, B. W. G., van Tilborg, A. A. G., Lurkin, I., Bonaventure, J., de Vries, A., Thiery, J.-P., van der Kwast, T. H., Zwarthoff, E. C., and Radvanyi, F. Novel fibroblast growth factor receptor 3 (fgfr3) mutations in bladder cancer previously identified in non-lethal skeletal disorders. *Eur J Hum Genet 10*, 12 (Dec 2002), 819–824.

[218] Vieira, A. V., Lamaze, C., and Schmid, S. L. Control of egf receptor signaling by clathrin-mediated endocytosis. *Science 274*, 5295 (1996), 2086–9.

[219] Vuoriluoto, K., Haugen, H., Kiviluoto, S., Mpindi, J.-P., Nevo, J., Gjerdrum, C., Tiron, C., Lorens, J. B., and Ivaska, J. Vimentin regulates emt induction by slug and oncogenic h-ras and migration by governing axl expression in breast cancer. *Oncogene 30*, 12 (Mar 2011), 1436–1448.

[220] Wang, W., Wyckoff, J. B., Frohlich, V. C., Oleynikov, Y., Haettelmaier, S., Zavadil, J., Cermak, L., Bottinger, E. P., Singer, R. H., White, J. G., Segall, J. E., and Condeelis, J. S. Single cell behavior in metastatic primary mammary tumors correlated with gene expression patterns revealed by molecular profiling. *Cancer Res 62*, 21 (2002), 6278–6288.

[221] Wang, Z., Edwards, J. G., Riley, N., Provance, D. W., J., Karcher, R., Li, X. D., Davison, I. G., Ikebe, M., Mercer, J. A., Kauer, J. A., and Ehlers, M. D. Myosin vb mobilizes recycling endosomes and ampa receptors for postsynaptic plasticity. *Cell 135*, 3 (2008), 535–48.

[222] Watson, F. L., Heerssen, H. M., Bhattacharyya, A., Klesse, L., Lin, M. Z., and Segal, R. A. Neurotrophins use the erk5 pathway to mediate a retrograde survival response. *Nat Neurosci 4*, 10 (Oct 2001), 981–988.

[223] Webster, M. K., and Donoghue, D. J. Constitutive activation of fibroblast growth factor receptor 3 by the transmembrane domain point mutation found in achondroplasia. *EMBO J 15*, 3 (Feb 1996), 520–527.

[224] Welz, T., Wellbourne-Wood, J., and Kerkhoff, E. Orchestration of cell surface proteins by rab11. *Trends Cell Biol 24*, 7 (2014), 407–15.

[225] WHO. Histological typing of urinary bladder tumours. *WHO* (1973).

[226] Wilcke, M., Johannes, L., Galli, T., Mayau, V., Goud, B., and Salamero, J. Rab11 regulates the compartmentalization of early endosomes required for efficient transport from early endosomes to the trans-golgi network. *J Cell Biol 151*, 6 (2000), 1207–1220.

[227] Williams, S. V., Hurst, C. D., and Knowles, M. A. Oncogenic fgfr3 gene fusions in bladder cancer. *Hum Mol Genet 22*, 4 (Feb 2013), 795–803.

[228] Witjes, J. A., Compérat, E., Cowan, N. C., De Santis, M., Gakis, G., Lebret, T., Ribal, M. J., Van der Heijden, A. G., Sherif, A., and , E. A. o. U. Eau guidelines on muscle-invasive and metastatic bladder cancer: summary of the 2013 guidelines. *Eur Urol 65*, 4 (Apr 2014), 778–792.

[229] Wong, A., Lamothe, B., Lee, A., Schlessinger, J., Lax, I., and Li, A. Frs2 alpha attenuates fgf receptor signaling by grb2-mediated recruitment of the ubiquitin ligase cbl. *Proc Natl Acad Sci U S A 99*, 10 (May 2002), 6684–6689.

[230] Wu, C., Ramirez, A., Cui, B., Ding, J., Delcroix, J.-D. M., Valletta, J. S., Liu, J.-J., Yang, Y., Chu, S., and Mobley, W. C. A functional dynein-microtubule network is required for ngf signaling through the rap1/mapk pathway. *Traffic 8*, 11 (Nov 2007), 1503–1520.

[231] Wu, Y.-M., Su, F., Kalyana-Sundaram, S., Khazanov, N., Ateeq, B., Cao, X., Lonigro, R. J., Vats, P., Wang, R., Lin, S.-F., Cheng, A.-J., Kunju, L. P., Siddiqui, J., Tomlins, S. A., Wyngaard, P., Sadis, S., Roychowdhury, S., Hussain, M. H., Feng, F. Y., Zalupski, M. M., Talpaz, M., Pienta, K. J., Rhodes, D. R., Robinson, D. R., and Chinnaiyan, A. M. Identification of targetable fgfr gene fusions in diverse cancers. *Cancer Discov 3*, 6 (Jun 2013), 636–647.

[232] Yasoda, A., Komatsu, Y., Chusho, H., Miyazawa, T., Ozasa, A., Miura, M., Kurihara, T., Rogi, T., Tanaka, S., Suda, M., Tamura, N., Ogawa, Y., and Nakao, K. Overexpression of cnp in chondrocytes rescues achondroplasia through a mapk-dependent pathway. *Nat Med 10*, 1 (Jan 2004), 80–86.

[233] Yin, Y. X., Shen, F., Pei, H., Ding, Y., Zhao, H., Zhao, M., and Chen, Q. Increased expression of rab25 in breast cancer correlates with lymphatic metastasis. *Tumour Biol 33*, 5 (Oct 2012), 1581–1587.

[234] Yuan, L., Liu, Z.-H., Lin, Z.-R., Xu, L.-H., Zhong, Q., and Zeng, M.-S. Recurrent fgfr3-tacc3 fusion gene in nasopharyngeal carcinoma. *Cancer Biol Ther 15*, 12 (2014), 1613–1621.

[235] Zhang, X., Ibrahimi, O. A., Olsen, S. K., Umemori, H., Mohammadi, M., and Ornitz, D. M. Receptor specificity of the fibroblast growth factor family. the complete mammalian fgf family. *J Biol Chem 281*, 23 (2006), 15694–700.

[236] Zhang, X., Tang, N., Hadden, T. J., and Rishi, A. K. Akt, foxo and regulation of apoptosis. *Biochim Biophys Acta 1813*, 11 (Nov 2011), 1978–1986.

[237] Zimmermann, P., Zhang, Z., Degeest, G., Mortier, E., Leenaerts, I., Coomans, C., Schulz, J., N'Kuli, F., Courtoy, P. J., and David, G. Syndecan recycling [corrected] is controlled by syntenin-pip2 interaction and arf6. *Dev Cell 9*, 3 (Sep 2005), 377–388.

Rôle des GTPases RAB25 et RAB11 dans la tumorigénèse des cancers de la vessie

Résumé : L'activation constitutive de FGFR3 par mutation ou translocation est l'un des évènements les plus fréquents dans le cancer de la vessie. Une dérégulation de RAB25, une protéine impliquée dans le processus de recyclage des récepteurs de surface, a été montrée dans différents cancers. Des données du transcriptome des cancers de vessie ont montré que *RAB25* est surexprimé dans les tumeurs présentant des altérations de FGFR3. L'objectif de cette thèse a été d'étudier l'implication possible de RAB25, des protéines de la même famille, RAB11A et RAB11B, et leur effecteurs RAB11FIP2 et MYO5B dans 1) la tumorigénèse des tumeurs altérées pour FGFR3 et 2) le trafic et la signalisation de FGFR3. Nos résultats montrent que l'extinction de ces protéines par des siARNs induit une diminution significative de la viabilité cellulaire des cellules exprimant des formes constitutivement activées de FGFR3. Les effets de la déplétion de RAB25 et RAB11 sur le recyclage de FGFR3, sur les voies de signalisation de FGFR3 et sur l'expression des gènes cibles de FGFR3 suggèrent que le recyclage de FGFR3 régulé par RAB25 et RAB11 peut prolonger le signal de FGFR3 et peut fournir une plateforme pour la signalisation de FGFR3. Nous avons également comparé la distribution cellulaire des formes sauvage et muté (S249C) de FGFR3 portant une étiquette GFP dans des cellules HeLa. Les deux formes de FGFR3 se trouvent dans plusieurs compartiments intracellulaires mais FGFR3 muté se localise préférentiellement dans le compartiment de recyclage. Ce projet nous a permis de mieux caractériser la trafic de FGFR3 dans le cancer de la vessie et son lien avec la signalisation et l'activité de FGFR3.

Mots-clés : FGFR3, cancer de la vessie, recyclage, GTPases RAB, sous-famille RAB11

Role of RAB25 and RAB11 GTPases in bladder tumorigenesis

Abstract : Activation of FGFR3 by point mutation, translocation and overexpression is one of the most frequent events in bladder cancer. The dysfunction of RAB25, a GTPase involved in endocytic recycling of transmembrane receptor, has been shown in many cancers. Gene expression data in bladder cancer indicates that *RAB25* expression is significant higher in tumors carrying altered FGFR3. The thesis project aimed to investigate the potential role of RAB25, proteins from the same family (RAB11A and RAB11B) and their effectors RAB11FIP2 and MYO5B in 1) the tumorigenesis of tumors carrying altered FGFR3 and 2) the trafficking and the signaling of FGFR3. Our results demonstrate that depletion of these proteins by siRNA significantly reduces cell viability in cells expressing constitutively activated forms of FGFR3. The effects of RAB25 and RAB11 silencing on FGFR3 trafficking and signaling and the expression of FGFR3 target genes suggest that the RAB11- and RAB25-mediated recycling can sustain the signaling by protecting altered FGFR3 from the degradation pathway, and can provide a platform for FGFR3 signaling We also compared the subcellular distribution of wild type and mutant (S249C) forms of FGFR3. These two forms localize to different compartments including early endosomes, late endosomes and recycling compartments. The S249C FGFR3 mutant preferentially localizes to the endocytic recycling compartment. Our findings shed light to the molecular mechanisms underlying the relationships between the trafficking and signaling of FGFR3 in the context of bladder cancer.

Keywords : FGFR3, bladder cancer, oncogene, recycling, RAB GTPases, RAB11 subfamily